Département de Géomatique Appliquée
Faculté des Lettres et Sciences Humaines
Université de Sherbrooke

Assimilation des données GRACE dans le modèle MESH pour l'amélioration de l'estimation de l'équivalent en eau de la neige

Assimilation of GRACE data into the MESH model to improve the estimation of snow water equivalent

Ala Bahrami

Directeur de recherche: Kalifa Goïta
Codirecteur de recherche: Ramata Magagi

Thèse présentée pour l'obtention du grade Philosophiae Doctor (PhD) en télédétection, cheminement en physique de la télédétection

August 2020

To Freedom of Thought and Speech

Identification du jury

Directeur de recherche: Professor Dr. Kalifa Goïta, Université de Sherbrooke, Canada

Codirecteur de recherche: Professor Dr. Ramata Magagi, Université de Sherbrooke, Canada

Membre du jury externe: Professor Dr. Barton Forman, University of Maryland, USA

Membre du jury interne: Professor Dr. Alexandre Langlois, Université de Sherbrooke, Canada

Membre du jury interne: Professor Dr. Yacine Bouroubi, Université de Sherbrooke, Canada

Abstract

Water storage changes over space and time play a major rule in the Earth's climate system through the exchange of water and energy fluxes among the Earth's water storage compartments and between atmosphere, continents, and oceans. In many parts of northern-latitude areas spring meltwater controls the availability of freshwater resources. With respect to terrestrial hydrologic process, snow water equivalent (SWE) is the most critical snow characteristic to hydrologists and water resource managers. The first objective of this study examined the spatiotemporal variations of terrestrial water storages and their linkages with SWE variabilities over Canada. Terrestrial water storage anomaly (TWSA) from the Gravity Recovery and Climate Experiment (GRACE), the WaterGAP Global Hydrology Model (WGHM), and the Global Land Data Assimilation System (GLDAS) were employed. SWE anomaly (SWEA) products were provided by the Global Snow Monitoring for Climate Research version 2 (GlobSnow2), Advanced Microwave Scanning Radiometer-Earth Observing System (AMSR-E), and Canadian Meteorological Centre (CMC). The grid cell (1°×1°) and basin-averaged analyses were applied to find any possible relationship between TWSA and SWEA over the Canadian territory, from December 2002 to March 2011. Results showed that GRACE versus CMC provided the highest percentage of significant positive correlation (62.4% of the 1128 grid cells), with an average significant positive correlation coefficient of 0.5, and a maximum of 0.9. In western Canada, GRACE correlated better with multiple SWE data sets than GLDAS. Yet, over eastern Canada, mainly in the northern Québec area (~ 55ºN), GRACE provided weak or insignificant correlations with all snow products, while GLDAS appeared to be significantly correlated. For the TWSA-SWEA analysis at the basin-averaged scale, significant relationships were observed between TWSA and SWEA for most of the fifteen basins considered (53% to 80% of the basins, depending on the SWE products considered). The best results were obtained with the CMC SWE products, compared to satellite-based SWE data. Stronger relationships were found in snow-dominated basins (R_s >= 0.7), such as the Liard [root mean square error (RMSE) = 21.4 mm] and Peace Basins (RMSE = 26.76 mm). However, despite high snow accumulation in northern Québec, GRACE showed weak or insignificant correlations with SWEA, regardless of the data sources. The same behavior was observed in the western Hudson Bay Basin. In both regions, it was found that the contribution of non-SWE compartments, including wetland, surface water, as well as soil water storages has a

significant impact on the variations of total storage. These components were estimated using the WGHM simulations and then subtracted from GRACE observations. The GRACE-derived SWEA correlation results showed improved relationships with three SWEA products (CMC, GlobSnow2, AMSR-E). The improvement is particularly important in the sub-basins of the Hudson Bay, where very weak and insignificant results were previously found with GRACE TWSA data. GRACE-derived SWEA showed a significant relationship with CMC data in 93% of the basins (13% more than GRACE TWSA). In general, results revealed the importance of SWE changes in association with the terrestrial water storage (TWS) variations.

The second objective of this thesis investigates whether integration of remotely sensed terrestrial water storage (TWS) information, which is derived from GRACE, can improve SWE and streamflow simulations within a semi-distributed hydrology land surface model. A data assimilation (DA) framework was developed to combine TWS observations with the MESH (Modélisation Environnementale Communautaire – Surface Hydrology) model using an ensemble Kalman smoother (EnKS). This study examined the incorporation and development of the ensemble-based GRACE data assimilation framework into the MESH modeling framework for the first time. The snow-dominated Liard Basin was selected as a case study. The proposed assimilation methodology reduced bias of monthly SWE simulations at the basin scale by 17.5% and improved unbiased root-mean-square difference (ubRMSD) by 23%. At the grid scale, the DA method improved ubRMSD values and correlation coefficients of SWE estimates for 85% and 97% of the grid cells, respectively. Effects of GRACE DA on streamflow simulations were evaluated against observations from three river gauges, where it could effectively improve the simulation of high flows during snowmelt season from April to June. The influence of GRACE DA on the total flow volume and low flows was found to be variable. In general, the use of GRACE observations in the assimilation framework not only improved the simulation of SWE, but also effectively influenced the simulation of streamflow estimates.

Key words: Gravity Recovery and Climate Experiment (GRACE), Terrestrial Water Storage (TWS), MESH (Modélisation Environnmentale Communautaire – Surface Hydrology), Snow Water Equivalent (SWE), Data Assimilation (DA), Ensemble Kalman smoother (EnKS).

Résumé

Les variations dans l'espace et le temps du stock d'eau à travers jouent un rôle important dans le système climatique de la Terre à travers l'échange des flux d'eau et d'énergie entre les compartiments du stock d'eau de la Terre, et entre l'atmosphère, les continents et les océans. Dans les régions nordiques, la fonte de la neige contrôle la disponibilité des ressources en eau. Concernant le processus hydrologique terrestre, l'équivalent en eau de la neige (SWE) est la caractéristique de neige la plus importante pour les hydrologues et les gestionnaires des ressources en eau. Le premier objectif de cette étude a examiné les variations spatio-temporelles des réservoirs terrestres d'eau et leurs liens avec les variabilités de SWE au Canada. Des anomalies de stockage d'eau terrestre (TWSA) provenant de GRACE (Gravity Recovery and Climate Experiment), du modèle hydrologique mondial WaterGAP (WGHM) et du modèle GLDAS (Global Land Data Assimilation System) ont été utilisées. Les produits du SWEA (Snow Water Equiavalent Anomaly) sont fournis par le GlobSnow2 (Global Snow Monitoring for Climate Research version 2), le AMSR-E (Advanced Microwave Scanning Radiometer-Earth Observing System) et le Centre météorologique canadien (CMC). L'analyse par cellule de grille (1°×1°) a été appliquée pour trouver toute relation possible entre TWSA et SWEA sur le territoire canadien, de décembre 2002 à mars 2011. Les résultats montrent que GRACE par rapport à CMC a fourni le pourcentage le plus élevé de corrélation positive significative (62,4% des 1128 cellules de la grille), avec un coefficient de corrélation positif significatif moyen de 0,5 et un maximum de 0,9. Dans la partie ouest du pays, GRACE a montré un meilleur accord avec plusieurs produits SWE que GLDAS. Pourtant, dans l'est du Canada, principalement dans le nord du Québec (~ 55° N), GRACE a fourni des corrélations faibles ou insignifiantes avec tous les produits SWE, contrairement à GLDAS qui semblait être significativement corrélé. Dans le cas de l'analyse à l'échelle du bassin versant, les relations significatives ont été observées entre TWSA et SWEA pour la plupart des quinze bassins considérés (53% à 80% des bassins, selon les produits SWE considérés). Les meilleurs résultats ont été obtenus avec les produits CMC SWE, par rapport aux données SWE satellitaires. Des relations plus fortes ont été trouvées dans les bassins dominés par la neige (Rs> = 0,7), tels que le bassin versant de Liard [erreur quadratique moyenne (RMSE) = 21,4 mm] et le bassin versant de Peace (RMSE = 26,76 mm). Cependant, malgré une forte accumulation de neige dans le nord du Québec, GRACE a montré des corrélations faibles ou insignifiantes avec SWEA, peu importent

les sources de données. Le même comportement a été observé dans le bassin versant ouest de la Baie d'Hudson. Dans les deux régions, il a été constaté que la contribution des compartiments non-SWE, y compris les zones humides, les eaux de surface, ainsi que les stocks d'eau du sol a un effet significatif sur les variations du stock total. Ces composantes ont été estimées à l'aide des simulations du modèle WGHM, puis soustraites des observations GRACE. Ces résultats de corrélation SWEA dérivés de GRACE ont montré une amélioration des relations avec les trois produits SWE (CMC, GlobSnow2, AMSR-E). L'amélioration est particulièrement importante dans les sous-bassins de la Baie d'Hudson, où des résultats très faibles et insignifiants avaient été précédemment trouvés avec les données GRACE TWSA. La SWEA dérivée de GRACE a montré une relation significative avec les données CMC dans 93% des bassins (13% de plus que GRACE TWSA). En somme, les résultats obtenus dans ce premier objectif ont montré le rôle important du SWE dans les variations du stock terrestre de l'eau dans la région d'étude.

Le deuxième objectif de cette thèse examine si l'intégration des informations de TWS (terrestrial water storage) dérivées de GRACE (Gravity Recovery and Climate Experiment), peut améliorer les simulations du SWE et du débit d'eau dans un modèle hydrologique semi-distribué de schéma de surface. Un cadre d'assimilation de données (DA) a été développé pour combiner les observations TWS avec le modèle MESH (Modélisation Environnementale Communautaire - Hydrologie de Surface) en utilisant un ensemble Kalman Smoother (EnKS). Cette étude était la première du genre à tenter une assimilation des données GRACE dans le modèle MESH pour améliorer l'estimation du SWE. Le bassin versant de la Liard dominé par la neige a été choisi pour le site d'étude. À l'échelle du bassin versant, la méthodologie d'assimilation proposée a réduit le biais des simulations mensuelles de SWE à 17,5% et amélioré le ubRMSD (unbiased root-mean-square difference) de 23%. À l'échelle de la grille, la méthode DA a amélioré l'estimation du SWE pour les valeurs ubRMSD et les coefficients de corrélation pour 85% et 97% des cellules de la grille, respectivement. Les effets de GRACE DA sur les simulations de débit ont été évalués par rapport aux observations de trois stations des débits, où il pourrait effectivement améliorer la simulation des débits élevés pendant la saison de fonte de la neige d'avril à juin. L'influence de GRACE DA sur le volume total et les faibles débits d'eau a été trouvée variable. En général, l'utilisation des observations GRACE dans le cadre d'assimilation non seulement a amélioré la simulation de SWE, mais a également influencé efficacement la simulation des estimations de débit.

Mots-clés: Gravity Recovery and Climate Experiment (GRACE), Stock d'eau Terrestre (TWS), MESH (Modélisation Environnmentale Communautaire – Surface et Hydrologie), équivalent en eau de la neige (SWE), Assimilation de Données (DA), Ensemble Kalman smoother (EnKS).

Table of Contents

List of Figures

List of Tables

Acronyms

AI	Analysis Increments
AMSR-E	Advanced Microwave Scanning Radiometer for Earth Observing System
ANU	Australian National University
CaPA	Canadian Precipitation Analysis
CCMEO	Canada Centre for Mapping and Earth Observation
CCRS	Canada Centre for Remote Sensing
C/DA	Calibration and Data Assimilation
CDED	Canadian Digital Elevation Data
CMC	Canadian Meteorological Centre
CLASS	Canadian Land Surface Scheme
CaLDAS	Canadian Land Data Assimilation System
CLM	Community Land Model
CRCM	Canadian Regional Climate Model
CSR	Center for Space Research
DA	Data Assimilation
DCS	Data Collection System
DEM	Digital Elevation Model
DLR	Deutsches Zentrum für Luft- und Raumfahrt
DZTR	Dynamically Zoned Target Release
EAKF	Ensemble Adjustment Kalman Filter
ECCC	Environment and Climate Change Canada
EnKF	Ensemble Kalman filter
EnKS	Ensemble Kalman Smoother
EnSRF	Ensemble Square-Root Filter
FFT	Fast Fourier Transform
FRWS	Frozen Water Storage

GEM	Global Environmental Multiscale
GEM-Hydro	GEM Hydrological
GFZ	GeoforschungsZentrum Potsdam
GIA	Glacial Isostatic Adjustment
GIWS	Global Institute for Water Security
GlobSnow	Global Snow Monitoring for Climate Research
GLDAS	Global Land Data Assimilation System
GMAO	Global Modeling and Assimilation Office
GOES	Geostationary Satellites
GPS	Global Positioning System
GRACE	Gravity Recovery and Climate Experiment
GRACE-FO	GRACE Follow-On
GRU	Grouped Response Units
H-LSM	Hydrological and Land Surface Models
JPL	Jet Propulsion Laboratory
LAI	Leaf Area Index
LCC	Land Cover of Canada
LQWS	Liquid Water Storage
LRI	Laser Ranging Interferometer
LSM	Land Surface Model
LZS	Lower Zone Storage
MAGS	Mackenzie GEWEX Study
MCMC	Markov Chain Monte Carlo
MEC	Modélisation Environnementale Communautaire
MESH	Modélisation Environnementale Communautaire – Surface Hydrology
MESH-CLASS	MESH and CLASS
MESH-GRACE	MESH and GRACE
MODIS	Moderate Resolution Imaging Spectroradiometer
MRB	Mackenzie River Basin

NASA	National Aeronautics and Space Administration
NOAA	National Oceanic and Atmospheric Administration
NSE	Nash-Sutcliffe Efficiency
NSIDC	National Snow and Ice Data Center
NWP	Numerical Weather Prediction
OL	Open-Loop
PBIAS	Percentage Bias
PBSM	Prairie Blowing Snow Model
PCR-GLOBWB	PCRaster Global Water Balance
PDF	Probability Density Functions
PDMROF	Probability Distribution Model based RunOff
PF	Particle Filters
PFT	Plant Functional Type
PMW	Passive Microwave
R&D	Research and Development
RMSD	Root Mean Square Difference
RMSE	Root Mean Square Error
SD	Snow Depth
SDS	Science Data System
SEIK	Singular Evolutive Interpolated Kalman
SLC	Soil Landscapes of Canada
SMOS	Soil Moisture and Ocean Salinity
SnowMIP	Snow Model Intercomparison Project
SQRA	Square Root Analysis
SVS	Soil, Vegetation, and Snow
SWE	Snow Water Equivalent
SWEA	Snow Water equivalent Anomaly
SWEM	Maximum SWE

TWS	Terrestrial Water Storage
TWSA	Terrestrial Water Storage Anomaly
UbRMSD	Unbiased Root-Mean-Square Difference
WaterGAP	Water-Global Assessment and Prognosis
WGHM	WaterGAP Global Hydrology Model
WSC	Water Survey of Canada
W3RA	World-Wide Water Resources Assessment
1D-EnKF	One-Dimensional Ensemble Kalman Filter

Acknowledgments

First of all, I would like to thank my supervisor Prof. Dr. Kalifa Goïta who offered me this opportunity to undertake my PhD studies at Université de Sherbrooke. I am very grateful for all the supports, valuable suggestions, guidance and freedom that gave me the opportunity to build my own research profile. His valuable insights and professional attitudes helped me to improve the results of this work through the process from beginning to end. Extended gratitude also goes to my co-supervisor Prof. Dr. Ramata Magagi for her generous support of my work, her patience and inspiration, and her immense knowledge in helping me to manage the complex task of completing this work. I would like to acknowledge the financial supports, awarded by the Natural Sciences and Engineering Research Council of Canada (NSERC).

My deep gratitude goes to Prof. Dr. Barton Forman (University of Maryland, USA), Prof. Dr. Alexandre Langlois (Université de Sherbrooke, Canada), and Prof. Dr. Yacine Bouroubi (Université de Sherbrooke, Canada) for their evaluations of my thesis. Their constructive comments helped me to improve the quality of this dissertation.

During my PhD studies, I had the unique chance to spend six months as a visiting researcher in the School of Environment and Sustainability at the University of Saskatchewan. I would like to thank the researchers and employees of the Environment and Climate Change Canada, Global Institute for Water Security, and the Centre for Hydrology at the University of Saskatchewan. I would like to acknowledge and thank Dr. Bruce Davison for providing me this chance to collaborate with a group of researchers in this project. His valuable guidance helped me to improve my skills and understanding through my PhD studies. My special thanks go to Prof. Dr. Saman Razavi for supporting me during my stay at Saskatoon to work in a productive and friendly environment. Very special thanks go to Dan Princz who has provided me valuable insights and suggestions that without doubts helped me to deal with technical programming issues of MESH open-source software. I would thank Mohamed Elshamy for taking his time and providing technical and scientific supports regarding the MESH configuration, and analysis of the model outputs. His helpful suggestions had a tremendous positive impact on my experience. I would like to thank Dr. Amin Haghnegahdar for the fruitful discussions during my stay in Saskatoon. I am grateful for the administrative support of Michelle Martel-Andre who helped me with her warm

and friendly guidance during my visit to Saskatoon.

During my PhD studies, I had the unique chance to have fruitful discussions with Dr. Ally M. Toure, Dr. Alexandre Roy, Dr. Hannes Müller Schmied, and Dr. Ehsan Forootan. I would also like to thank the faculty and staff at Université de Sherbrooke for all their work and support through different stages of my studies. I like to thank Odile Couture who helped me with her smiles to cope with administrative tasks. I would like to thank my colleagues at Université de Sherbrooke. During my graduate studies, I met many nice, friendly, outgoing colleagues who inspired me a lot for having various social and sportive activities. My special thanks go to Jean-Benoît Madore (JB) for his tremendous support and help. I like to thank: Brice Caillié, Nicolas Marchand, Bruno-Charles Busseau (BC), Joris Ravaglia, Michael Prince, Olivier Saint-Jean-Rondeau, Daniel Kramer, Simon Levasseur, Guillaume Couture, Julien Meloche, Ali Ben Abbes, Florentin Bourge, Paul Billecocq, Carina Poulin, Homayoun Harirforoush, Joëlle Voglimacci, Vincent Beauregard, Nathalie Thériault, Caroline Dolant, Fanny Larue, Adrien Letellier, Vincent Sasseville, Céline Vargel, and Alex Mavrovic.

I am fortunate in my life to have a group of adorable friends. I am very grateful to my best friend Arvin Morattab. I always enjoyed spending time with him. The loss of Arvin and his lovely wife Aida, in the crash of Ukrainian flight PS752, was an unbelievable tragedy for me. I owe particular thanks to Armin Morattab, Arash Morattab, Fereshteh Farokhi, Saman Pournahavandi, Iraj Yadegari, Hamid Dehghan, Jamil Bahrami, Babak Hejrani, Fardin Nili, and Babak Roshani.

I would like to thank my parents, Sheida and Alaeddin, who have stood beside and supported me in entire life. Special thanks also go to my lovely and supportive sister and brother, Nishtman and Azad, who have always encouraged and inspired me with their kind motivations and inspirations throughout my life. Without the support of my family, none of this work would have been possible, and their contribution is unmatched by my own effort. I would like to thank my uncle, Saadi, for his encouragement and kind assistance during my life.

Finally, but very certainly not least, my most warm and exceptional gratitude goes to Soma for bearing me during this adventure, particularly during difficult times. She has filled my life with so much joy and supported me in all aspects. Finishing this thesis would not be possible without her immense support.

Reading Guide

As part of this research project, we have published one article in the Hydrological Processes Journal. One article has been also submitted to the Journal of Hydrology. One article is also prepared for submission to the Journal of Remote Sensing.

Therefore, this thesis is presented in the form of articles based on three journal publication/submissions. Three technical chapters of the thesis are devoted to the articles. Each chapter contains the following sections: introduction, study site and data, methodology, results, and discussion. Chapter 1 explains the research problematics, objectives, research questions, and hypotheses. Chapter 2 is an overview of the scientific background and applications. Chapter 3 explains the summary of datasets and study sites. Chapters 4, 5, and 6 in the form of articles, present the TWSA-SWEA relationship analysis and data assimilation implementation, respectively. Chapter 7 is dedicated to overall discussions. Finally, the findings of the thesis, general perspectives, and outlooks are described in chapter 8.

1. Introduction

1.1. The Global water cycle

Continental water storage changes in space and time play a major rule in the Earth's climate system via the exchange of water and energy fluxes among the Earth's water storage compartments and between atmosphere, continents, and oceans (Döll *et al.,* 2014a). Global observations of water and ice mass distribution at monthly to decadal time scales are crucial for the forecast of climate change, weather, biological and agricultural productivity, flooding, and a wide variety of studies in the geoscience (Rodell *et al.*, 2004; Tapley *et al.*, 2019). Thus, the critical challenge for this century may be the globally sustainable management of water resources (Rodell *et al.*, 2018).

Terrestrial water storage (TWS) as a major variable of the Earth's water cycle is defined as the summation of key hydrologic reservoirs, including soil water (i.e, near surface in unsaturated zone and in deeper groundwater reservoirs), surface water (i.e., rivers, lakes), the cryosphere water storage (including seasonal snowpack, mountain glaciers, polar ice sheets), and biomass water storage (Famiglietti and Rodell, 2013; Margulis, 2014). In Table 1.1 the approximate estimate of water storage in the key reservoirs in the global system is presented. After the ocean reservoir, the largest source of water storage is the ice caps and glaciers which contain valuable sources of freshwater in frozen form (Margulis, 2014).

Table 1.1. Estimates of storage in primary global hydrologic reservoirs (Bras, 1990)

Reservoir	Volume (km^3)	% Total water
Oceans	1,322,000,000	97.2
Ice caps & glaciers	29,199,700	2.1
Groundwater (near surface)	4,171,400	0.31
Lakes & rivers	130,700	0.017
Soil moisture	66,700	0.005
Atmoshpere	12,900	0.0009

The general schematic of water distribution in surface and sub-surface water storage, as well as mass variation within and between ocean and atmosphere, is presented in Figure 1.1.

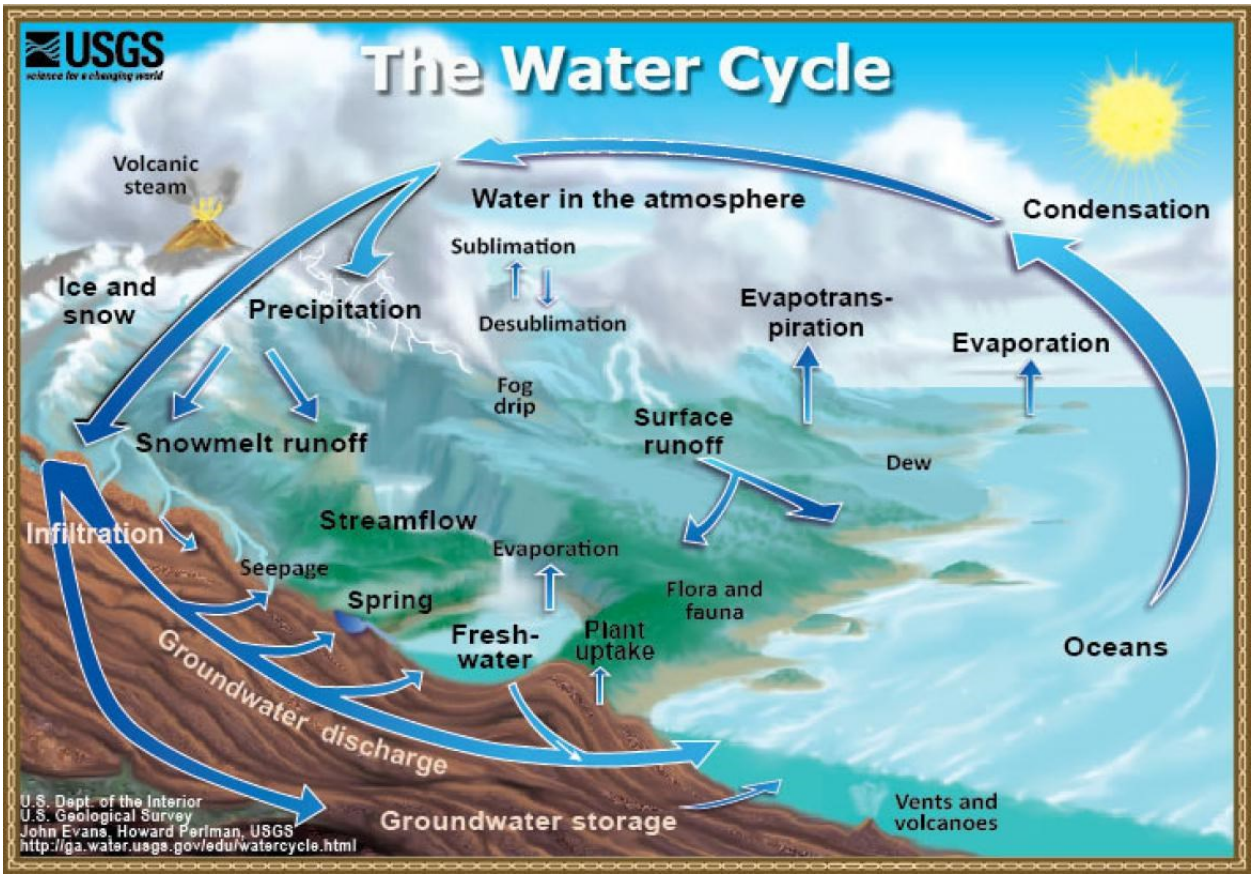

Figure 1.1. The schematic overview of the Earth's water movement (Retrieved from https://www.usgs.gov/media/images/water-cycle-natural-water-cycle)

1.2. The importance of snow

Snow as one of the most noticeable elements of the hydrologic cycle has considerable influence on the short- and long-term weather and climate systems of various regional and hemispheric phenomena (Cohen and Entekhabi, 1999; Su *et al.*, 2010; Walsh, 1984). In the Northern hemisphere, energy budget, water balance, and geochemical cycles are influenced by the seasonal cycle of the terrestrial snow and snow mass (Mudryk *et al.,* 2015). Snow is a critical component of the hydrologic cycle due to the pivotal impact of snow albedo (reflectivity) and surface temperature feedbacks on weather and climate (Barnett *et al.*, 1989; Cohen, 1989; Fletcher *et al.*, 2009; Gong *et al.*, 2004; Kelly, 2009; Robinson *et al.*, 1993; Yang *et al.*, 2001). There are different

ways in which snow cover alters the exchange of energy between the surface and the atmosphere. First, the albedo of fresh snow is 0.8-0.85 for sunlight, while the reflectivity of bare land and ice-free ocean is typically between 0.05 and 0.3 (Walsh, 1984). Therefore, snowpack helps to cool the surface temperature due to high albedo of snow, more outgoing thermal radiation due to high emissivity of snow, and more outgoing heat flux due to snowmelt, evaporation and/or sublimation (Gong *et al.*, 2004). Second, snow as a highly effective insulator has low thermal conductivity. The soil temperature can remain unfrozen for several weeks beneath a snow cover of 20-30 cm, even when the air temperature drops to 10-20º C below freezing point (Walsh, 1984).

In many parts of northern-latitude areas, as well as the mountainous regions, spring meltwater controls the availability of freshwater resources for approximately more than one-sixth of the world's population (Barnett *et al.*, 2005; Déry *et al.*, 2005; Stieglitz *et al.*, 2001). With respect to the terrestrial hydrologic process, three fundamental parameters for climatology and hydrology include snow water equivalent (SWE), snow extent, and melt onset (Foster *et al.*, 2011). SWE is defined as the equivalent amount of liquid water mass that be acquired if the entire snowpacks were melted (Margulis, 2014). Thus, the accurate presentation of SWE is the most critical snow characteristic to hydrologists and water resource managers for operational run-off and river discharge forecasts (McCreight *et al.*, 2014; Pulliainen, 2006). However, estimation of SWE over time and space is a challenging task.

1.3. SWE estimation

SWE can be estimated using ground-based techniques, remote sensing, and land surface model (LSM) simulations. Ground-based SWE information can be estimated using the interpolation of SWE in-situ measurements or as the product of snow depth (SD) and snow density observations. SD is easier and quicker to measure than SWE (Sturm *et al.*, 2010). However, the accuracy of the snow depth measurements is influenced by the interpolation of observations from gauging networks and snow courses, or daily synoptic weather station-based measurements (Pulliainen, 2006). In addition to the limitations of snow depth products, snow density measurements (e.g., snow tubes, triangular sampler) have their uncertainties. Snow density has around 10% uncertainty in the density measurement. The uncertainty of SWE estimates is negatively influenced by inadequate spatial coverage, especially in the northern regions where observations become sparse

and also biased toward coastal location that may not be representative of the general area (Derksen *et al.*, 2010; Rott *et al.*, 2010; Verseghy *et al.*, 2017b). Due to limitations of ground-based SWE methods, satellite remote sensing measurements and land surface model simulations are considered as alternative solutions to obtain more accurate snow products (Zhang *et al.*, 2014). Among remote sensing SWE estimation approaches, satellite passive microwave (PMW) retrievals have been used since 1978 and SWE estimates have been offered at all weather conditions with good temporal (daily) and moderate (~25 km) spatial resolution. Despite the benefits of PMW SWE products, they have several major drawbacks in forest land cover types and wet and deep snow conditions (when SWE is higher than 150 mm). These limitations can cause high uncertainties (up to 50% in boreal forest) in SWE estimates such that the usage of PMW SWE retrievals faces important challenges (Chang *et al.*, 1996; Roy, 2014; Roy *et al.*, 2010, 2012; Vachon *et al.*, 2010). Therefore, due to the limitations of PMW SWE estimates, other satellite remote sensing observations should be considered as alternative products. More information on SWE estimation using microwave remote sensing can be found in the work of Tedesco *et al.* (2014) and Saberi *et al.* (2020).

Among satellite measurement techniques, the Gravity Recovery and Climate Experiment (GRACE, Tapley *et al.*, 2004a) added a unique component to the existing suite of Earth observations by measuring the redistribution of terrestrial water storage anomaly (TWSA) around the world. Water mass movement can influence the Earth's gravity in a way that can be observed and quantified by gravity-based measurements (Reager, 2012). GRACE is a unique data source that can detect the spatiotemporal changes of the Earth's water storage and improve the estimation of the water cycle at regional to global scales (Güntner, 2008). GRACE observations are fundamental to understand the complex interactions and transitions involved in today's changing climate (Tapley *et al.*, 2019). The satellite observation of TWSA provides large-scale changes of total quantity of water as the summation of groundwater, soil moisture, SWE, surface water, ice, and water in biomass (Famiglietti and Rodell, 2013). This remote sensing product offers broad spatial coverage and provides much greater insight into global problems. The TWSA retrievals have monthly temporal resolution with an effective spatial (horizontal) resolution no better than a few hundred kilometers (Landerer and Swenson, 2012). GRACE unlike other satellite-based instruments, such as passive microwave sensors, does not rely on surface conditions and can measure total precipitation accumulation with no need for empirical parametrization and ground-

based calibration (Behrangi *et al.*, 2017, 2018). Over snow-dominated areas, the total water storage changes captured by GRACE are highly dominated by snow mass changes during snow accumulation and ablation phase (Forman *et al.*, 2012). In the mountainous regions during cold seasons, GRACE has provided the accumulated precipitation which appeared to be advantageous compared to conventional hydro-meteorological observing systems which faced the highest detection and retrieval uncertainty (Behrangi *et al.*, 2017, 2018).

A large number of LSMs has been developed to simulate the spatiotemporal variability of TWS changes on small to large scales in order to improve the estimation of the global water cycle (Schumacher, 2016; Sood and Smakhtin, 2015). Environment and Climate Change Canada (ECCC) designed a community-based hydrological-land surface model (H-LSM) called MESH (Modélisation Environnementale Communautaire (MEC) – Surface Hydrology; Pietroniro *et al.*, 2007). MESH, as a semi-distributed coupled model, has been developed for large-scale watershed modeling with consideration of cold region processes common in Canada. MESH is configured with the Canadian Land Surface Scheme (CLASS, Verseghy, 1991; Verseghy et al., 1993), the hydrological routing from WATFLOOD (Kouwen, 1988; Kouwen *et al.*, 1993), and other lateral flow processes (Mekonnen *et al.*, 2014; Soulis *et al.*, 2000, 2011; Yassin *et al.*, 2019). In this study, CLASS version 3.6 (Verseghy, 2012) is used to simulate the vertical energy and water fluxes for the vegetation canopy, snow, and different soil layers. The MESH model prognostic state (e.g., SWE) and flux simulation similar to other hydrological models are subject to several sources of uncertainty. Several important sources that influence model simulation include input data (e.g., climate forcing), model structure, and model parametrization (Müller Schmied *et al.*, 2014). Therefore, it may be useful to constrain model-derived water storage states by using auxiliary information in order to improve model simulation (Schumacher, 2016).

1.4. Challenge of SWE estimation methods

1.4.1. Modeled SWE

The seasonal snowpack estimates in CLASS is simulated using a single thermal layer with a bulk temperature and surface skin temperature. The evaluation of CLASS-derived SWE estimates in the Snow Model Intercomparison Project (SnowMIP) demonstrated that the single-layer model performed well compared to the multi-layer snowpack (Brown *et al.*, 2006; Essery *et al.*, 2009;

Etchevers *et al.*, 2002, 2004; Rutter *et al.*, 2009).

The first performance of the MESH model configured with CLASS (MESH-CLASS) version 3.0 in the simulation of snow mass was evaluated in the Ottawa river basin (Pietroniro *et al.*, 2007). The validation of results against snow survey observations showed that MESH-CLASS underestimated the SWE estimates. The Root Mean Square Error (RMSE) values of modeled SWE for years 2002 to 2005 fell between the range of 54 mm to 86 mm. The evaluation of MESH-CLASS in the SWE estimation has not been conducted in other studies. However, the individual performance of CLASS coupled with regional models was evaluated in a number of studies.

Langlois *et al.* (2014) evaluated the modeled SWE of CLASS versions 2.7 and 3.5 coupled to the Canadian Regional Climate Model, version 4 (CRCM4) over northern Québec. The assessment of results against snow course data revealed an overall overestimation of SWE with the RMSE values of 78.8 mm and 73.9 mm for both experiments respectively. The results show that the uncertainty of the model in the estimation of SWE is quite higher than the expected uncertainty limits of 30 mm for SWE < 300 mm (Rott *et al.*, 2010; Roy, 2014).

Recently, two studies evaluated the performance of CLASS-derived SWE estimates coupled to the CRCM5 on a regional scale over eastern and western Canada (Verseghy *et al.*, 2017; Verseghy and MacKay, 2017). The assessment analysis for the 12-year period of 1998-2010 demonstrated that CLASS has a substantial positive bias compared to the Canadian Meteorological Center (CMC) SWE data for March to May in Labrador and in the northern part of the Quebec (Verseghy *et al.*, 2017). Furthermore, for the first time over the western regions of Canada, the performance of CLASS was evaluated against monthly CMC and Global Snow Monitoring for Climate Research (GlobSnow) data sets, by excluding the mountainous regions (Verseghy and MacKay, 2017). The seasonal cycle of monthly modeled SWE (with and without lakes simulation), in addition to CMC and GlobSnow for the tundra, boreal, and southern zones are shown in Figure 1.2. Even though Verseghy and MacKay (2017) indicated that the CLASS model was deemed to have acceptable performance, they have not presented any statistical skill to illustrate the uncertainty of model simulation.

Based on the above-mentioned studies, valuable insights about the uncertainties and challenges in simulating snow mass using CLASS were highlighted. There is a substantial need to accurately

represent the snow budget. To achieve this objective, a robust method should be implemented to improve the modeled SWE estimation. Note that, the simulation of energy and water budgets within a tile (basin computational unit) in the MESH model is derived using different physically-based solver routines of the CLASS model. Then in the MESH model, the water storage, energy, and soil prognostic variables for each grid cell are weighted according to the land cover percentage area that is occupied inside the grid.

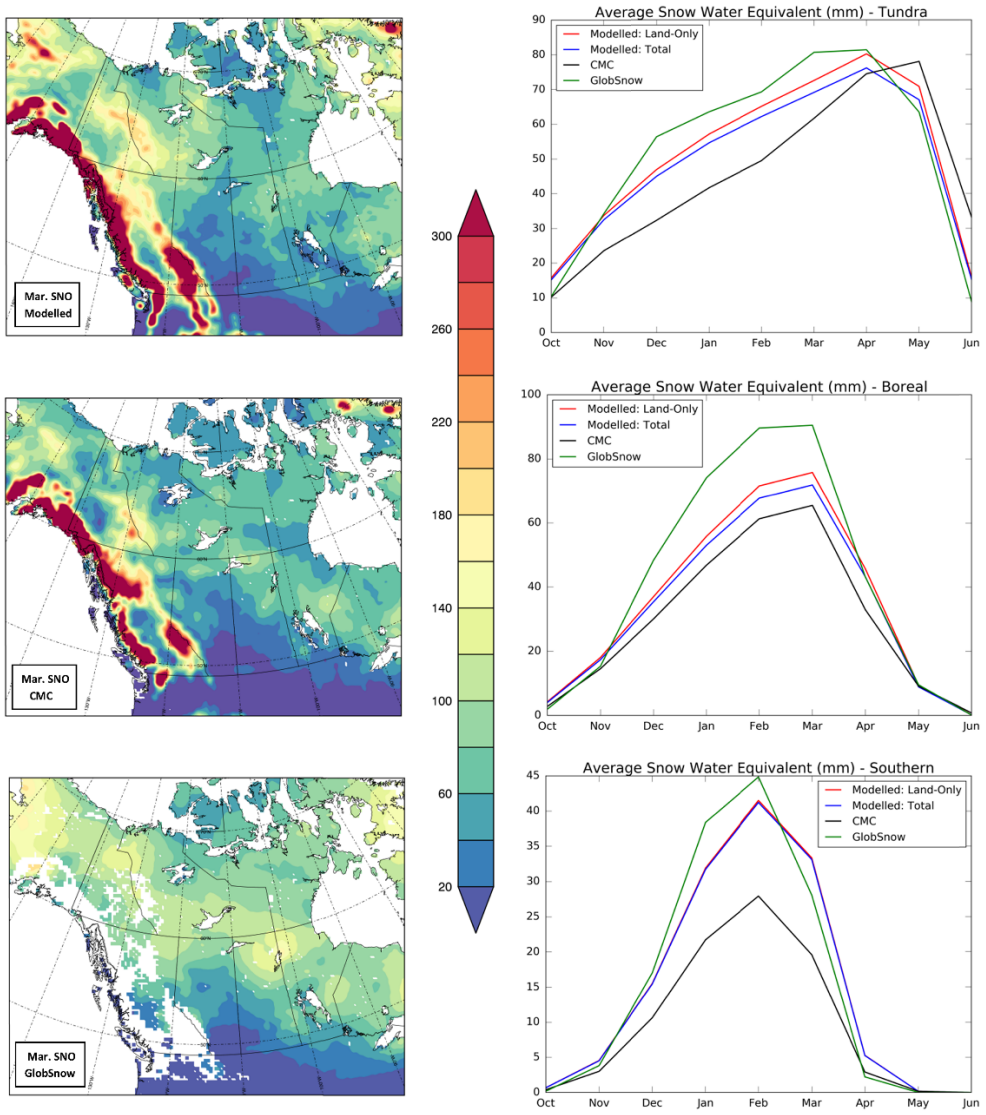

Figure 1.2. The evaluation of modeled and observed SWE over 12 year period. Left images present the time mean of SWE (mm) in March for CLASS, CMC, and GlobSnow. Left images show seasonal cycles of the total modeled, land only (exclusion of lakes), CMC, and GlobSnow SWE for the tundra, boreal, and southern zones (Verseghy and MacKay, 2017).

1.4.2. Estimation of SWE using GRACE observations

For the first time in the history of geoscience, satellite-based observations of global water cycle from the GRACE mission have provided the free-access of freshwater resource changes across the globe (Rodell *et al.*, 2018). This unique potential of gravimetric measurements enables the analysis of TWS anomalies over the continents, river basin and local scales, which is not feasible using traditional microwave, infrared, or visible remote sensing measurements (Forman and Reichle, 2013). Even though GRACE observations are employed for different hydrological applications, different challenges are associated with TWS data.

Two main issues are linked to GRACE-derived TWSA products. First, GRACE is not able to sense individual sources of TWSA retrievals (e.g., snow, soil moisture). Even though in some regions snow mass changes might have a major influence on the variation of the water mass, the individual storage compartment, e.g., SWE compartment, is not retrieved directly from GRACE observations. Second, the critical limitation concerning the usage of GRACE observations is linked to their coarse spatial (~300 km at midlatitudes) and temporal (monthly) resolutions.

In order to overcome the scientific challenges related to the GRACE observations, complementary data should be used. One simple way to obtain SWE changes from GRACE observation is to subtract the contributions of soil moisture, groundwater, and eventually surface water storage changes from GRACE-derived TWSA. These different contributions may be obtained from models simulations. Niu *et al.* (2007) retrieved snow mass from GRACE observation for different large basins in Arctic regions by subtracting the contribution of groundwater storage changes, which was calculated from the Community Land Model (CLM) model. The drawback of this method is that the uncertainty of the model and observations are not included in the final SWE product. Another solution is suggested by merging GRACE observations into hydrological models using sophisticated data assimilation (DA) method (Zaitchik *et al.*, 2008). In the DA methods, observations are downscaled from coarse spatial and temporal resolutions to the finer scales. For example, in this application, the column integrated GRACE-derived TWSA are downscaled from the coarse-scale (~150,000 km^2) to finer scale (~100 km^2) MESH model resolution. On the other side, GRACE data contain valuable information that helps to constrain the individual model compartments of the MESH model.

1.5. Research objectives

1.5.1. General objective

The general objective of this thesis focuses on developing a framework to improve SWE estimation in the MESH model over Canada through the assimilation of TWSA retrievals provided by the GRACE satellites. Recent studies have shown that the assimilation of GRACE-derived TWSA into National Aeronautics and Space Administration (NASA's) catchment land surface model (CLSM) and CLM yielded improvements in the simulation of SWE over some parts of North American (sub-) basins, e.g., Mackenzie basin (Forman *et al.*, 2012; Su *et al.*, 2010). It is worth mentioning that even though the general methodology of this work is similar to the work of Forman *et al.* (2012), several major points distinguish this study from their findings. It should be pointed out that, the MESH model differs from the CLSM model in terms of model physics (treatment of the spatial variation of soil water and water table depth, calculation of snow budget within each computational unit), input forcing set, model configuration (spatial and temporal resolution), routing scheme, treatment of geophysical heterogeneity, calibration, model parameter ranges, initial values. Furthermore, in this study different datasets are used to evaluate the results. Therefore, based on the mentioned reasons, the practical implementation of the MESH data assimilation framework requires different approaches.

1.5.2. Specific objectives

Before developing the data assimilation framework in maintaining the improvement in the model state estimates, it is required to find out the hydrological connection between the SWE anomaly (SWEA) and TWSA during snow seasons over the Canadian landmass. The first contribution and originality of this thesis focus on the exploration of the TWSA-SWEA relationship to identify suitable regions where snow mass changes have a high impact on the TWS changes. After investigating the TWSA-SWEA relationship, the plausible areas for integrating the GRACE observations with the MESH hydrological model are identified.

As the development of the MESH model continues, the attention of some scientists and collaborators is being focused on using remotely sensed products into the modeling system, especially for forecast applications (Xu *et al.*, 2015; Yassin *et al.*, 2017). Given the significance

of GRACE observations in improving the estimation of water storage compartments in different hydrological and land surface models (Forman *et al.*, 2012; Girotto *et al.*, 2016; Houborg *et al.*, 2012; Kumar *et al.*, 2016; Reager *et al.*, 2015; Schumacher *et al.*, 2018; Van Dijk *et al.*, 2014; Zaitchik *et al.*, 2008), an interesting question is the effectiveness of integrating GRACE observations into the MESH. Another novel and original research subject of this thesis explores the assimilation of GRACE observations into the MESH model for the purpose of improving model state simulation.

More specifically, this thesis addresses two main objectives as the following:

1. Analyze the spatial and temporal relationship between GRACE-derived TWSA retrievals and multisource SWE products.

2. Assimilate GRACE TWSA observations into the MESH model in a Canadian basin to improve SWE and streamflow simulations by making use of the ensemble Kalman smoother (EnKS) approach.

Focusing on the main objectives, this study addresses the following research questions:

- Does the relationship between GRACE TWSA and multisource SWEA products on a basin and gridded spatial resolution scale provide useful information for monitoring snow mass changes in Canada?

- Can the assimilation of GRACE observations into the MESH model improve modeled SWE estimates? If any, how the improvements are applied in the spatial and temporal resolution scales?

1.6. Hypothesis

Following the specific objectives of this dissertation, two main hypotheses are considered:

- The hypothesis I of this thesis states that during snow accumulation and ablation seasons, the total water mass changes are highly influenced by the variations of the snow mass changes (Forman *et al.*, 2012; Niu *et al.*, 2007).

- The hypothesis II of this thesis states that improved performance in the estimation of SWE can be acquired through the assimilation of GRACE-derived TWSA into the MESH model.

1.7. Structure of thesis

This dissertation is organized into eight chapters. In this introductory chapter 1, the importance of the research topic is discussed. The research problematics and the challenges of SWE estimation methods are explained. It also discusses in details the objectives, research questions, and hypotheses of the research. The rest of the thesis is organized as follows.

In chapter 2, an overview of the scientific background and geoscience applications is described. The mathematic basis of satellite gravimetric measurements, as well as the calculation of water storage changes from these measurements, are explained in section 2.1. The general description of the MESH model in addition to the model set-up and configuration are discussed in section 2.2. In section 2.3 the main principles and applications of data assimilation methods are presented. The mathematical principle of the proposed assimilation methods and the generation of pseudo random fields are also presented in this section.

The summary of datasets, as well as the explanation of study sites, are given in chapter 3. The description of methodologies related to the specific objectives of the thesis is discussed in detail.

In chapter 4 of this dissertation, the implementation of the spatiotemporal TWSA-SWEA relationship on a gridded scale spatial resolution is explained. The statistical interrelations between TWSA derived from GRACE and Global Land Assimilation System (GLDAS), along with SWEA data obtained from various sources of snow products are discussed. The major findings of this chapter provide detailed information related to the influence of snow mass changes on the TWS changes over the Canadian landmass. This chapter is prepared for submission to the Journal of Remote Sensing.

Chapter 5 follows the second part of the first objective of the work. The aim of this chapter is to quantify the spatiotemporal relationship between TWSA/SWEA-derived from GRACE and multisource SWE products. Based on the findings of this chapter, potential basins are identified such that the assimilation of GRACE observations into the hydrological model has an impact on the improvement of storage and flux simulations. Some important points distinguish findings of

chapter 5 from chapter 4. Indeed, in chapter 5, model simulations of WaterGAP Global Hydrology Model (WGHM) during the snow season were used to extract the contribution of different water storage compartments from GRACE-derived TWSA data. It is examined whether the subtraction of WGHM TWS estimates from GRACE observations (especially around Hudson Bay area) improves the relationship between GRACE and multisource snow products. This chapter is formed of an article entitled “Analyzing the contribution of snow water equivalent to the terrestrial water storage over Canada” which was published in the Hydrological Processes Journal.

The implementation of the assimilation of GRACE-derived TWSA retrievals into the MESH model is explained in Chapter 6. The framework of the developed assimilation methodology is explained in detail. The influence of the integration of GRACE measurements in the improvement of SWE and streamflow estimations in the Liard basin is discussed. This chapter is formed of a manuscript entitled “Data Assimilation of satellite-based terrestrial water storage changes into a hydrology land-surface model” which is in evaluation for the Journal of Hydrology.

The major issues regarding the specific objectives of this dissertation are discussed in Chapter 7.

In Chapter 8, the important findings of the thesis, which are explained in Section 4, Section 5, and Section 6 are summarized. The general perspectives and outlooks for future works are described in Section 8.2.

2. Background

This chapter describes the scientific background of GRACE (2.1), the MESH model (2.2), and data assimilation (2.3). An overview of the theoretical basis in addition to the scientific application of each section are provided in detail.

2.1. GRACE observations

2.1.1. Overview of GRACE Mission

The GRACE is a joint project between the United States NASA and the German Aerospace Center (Deutsches Zentrum für Luft-und Raumfahrt, DLR). The GRACE mission was launched on March 2002 and provided semi-continuous gravity measurements over 15 years including 163 monthly solutions of the time-variable gravity field, out of 187 possible months (Tapley *et al.*, 2019). The objectives of the project were to monitor time-variable components of the Earth's gravity field variations to track mass distribution on a large scale in the hydrosphere, cryosphere and oceans (Tapley *et al.*, 2004b). GRACE also enlightened the view of mass distribution associated with glacial isostatic adjustment (GIA) and earthquakes. The mission was extended by launching the GRACE Follow-On (GRACE-FO) in May 2018 with the purpose of continuing the observation of Earth's mass changes, in particular those related to large-scale water mass distribution (Cooley and Landerer, 2019).

GRACE used a constellation of two almost-identical satellites following each other in a near-circular orbit with a separation distance of about 220 ± 50 km. The orbit has an inclination of 89.5° with an initial altitude of ~ 500 km. Due to atmospheric drag, the altitude of the satellite had been decreased to 357 km over 15 years of operation (« GRACE Mission Operation Status », 2016). GRACE-FO similar to GRACE uses the same method to detect the gravitational changes of Earth's mass movements with small modifications in the mission design.

The general concept of GRACE satellite measurements flying at low altitudes with satellite to satellite tracking originated from a methodology proposed by Wolff (1969) for obtaining a more accurate gravity field model (Figure 2.1). Gravitational variation in the Earth's gravity field influence the distance between twin satellites. For instance, if the leading satellite passes over areas

of stronger gravity, *i.e*, greater mass concentration, the change in the gravitational field increases the distance between the two satellites. Then, the tailing satellite approaches the gravity anomaly, leading to a higher attraction and therefore to a decrease in distance between the satellites.

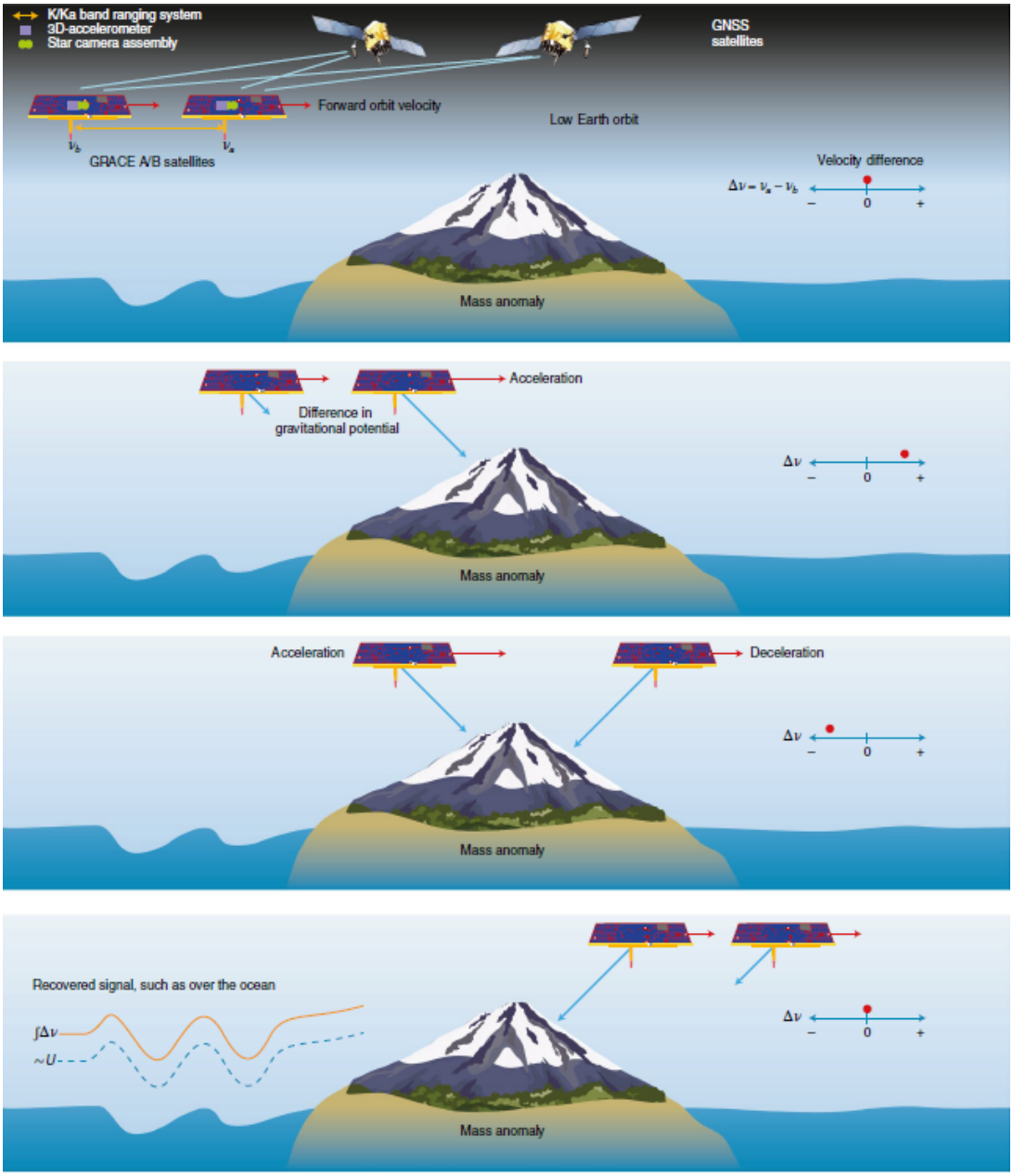

Figure 2.1. GRACE mission concept (Tapley et al., 2019).

Small changes in the distance between the two satellites are measured using a K-band Ranging system (Tapley *et al.*, 2004b). This ranging system can detect changes in separation distance between two GRACE satellites within one micron by using the dual-frequency one-way of K- and Ka-band phase measurement transmitted and received by both satellites (Dunn *et al.*, 2003).

GRACE-FO as a rebuild of the GRACE mission is equipped with microwave ranging for measuring changes of intersatellite distance, and a laser ranging interferometer (LRI) as a demonstrator experiment (Sheard *et al.*, 2012). A design precision of laser interferometry is approximately 26 times better than the K-band ranging system and it is expected to increase the accuracy of measurements by tenfold or more (Tapley *et al.*, 2019). Furthermore, the position and timing of satellites with an accuracy of centimeter is determined with the Global Positioning System (GPS). The non-gravitational forces acting on satellites are removed from along-track observations using the precise accelerometers to make sure that only accelerations caused by gravity are considered in the distance measurements (Tapley *et al.*, 2004b). The precise attitude estimations of inertial orientation for the GRACE satellites are determined using star camera assembly.

2.1.2. GRACE science data

The GRACE Science Data System (SDS) distributes monthly gravity field processing for both GRACE and GRACE-FO missions through all tasks required for the production of the monthly and mean gravity field solutions (Figure 2.2). The monthly satellite gravimetric solutions are found in the Jet Propulsion Laboratory (JPL), the Center for Space Research (CSR) of the University of Texas at Austin, and the GeoforschungsZentrum Potsdam (GFZ) of Germany. Each center uses parameter choices and solution strategies to convert relative ranging observations between twin satellites to gravity changes (Bettadpur, 2012).

Both GRACE and GRACE-FO data products appear at different levels, including, level-1, level-2, and level-3 processing. The level-1 is as a result of the irreversible processing steps applied to GRACE and GRACE-FO raw data. In level-1 products, the data sample rate is reduced and data are time-tagged to the respective satellite receiver clock time. The Level-1 data include the ancillary data products required for further processing (Bettadpur, 2012). GRACE and GRACE-FO level-2 time-variable gravity field data consist of a set of normalized geopotential spherical harmonic coefficients or more recently as gridded mascon (mass concentration blocks, Watkins *et al.*, 2015). The geopotential term is referred to the exterior potential of the Earth system including the entire solid and fluid (ocean and atmosphere) compartments (Bettadpur, 2018). Following the conventional methods (Heiskanen and Moritz, 1967), the gravitational potential attraction between

a unit mass and the Earth System can be expressed in terms of spherical harmonic expansion as :

$$V(\lambda,\theta,r) = \frac{GM}{R}\sum_{l=0}^{l_{max}}\left(\frac{R}{r}\right)^{l+1}\sum_{m=0}^{l}\bar{P}_{lm}(\cos\theta)\,[C_{lm}\cos(m\lambda) + S_{lm}\sin(m\lambda)] \qquad (2.1)$$

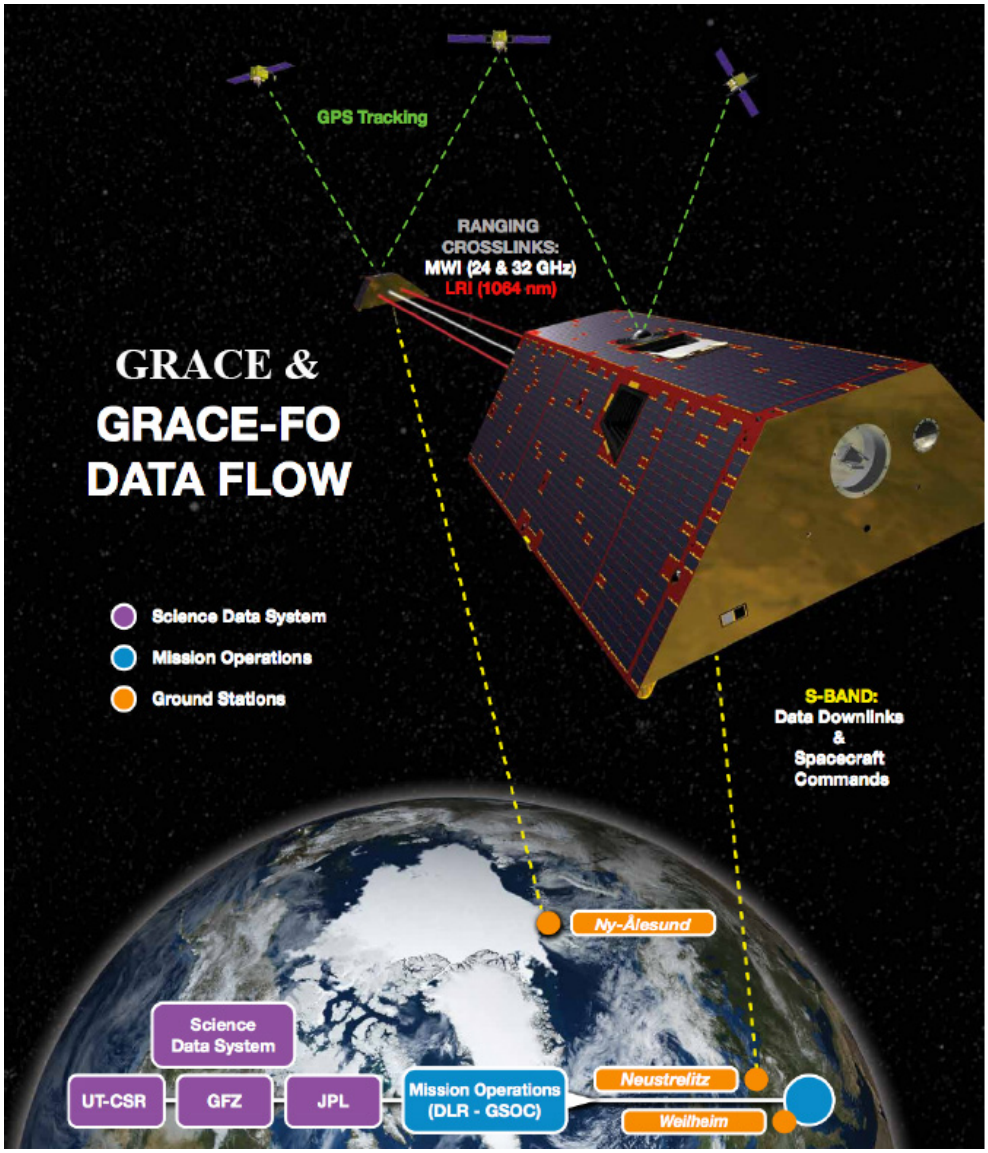

Figure 2.2. GRACE and GRACE-FO mission data flow (Cooley and Landerer, 2019).

Where C_{lm} and S_{lm} are fully normalized spherical harmonic coefficients of degree l and order m, $\bar{P}_{lm}$ are fully normalized associated Legendre functions of degree l and order m, M is the total mass of the Earth (kg), G is Newton's gravitational constant ($m^3/(kg\ s^2)$), R (m) is the Earth's radius, and

θ, λ, r are the spherical coordinates. The summation can be truncated to a maximum degree (l_{max}). For GRACE and GRACE-FO monthly fields, the l_{max} is limited to the 60-100 range based on the solution of the processing center. Because of the limited range of spherical harmonics, the surface spatial resolution of GRACE-derived TWSA products is limited to about 330 km at low latitudes (Cooley and Landerer, 2019) with an error level of 2 cm in terms of equivalent water height (Vishwakarma *et al.*, 2018).

Wahr *et al.* (1998) assumed that the change in surface density (i.e., mass/area) causing temporal changes of the gravitational potential is concentrated in a thin layer at the surface of the Earth as a function of the spherical harmonic coefficient changes. The density change (Δσ) is expressed as

$$\Delta\sigma(\lambda,\theta) = \frac{M}{4\pi R^2} \sum_{l=1}^{l_{max}} \sum_{m=0}^{l} \frac{(2l+1)}{(1+k_l)} \bar{P}_{lm}(\cos\theta) \left[\Delta C_{lm} \cos(m\lambda) + \Delta S_{lm} \sin(m\lambda)\right] \qquad (2.2)$$

where k_l is load love number of degree l. The spherical harmonic changes ΔC_{lm} and ΔS_{lm} are obtained by subtracting the temporal mean value from each month of GRACE or GRACE-FO level-2 products. In the next step, the equivalent water heights, i.e., TWSA (mm) is retrieved by dividing the surface density changes by the mean density of water ρ_w = 1025 (kg/m^3) as:

$$\Delta E(\lambda,\theta) = \frac{M}{4\pi R^2 \rho_w} \sum_{l=1}^{l_{max}} \sum_{m=0}^{l} \frac{(2l+1)}{(1+k_l)} \bar{P}_{lm}(\cos\theta) \left[\Delta C_{lm} \cos(m\lambda) + \Delta S_{lm} \sin(m\lambda)\right] \qquad (2.3)$$

Due to the measurement errors (including systematic and random), GIA effects, as well as background model corrections, a set of nontrivial processing steps are applied over level-2 data products in order to be used in hydrological applications. The GRACE and GRACE-FO quality controlled gridded mass change processed products called level-3 can be accessed via the JPL's GRACE Tellus website (available at https://podaac-tools.jpl.nasa.gov). In this thesis, the GRACE-derived TWSA level-3 gridded data are used for different analysis approaches. The details of the processing steps are beyond the scope of this study and can be found in the handbooks of level-2 (Bettadpur, 2018) and level-3 (Cooley et Landerer, 2019) products. Note that the mascon solutions that are processed with domain-optimized filters can also be deployed. However, the preliminary analyses in this study showed no significant differences between harmonic and mascon solutions.

Therefore, the mascon data were not used in this thesis.

The GRACE Tellus data are provided at 1º×1º in both longitude and latitude. To restore the signal loss as a result of processing, Landerer and Swenson (2012) provided scaling gain factors. It is worth mentioning that even though the GRACE and GRACE-FO products are resampled to 1º, it does not mean that observations at two neighboring cells are independent.

2.1.3. GRACE science applications

Based on the U.S. government's civilian science programs, GRACE and GRACE-FO data cover major application objectives to guide the space-based Earth observations (Cooley et Landerer, 2019). The GRACE observations have provided unprecedented insight to quantify regional to global water cycle changes from both natural variability and anthropogenic climate impacts on ice-loss (Rignot *et al.*, 2011; Sasgen *et al.*, 2012, 2013; Shepherd *et al.*, 2018; Velicogna *et al.*, 2014; Velicogna and Wahr, 2005; Wouters *et al.*, 2008, 2013), sea-level rise and ocean heat uptake (Chambers *et al.*, 2004, 2016; Llovel *et al.*, 2014), and the magnitude and frequency of droughts and flood events (Houborg *et al.*, 2012; Kumar *et al.*, 2016; Reager *et al.*, 2014, 2015; Reager and Famiglietti, 2009). Recently, efforts have been made to shorten the time-lag of GRACE-data availability to near real-time, to support new climate service applications that are critical to regional water management, snow/ice melt prediction, flood and drought alarming, providing a database for political decisions or emergency management (Tapley *et al.*, 2019).

During cold seasons in mid-to-high latitudes, snow mass changes appear to have a major impact on the TWS variabilities (Bahrami *et al.*, 2020). Few studies have focused on using GRACE TWS retrievals for the purpose of SWE estimations (Frappart *et al.*, 2006, 2011; Niu *et al.*, 2007; Ramillien *et al.*, 2005). The results of these studies unveiled the importance of GRACE observation to quantify the contribution of snow mass changes to terrestrial water storage changes. Furthermore, the estimation of hydrological fluxes at a global scale is a critical issue. Using mass conservation principles, GRACE measurement of the TWS-change allows the derivation of basin scale flux estimates of evapotranspiration (Ramillien *et al.*, 2006; Rodell *et al.*, 2011), river discharge (Syed *et al.*, 2005), and precipitation (Behrangi *et al.*, 2017, 2018; Seo *et al.*, 2010; Swenson, 2010).

One of the key applications of GRACE data is to estimate groundwater depletion in regions with a lack of observations (Rodell *et al.*, 2007). GRACE has also demonstrated the anthropogenic induced variations in water availability that, before GRACE, were known only anecdotally (e.g., TWS depletion in northern India, Middle East) or not at all were known, e.g., in northwestern China (Rodell *et al.*, 2018). For the first time, GRACE has revealed the quantification of groundwater storage changes around the world induced by natural changes or unsustainable water consumption for agriculture and other human uses (Döll, *et al.*, 2014b; Famiglietti *et al.*, 2011; Forootan *et al.*, 2014; Richey *et al.*, 2015; Rodell *et al.*, 2009, 2018; Voss *et al.*, 2013; Yeh *et al.*, 2006).

GRACE data have been used to address the land surface and hydrological model limitations (Scanlon *et al.*, 2018, 2019; Swenson and Lawrence, 2015) in order to refine model parameters and structural elements (Eicker *et al.*, 2014; Güntner, 2008; Güntner *et al.*, 2007; Lo *et al.*, 2010; Niu and Yang, 2006; Schumacher *et al.*, 2016, 2018; Sun *et al.*, 2012; Swenson and Lawrence, 2014; Trautmann *et al.*, 2018; Yassin *et al.*, 2017). The integration of GRACE-derived TWS anomalies within a land-data assimilation system has been shown to improve the accuracy of hydrological and land surface simulations (Forman *et al.*, 2012; Girotto *et al.*, 2016, 2019; Houborg *et al.*, 2012; Khaki and Awange, 2019; Kumar *et al.*, 2016; Li *et al.*, 2012; Reager *et al.*, 2015; Schumacher *et al.*, 2016, 2018; Su *et al.*, 2010; Tangdamrongsub *et al.*, 2015; Van Dijk *et al.*, 2014; Zaitchik *et al.*, 2008).

2.2. The MESH framework

2.2.1. Overview of the MESH model

There has been an intensive global research effort to couple atmospheric and hydrological models, by means of LSMs, to improve streamflow simulations and atmospheric predictions in both climate (Soulis *et al.*, 2000) and weather prediction models (Benoit *et al.*, 2000). In Canada following global research efforts, scientific initiatives have been carried out since mid-90s to couple atmospheric and hydrological models using LSMs. The initial coupling framework was conducted by Soulis *et al.* (2000). They designed an approach to couple the CLASS for the simulation of runoff and WATFLOOD for proper streamflow routing between elements. The combined model, WAFLOOD/CLASS or WATCLASS, forms the benchmark for coupling

atmospheric and hydrological models (Pietroniro and Soulis, 2003). The coupling framework can be run either two-way coupled to the atmospheric Canadian Global Environmental Multiscale (GEM, Côté *et al.*, 1998a; Côté *et al.*, 1998b; McTaggart-Cowan *et al.*, 2019a; McTaggart-Cowan *et al.*, 2019b) model or off-line (stand-alone) mode, reading GEM or other climate forcing data sets (Pietroniro and Soulis, 2003; Soulis *et al.*, 2005). The modeling strategy which focused on the creation of WATCLASS at different steps for the Mackenzie River Basin is summarized in Figure 2.3 (Soulis and Seglenieks, 2008).

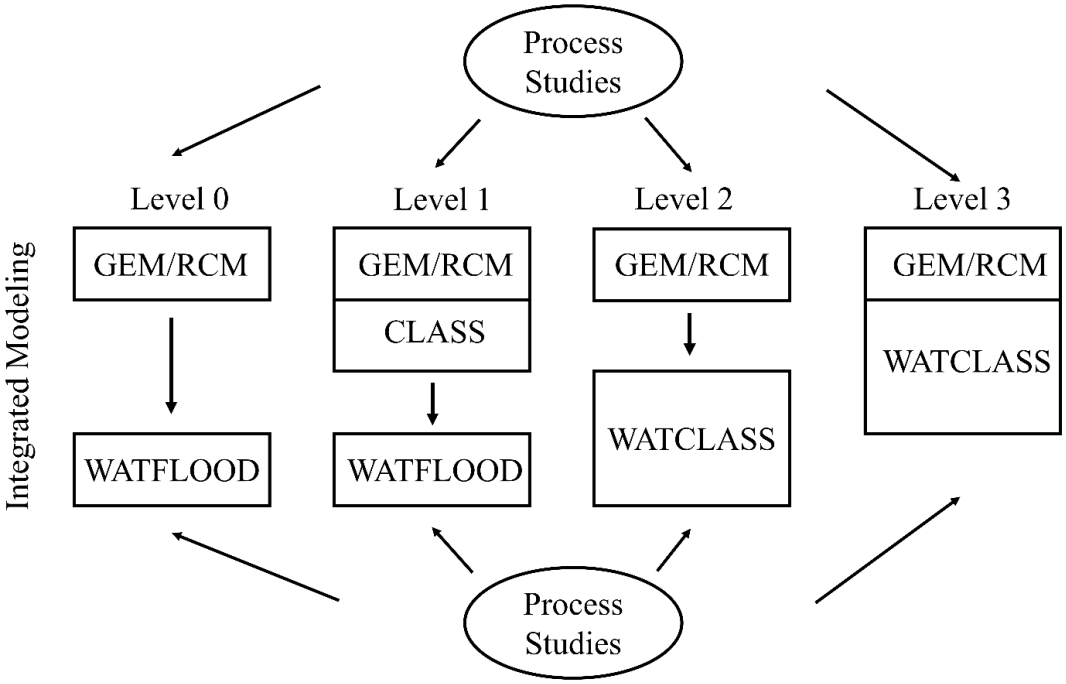

Figure 2.3. Mackenzie GEWEX Study (MAGS) modeling strategy (Soulis and Seglenieks, 2008).

Even though the development of a suite of hydrological-land surface models is appropriate for research purposes, their application in hydrometeorological forecasting systems are limited (Pietroniro *et al.*, 2007). Therefore, to optimize the research and development (R&D), a community environmental modeling called MEC has been developed by the ECCC in collaboration with a team of researchers to share a unified modeling framework (Soulis *et al.*, 2005). The community framework of the MEC modeling provides this advantage to researchers and end-users, e.g., water resource managers, benefiting from continuous improvements made to

the modeling system for research and operation purposes, such as streamflow forecasting. Pietroniro *et al.* (2007), based on the model coupling strategies outlined in Soulis *et al.* (2000) and Soulis *et al.* (2005), introduced the concept of MESH (MEC – Surface Hydrology) modeling framework. They used MEC and WATFLOOD, as a part of an operational ensemble forecasting system at ECCC and called the overall system as MESH. To implement the concept of community-based platform independent of a single institution, and address important R&D and operational issues based on GEM, WATCLASS was renamed to MESH (Davison, 2016).

In the MESH modeling framework, different LSMs can coexist so that the simulation results can be compared for the same experiment using the same input climate forcings and model configuration set-ups (Pietroniro *et al.*, 2007). The MESH model allows coupling of a LSM, either CLASS version 3.6 (Verseghy, 2012) or the Soil, Vegetation, and Snow (SVS, Alavi *et al.*, 2016; Husain *et al.*, 2016) scheme with hydrological routing implemented from WATFLOOD (Kouwen, 1988; Kouwen *et al.*, 1993), together with other lateral flow processes (Mekonnen *et al.*, 2014; Soulis *et al.*, 2000, 2011; Yassin *et al.*, 2019). The MESH model is under continuous development by a collaborative team of researchers from ECCC, the Global Institute for Water Security (GIWS, University of Saskatchewan, Haghnegahdar *et al.*, 2017), and other academic institutions (e.g., McMaster, Waterloo, Wilfrid Laurier Universities).

Similar to MESH, over the past decade ECCC has also developed an operational GEM hydrological modeling platform (GEM-Hydro, Gaborit *et al.*, 2017) which is tied to the Canadian Meteorological Centre (CMC) infrastructure. Both MESH and GEM-Hydro have in common to incorporate the distributed nature of watershed parameters in a basin and a structure established around two main components: a LSM for the representation of surface processes and a horizontal routing component for simulating water transport in the streams (Gaborit *et al.*, 2017). Yet, some differences exist between MESH and GEM-Hydro, such as streamflow simulation with regard to the baseflow component of the streamflow.

2.2.2. MESH model description

MESH hydrological processes consist of three main components: (i) a vertical exchange of moisture fluxes between soil, vegetation canopy and atmosphere within a grid cell; (ii) lateral water movement within soil inside a grid cell; and (iii) horizontal transfer (between grid routing)

of water in the model within the stream network (Mekonnen *et al.*, 2014). The general framework of MESH modeling is presented in figure 2.4. In this research, the MESH model has been set up at a 0.125º × 0.125º (longitude/latitude) spatial resolution and half-hourly temporal resolution based on the spatial and temporal resolution of climate input forcing data. The spatial and temporal resolution can be modified according to user needs based on the model configuration set-up.

A set of seven meteorological inputs are required for the model: incoming shortwave and longwave radiation; precipitation; temperature; barometric pressure; specific humidity; and wind speed. In addition to the climate forcing data the MESH model requires three initialization files (.ini, e.g., CLASS parameters, see Appendix I), four other input text files (.txt, e.g., soil levels), the MESH drainage database file (.r2c), and output directories to run the MESH model.

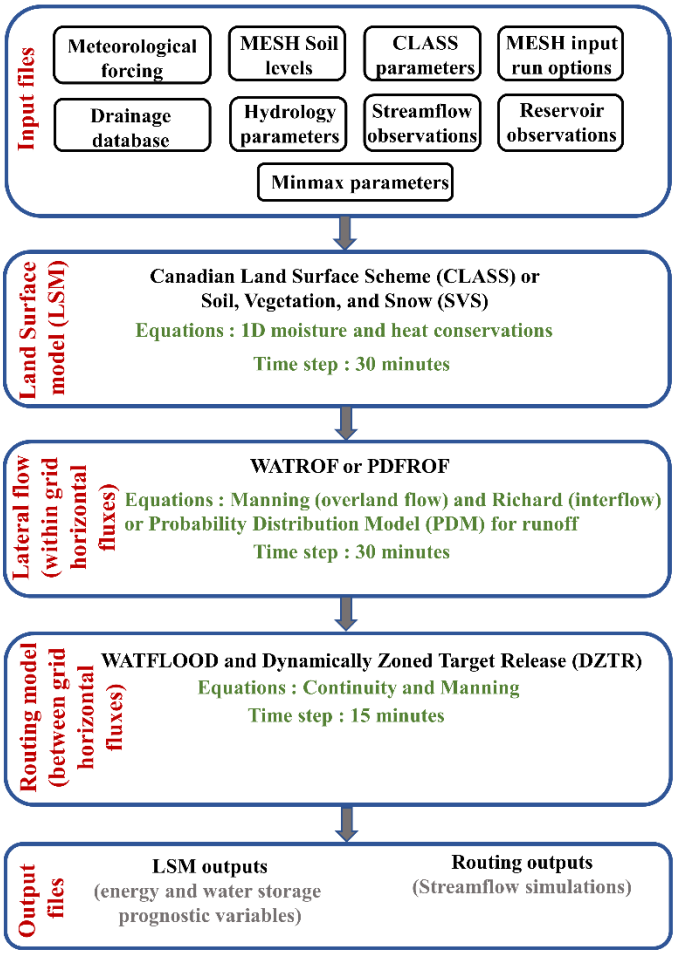

Figure 2.4. MESH modeling framework (modified after Mekonnen *et al.*, 2014).

2.2.2.1. Subgrid heterogeneity

In the physically-based hydrological models, to better simulate the observed hydrologic and hydraulic phenomena, it is required to downscale the watershed into smaller units (Pietroniro and Soulis, 2003). Hydrological models in the treatment of geophysical heterogeneity can be classified into two categories, including lumped and distributed models. In the lump hydrological models, the spatial distribution of input data or model parameters characterizing the physical processes is not taken account, whereas distributed models are defined by their ability to incorporate the distributed nature of watershed parameters and inputs into a modeling framework (Clarke, 1973). Distributed models are further sub-divided into fully distributed and semi-distributed models (Pietroniro and Soulis, 2003). Fully distributed models that are designed to enable the spatial distribution of physical properties across the watershed are explicitly considered for a network of grid points (Refsgaard, 1997). Because of detailed physics considered in these models, fully distributed models are too complex and computationally intensive to calibrate, especially for large basins (Soulis *et al.*, 2005). In contrast, in semi-distributed models, such as WATFLOOD and MESH, all areas with a similar land cover (or other attributes) are regrouped within a gridded cell inside a desired basin. In other words, each grid is composed of a number of Grouped Response Units (GRUs; Kouwen et al., 1993). The tile (a specific GRU within a given grid) is the basic computational unit that aggregates different attributes, such as soil and vegetation properties within the grid (Pietroniro et Soulis, 2003). Figure 2.5 shows the concept of basin discretization for two grids and four GRUs including irrigated crops, grass, urban, and mixed forest. The number of tiles based on the land cover information for two grids is accounted for seven tile members. The treatment of geophysical heterogeneity within each grid cell can be defined, based upon other variables, such as digital elevation model (DEM), and soil characteristics (Davison *et al.*, 2019). However, in the MESH model, land cover types are the basis to define the subgrid heterogeneity in the model.

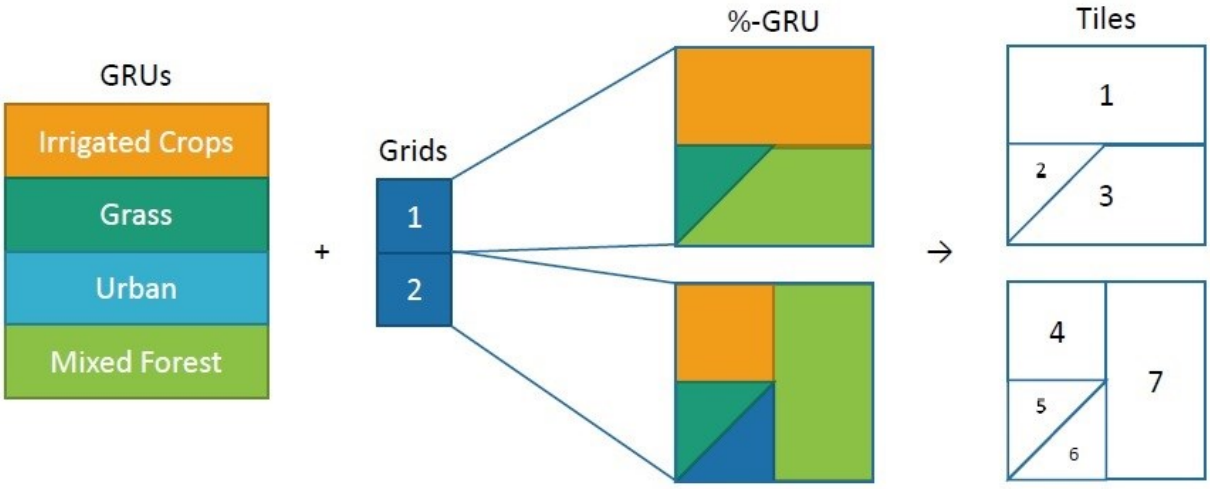

Figure 2.5. The GRU approach to basin discretization used in MESH (Princz, 2017).

2.2.2.2. CLASS

CLASS model (Figure 2.6) is a physically-based model that simulates the energy and water balances of the land surface, forward in time, from an initial starting point by making use of meteorological forcing data (Verseghy, 1991, 2012; Verseghy *et al.*, 1993). CLASS further sub-divides each tile into a mixture of four sub-areas, including bare soil, vegetation, snow over bare soil, and snow with vegetation (Davison *et al.*, 2006). Each sub-area activates different physically-based solver routines. For example, snow related routines are active in the snow over bare soil and snow with vegetation sub-areas, but not for bare soil or vegetation, which omit snow. The energy and water budget are first calculated for each sub-area individually and then combined using the relative fractions of these sub-areas inside the tile. These sub-area fractions vary in time; for example, with and without the presence of snow. Outside of CLASS, the energy and water budget of the tiles is calculated as a weighted average by their respective GRU percentage area that is occupied inside the grid (Kouwen *et al.*, 1993). The vegetation properties are determined based on four main vegetation types identified by CLASS including needleleaf trees, broadleaf trees, crops, and grasses, which are aggregated to form a representative parameterization used within the active sub-areas for each tile (Verseghy, 2012). The structural attributes, namely leaf area index (LAI), roughness length, canopy mass, and rooting depth of each of the vegetation groups are varied over seasonal timescales (Soulis *et al.*, 2005).

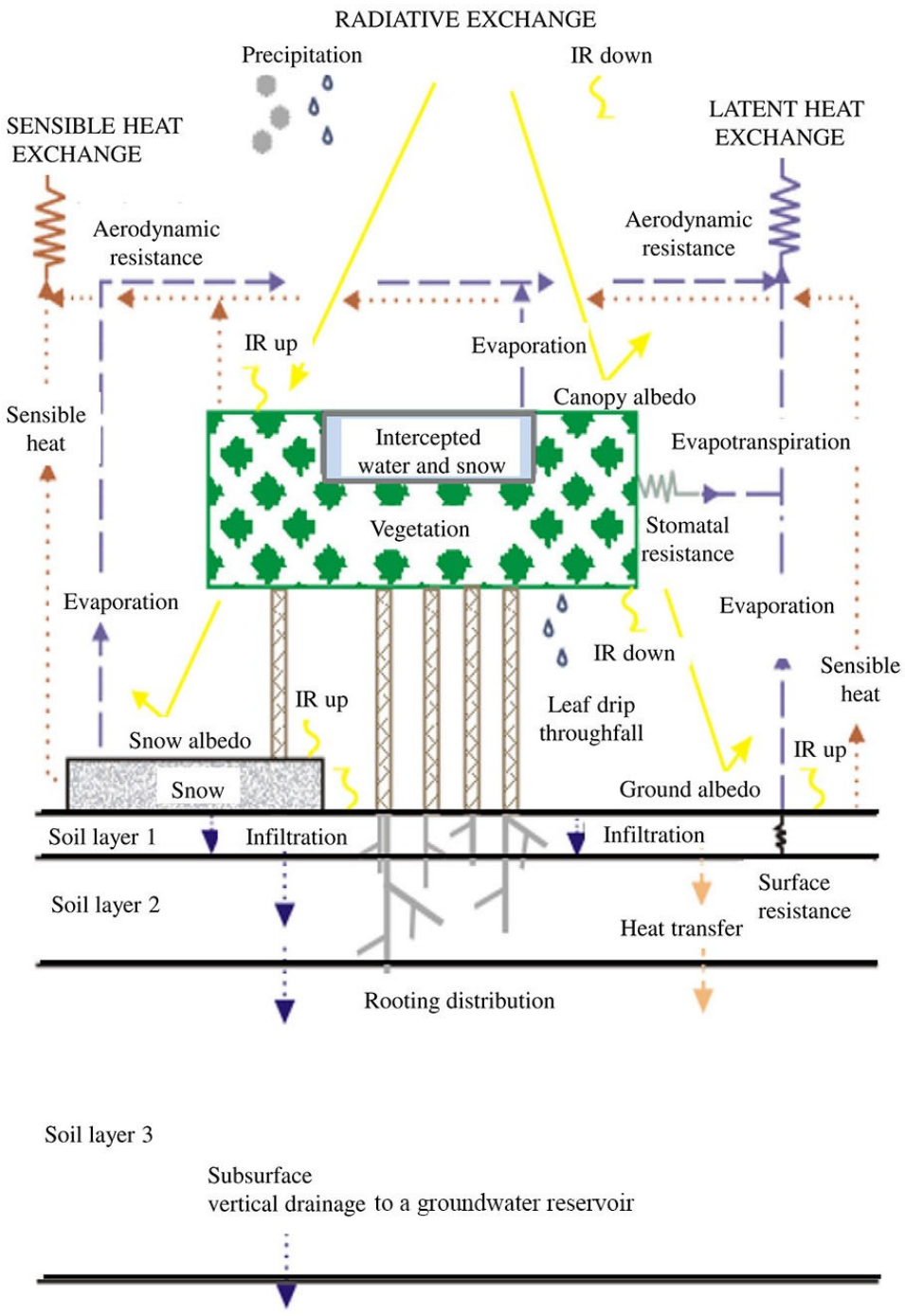

Figure 2.6. Schematic diagram of CLASS (Verseghy, 2012)

By default, CLASS divides the soil column into three soil layers of 0.1 m, 0.25 m, and 3.75 m. Since the release of version 3.0, a flexible soil-layering scheme is implemented in the CLASS model, so that the total depth and the thickness of soil layers can be varied for the application of frozen land and other related processes (Elshamy *et al.*, 2020; Ganji *et al.*, 2015; Sapriza-Azuri *et*

al., 2018). In this study, four soil layers with thicknesses of 0.1 m, 0.25 m, 0.75 m and 3.0 m are used for the MESH model, yielding a total thickness of 4.1 m for the soil column. The layer temperatures and liquid and frozen water storage compartments as prognostic variables are evolved forward in time on the basis of the energy and moisture fluxes at the top and bottom of each layer (Soulis *et al.*, 2005). The simulated terrestrial water storage in the MESH-CLASS model is the sum of several prognostic variables, including intercepted precipitation by the canopy (rain or snow), SWE, snowmelt held in the snow mass, water ponded on the surface, and liquid and frozen water storage (LQWS and FRWS) content of soil layers. The temperature of each of these TWS compartments, along with snow albedo and density, vegetation growth index are calculated for each of the tiles between time steps (Verseghy, 2012).

A single-layer snow model is used in CLASS to simulate snow mass on bare soil (Verseghy, 1991; Verseghy *et al.*, 1993). Evaluation of the seasonal snowpack evolution derived from CLASS in the Snow Model Intercomparison Project (SnowMIP) demonstrated that this single-layer model performed as well as multilayer models (Brown *et al.*, 2006). The snow density increases and snow albedo decreases with time from fresh snow values based on empirically exponential decay functions (Verseghy *et al.*, 2017). Snowmelt is modeled either from the top of the snowpack in response to surface energy fluxes or from the bottom as a result of conduction from the underlying soil. When melting of snow happens at the top, percolation and refreezing of meltwater in the snowpack occurs until the snow temperature is set back to 0^{o}, after which the meltwater is allowed to infiltrate into the soil. The snow depth is assumed to be complete if the diagnosed snow depth does not fall below a threshold value of 0.1 m (Soulis *et al.*, 2005). When it occurs, the snow depth is set to the threshold values and fractional snow coverage is calculated on the basis of conservation of snow mass (Verseghy et MacKay, 2017). Furthermore, blowing snow processes as an option can be incorporated into the CLASS model. Snow accumulation and redistribution can be simulated using the physically-based Prairie Blowing Snow Model (PBSM) that takes into account wind direction and speed, and other aspects (MacDonald *et al.*, 2009).

2.2.2.3. Runoff and routing

Soulis *et al.* (2000) developed physically-based functions in the MESH-CLASS model based on the idea of a sloping soil layer with a horizontal hydraulic conductivity that allows movement of

water from the soil column (Figure 2.7). The developed algorithm called WATROF, have two major runoff components: overland flow that drains the excess surface water and interflow (or horizontal near-surface) that leaves the sloping soil column through the seepage face. Runoff from the surface water follows Manning's equations, while interflow for saturated and unsaturated soil conditions is generated using a parametrization of Richard's equation (Soulis *et al.*, 2000, 2011). In the recent configuration of the MESH model, it is possible to maintain lower zone storage (LZS), representing superficial aquifer, then releases the baseflow to the streams (Princz, 2017). The simulation of the baseflow can be carried out either based on Luo *et al.* (2012) algorithm or the method described by Kouwen (2018).

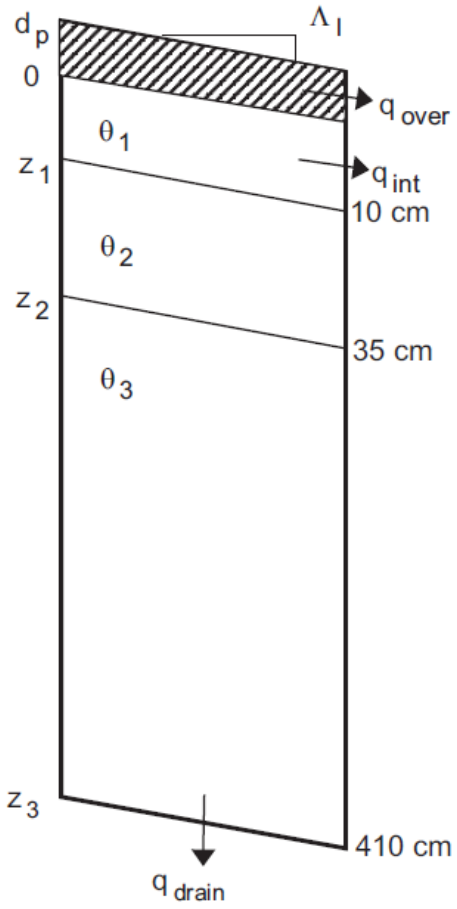

Figure 2.7. Soil moisture and land-surface drainage representation in MESH-CLASS. In this figure d_p, z, θ, Λ, and q present water ponded on the surface, soil depth, volumetric soil moisture, soil slope, and flow respectively (Soulis *et al.*, 2000).

Instead of WATROF, the lateral flow in the soil can be simulated by the PDMROF (Probability Distribution Model based Runoff generation, Mekonnen *et al.*, 2014) algorithm, which is based on the probability distribution runoff generation concept (Moore, 2007). The PDMROF, as an alternative approach, permits simulation of the Prairie hydrology in large scale hydrological models (Mekonnen *et al.*, 2014).

The total runoff to a basin outlet is generated based on the overland flow (from the pervious and impervious areas) and the interflow and the baseflow (Kouwen, 1988). In the WATFLOOD (Figure 2.8), a 1-D hydrologic routing model based on flow directions and elevation data simulates flows from upstream grids and route them through the grid to the next downstream grid (Kouwen, 2018). Recently, Yassin *et al.* (2019) also integrated a reservoir operation model into the MESH model. This model is called the dynamically zoned target release (DZTR) model that improves reservoir operation simulation of horizontal transfer (between grid routing) of water in the model compared with other widely used approaches.

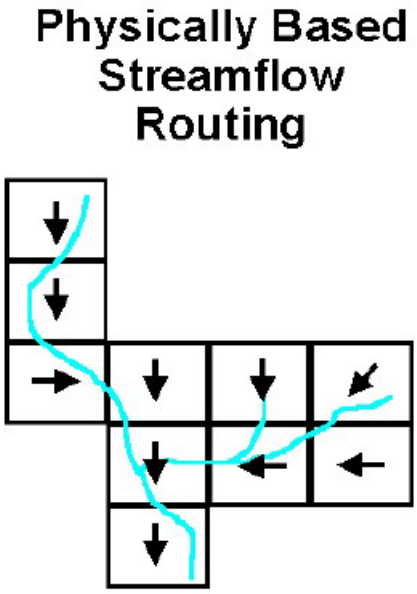

Figure 2.8. Runoff routing concept (Kouwen, 2018).

2.2.3. MESH science application

Different modeling and calibration efforts have been undertaken to improve the performance of MESH in hydrological simulations (Davison *et al.*, 2019, 2006; Dornes *et al.*, 2008; Haghnegahdar and Razavi, 2017; Haghnegahdar *et al.*, 2017, 2015; MacDonald *et al.*, 2009; Mekonnen *et al.*,

2014; Soulis *et al.*, 2011; Yassin *et al.*, 2017). More capabilities have been developed, such as the representation of water management (Yassin *et al.*, 2019) and permafrost (Elshamy *et al.*, 2020).

As the development of the MESH model continues, some researchers and collaborators have focused upon incorporating remotely sensed products into the modeling system, especially for forecasting applications. Yirdaw *et al.* (2009) compared MESH-derived TWSA with GRACE observations in the Mackenzie Basin and found a general agreement between model simulations and satellite retrievals. The integration of satellite-based observations within the MESH system has been shown to improve the accuracy of model simulations. Xu *et al.* (2015) applied a one-dimensional Ensemble Kalman filter (1D-EnKF) over the Great Lakes by integrating SMOS soil moisture retrievals into the MESH model. Results highlighted that the developed DA methodology can improve moisture estimation in both the surface soil and root zone over the crop-dominated grids. Yassin *et al.* (2017) incorporated GRACE observations into the MESH model in the Saskatchewan River Basin using a multiobjective calibration approach to constrain the model parameters. This study examines the development of the state-of-the-art MESH-GRACE framework into the ECCC community environmental modeling for improving model simulations.

2.3. Data assimilation

Even though data assimilation is a common process in numerical weather forecast, its application has been extended in other research areas, such as climate, atmosphere, ocean and environment modeling, where one needs to estimate the state of a large dynamical model based on limited knowledge about the initial and boundary conditions (Carrassi *et al.*, 2018; Evensen, 2009). DA has an interdisciplinary nature. The choice of an efficient DA approach depends on the requirements of the research, both in terms of model resolution and forecast time horizon (Carrassi *et al.*, 2018, Figure 2.9). Therefore, geoscientists should find state-of-the-art data assimilation strategies according to application, model resolution, computational efficiency, observing systems, and other requirements.

In this section, an introduction to sequential DA methods is discussed. Then, the mathematical foundations of the EnKS (the approach used is in this study) are explained. Thereafter, the procedure of generating a temporally correlated pseudo random field is discussed. Finally, the science applications of data assimilation methods are presented.

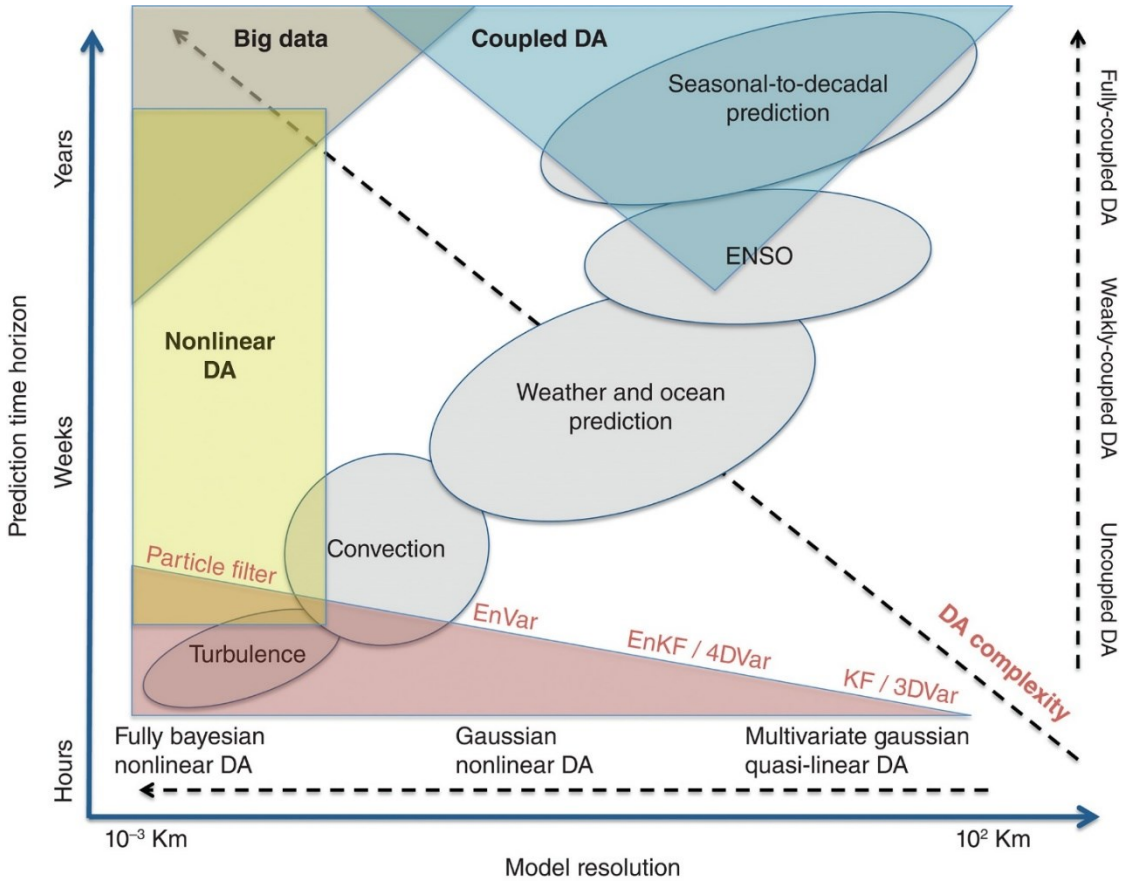

Figure 2.9. Required data assimilation method based on mode resolution and prediction time horizon (Carrassi *et al.*, 2018).

2.3.1. Sequential data assimilation

In sequential data assimilation methods, which are the most common in geophysical applications, observations are utilized to correct the present states of a model when they become available (Evensen, 2009). In Figure 2.10 the concept of sequential data assimilation is presented. The model is propagated forward from time t_k, when an analysis (red square) is issued using the forecast (green circle) and observation (blue star). In this illustration, the estimated uncertainties of observation, model forecast (or prediction), and analysis (or update) are displayed in terms of probability density functions (PDF) using ellipsoids of proportional sizes (Carrassi *et al.*, 2018). Then, a prediction is produced from the analysis at time t_k until the next observations at t_{k+1}. This process is repeated sequentially for each time step, whenever observations are available. The sequential method is appropriate when models are driven by a set of meteorological inputs (e.g., precipitation, radiations, and other climate variables), and when knowledge about the initial

conditions are less relevant (Schumacher, 2016).

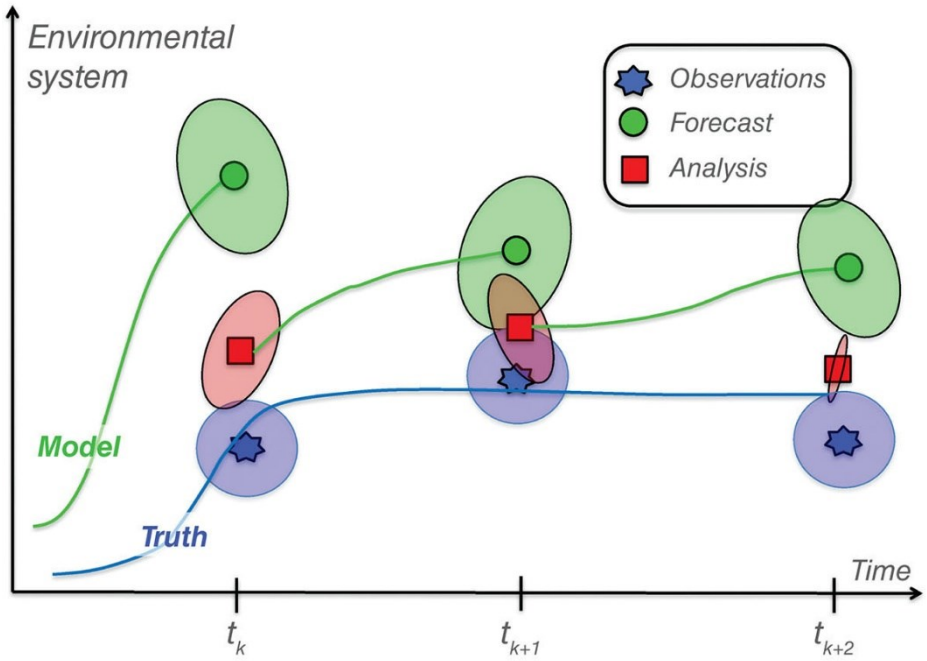

Figure 2.10. Illustration of sequential data assimilation. Observations (blue), forecast (green), and analysis (red). The true signal is presented by the blue line, (Carrassi *et al.*, 2018).

2.3.2. Ensemble methods

A Markov Chain Monte Carlo (MCMC) approach is the basis of a class of algorithms referred to ensemble-based methods, among them are the ensemble Kalman filter (EnKF, Evensen *et al.*, 1994) and the EnKS (Evensen and Van Leeuwen, 2000). The latter is an extension of EnKF developed by Evensen and Van Leeuwen (2000). For both EnKF and EnKS methods, it is assumed that model errors have a Gaussian distribution. Several variations of the original algorithms have been successfully applied in geoscience (Evensen, 2009). For instance, since 2005 a global EnKF coupled with the Canadian GEM model has been implemented operationally at CMC to provide the initial conditions for a global ensemble prediction system (Houtekamer *et al.*, 2005). The ensemble-based Canadian Land Data Assimilation System (CaLDAS), based on the EnKF method, has been developed at ECCC to generate land surface analyses (Carrera *et al.*, 2015) and provide short-range numerical weather predictions (Milbrandt *et al.*, 2016).

In the MCMC experiments, a numerical tool such as a forecast model is performed in sequence to

generate an ensemble of outputs from an ensemble of inputs (Houtekamer and Zhang, 2016). Based on the MCMC method, each of the model states represents one point in the *n*-dimensional state space. All the ensemble members together will generate a cloud of points in the state space. The cloud of points in the state space can be described using a PDF with an infinite ensemble size (Evensen, 2003). However, in practice, the PDF is defined based on a finite ensemble:

$$p(x) = \lim_{N\to\infty} \frac{dN}{N} \tag{2.4}$$

where *dN* is the number of points in a small unit volume, *N* is the total number of points (or ensemble). With knowledge of either the PDF or the ensemble representing *p(x)*, one can calculate statistical moments (e.g., mean, covariance) which are required in assimilation procedure (Evensen, 2003, 2009). In the ensemble-based methods, when a best estimate is needed, the ensemble mean can be used and the ensemble spread around the mean should provide a reliable estimate of error (Houtekamer and Zhang, 2016).

2.3.2.1. Ensemble Kalman Smoother method

A Forecast and an analysis steps are two major components of the EnKS approach (Evensen, 2003). During the forecast step, the EnKS evolves an ensemble of model states forward in time. In the analysis step, observations are used to obtain a posteriori state estimate (or update) for the time period of interest. For instance, the beginning and end of the assimilation window correspond to the first (t_o) and last day (t_f) of the month.

In the EnKS, the nonlinear land surface model *G(.)* propagates an ensemble of *N* initial or analysis model states $\mathbf{x}_{k-1,i}^{a}$ with model error of $\mathbf{q}_{k,i}$ from time *k-1* to the next time step *k* to obtain model forecast $\mathbf{x}_{k,i}^{f}$, as the following:

$$x_{k,i}^{f} = G(x_{k-1,i}^{a}, q_{k,i}) \qquad for\ i\ \in\ N \tag{2.5}$$

In practice, to reflect the uncertainty in the model forecasts, perturbations are applied to model states and inputs of climate forcing at each time step to generate *N* ensemble forecast. Here, for the sake of simplicity, the ensemble index *i* is dropped. In the EnKS method, when observations $\mathbf{y_k}$ are available, the analyzed states $\mathbf{x}_k^a$ are reinitialized by a weighted linear combination of the

model forecast $\mathbf{x}_k^f$ and the vector of measurement as:

$$x_k^a = x_k^f + K_k\left((y_k + \varepsilon_k) - Hx_k^f\right) \tag{2.6}$$

where $\mathbf{K_k}$ is the Kalman gain and **H** is the measurement vector (or operator) that maps the model states into the observation space. The observations are perturbed by adding random realizations $\boldsymbol{\varepsilon_k}$ of the measurement error (Burgers *et al.*, 1998).

The second matrix in equation (2.6), i.e., $K_k((y_k + \varepsilon_k) - Hx_k^f))$, is called the analysis increments (AI). The analysis increments (or updates) transfer the vector of observation-minus-forecast residuals to the model prognostic state at the model spatial and temporal resolution, based upon the partitioning that is given by Kalman gain (Girotto *et al.*, 2019). The Kalman gain ($\mathbf{K_k}$) represents the relative weights given to the model forecast states $\mathbf{x}_k^f$ and the observations $\mathbf{y_k}$ during the update state. $\mathbf{K_k}$ is expressed as:

$$K_k = P_k^f H^T\left(HP_k^f H^T + R\right)^{-1} \tag{2.7}$$

Here, **R** is the time-invariant measurement covariance and *T* denotes the transpose operator. The observation errors of GRACE TWSA retrievals can either be treated as spatially uncorrelated (Forman *et al.*, 2012; Girotto *et al.*, 2016; Kumar *et al.*, 2016; Su *et al.*, 2010; Zaitchik *et al.*, 2008) or correlated (Eicker *et al.*, 2014; Schumacher *et al.*, 2016, 2018). In this study, the observation errors are considered to be spatially uncorrelated. The model forecast (background) error covariance $\mathbf{P_k^f}$ is diagnosed from the sample covariance of the ensemble as:

$$P_k^f = \overline{\left(x_k^f - \overline{x_k^f}\right)\left(x_k^f - \overline{x_k^f}\right)^T} \tag{2.8}$$

where the overlines denote an average over the ensemble.

2.3.3. Generating pseudorandom fields

In the data assimilation experiment, the ensemble spread is generated by adding perturbations to meteorological forcing and model states (Reichle et Koster, 2003). Note that, log-normally distributed multiplicative perturbations or normally distributed additive perturbations are applied

based on the variable type. (Reichle *et al.*, 2007). Therefore, the focus is now to simulate pseudo random fields with mean equal to zero, variance equal to one, and a specified covariance which determines the smoothness of the fields (Evensen, 2003). The mathematical descriptions follow (Evensen *et al.*, 1994), (Evensen, 2003), and (Evensen, 2009). Note that, here x and y represent coordinates of a two-dimensional random field.

A continuous field $q = q(x,y)$ using an $n_x \times n_y$ grid can be described by its Fourier transform

$$q(x,y) = \int_{-\infty}^{+\infty} \int_{-\infty}^{+\infty} \hat{q}(\boldsymbol{k})\ e^{i\boldsymbol{k}.\boldsymbol{x}}\, d\mathbf{k} \tag{2.9}$$

We define $\boldsymbol{k} = (k_l, \lambda_p)$, where l, p are counters and k_l and λ_p are wave numbers in x and y directions, respectively. A discrete version of Eq. (2.9) can be written as

$$q(x_n, y_m) = \sum_{l,p} \hat{q}(k_l, \lambda_p)\ e^{i(k_l x_n + \lambda_p y_m)} \Delta\mathbf{k} \tag{2.10}$$

where $x_n = \mathrm{n}\,\Delta x$, $y_m = \mathrm{m}\,\Delta y$, $k_l = \frac{2\pi l}{n_x \Delta x}$, $\lambda_p = \frac{2\pi p}{n_y \Delta y}$, and $\Delta\mathbf{k} = \Delta k\,\Delta\lambda = \frac{(2\pi)^2}{n_x n_y \Delta x \Delta y}$.

In Evensen *et al.* (1994) for the Fourier coefficients, the following Gaussian form was used,

$$\hat{q}(k_l, \lambda_p) = \frac{c}{\Delta\mathbf{k}} e^{-(k_l^2 + \lambda_p^2)/r^2} e^{2\pi i \phi_{l,p}} \tag{2.11}$$

where $\phi_{l,p} \in [0\ 1]$ is a uniformly distributed random number that introduces a random phase shift. When l and p increase, the wave number k_l and λ_p will give an exponentially decreasing contribution. This representation of Fourier coefficients leads to generate isotropic covariances field, i.e the smoothness is the same in all directions. Now, Eq. (2.11) is inserted into Eq. (2.10) and the following equation is obtained for the inverse Fourier transform that defines the random fields:

$$q(x_n, y_m) = \sum_{l,p} \frac{c}{\Delta\mathbf{k}} e^{-(k_l^2 + \lambda_p^2)/\sigma^2} e^{2\pi i \phi_{l,p}}\ e^{i(k_l x_n + \lambda_p y_m)} \Delta\mathbf{k} \tag{2.12}$$

It should be noted that it is required to produce real fields only. Therefore, when the summation of

Eq. (2.12) over l and p is performed, all the imaginary contributions must add up to zero. This condition is satisfied whenever:

$$\hat{q}(k_l, \lambda_p) = \hat{q}^*(k_{-l}, \lambda_{-p}) \tag{2.13}$$

where the asterisk indicates complex conjugate, and in addition:

$$Im\ \hat{q}(k_0, \lambda_0) = 0 \tag{2.14}$$

Eq. (2.12) can be used to generate an ensemble of random fields with a covariance determined by the parameters c and σ. By assuming that the fields are uncorrelated in wave space, that is, there is only a distance dependence (isotropy) for the covariance, then the expression of the covariance is given by:

$$\overline{q(x_1, y_1)q(x_2, y_2)} = \Delta\mathbf{k}c^2 \sum_{l,p} e^{-2(k_l^2+\lambda_p^2)/\sigma^2}\, e^{i[k_l(x_l-x_2)+\lambda_p(y_l-y_2)]} \tag{2.15}$$

By requiring that the variance of random field equals to 1 in Eq. (2.15), then we get the equation:

$$1 = \Delta\mathbf{k}c^2 \sum_{l,p} e^{-2(k_l^2+\lambda_p^2)/\sigma^2} \Rightarrow c^2 = \frac{1}{\Delta\mathbf{k}\sum_{l,p} e^{-2(k_l^2+\lambda_p^2)/\sigma^2}} \tag{2.16}$$

Further, a decorrelation length r_h is defined, so that the covariance at the x direction (i.e., x_1- x_2 = r_h) and y direction (y_1- y_2 = 0) to be equal to e^{-1}. Therefore, we obtain:

$$e^{-1} = \Delta\mathbf{k}c^2 \sum_{l,p} e^{-2(k_l^2+\lambda_p^2)/\sigma^2}\, e^{ik_l r_h} = \Delta\mathbf{k}c^2 \sum_{l,p} e^{-2(k_l^2+\lambda_p^2)/\sigma^2}\, cos(k_l r_h) \tag{2.17}$$

By inserting c^2 from Eq. (2.16), then:

$$e^{-1} = \frac{\sum_{l,p} e^{-2(k_l^2+\lambda_p^2)/\sigma^2}\, cos(k_l r_h)}{\sum_{l,p} e^{-2(k_l^2+\lambda_p^2)/\sigma^2}} \tag{2.18}$$

The nonlinear scalar equation (2.18) can be solved for σ using some numerical routines (e.g., a Newton method). Then, a value for c is determined from Eq. (2.16). When the values of c and σ are defined, one can use the formula (2.12) to simulate an ensemble of random fields with variance

1 and covariance determined by the decorrelation length r_h. An efficient way for finding the inverse transform in equation (2.12) is to apply a two-dimensional fast Fourier transform (FFT) algorithm.

2.3.4. Model error evolution

A simple formula can be used for simulating time evolution of correlated model errors:

$$q_k = \alpha q_{k-1} + \sqrt{1-\alpha^2} w_k \tag{2.19}$$

Here it is assumed that w_k is a random realization that is sampled from a distribution with zero mean and variance equal to one, while q_{k-1} is the previous model error, to which q_k should be correlated. The generation of q_k can be implemented similar to the method that is described in the previous section. The coefficient $\alpha \in [0\ 1]$ determines the time correlation of the model error, e.g., $\alpha = 0$ generates a white sequence in time, while $\alpha = 1$ will remove the stochastic forcing. The factor α can be related to the time step used and a specified time decorrelation length τ, such that q is damped with a ratio of e^{-1} over a time period of $t = \tau$. A numerical approximation becomes:

$$q_k = \left(1 - \frac{\Delta t}{\tau}\right) q_{k-1} \tag{2.20}$$

where Δt is the time step. Thus, the factor α is defined as:

$$\alpha = 1 - \frac{\Delta t}{\tau} \qquad for\ \ \tau \geq \Delta t \tag{2.21}$$

Based on equation (2.19), the temporal correlations of error perturbations are imposed using a first-order autoregressive model (AR(1)) for all perturbation fields. The time error perturbations using higher orders (e.g., a second order) was considered as beyond the scope of this study, and was not investigated.

2.3.5. GRACE Data assimilation for geoscience applications

Finding an appropriate data assimilation method for the integration of satellite observations into a prognostic model is not straightforward. The selection of the data assimilation method can be defined based on different criteria, such as the treatment of model and observation errors, model specification, and the purpose of the study. Each of the methods might have advantages but at the same time shortcomings and complications of implementation (Schumacher, 2016). Among

assimilation methods, ensemble-based Kalman filtering and smoothing algorithms have been recognized as the most common and the most encouraging method for land data assimilation (Reichle *et al.*, 2009).

In the past two decades, key research contributions at the NASA Global Modeling and Assimilation Office (GMAO) include the continued development and application of land data assimilation to satellite retrievals of surface soil moisture, TWS observations, land surface temperature, and the other products. In the application of using TWS observations into the GMAO, Zaitchik *et al.* (2008) assimilated GRACE retrievals into the CLSM model in the Mississippi Basin. They demonstrated the potential of the developed DA method for the improvement of surface and subsurface model simulations. Later, the ensemble-based smoother method has been applied for the purpose of snow, groundwater, subsurface and soil moisture applications (Forman *et al.*, 2012; Girotto *et al.*, 2016, 2017, 2019; Houborg *et al.*, 2012; Kumar *et al.*, 2016; Li *et al.*, 2012, 2019; Reager *et al.*, 2015).

A data assimilation/calibration project (www.globalcda.de) has been conducted at the Goethe University Frankfurt and the University of Bonn with different partners. The purpose of this project was to develop a multi-observation ensemble-based calibration and data assimilation (C/DA) methodology to combine remotely sensed observations, such as GRACE/GRACE-FO TWS retrievals with the WGHM. For the first time, Schumacher (2012) examined the potential of assimilating GRACE observations into the WGHM model based on the C/DA framework using the EnKF method. This framework was further developed and examined in other studies by using gridded (5º×5º) GRACE observations (Eicker *et al.*, 2014; Schumacher, 2012, 2016; Schumacher *et al.*, 2016, 2018).

Su *et al.* (2010) examined the potential multisensor data assimilation approach on improving snow estimates over North America and found that the multivariate DA can provide significant improvements over the single sensor assimilation approach. Van Dijk *et al.* (2014) reported other DA experiments using the ensemble-based EnKF approach to assimilate GRACE observations into the World-Wide Water Resources Assessment (W3RA) model and four variants of the GLDAS model at the Australian National University (ANU, Australia). An overview of integrating GRACE TWS retrievals into different models is summarized in Table 2.1, 2.2 , and 2.3.

Table 2.1. Summary of GRACE data assimilation experiments into the CLSM and CLM models

Hydrologic objective	DA method	Model	Region	Findings	Reference
Surface and subsurface hydrology	Ensemble smoother	CLSM	Mississippi	DA can improve the simulation of groundwater, runoff, drought indicators	(Zaitchik *et al.*, 2008)
Snow	Ensemble smoother	CLSM	Mackenzie	1) For SWE, modest improvements are achieved. 2) GRACE assimilation has little influence on runoff simulation	(Forman *et al.*, 2012)
Surface and subsurface hydrology	Ensemble smoother	CLSM	Europe	DA has significant influence on groundwater estimates including trend and seasonality	(Li *et al.*, 2012)
Surface and subsurface hydrology	Ensemble smoother	CLSM	North America	Results highlight the potential for improving drought detection	(Houborg *et al.*, 2012)
Surface and subsurface hydrology	Ensemble smoother	CLSM	Missouri	Assimilation offers a useful tool for flood potential assessment	(Reager *et al.*, 2015)
Surface and root zone soil moisture	Ensemble smoother	CLSM	USA	1) DA has a positive effect on the simulation of groundwater 2) Smaller improvements are observed in the simulation of snow depth 3) The effect of DA on river discharge and evapotranspiration is variable 4) Assimilation of gridded GRACE data does not add significant information content relative to the basin average	(Kumar *et al.*, 2016)
Soil moisture and subsurface hydrology	Ensemble smoother	CLSM	USA	1) DA scheme yields improved groundwater simulations 2) It has smaller impact on surface and root-zone moisture	(Girotto *et al.*, 2016)
Subsurface hydrology	Ensemble smoother	CLSM	India	DA improves the interannual variability of groundwater simulation but introduces a negative trend in simulated evapotranspiration	(Girotto *et al.*, 2017)
Soil moisture and subsurface hydrology	EnKF, Ensemble smoother	CLSM	USA	1) The assimilation of GRACE TWS improves groundwater estimates, while SMOS[1] DA improves surface soil moisture estimates 2) The multi-sensor assimilation of GRACE and SMOS maintains the single-sensor assimilation benefits	(Girotto *et al.*, 2019)
Subsurface hydrology	Ensemble smoother	CLSM	Global	GRACE DA improves the simulation of groundwater in regions with large interannual variability in precipitation	(Li *et al.*, 2019)
Snow	EnKF, EnKS	CLM	North America	The multisensor method can provide significant improvements over a MODIS[2] only approach	(Su *et al.*, 2010)
Soil moisture and snow	EAKF[3]	CLM	Global	1) Assimilation of MODIS snow cover fraction slightly improves snow estimation. 2) AMSR-E[4] plays complementary role in improving soil moisture and snow estimates. 3) Assimilation of GRACE tends to degrade global soil moisture but poses potential in improving snow depth estimation in high latitude regions	(Zhao and Yang, 2018)

Note: (1) Soil Moisture and Ocean Salinity (SMOS) mission; (2) Moderate Resolution Imaging Spectroradiometer (MODIS); (3) ensemble adjustment Kalman filter (EAKF); (4) Advanced Microwave Scanning Radiometer for Earth Observing System (AMSR-E).

Table 2.2. Summary of GRACE data assimilation experiments into the WGHM and W3RA models

Hydrologic objective	DA method	Model	Region	Findings	Reference
Total water storage	EnKF	WGHM	Mississippi	Assimilating gridded GRACE data (at 5º) resolution provides results that appear superior to the assimilation of basin averages	(Eicker *et al.*, 2014)
Surface and subsurface hydrology	EnKF, SQRA[1], SEIK[2]	WGHM	Mississippi	1) Hydrological parameters are sensitive to TWSA assimilation 2) Spatial error correlation has a significant influence on the adjusted water states and model parameters	(Schumacher *et al.*, 2016)
Surface and subsurface hydrology	EnKF	WGHM	Murray-Darling (Australia)	1) Integrating GRACE data into WGHM does not only improve simulation of seasonality and trend of TWSA but also it ameliorates the simulation of individual water storage components 2) parameter updating using GRACE observations is very challenging 3) Calibration/assimilation method does not improve river discharge simulation	(Schumacher *et al.*, 2018)
Surface, snow and subsurface hydrology	EnKF	GLDAS, W3RA	Global	The DA scheme generally behaves as desired, but in hydrologically complex regions the analysis can be affected by poorly constrained prior estimates and error specification.	(Van Dijk *et al.*, 2014)
Surface and subsurface hydrology	EnKF, EnKS	W3RA	Australia	The multisensor GRACE/SMOS can produce improved estimates of surface and root-zone soil moisture as well as groundwater estimates	(Tian *et al.*, 2017)
Soil moisture and subsurface hydrology	Stochastic and deterministic EnKF, PF[3]	W3RA	Australia	1) All implemented filters improve the estimation of water storage simulations of W3RA 2) The best results are obtained using two versions of deterministic EnKF, including SQRA and EnSRF[4].	(Khaki, *et al.*, 2017a)
Soil moisture and subsurface hydrology	SQRA	W3RA	Australia	Results show that local analysis within the SQRA filter leads to less errors for all spatial scales	(Khaki, *et al.*, 2017b)
Soil moisture and subsurface hydrology	EnSRF	W3RA	Iran	The EnSRF method improves model derived water storage simulations by introducing missing trends and correcting the amplitude and phase of seasonal water storage variations.	(Khaki *et al.*, 2018)
Surface and subsurface hydrology	EnSRF	W3RA	South America	DA of GRACE/SMOS/AMSR-E improves the estimation of groundwater and soil moisture variations	(Khaki and Awange, 2019)

Note: (1) square root analysis (SQRA); (2) singular evolutive interpolated Kalman (SEIK); (3) Particle filters (PF); (4) Ensemble Square-Root Filter (EnSRF)

Table 2.3. Summary of GRACE data assimilation experiments into the HBV-96 and PCR-GLOBWB models

Hydrologic objective	DA method	Model	Region	Findings	Reference
Subsurface hydrology	EnKF	HBV-96	Rhine	Results show a noticeable improvement in groundwater estimates when GRACE data were assimilated	(Tangdamrongsub *et al.*, 2015)
Surface and subsurface hydrology	EnKS	PCR-GLOBWB[1]	Hexi Corridor (China)	The GRACE DA adjusts TWS estimates and improves the accuracy of groundwater estimates.	(Tangdamrongsub *et al.*, 2017)
Subsurface hydrology	EnKS	PCR-GLOBWB	China, Australia	GRACE DA also improves the estimation of groundwater depletion due to the incorrect information of the groundwater demand or the unavailability of a groundwater consumption routine	(Tangdamrongsub *et al.*, 2018)

Note: (1) PCRaster Global Water Balance (PCR-GLOBWB)

3. Data and general method

In this chapter, the study site and the different data sources used are presented. An overview of the methods of the research is also presented, including a general methodological flowchart. The detailed methods on each aspect of the study are described in the respective articles manuscripts presented in Chapters 4, 5 and 6.

3.1. Study site

Study sites considered in this research are grouped into two categories based on the objectives of this research: 1) Gridded study domain; and 2) basin study domain. The gridded domain at 1°×1° spatial resolution covers the Canadian landmass except for the arctic latitudes and areas of high elevation between 42°N to 72°N latitude, and 141°W to 54°W longitude. Following the first part of the objective 1, gridded GRACE/GLDAS-derived TWSA data along with multisource SWE dataset are used to realize the spatiotemporal TWSA-SWEA relationship. The geophysical properties over the Canadian landmass can be defined, based upon DEM and land-cover classification. Land cover information (Figure 3.1) is extracted from the Land Cover of Canada (LCC, 2010), which was produced based on Landsat satellite images by the Canada Centre for Mapping and Earth Observation (CCMEO), formerly the Canada Centre for Remote Sensing (CCRS). For the TWSA-SWEA analysis at the basin-averaged domain, in the thesis, topographic data (Figure 3.2) is based upon the U.S. Geological Survey's data center with a horizontal grid spacing of 30 arc seconds (www.usgs.gov). To pursue the second part of the objective 1, the spatiotemporal relationship between TWSA/SWEA-derived from GRACE and multisource SWEA is analyzed at the basin-averaged spatial resolution. Basins (Figure 3.3) considered in the study cover most parts of the Canadian landmass. Except for the Fraser basin (basin 1 in Figure 3.3), they are all included within three large scale basins, namely Mackenzie (including Athabasca, Bear and Peel, Liard, Peace, and Slave), Hudson Bay (including Churchill, Southwestern of Hudson Bay, La Grande, Nelson, Northeastern Hudson Bay, Nottaway, Ungava Bay, Western Hudson Bay), and Saint Lawrence (including Saint Lawrence River). In summary, the basin study domain contains fifteen basins (Figure 3.3, Table 3.1) where the regional TWSA-SWEA relationships are analyzed.

Considering the second objective of this study, the Liard Basin (basin 12 in Figure 3.3) was chosen

as one of the sub-basin of the Mackenzie Basin. The watershed of the Liard River drains portions of British Columbia and Alberta, and the Yukon and Northwest Territories of boreal northwestern Canada, spanning longitudes 132°W to 118°W and latitudes 57°N to 63°N. Land cover of the Liard Basin is dominated by sub-polar needleleaf and mixed forest (71%) and grasslands (16%), followed by barren land (7%) and wetlands (4%); a small fraction of its area is covered by water bodies (1.5%) and glaciers (0.5%). The basin drains approximately 85.64 billion cubic meters per year which is about 27% of Mackenzie Basin outflow. The basin drainage area is about 275 000 km^2.

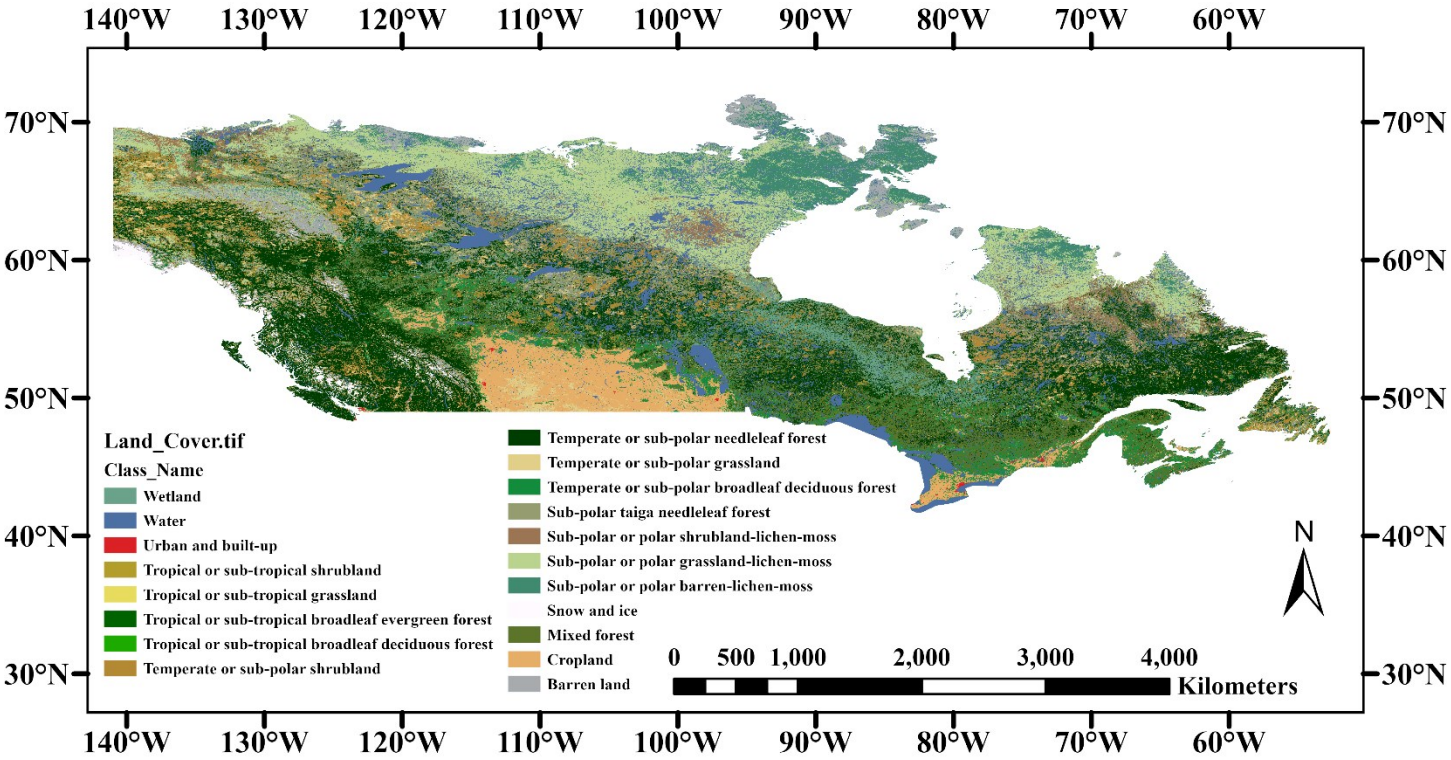

Figure 3.1. Map of land cover types.

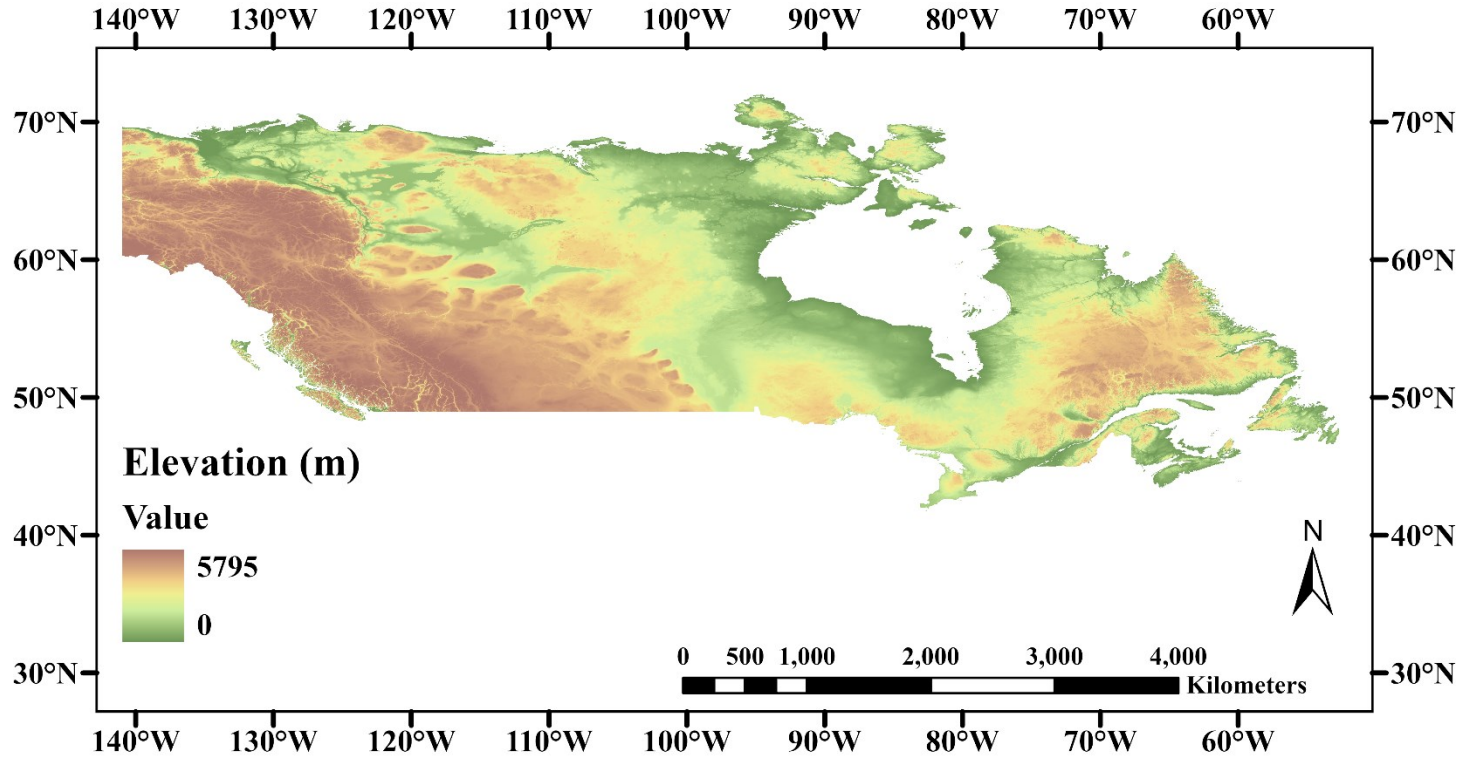

Figure 3.2. Map of digital elevation model (DEM).

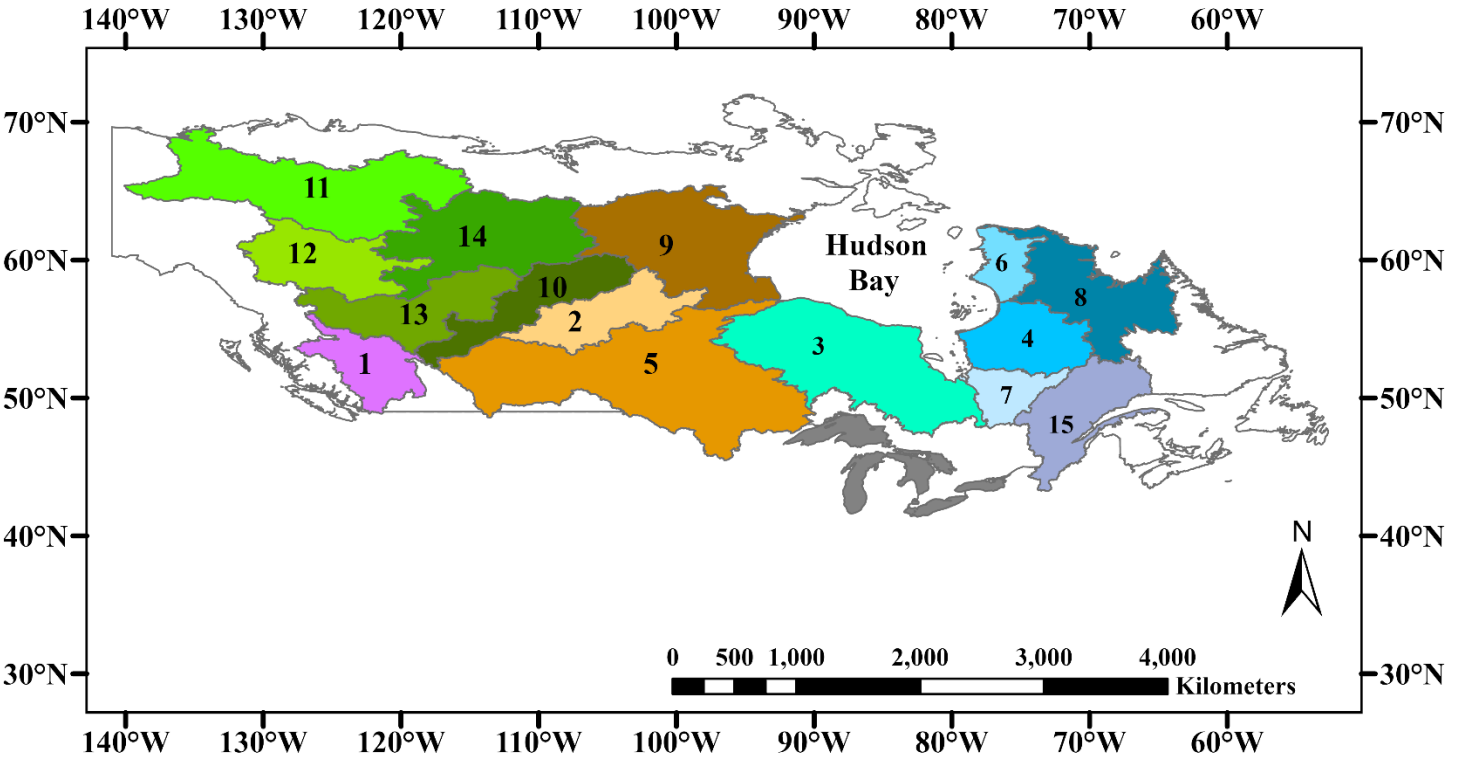

Figure 3.3. Location of the fifteen Canadian river basins

Table 3.1. Basin areas, forest fractional cover, and elevation. Basin locations can be seen in Figure 3.3.

Basin ID	Basin Name	Area (km^2)	Percentage of the forest cover (%)	Average elevation (m)
1	Fraser	231924.0	70.2	1192.8
2	Churchill	258817.1	60.7	446.7
3	Southwestern of Hudson Bay	735761.7	63.3	205.9
4	La Grande	268720.9	58.7	329.4
5	Nelson	1112976.0	32.7	525.7
6	Northeastern Hudson Bay	100467.4	2.7	160.1
7	Nottaway	144967.9	63.2	326.4
8	Ungava Bay	380791.9	25.7	352.9
9	Western Hudson Bay	492467.5	21.2	232.9
10	Athabasca	272726.4	64.3	610.4
11	Bear and Peel	498350.3	34.2	538.7
12	Liard	274955.2	71.3	992.2
13	Peace	323134.6	74.3	845.4
14	Slave	430091.1	53.5	342.3
15	Saint Lawrence River	365385.0	79.8	431.4

Four main reasons motivated the selection of the Liard Basin for the assimilation of GRACE observations into the MESH model. First, data analysis between GRACE and multisource SWE products revealed that GRACE TWSA seasonal amplitudes in the Liard Basin are dominated by snow mass changes during the snow season (Bahrami *et al.,* 2020). Second, contributions of surface water mass changes from lakes, reservoirs, and river storage to total water storage. As the contribution of large water bodies and wetlands might have effects on the total water storage variations sensed by GRACE satellites during cold seasons, in the Liard Basin these components are not significant. Third, the basin size (~275 000 km^2) is not substantially larger than the true resolution of observations in the Liard Basin. The smallest spatial scale in which GRACE observations can be reasonably resolved in high latitudes is about 150 000 km^2. Fourth, this study is part of a study that focuses on developing a large-scale hydrological model for the Mackenzie River Basin (MRB) (Figure 3.4). The MESH framework is employed to study the effects of climate and land use/cover changes on various aspects of the MRB hydrology.

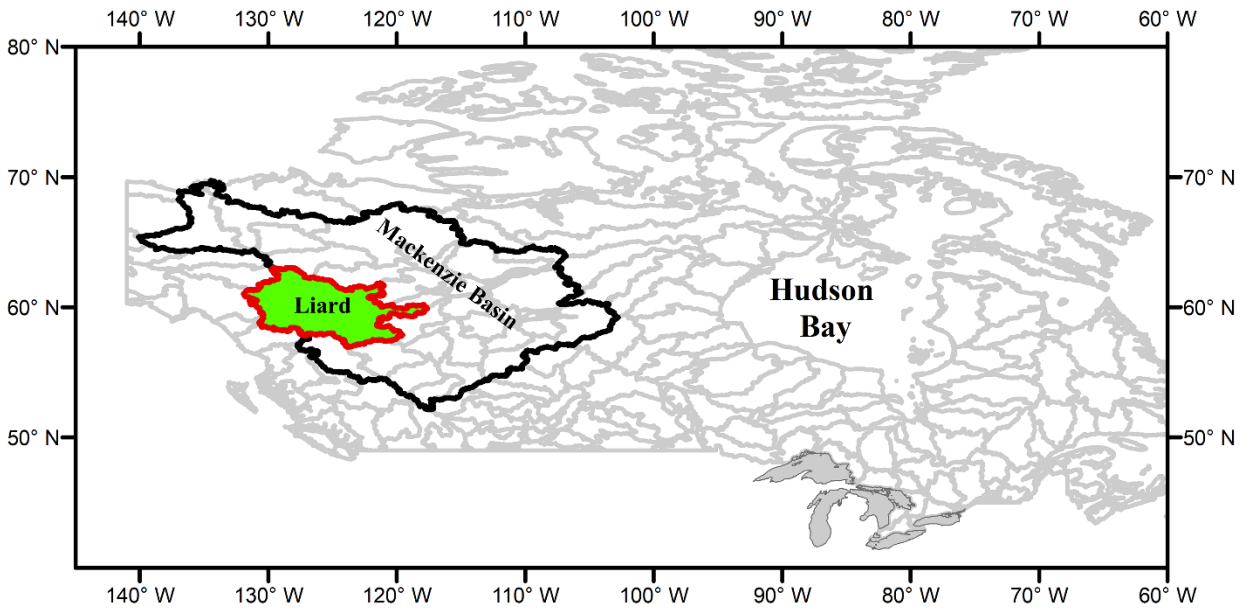

Figure 3.4. Mackenzie and Liard basin boundary discretizations.

3.2. Data sets

3.2.1. TWS data

3.2.1.1. GRACE observations

A set of nontrivial processing steps (Section 2.1.2) are applied across GRACE gravity solutions to produce gridded equivalent water heights, i.e., TWSA (mm) products that can be used in hydrological applications (Cooley and Landerer, 2019). The gridded (1°×1°) GRACE-derived TWSA retrievals are publicly available from April 2002 to October 2014, through the NASA JPL TELLUS website (Swenson, 2012). As mentioned in Section 2.1.2, to effectively reduce the noise in the GRACE data, the arithmetic mean of all three data processing centers were used in this study (Sakumura *et al.*, 2014). In each year, GRACE TWSA retrievals corresponding to the snow season (from December to March) were extracted to compare against multisource SWE products. The reason for selecting this period was based on the preliminary analyses which showed that GRACE/GLDAS were strongly related to SWE.

3.2.1.2. GLDAS simulations

The GLDAS-derived TWSA is obtained from NOAH LSM, version 2.7.1 (Chen *et al.*, 1996;

Koren *et al.*, 1999), within the GLDAS system (Rodell *et al.*, 2004). The model TWS estimates are presented at 1°×1° spatial resolution on a monthly temporal resolution from December 2002 to March 2011. In this study, we used GLDAS TWS data related to snow seasons (December to March). The simulated TWS of the GLDAS-NOAH is the sum of state variables, including intercepted precipitation by the canopy, snow, and soil moisture from four soil layers with thicknesses of 0.1, 0.3, 0.60 and 1.0 m. The reason for using GLDAS data is that the total water content is directly comparable to GRACE observations over land. However, it should be mentioned that GLDAS TWS estimates do not include groundwater and surface water components (e.g., river and lakes).

3.2.1.3. WGHM simulations

The Water-Global Assessment and Prognosis (WaterGAP) model contains two important parts, including the water use models and the WGHM model (Döll, *et al.*, 2014b; Müller Schmied *et al.*, 2014). WGHM simulates water storage variations and fluxes globally with the exception of Antarctica at 0.5°×0.5° spatial resolution on a monthly temporal resolution from December 2002 to March 2011. The WGHM TWS simulation for each grid cell was calculated by summing different water storage components, including canopy, snow, soil, groundwater, lakes, man-made reservoirs, wetlands, and rivers. The spatial representation of model outputs is converted to 1°×1° by averaging all grid points falling in a 1° grid cell corresponding to GRACE grid.

3.2.2. SWE Products

3.2.2.1. CMC

Monthly CMC SWE analysis data is provided at a spatial resolution of 0.25°×0.25° (~24 km × ~24 km) over the Northern Hemisphere from December 2002 to October 2014 (Brown and Brasnett, 2010). Monthly SWE estimates for the October to June period of each year were derived from monthly averaged snow depth analyses and using the corresponding mean monthly snow density lookup table that was identified by Sturm *et al.* (1995). Data sets are provided by the National Snow and Ice Data Center (NSIDC). Note that, CMC snow depth observations in northern latitudes (~ 55°N) are shown to have negative biases. In section 7.1, limitations of CMC SWE values are discussed in detail.

3.2.2.2. GlobSnow2

Monthly GlobSnow version 2.0 (GlobSnow2) is a source of SWE product that was used in this study. GlobSnow2 SWE, as a data assimilated product, is obtained from a combination of ground-based weather station data, passive microwave remote sensing observations, and model estimates (Takala *et al.*, 2011). The SWE products cover the terrestrial non-mountainous regions of Northern hemisphere (between latitudes 35° to 85°), except for glaciers and Greenland. Data are provided with a spatial resolution of 25 km × 25 km from December 2002 to March 2011. They are accessed through the Finnish Meteorological Institute website (http://www.globsnow.info/swe).

3.2.2.3. AMSR-E

Monthly level-3 SWE product of AMSR-E from passive microwave measurements was employed for the purpose of analyzing the relation between GRACE TWSA and SWE products. Data are provided with a spatial resolution of 25 km × 25 km (Tedesco *et al.*, 2004). The AMSR-E SWE data cover the Canadian landmass from December 2002 to March 2011 which corresponds to a snow season (December to March). The AMSR-E SWE products have negative biases in mountainous and/or forest areas. The mitigation of these biases has not been applied to AMSR-E products. The limitations of AMSR-E data are given in section 7.1.

3.2.2.4. Snow survey observations

The station-based snow surveys were conducted by the British Columbia Ministry of Environment in Canada on a daily basis over the winter/spring season. Automated snow observations were collected through the Data Collection System (DCS) on Geostationary Satellites (GOES) operated by the National Oceanic and Atmospheric Administration (NOAA). The archived daily snow SWE observations can be accessed and used through the provincial snow survey network website (https://www2.gov.bc.ca/gov/content/environment). In this study, we used snow surveys from November 2012 to April 2014 and converted them to monthly observations. Monthly SWE observations during the snow seasons (November to April) are used for the evaluation of modeled SWE estimates. Snow monitoring stations include the 4C22P (Kiwigana Climate), the 4C21P (Two Island Climate), and 4C20P (Sierra Climate).

3.2.3. MESH model data configuration

The MESH model version 1.4.1037 has been set-up at a 0.125º × 0.125º (longitude/latitude) spatial resolution and half-hourly temporal resolution. For the configuration of the MESH model, the topographic data are extracted based upon the Canadian Digital Elevation Data (CDED, 2016) at a scale of 1:50 000. Land cover information is acquired from the Land Cover of Canada (LCC, 2010), which is produced by the CCMEO and based on Landsat satellite images. Soil texture information comes from Soil Landscapes of Canada (SLC, 2010) data of Agriculture and Agri-Food Canada. Based on the CCMEO's dataset, seven GRU types, including forest, grass, wetland, barren land, urban, water, and glaciers have been assigned for the Liard Basin. Four soil layers with thicknesses of 0.1, 0.25, 0.75, and 3.0 m are used for this model, yielding a total thickness of 4.1 m of the soil column.

3.2.3.1. Meteorological forcing data

The MESH model is driven by a set of seven climate forcing data acquired from ECCC based on personal communication with Daniel Princz. The input forcing variables include incoming shortwave and longwave radiation; precipitation; temperature; barometric pressure; specific humidity; and wind speed. Precipitation data were acquired from the Canadian Precipitation Analysis (CaPA, Fortin *et al.*, 2018; Lespinas *et al.*, 2015; Mahfouf *et al.*, 2007), while the rest of input forcing variables were obtained from ECCC's GEM Numerical Weather Prediction (NWP) model (Côté *et al.*, 1998a; Côté *et al.*, 1998b; McTaggart-Cowan *et al.*, 2019a; McTaggart-Cowan *et al.*, 2019b).

3.2.3.2. Streamflow observations

The Streamflow observations are available from the Water Survey of Canada (WSC) website (http://www.ec.gc.ca/rhc-wsc). Three streamflow records of three stations, including Liard River at Lower Crossing, Liard River at Fort Liard, and Liard River Near the Mouth are employed for the calibration and evaluation of MESH model simulations.

3.2.4. Summary of data use

An overview of the pros and cons of different data products is summarized in Table 3.2 and Table 3.3.

Table 3.2. Pros and Cons of datasets

Dataset	Description	
	Advantage	Limitation
GRACE	1. Provide semi-continuous observations from the redistribution of water mass changes globally 2. Does not rely on surface conditions	1. Has coarse spatial and temporal resolution with a median error level around 33 mm over the Canadian landmass 2. TWSA data are vertically integrated and they are not separated into individual components (e.g., SWE) 3. In areas surrounding Hudson Bay, GRACE observations are more uncertain and exhibit considerable noises
GLDAS	1. This a NASA product that can be compared against GRACE TWSA retrievals	1. The contribution of groundwater and surface water is not considered 2. Has limitation in capturing snow mass variations in high latitudes and mountainous regions
WGHM	1. Simulate water storage changes and fluxes for all continents excluding Antarctica 2. Water storage changes in different compartments are provided (e.g., canopy, snow, soil moisture, groundwater, surface water, wetland)	1. Underestimate GRACE TWSA seasonal amplitudes by 3% with the RMSE value of 52.7 mm in northern to midlatitudes (2`0-50ºN) areas
CMC	1. The SWE analysis product is acquired from snow observations and model simulations 2. SWE gridded product is considered as one of the most useful global data sources for evaluating SWE	1. GEM precipitation in northern areas tends to be biased low, by around 0.1–0.4 mm day^{-1} 2. In northern areas (~ 55º N), snow depth observations come from coastal locations or large open areas at airports. Due to early loss of snow in the spring, the shallow bias of snow depth reported from observing sites 3. CMC understimates maximum SWE with RMSE = 81.3 mm and BIAS = -58.1 mm (over the Saint-Maurice River Basin)
GlobSnow2	1. SWE dataset is a data assimilation product by combining PMW data, ground-based observations, and model simulations 2. Data are provided at spatial resolution (~ 25 km) on a daily, weekly, and monthly temporal resolution over the Northern Hemisphere from 1979 to 2018	1. Highest SWE uncertainties were reported in both dense vegetation and deep boreal forest (SWE > 150 mm) 2. The underestimation of SWE with RMSE of 94.1 ± 20.3 mm was reported in eastern Canada 3. In northern areas observation are sparsely located

Table 3.3. Pros and Cons of datasets

Dataset	Description	
	Advantage	Limitation
AMSR-E	1. It is NASA satellite-based SWE product and is considered as one of the key science product suites for cryospheric and hydrological applications 2. It is presented in a 25×25 km spatial resolution with daily, five-day, and monthly temporal resolution	1. The accuracy of SWE is low in deep snow conditions (SWE > 60 mm) 2. An underestimation of SWE with a large RMSE value of 165.6 mm was reached in areas covering eastern Canada 3. Data shows very week SWE variability
Snow survey	1. The observations can be used to evaluate hydrological and climate model simulations	1. It is punctual and prevails local-scale variability 2. Time series of observations is not provided over a long period
MESH	1. MESH model is a community-based modeling framework developed for large scale watershed modeling 2. A Multi-modeling framework can coexist 3. It is under continuous development for current and future climate runs, water management, water quality applications	1. Some modifications are required to incorporate groundwater, small lakes, and wetland components
Climate forcing	1. An archive of pre-operational and operational CaPA products can be used for many application (weather forecasting, flood forecasting, hydropower production) 2. GEM can be deployed at resolution ranging from 1 to 10 km	1. Multiple studies identified limitations of CaPA, in particular for soild preciptation, in complex terrain and for snowpack simulation
Streamflow	1. Daily observations can be used for both the purpose of model calibration and evaluation	1. Multiple sources of uncertainties (e.g., observations of stream stage, periodic measurements, a rating curve) influence streamflow records

3.3. Methods

In this section, brief explanations on how to meet the general methodologies of the different objectives of this research are given. A more detailed description of the methodologies can be found in sections 4, 5, and 6. The general methodology of the study is summarized in Figure 3.5.

3.3.1. General methodology of Objective I

In part 1 of objective 1, gridded spatiotemporal relationship between GRACE/GLDAS and three multisource products of snow is analyzed over the Canadian landmass. First, all data sets were treated in a harmonized way. Both GRACE and GLDAS data are provided at 1º×1º spatial

resolution. The spatial resolution of SWE products, including GlobSnow2, AMSR-E, CMC was harmonized by computing the simple average of all data points falling into a 1º×1º grid cell in each case. As the mountainous areas were excluded in the GlobSnow products, a topography masking was applied to each data, including GRACE, GLDAS, AMSR-E, and CMC to exclude areas of high elevation. For the calculation of data anomalies, all available data from December to March (hereafter referred to as DJFM) are extracted. DJFM corresponds to snow accumulation period. The month of April was not considered, because of the quality of passive microwave remote sensing SWE products (melting effects). Then, the temporal means from the available DJFM for each source of data were subtracted in order to calculate corresponding data anomaly. Finally, a 1º×1º grid cell TWSA versus SWEA Pearson's correlation coefficient (R) was determined for the data sets over the time period considered. The statistical significance of the TWSA-SWEA relationship was assessed at the 95% confidence intervals.

In part 2 of objective 1, the spatial and temporal relationship between TWSA/SWEA-derived from GRACE and multisource SWEA was investigated over 15 Canadian basins. First, to consider the contribution of water storage compartments during the snow season, the time-mean WGHM water storage compartments were plotted as pie charts. Second, three processing steps, including topography masking, spatial averaging, and anomaly calculation were not only applied for GRACE derived TWSA/SWEA data but also for multisource SWE products. Then, the Spearman's rank correlation coefficient (Iman et Conover, 1979) between GRACE and GloSnow2/AMSR-E/CMC was calculated and the statistical significance of the relationship was computed based on the *t*-statistic test. Finally, an evaluation metric, such as RMSE between GRACE and each snow product was performed to evaluate the overall performance of the analysis.

3.3.2. Objective II

The MESH model was set-up for the Liard Basin. The calibration of the model was implemented using a pseudo multi-objective approach that aggregated three streamflow error metrics. The calibration was performed over October 2003 to October 2008 period. The model calibration set-up was acquired based on personal communication with Dr. Mohamed Elshamy (GIWS, University of Saskatchewan). From October 2008 to October 2014, the MESH model was run in either the Open-loop (OL, without assimilation but with perturbation) or DA mode. In this study,

the generation of ensemble members was conducted by adding perturbations to meteorological forcing and model states by following the work of Reichle and Koster (2003) and Forman *et al.* (2012).

The data assimilation method using the EnKS approach was developed for the MESH model. The DA method contains two main steps including the forecast and analysis step. In the forecast step, uncertainties in the model predictions were determined and monthly forecast prediction of GRACE TWS observations at the basin scale was computed. In the analysis step, the prior model simulations were updated daily for month *k.* This two-step procedure (forecast-analysis) was repeated for the next month until the end of the simulation.

The evaluation of both OL and DA experiments at basin-averaged and gridded spatial resolutions was performed using the Spearman's rank correlation, Percentage Bias (PBIAS), and the unbiased root-mean-square difference (ubRMSD, Entekhabi *et al.*, 2010). The performance of streamflow simulations at three stations was assessed using PBIAS, Nash-Sutcliffe Efficiency (NSE, Nash and Sutcliffe, 1970), with logarithmic transformation of NSE. Finally, two assimilation system diagnostics (ensemble spread, assimilation increment) were used to better understand the effect of GRACE observations on the model simulations.

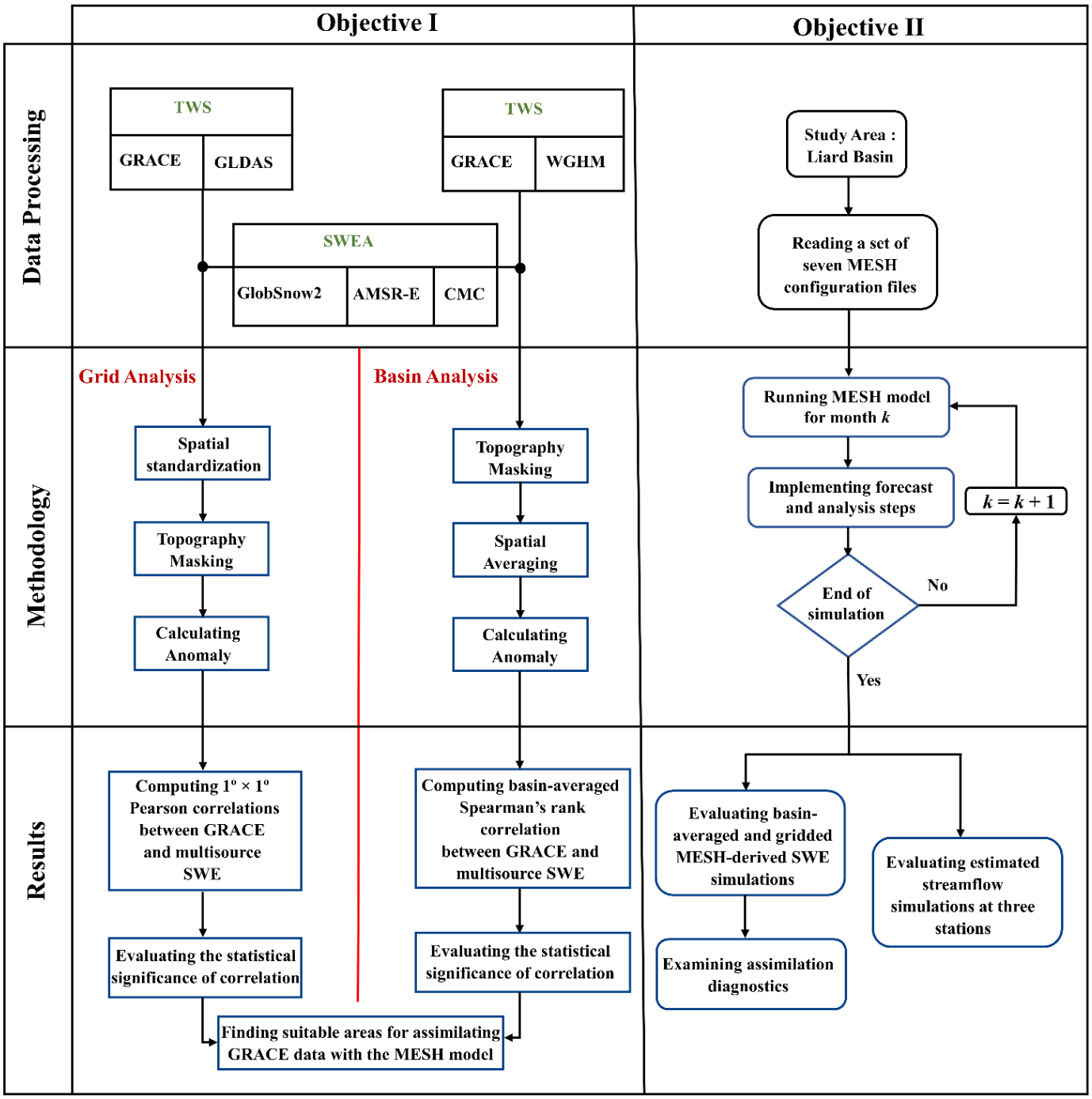

Figure 3.5. General methodology of this study

4. Understanding the Spatial and Temporal Variations of Water Storages and their Associations with Snow Water Equivalent Variabilities

4.1. Article presentation

This article is a part of the first objective of the thesis related to analyzing the spatiotemporal relationship between GRACE-derived TWS retrievals and multisource SWE products. GRACE observations and GLDAS simulations were chosen as the TWSA data sets. SWE data were extracted from three different sources: GlobSnow2, AMSR-E, and CMC. The comparison was conducted to understand the impacts of snow mass on terrestrial water storage during the winter.

The general methodology proposed to analyze the association between TWSA and SWEA is summarized in Section 3.3.1. The details of the manuscript, including the methodology and the results, are presented in the following pages.

Understanding the Spatial and Temporal Variations of Water Storages and their Associations with Snow Water Equivalent Variabilities

by Ala Bahrami, Kalifa Goïta, Ramata Magagi

To be submitted to Remote Sensing

Understanding the Spatial and Temporal Variations of Water Storages and their Associations with Snow Water Equivalent Variabilities

Ala Bahrami[1], Kalifa Goïta [1], Ramata Magagi [1]

[1] Centre d'applications et de recherches en télédétection (CARTEL), Département de géomatique appliquée, Université de Sherbrooke, Sherbrooke, Québec, Canada

Corresponding author: Ala Bahrami (ala.bahrami@usherbrooke.ca)

Abstract: Water storage changes in space and time play a major rule in the Earth's climate system via the exchange of water and energy fluxes among the Earth's water storage compartments and between atmosphere, continents, and oceans. In many parts of northern-latitude areas spring meltwater controls the availability of freshwater resources. With respect to terrestrial hydrologic processes, snow water equivalent (SWE) is the most critical snow characteristic to hydrologists and water resource managers. The main focus of this study is to examine the spatiotemporal variations of terrestrial water storages and their linkages with snow water equivalent variabilities over Canada. For the terrestrial water storage anomaly (TWSA), satellite measurements from the Gravity Recovery and Climate Experiment (GRACE) and model simulations from the Global Land Data Assimilation System (GLDAS) are used. SWE products are provided by the European Space Agency (ESA) Global Snow Monitoring for Climate Research version 2 (GlobSnow2), Advanced Microwave Scanning Radiometer-Earth Observing System (AMSR-E), and Canadian Meteorological Centre (CMC). The grid cell (1°×1°) analysis was applied to find any possible relationship between TWSA and SWE anomalies over the Canadian territory, from December 2002 to March 2011. Results show that GRACE versus CMC provided the highest percentage of significant positive correlation (62.4% of the 1128 grid cells), with an average significant positive correlation coefficient of 0.5, and a maximum of 0.9. In the western part of the country, GRACE showed better agreement with multiple SWE source than GLDAS. Yet, over eastern Canada, mainly in the northern Québec area (~ 55ºN), GRACE provided weak or insignificant correlations with all snow products, while GLDAS appeared to be significantly correlated. In general, results revealed the importance of SWE changes in association with the terrestrial water storage variations.

Keywords: GRACE, GLDAS, Snow water equivalent, Terrestrial water storage.

Résumé: Les variations du stock l'eau dans l'espace et dans le temps jouent un rôle majeur dans le système climatique de la Terre via l'échange des flux d'eau et d'énergie entre les compartiments de stockage terrestres, et entre l'atmosphère, les continents et les océans. Dans de nombreuses régions nordiques, la fonte de la neige contrôle la disponibilité des ressources en eau. Dans les processus hydrologiques terrestres, l'équivalent en eau de la neige (SWE) est la caractéristique de neige la plus importante pour les hydrologues et les gestionnaires des ressources en eau. L'objectif principal de cette étude est d'examiner les variations spatio-temporelles des stockes d'eau terrestres et leurs liens avec les variabilités de l'équivalent du SWE au Canada. Les données d'anomalies de stocks d'eau (TWSA) proviennent des mesures satellitaires de GRACE (Gravity Recovery and Climate Experiment) et des simulations du modèle GLDAS (Global Land Data Assimilation System). Les données de SWE sont extraites des produits du Global Snow Monitoring for Climate Research version 2 (GlobSnow2) de l'Agence spatiale européenne (ESA), de AMSR-E (Advanced Microwave Scanning Radiometer-Earth Observing System) et du Centre météorologique canadien (CMC). L'analyse par cellule de grille (1°×1°) est appliquée pour trouver toute relation possible entre TWSA et SWEA sur le territoire canadien, de décembre 2002 à mars 2011. Les résultats montrent que GRACE par rapport à CMC fourni le pourcentage le plus élevé de corrélation positive significative (62,4% des 1128 cellules de la grille), avec un coefficient de corrélation positif significatif moyen de 0,5 et un maximum de 0,9. Dans la partie ouest du pays, GRACE a montré un meilleur accord avec les autres sources de données SWE contrairement à GLDAS. Et, dans l'est du Canada, principalement dans le nord du Québec (~ 55° N), GRACE fourni des corrélations faibles ou insignifiantes avec tous les produits de la neige; tandis que GLDAS semblait être significativement corrélé. De façon générale, les résultats révèlent le contrôle important du SWE sur les variations du stock total d'eau terrestre.

Mots-clés : GRACE, GLDAS, Équivalent en eau de la neige, Stock d'eau terrestres

4.2. Introduction

Global observations of water and ice mass distribution at monthly to decadal time scales are crucial for the forecast of climate change, weather, biological and agricultural productivity, flooding, and a wide variety of studies in the geoscience (Rodell et al., 2004; Tapley et al., 2019). Thus, the global sustainable management of water resources may be one of the critical challenges for this century (Rodell et al., 2018). Terrestrial water storage (TWS) as a major variable of the Earth's water cycle is defined as the summation of key hydrologic reservoirs, including soil water, surface and subsurface water, snowpack and biomass water storage (Famiglietti and Rodell, 2013). Snow as one of the most noticeable elements of the hydrologic cycle has considerable influence on the weather and climate systems (Cohen and Entekhabi, 1999). In many parts of northern-latitude areas, as well as the mountainous regions, spring meltwater controls the availability of freshwater resources for approximately more than one-sixth of the world's population (Barnett et al., 2005; Déry et al., 2005; Stieglitz et al., 2001). With respect to terrestrial hydrologic processes, snow water equivalent (SWE) is one of the important parameters for climatology and hydrology (Foster et al., 2011). Therefore, the accurate estimation of SWE over space and time is required.

Among satellite measurement techniques, the Gravity Recovery and Climate Experiment (GRACE, Tapley et al., 2004) has provided a unique component to the existing suite of Earth observations by measuring the redistribution of terrestrial water storage anomaly (TWSA) around the world. GRACE compared to other satellite-based instruments, such as passive microwave sensors, has this advantage that it does not rely on surface conditions and can detect accumulated water storage without the need of empirical parametrization and ground-based calibration (Behrangi et al., 2018). In the snow-covered regions, the seasonal component of TWSA is dominated by the snow mass anomaly (Bahrami et al., 2020).

GRACE TWS retrievals were used for the purpose of SWE estimations (Frappart et al., 2011, 2006; Niu et al., 2007; Ramillien et al., 2005). The results of these studies highlighted the importance of GRACE observation to quantify the contribution of snow mass changes to terrestrial water storage changes. Based on the mass conservation approach, GRACE TWSA retrievals are used to estimate cold-season precipitation (Behrangi et al., 2018, 2017; Seo et al., 2010; Swenson, 2010). Bahrami et al. (2020) examined the linkage between GRACE TWSA retrievals and

multisource snow water equivalent anomaly (SWEA) data sets at the basin scale and found important insights on the patterns of TWSA-SWEA association.

GRACE data have been used to address the land surface and hydrological model estimates. The integration of GRACE-derived TWSA observations within a land-data assimilation system has proven valuable for improving the accurate estimation of snow budgets (Forman et al., 2012; Kumar et al., 2016; Su et al., 2010; Van Dijk et al., 2014).

In this study, it is hypothesized that a strong correlation between TWSA and SWEA is found whether the variability of SWE contributes mainly to TWS change during the cold season. The objective of this research focuses on the spatial and temporal relationships between TWSA derived from GRACE, as well as Global Land Assimilation System (GLDAS), and multisource SWE anomalies. SWE data were extracted from three different sources: the European Space Agency (ESA) Global Snow Monitoring for Climate Research (version 2.0 – GlobSnow2), the Advanced Microwave Scanning Radiometer-Earth Observing System (AMSR-E), and the Canadian Meteorological Centre (CMC). The comparison was conducted to understand the impacts of snow mass on terrestrial water storage during the winter.

4.3. Study area and data

4.3.1. Domain of study

The Canadian landmass with the exclusion of the arctic latitudes and areas of high elevation between 42°N to 72°N latitude, and 141°W to 54°W longitude was selected as the study area. Following the objective of this study, gridded GRACE/GLDAS-derived TWSA data along with multiple SWE data sources are used to analyze the TWSA-SWEA spatiotemporal relationship. Here, the geophysical property based upon the land-cover classification is shown in Figure 4.1. Land cover information is acquired from the Land Cover of Canada (LCC, 2010), which is based on Landsat satellite images.

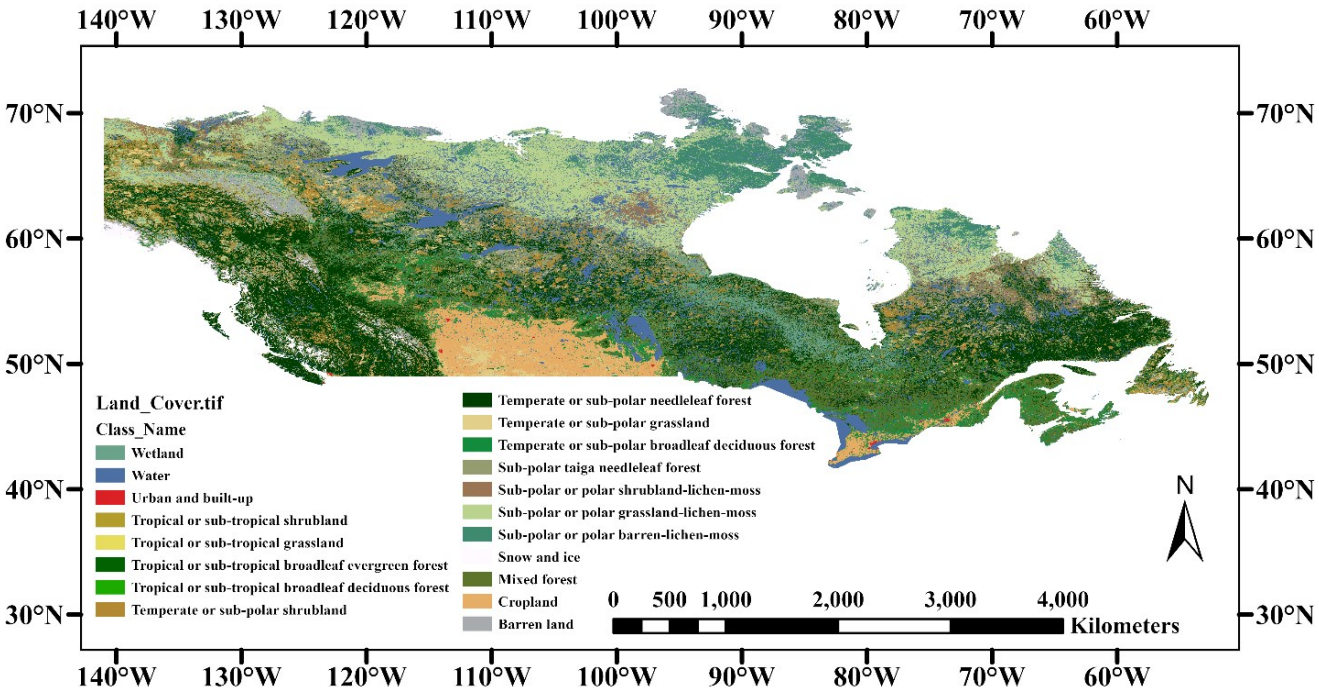

Figure 4.1. Map of study domain. Nineteen land-cover classes cover the study area.

4.3.2. Terrestrial Water Storage Data

4.3.2.1. GRACE TWSA

The aim of the GRACE project was to monitor time-variable components of the Earth's gravity field variations to track mass distribution on a large scale in the hydrosphere, cryosphere, oceans, and mass distribution associated with glacial isostatic adjustment (GIA) and earthquakes (Tapley et al., 2004). The hydrological signal detected by GRACE can provide the column integrated TWSA product with a surface spatial resolution of about 330 km at low latitudes (Cooley and Landerer, 2019) with an accuracy of 1.5 cm equivalent water height (Famiglietti and Rodell, 2013). Different filters are applied to land and ocean grids to best filter out noise while preserving real geophysical signals (Cooley and Landerer, 2019). To restore the signal loss as a result of processing, Landerer and Swenson (2012) provided scaling gain factors. Gridded (1°×1°) scaling factors, as long as post-processed GRACE retrievals can be accessed via the Jet Propulsion Laboratory (JPL)'s GRACE Tellus website (available at https://podaac-tools.jpl.nasa.gov). Monthly satellite gravimetric solutions are found in the JPL, the Center for Space Research (CSR) of the University of Texas at Austin, and the GeoforschungsZentrum Potsdam (GFZ) of Germany. Each center uses parameter choices and solution strategies to convert relative ranging

observations between twin satellites to gravity changes. In this study, the GRACE-derived TWSA level-3 gridded (1°×1°) data were used. For the purpose of noise reduction, the ensemble product from the arithmetic mean of all three processing centers was employed (Sakumura et al., 2014).

4.3.2.2. GLDAS

The GLDAS terrestrial water content used was from NOAH Land Surface Model, version 2.7.1 (Chen et al., 1996; Koren et al., 1999), within the GLDAS system (Rodell et al., 2004). The Model TWS simulations were calculated by summing different water compartments, including intercepted precipitation by the canopy, snowpack, and soil moisture. Noted that in the GLDAS-NOAH model estimates, groundwater and surface water are not simulated. The GLDAS-derived TWS simulations are provided at 1°×1° spatial resolution on a monthly temporal resolution. In this study, GLDAS TWS data related to snow season (December to March) was used for the period from December 2002 to April 2011. The GLDAS land water content datasets are chosen for this reason that they are directly comparable to GRACE total water storage changes. It is interesting to investigate whether the association between GLDAS and multisource SWE provides the same patterns as GRACE. Some patterns of the spatiotemporal discrepancy from the relationship between GRACE versus multisource SWE and GLDAS versus snow products may be observed. Note that it is expected that the GLDAS total water storage estimates deviate from GRACE TWSA retrievals as groundwater and separate surface water components (such as rivers and lakes) were not included in NOAH model simulations.

4.3.3. Snow Water Equivalent Products

SWE products come from different sources, briefly presented below. A summary of the products used is given in Table 4.1.

4.3.3.1. CMC SWE product

Monthly mean estimates of SWE are considered in this study. These values were obtained from monthly averaged snow depth analyses using the corresponding mean monthly snow density values (Brown and Brasnett, 2010). Snow density values were based on the Canadian snow course observations corresponding to snow-climate classes in the Sturm et al. (1995) classification. This

monthly data set is provided at a horizontal resolution of 0.25°×0.25° (~24 km × ~24 km) over the Northern Hemisphere, and it can be accessed through the National Snow and Ice Data Center (NSIDC). Despite some limitations of the CMC SWE data set, such as scarcity of observations in the northern latitudes, the products are frequently used for evaluating land surface models (LSMs), reanalyses, and remote sensing products (Brown et al., 2018; Forman et al., 2012; Mudryk et al., 2015; Reichle et al., 2017, 2011; Toure et al., 2016; Verseghy et al., 2017).

4.3.3.2. GlobSnow2 SWE product

Monthly GlobSnow2 SWE product was used as another source of SWE data sets. GlobSnow2 SWE, as a data assimilated product, is obtained from a combination of ground-based weather station data, passive microwave remote sensing observations, and model estimates (Takala et al., 2011). The SWE data is projected into Equal-Area Scalable Earth Grid (EASE-Grid), and covers the terrestrial non-mountainous regions of Northern hemisphere, with the exception of glaciers and Greenland. SWE data are provided at a spatial resolution of 25 km × 25 km. Data products are available by the Finnish Meteorological Institute website (http://www.globsnow.info/swe).

4.3.3.3. AMSR-E SWE data

Monthly level-3 AMSR-E SWE product was used in this study. SWE retrievals were performed based on methods described in Chang et al. (1987) and Kelly (2009). This algorithm retrieves SWE using the simple brightness temperature difference at 19 and 37 GHz. Monthly SWE data are projected to the 25 km the Equal-Area Scalable Earth Grids (EASE-Grids) domain and they are available through the NSIDC website (Tedesco et al., 2004). A number of studies on the assessment of AMSR-E data, reported that SWE retrievals were underestimated compared to validation data (Tedesco et al., 2004; Tedesco and Narvekar, 2010).

Table 4.1. Summary of the SWE data sets used in this study.

Dataset	Description	Resolution	Domain
CMC	SWE estimates are derived from monthly snow depth analyses and snow density lookup table	0.25°×0.25° (~24 km × ~24 km)	Northern Hemisphere
GlobSnow2	SWE retrievals are obtained from a combination of ground-based, satellite-based observations, and model estimates	25 km × 25 km	Between 35° to 85° northern latitudes (except for glaciers and Greenland)
AMSR-E	SWE product was obtained from empirical equations obtained from remote sensing observations	25 km × 25 km	Northern and Southern Hemisphere

4.4. Methods

The grid-based analysis depicts a comprehensive image of the linkage between TWSA versus SWEA covering the entire domain of study with various geophysical characteristics. The methodology proposed to analyze the association between TWSA and SWEA (e.g., GRACE and GlobSnow2) is summarized in Figure 4.2. TWSA data from GRACE/GLDAS were compared to SWEA data from three different sources respectively: GlobSnow2, AMSR-E, and CMC.

In the spatial standardization step, the spatial resolution of all data sets was equalized in order to represent the same grid format. Both monthly GRACE and GLDAS data were provided at a spatial resolution of 1°×1° (latitude-longitude). Monthly SWE products including GlobSnow2, AMSR-E, and CMC were interpolated on the 1° grid cell spatial resolution using the nearest-neighbor approach. In the masking step, the lake/mountain mask was applied to GRACE/GLDAS and multisource SWE datasets. Grid cells that fall inside large lakes or mountainous areas with a height standard deviations above 200 m were masked out (Takala et al., 2011), as the GlobSnow SWE products were not reliable in those areas.

The grid cell anomaly calculation for each data source was done individually. This process consisted of two main steps. First, the time-baseline from December 2002 to March 2011 was selected. Second, only monthly data corresponding to a snow season from December to March

(hereafter referred to as DJFM) was considered. Based on the time-baseline of study (2002-2011), a total number of nine snow seasons covered the period of study. For months when GRACE data were not available (e.g., January 2001), missing values were assigned. Then, the time-mean field for each grid cell was calculated. Finally, this time-mean grid was subtracted from all monthly DJFM data.

A grid-by-grid TWSA versus SWEA Pearson's correlation coefficients (R) were calculated for the data sets over the time period considered. The statistical significance of correlation results was assessed at the 95% confidence interval. Then, results were categorized into two groups, including significant (p-value < 0.05) and no-significant R (p-value ≥ 0.05). Possible reasons for disagreement, such as weak correlations (near zero) were discussed.

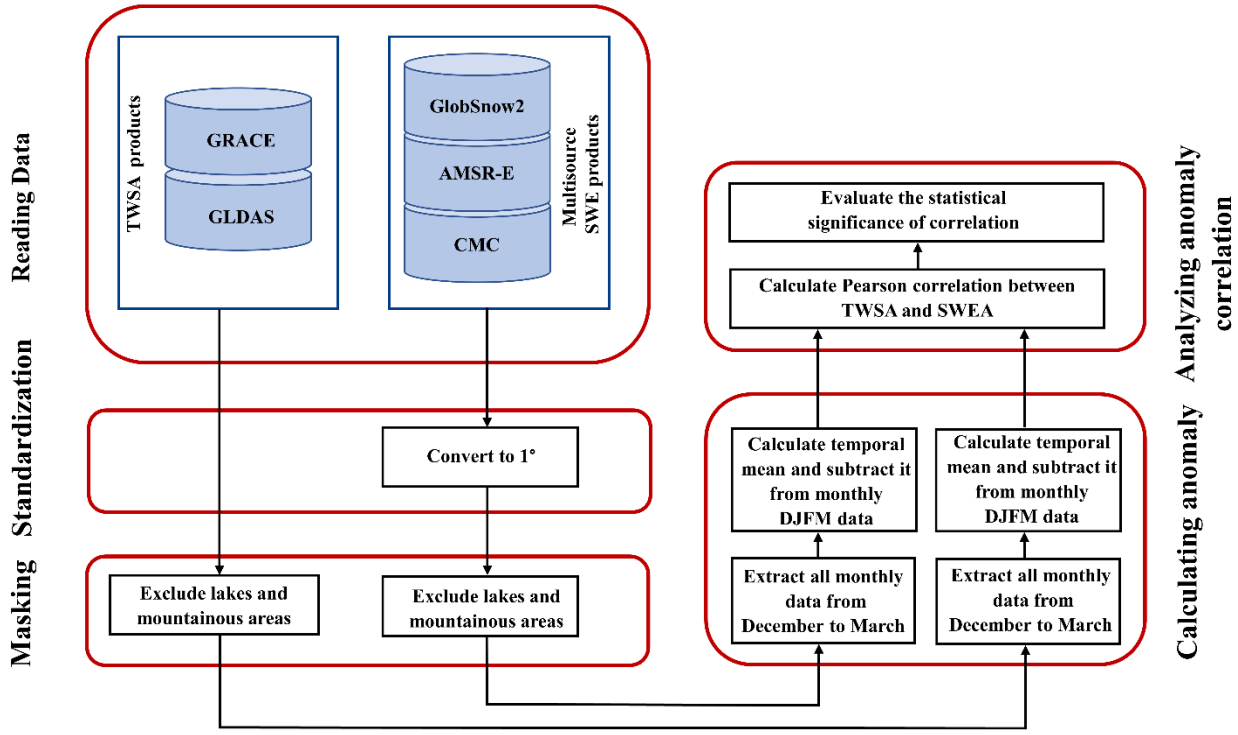

Figure 4.2. Flowchart for analyzing the TWSA-SWEA relationship.

4.5. Results

The grid-by-grid association between TWSA and SWEA was examined over the Canadian territory. TWSA data derived from GRACE/GLDAS were compared against GlobSnow2,

AMSR-E, and CMC SWEA during the cold season. The results are summarized in Figure 4.3, Figure 4.4, and Table 4.2.

4.5.1. GRACE against GlobSnow2

Figure 4.3(a) and Figure 4.4(a) present grid cell anomaly correlation and its associated p-value results between GRACE and GlobSnow2. Table 4.2 shows the summary of gridded significant Pearson's correlation results. The correlation values range from 0.3 to 0.7, with an average of 0.5. The results indicate a significant relationship between GlobSnow2 and GRACE observations for 56.8% of the grid cells covering the unmasked area of the territory. Insignificant results are found mainly in the northern and central Québec-Labrador area as well as a region covering partly western Hudson Bay. It can be seen in Table 4.2 that GRACE versus GlobSnow2 provided no data for negative significant correlation.

4.5.2. GRACE against AMSR-E

The gridded correlation analyses and the related p-values between GRACE and AMSR-E are shown in Figure 4.3(c) and Figure 4.4(c). The summary of the statistics is given in Table 4.2. Significant correlations vary between 0.7 and 0.3. The average significant positive correlation between GRACE TWSA and SWEA is 0.5. A total of 52.2% of the grid cells show significant associations between GRACE and AMSR-E. These statistics in terms of correlation and spatial distribution are quite similar to the GRACE-GlobSnow2 analysis results. With the exception of northern and central Québec and western Hudson Bay, AMSR-E agreed favorably with GRACE.

4.5.3. GRACE against CMC

Results between GRACE TWSA and CMC SWEA are shown in Figure 4.3(e) and Figure 4.4(e). Table 4.2 provides a summary of statistical analyses. Positive significant correlation values range from 0.3 to 0.9. Compared to GlobSnow2 and AMSR-E, stronger correlations are found between GRACE and CMC for 62.4% of the grid cells covering the region of study. However, we observe also some negative, but significant correlations, ranging from -0.5 to -0.3, for few grid cells (1.7%) located mainly at western Hudson Bay. Overall, GRACE observations during the cold season agree favorably with CMC SWE analysis product, except in areas located at northern Québec (~ 55º), western Hudson Bay, and Northwest Territories.

4.5.4. GLDAS against GlobSnow2

Figure 4.3(b) and Figure 4.4(b) illustrate correlation and p-value results between GLDAS and GlobSnow2 at 1º×1º gridded spatial resolution. As shown in Table 4.2, significant positive correlation values fall within the range of 0.3 to 0.9 (with an average value of 0.6) for 47% of the grid cells. Here also, we find significant negative correlations, ranging from -0.6 to -0.3, for a few grid cells (1.5%), especially in the western Hudson Bay. We can observe a significant relationship between GLDAS and GlobSnow2 in areas covering the eastern portion of Canada, especially the northern Québec and Labrador area as well as southwestern Hudson Bay. Several grid cells in the western region of the country show insignificant association, which is not the case when GRACE data are used.

4.5.5. GLDAS against AMSR-E

The correlations and p-values between GLDAS and AMSR-E are shown in Figure 4.3(d) and Figure 4.4(d), respectively. A summary of the statistics can be found in Table 4.2. Positive significant correlations range from 0.3 to 0.8, which are found in 39.8% of the grid-cells. Negative significant correlations vary from -0.5 to -0.3, but for only 1.6% of the grid cells. In general, moderate agreements between GLDAS and AMSR-E are found, with the exception of grid cells situated in the northeastern Hudson Bay and scattered areas located at the western part of the country.

4.5.6. GLDAS against CMC

The analysis results between GLDAS and CMC (Table 4.2) show that the significant positive correlation values fall within the range of 0.3 to 0.9, with an average value of 0.5. Overall, GLDAS TWSA agrees well with CMC during the snowfall season. A positive significant correlation is found in 47% of the grid cells. Significant negative relationship is found in about 3% of the grid cells, located mainly in the western Hudson Bay and around Slave Lake in northern Alberta.

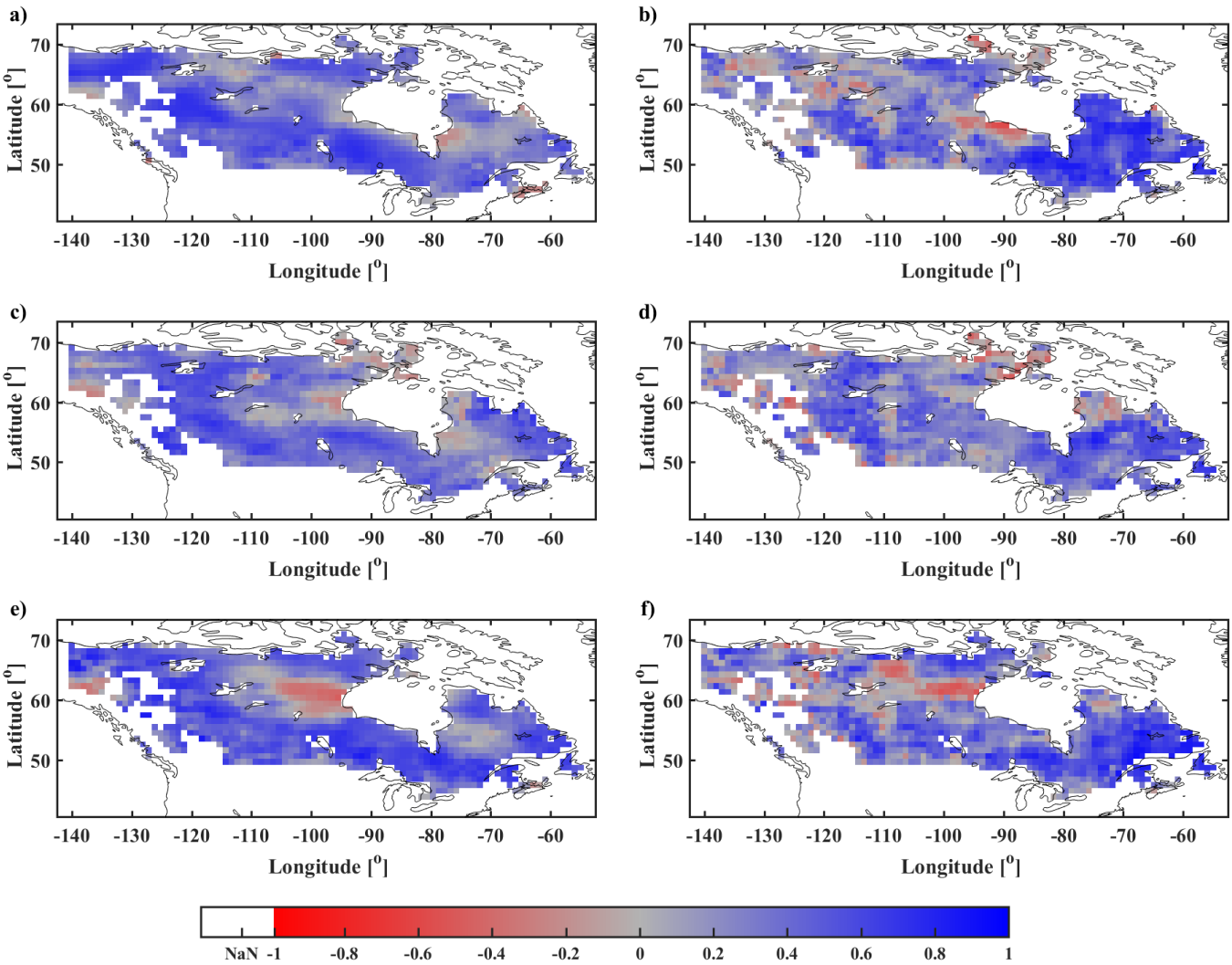

Figure 4.3. Gridded correlation coefficient analysis between GRACE/GLDAS-derived TWSA and GlobSnow2/AMSR-E/CMC-derived SWEA: (a) results for GRACE and GlobSnow2; (b) results for GLDAS and GlobSnow2: (c) results for GRACE and AMSR-E: (d) results for GLDAS and AMSR-E: (e) results for GRACE and CMC: (f) results for GLDAS and CMC.

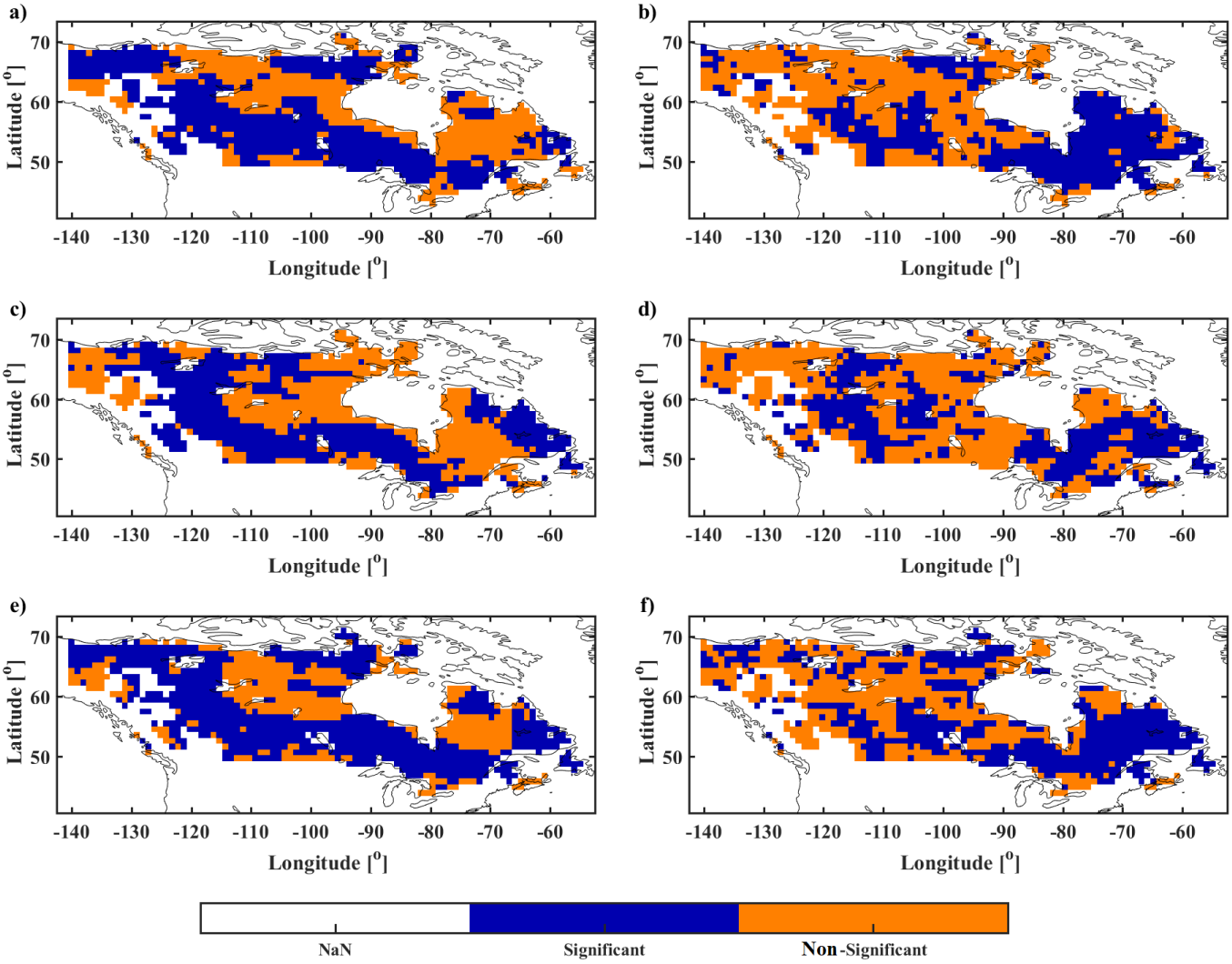

Figure 4.4. Gridded p-value analysis between GRACE/GLDAS-derived TWSA and GlobSnow2/AMSR-E/CMC-derived SWEA: (a) results for GRACE and GlobSnow2; (b) results for GLDAS and GlobSnow2: (c) results for GRACE and AMSR-E: (d) results for GLDAS and AMSR-E: (e) results for GRACE and CMC: (f) results for GLDAS and CMC.

Table 4.2. Summary of gridded correlation statistics of the comparison between GRACE/GLDAS-derived TWSA and SWEA from GlobSnow2, AMSR-E, and CMC.

	Total number of grid cells over the Canadian land mass	Range of observed Pearson correlation	% of grid cells with significant correlation	Range of significant positive correlation	Average significant positive correlation	% of grid cells with significant positive correlation	Range of negative significant correlation	Average negative significant correlation	% of grid cells with negative significant correlation
GRACE - GlobSnow2	1128	(0.3 – 0.7)	56.8	(0.3 – 0.7)	0.5	56.8	-	-	-
GRACE - AMSR-E	1128	(0.3 – 0.7)	52.2	(0.3 – 0.7)	0.5	52.2	-	-	-
GRACE - CMC	1128	(-0.5 – 0.9)	64.1	(0.3 – 0.9)	0.5	62.4	(-0.5) – (-0.3)	-0.4	1.7
GLDAS - GlobSnow2	1128	(-0.6 – 0.9)	48.5	(0.3 – 0.9)	0.6	47.0	(-0.6) – (-0.3)	-0.4	1.5
GLDAS - AMSR-E	1128	(-0.5 – 0.8)	41.4	(0.3 – 0.8)	0.5	39.8	(-0.5) – (-0.3)	-0.4	1.6
GLDAS - CMC	1128	(-0.5 – 0.9)	50.0	(0.3 – 0.9)	0.5	47.0	(-0.5) – (-0.3)	-0.4	3.0

4.6. Discussion

Regarding the gridded correlation results of GRACE-derived TWSA versus GlobSnow2/AMSR-E/CMC SWEA data, it appears that GRACE TWS anomalies are generally quite linked to SWE variations during the cold season. Stronger correlation values can be found in the areas with important snowfall. These findings are consistent, to some extent, with works of Frappart et al. (2006; 2011) who achieved strong GRACE-derived SWE signal over western Canada. They indicated that GRACE contains valuable information about the spatiotemporal changes of snow mass. Positive and significant correlation results are found mainly in southern Québec, Ontario and the Canadian Prairies. In areas where significant positive correlations are found between GRACE TWSA and GlobSnow2, AMSR-E, and CMC SWEA, the snow mass changes appear as an important component of TWS variabilities. However, in the northern Québec, Labrador, and western Hudson Bay areas, with weak and insignificant or even negative correlation values, different possible reasons may influence the relationships.

Due to GRACE measurement errors, including systematic (Swenson and Wahr, 2006) and random (Wahr et al., 2006), the glacial isostatic adjustment (GIA, Geruo et al., 2013), signal

leakage errors (Landerer and Swenson, 2012), as well as background model corrections, a set of nontrivial processing steps are applied to GRACE observation data products in order to be used in hydrological applications. The uncertainties and errors of GRACE observations are inherited from these processing steps (Cooley and Landerer, 2019).

GRACE TWSA signal can be decomposed into long-term (linear and inter-annual), seasonal, and sub-seasonal residual components based on the methodology mentioned by Humphrey et al. (2016). Each of these components is a signal of great scientific interest based on the application. GRACE observation tracks valuable information regarding ice-load histories, particularly near the locations of Hudson Bay areas. The secular trends have been removed from GRACE mass grid products based on the GIA model corrections by Geruo et al. (2013). However, the GIA corrections add some uncertainty in the estimation of surface mass changes. Lambert et al. (2013) found that the GIA correction using models were deficient and suggested to adjust GIA effects by using GPS vertical velocities. Another issue which should be considered is the dominance of the seasonal and residual component of the total water storage signal. A study conducted by Scanlon et al. (2019) showed that GRACE TWSA seasonal signal dominates other temporal components, accounting for 40%-80% of the signal regarding the region of study. It might be possible in the northern Québec and western Hudson Bay, where poor associations between GRACE and multisource SWE were found, the sub-seasonal component of signal is dominant. Therefore, the treatment of GRACE observations in these areas should be carried out carefully.

Based on the gridded analysis results, compared to GRACE moderate associations between GLDAS and multisource SWE data sets are found. Strong correlation values are found mainly in the Québec-Labrador area. This region, after the western Rocky Mountains, has the second-largest seasonal snow accumulation over Northern America (Verseghy et al., 2017). In areas where strong to moderate correlations are obtained, GLDAS derived-TWS anomalies vary in proportion to SWE changes. Furthermore, results obtained with GLDAS show a dependency on the latitudinal variations. Weak or insignificant correlation results between GLDAS and snow mass datasets are mainly concentrated in higher latitudes (> 55° N).

In this study, the errors of GRACE TWSA are considered to be spatially uncorrelated. This means that the errors in nearby pixels are not addressed, i.e. assuming white noise for GRACE TWSA

errors. The interpretation of how the correlated GRACE errors affect the gridded analysis results was not considered. Therefore, a correlation test between adjacent GRACE pixels could be conducted to verify how the consideration of GRACE TWSA autocorrelation errors influences the grid-based analysis result, especially in the case of GRACE versus multisource SWEA products.

Snow simulation results that were obtained in this study are consistent with Mudryk et al. (2015). They used different SWE products from three reanalysis-based datasets, GlobSnow2 and GLDAS-NOAH 3.3 model. They calculated the multi dataset mean correlation from pairs of SWE time series and found moderate correlation results in Canada. The spatial pattern of the correlation results between GLDAS and GlobSnow2 is consistent, to some extent, with their findings. Correlation results between GLDAS and multiple snow products may be affected by the shortcoming and uncertainty of GLDAS simulations. The major sources of errors in the estimation of GLDAS-derived TWS and its components are related to the quality of input forcing data, model physical parameterization, calibrated model parameters, and land surface characteristics data. First, a simple snow layer scheme is implemented in the NOAH 2.7.1 model. This simple snow model cannot capture snow mass variations, especially in high latitudes and mountainous regions over western Canada domain (Mudryk et al., 2015; Syed et al., 2008). The other possible reasons may be related to the contribution of water storage compartments which are not simulated in the GLDAS estimates. GLDAS also has limitations in capturing seasonal variations in monthly TWS changes compared to GRACE (Wang et al., 2016). Inconsistent association between GLDAS and SWE products in the northern latitudes, such as snow-covered areas of Northwest Territories may be related to this deficiency.

It is worth mentioning that, in addition to the limitations inherent to GRACE and GLDAS, the uncertainty of SWE products may influence the correlation results. Remote passive microwave SWE retrievals have still large uncertainties because of dense vegetation, wet snow, and deep snow conditions. Larue et al. (2017) validated the GlobSnow2 SWE values in comparison to in-situ SWE measurements in eastern Canada and found that GlobSnow2 underestimates the SWE estimates. They found a root mean square error (RMSE) of 94.1 ± 20.3 mm which is significantly higher than the objective value of 40 mm. Zhou et al. (2014) and Verseghy et al. (2017) found that GlobSnow2 appeared unreliable in the Québec-Labrador region because of signal saturation

for SWE values greater than 150 mm. Tedesco and Narvekar (2010) evaluated AMSR-E SWE retrievals with the Snow Data Assimilation System (SNODAS) SWE values and found a poor correlation between AMSR-E and SNODAS. Larue et al. (2017) also assessed AMSR-E SWE compared to in-situ observations from 2002 to 2009 over eastern Canada. Regarding their results, AMSR-E showed weak performance with the tendency to underestimate SWE (RMSE = 165.6 mm). For CMC SWE product, it is well-known that SWE estimations are not reliable in some areas, particularly in high latitudes, where surface snow depth observations are sparsely located and are unlikely to be representative of snow cover over the prevailing land cover (Brown et al., 2010). Brown et al., (2018) evaluated the annual maximum SWE (SWEM) based on manual gravimetric snow surveys over the Saint-Maurice River basin in southern Québec. They found that CMC underestimates SWEM over the study domain (RMSE = 81.3 mm, BIAS = -58.1 mm, R = 0.53). However, it is able to capture the interannual variability in regionally averaged SWEM. The poor correlation obtained from CMC SWE and GlobSnow in northern latitudes may be related to the reliance of these datasets on the real-time surface snow depth observations.

4.7. Conclusions

This paper analyzed the relationship between terrestrial water storage anomalies derived from GRACE and GLDAS (NOAH 2.7.1 land surface model), and snow water equivalent anomalies from three different sources (GlobSnow2, AMSR-E, and CMC) over the Canadian landmass from 2002 to 2011. The analysis was performed on a gridded (1°×1° grid cells) spatial resolution.

The results indicated significant relationships between GRACE and SWE anomalies for 52% to 62% of the grid cells covering the study area, depending on the SWE product used. The highest results were obtained with CMC SWE anomalies. With GLDAS, the percentage of significant relationships varied from 40% of the grid cells for AMSR-E product to 47% for both GlobSnow2 and CMC. This indicates a less dependency of GLDAS total water storage variations to SWE, compared to GRACE.

Overall, results highlight the important role of SWEA on TWS variations during the cold season. The analyses present insights into patterns of TWS and SWE anomalies relationships. In general, higher correlation values were found mainly in areas with dominant snow mass. GRACE correlated better with GlobSnow2, AMSR-E, and CMC data than GLDAS except in eastern

Canada. Indeed, in northern Québec, although the snow accumulation is high during the winter season, GRACE did not show consistent variations in comparison to SWE anomalies. The poor association obtained between GRACE and SWE products in particular areas (e.g., western Hudson Bay, northern Québec and Labrador) may be explained also by uncertainties of GRACE observations, the effects of GIA correction, the presence of sub-seasonal component of signal, and uncertainties of SWE datasets.

GRACE and GLDAS appeared as complementary sources of TWS data. However, the linkage between GRACE and SWE products was better than GLDAS, particularly over western Canada. Therefore, GRACE data may have the potential for validating and improving global and regional land surface models in these areas. Obviously, further works are required to consider the temporal decomposition of GRACE signal into its components. Undoubtedly, proper treatment of signal contamination from nearby land hydrology and adjusted GIA effects should be considered carefully.

Acknowledgment

The authors would like to thank the Natural Sciences and Engineering Research Council of Canada (NSERC) for the financial support of this project. We thank NASA MEaSUREs Program for supporting GRCTellus data. We are grateful to Goddard Earth Sciences Data and Information Services Center for providing GLDAS data, the National Snow and Ice Data Center for distributing CMC snow water equivalent data, as well as the Meteorological Service of Canada for supporting CMC data products.

References

Bahrami, A., Goïta, K., Magagi, R., 2020. Analyzing the contribution of snow water equivalent to the terrestrial water storage over Canada. Hydrol. Process. 34, 175–188. https://doi.org/10.1002/hyp.13625

Barnett, T.P., Adam, J.C., Lettenmaier, D.P., 2005. Potential impacts of a warming climate on water availability in snow-dominated regions. Nature 438, 303–9. https://doi.org/10.1038/nature04141

Behrangi, A., Gardner, A.S., Reager, J.T., Fisher, J.B., 2017. Using GRACE to constrain

precipitation amount over cold mountainous basins. Geophys. Res. Lett. 44, 219–227. https://doi.org/10.1002/2016GL071832

Behrangi, A., Gardner, A., Reager, J.T., Fisher, J.B., Yang, D., Huffman, G.J., Adler, R.F., 2018. Using GRACE to estimate snowfall accumulation and assess gauge undercatch corrections in high latitudes. J. Clim. 31, 8689–8704. https://doi.org/10.1175/JCLI-D-18-0163.1

[dataset] Brown, R., Brasnett, B., 2010. Canadian Meteorological Centre (CMC) Daily Snow Depth Analysis Data, Version 1. National Snow and Ice Data Center. https://doi.org/https://doi.org/10.5067/W9FOYWH0EQZ3

Brown, R., Derksen, C., Wang, L., 2010. A multi-data set analysis of variability and change in Arctic spring snow cover extent, 1967-2008. J. Geophys. Res. Atmos. 115, 1–16. https://doi.org/https://dx.doi.org/10.1029/2010JD013975

Brown, R., Tapsoba, D., Derksen, C., 2018. Evaluation of snow water equivalent datasets over the Saint-Maurice river basin region of southern Québec. Hydrol. Process. 32, 2748–2764. https://doi.org/10.1002/hyp.13221

Chang, A.T.C, Foster, J.L, Hall, D.K., 1987. Nimbus-7 SMMR Derived Monthly Global Snow Cover and Snow Depth. Ann. Glaciol. 9, 39–44. https://doi.org/https://doi.org/10.3189/S0260305500200736

Chen, F., Mitchell, K., Schaake, J., Xue, Y., Pan, H.-L., Koren, V., Duan, Q.Y., Ek, M., Betts, A., 1996. Modeling of land surface evaporation by four schemes and comparison with FIFE observations. J. Geophys. Res. Atmos. 101, 7251–7268. https://doi.org/https://dx.doi.org/10.1029/95JD02165

Cohen, J., Entekhabi, D., 1999. Eurasian snow cover variability and northern hemisphere climate predictability. Geophys. Res. Lett. https://doi.org/10.1029/1999GL900200

Cooley, S.S., Landerer, F.W., 2019. GRACE/GRACE-FO Level-3 Data Product User Handbook. California.

Déry, S.J., Sheffield, J., Wood, E.F., 2005. Connectivity between Eurasian snow cover extent and Canadian snow water equivalent and river discharge. J. Geophys. Res. 110, 1–14. https://doi.org/https://dx.doi.org/10.1029/2005JD006173

Famiglietti, J.S., Rodell, M., 2013. Environmental science. Water in the balance. Science 340, 1300–1. https://doi.org/https://dx.doi.org/10.1126/science.1236460

Forman, B.A., Reichle, R.H., Rodell, M., 2012. Assimilation of terrestrial water storage from GRACE in a snow-dominated basin. Water Resour. Res. 48, 1–14. https://doi.org/10.1029/2011WR011239

Foster, J.L., Hall, D.K., Eylander, J.B., Riggs, G.A., Nghiem, S. V., Tedesco, M., Kim, E., Montesano, P.M., Kelly, R.E.J., Casey, K.A., Choudhury, B., 2011. A blended global snow product using visible, passive microwave and scatterometer satellite data. Int. J. Remote Sens. 32, 1371–1395. https://doi.org/10.1080/01431160903548013

Frappart, F., Ramillien, G., Biancamaria, S., Mognard, N.M., Cazenave, A., 2006. Evolution of high-latitude snow mass derived from the GRACE gravimetry mission (2002–2004). Geophys. Res. Lett. 33, 1–5. https://doi.org/https://dx.doi.org/10.1029/2005GL024778

Frappart, F., Ramillien, G., Famiglietti, J.S., 2011. Water balance of the Arctic drainage system using GRACE gravimetry products. Int. J. Remote Sens. 32, 431–453. https://doi.org/https://dx.doi.org/10.1080/01431160903474954

Geruo, A., Wahr, J., Zhong, S., 2013. Computations of the viscoelastic response of a 3-D compressible Earth to surface loading: an application to Glacial Isostatic Adjustment in Antarctica and Canada. Geophys. J. Int. 192, 557–572. https://doi.org/https://dx.doi.org/10.1093/gji/ggs030

Humphrey, V., Gudmundsson, L., Seneviratne, S.I., 2016. Assessing Global Water Storage Variability from GRACE: Trends, Seasonal Cycle, Subseasonal Anomalies and Extremes. Surv. Geophys. 37, 357–395. https://doi.org/https://dx.doi.org/10.1007/s10712-016-9367-1

Kelly, R., 2009. The AMSR-E Snow Depth Algorithm: Description and Initial Results. J. Remote Sens. Soc. Japan 29, 307–317. https://doi.org/https://dx.doi.org/10.11440/rssj.29.307

Koren, V., Schaake, J., Mitchell, K., Duan, Q.-Y., Chen, F., Baker, J.M., 1999. A parameterization of snowpack and frozen ground intended for NCEP weather and climate models. J. Geophys. Res. Atmos. 104, 19569–19585. https://doi.org/https://dx.doi.org/10.1029/1999JD900232

Kumar, S.V., Zaitchik, B.F., Peters-Lidard, C.D., Rodell, M., Reichle, R., Li, B., Jasinski, M.,

Mocko, D., Getirana, A., De Lannoy, G., Cosh, M.H., Hain, C.R., Anderson, M., Arsenault, K.R., Xia, Y., Ek, M., 2016. Assimilation of Gridded GRACE terrestrial water storage estimates in the North American land data assimilation system. J. Hydrometeorol. 17, 1951–1972. https://doi.org/https://dx.doi.org/10.1175/JHM-D-15-0157.1

Lambert, A., Huang, J., van der Kamp, G., Henton, J., Mazzotti, S., James, T.S., Courtier, N., Barr, A.G., 2013. Measuring water accumulation rates using GRACE data in areas experiencing glacial isostatic adjustment: The Nelson River basin. Geophys. Res. Lett. 40, 6118–6122. https://doi.org/https://dx.doi.org/10.1002/2013GL057973

[dataset] Land Cover of Canada, 2010. Natural Resources Canada; Canada Centre for Remote Sensing. https://open.canada.ca/data/en/dataset/c688b87f-e85f-4842-b0e1-a8f79ebf1133 (accessed 11.12.19)

Landerer, F.W., Swenson, S.C., 2012. Accuracy of scaled GRACE terrestrial water storage estimates. Water Resour. Res. 48, 1–11. https://doi.org/https://dx.doi.org/10.1029/2011WR011453

Larue, F., Royer, A., De Sève, D., Langlois, A., Roy, A., Brucker, L., 2017. Validation of GlobSnow-2 snow water equivalent over Eastern Canada. Remote Sens. Environ. 194, 264–277. https://doi.org/https://dx.doi.org/10.1016/j.rse.2017.03.027

Mudryk, L.R., Derksen, C., Kushner, P.J., Brown, R., 2015. Characterization of Northern Hemisphere snow water equivalent datasets, 1981-2010. J. Clim. 28, 8037–8051. https://doi.org/https://dx.doi.org/10.1175/JCLI-D-15-0229.1

Niu, G.-Y., Seo, K.-W., Yang, Z.-L., Wilson, C., Su, H., Chen, J., Rodell, M., 2007. Retrieving snow mass from GRACE terrestrial water storage change with a land surface model. Geophys. Res. Lett. 34, 1–5. https://doi.org/https://dx.doi.org/10.1029/2007GL030413

Ramillien, G., Frappart, F., Cazenave, A., Guntner, A., 2005. Time variations of land water storage from an inversion of 2 years of GRACE geoids. Earth Planet. Sci. Lett. 235, 283–301. https://doi.org/https://dx.doi.org/10.1016/j.epsl.2005.04.005

Reichle, R.H., Draper, C.S., Liu, Q., Girotto, M., Mahanama, S.P.P., Koster, R.D., De Lannoy, G.J.M., 2017. Assessment of MERRA-2 land surface hydrology estimates. J. Clim. 30. https://doi.org/10.1175/JCLI-D-16-0720.1

Reichle, R.H., Koster, R.D., De Lannoy, G.J.M., Forman, B.A., Liu, Q., Mahanama, S.P.P., Toure, A., 2011. Assessment and enhancement of MERRA land surface hydrology estimates. J. Clim. 24, 6322–6338. https://doi.org/10.1175/JCLI-D-10-05033.1

Rodell, M., Famiglietti, J.S., Wiese, D.N., Reager, J.T., Beaudoing, H.K., Landerer, F.W., Lo, M.H., 2018. Emerging trends in global freshwater availability. Nature 557, 651–659. https://doi.org/10.1038/s41586-018-0123-1

Rodell, M., Houser, P.R., Jambor, U., Gottschalck, J., Mitchell, K., Meng, C.-J., Arsenault, K., Cosgrove, B., Radakovich, J., Bosilovich, M., Entin*, J.K., Walker, J.P., Lohmann, D., Toll, D., 2004. The Global Land Data Assimilation System. Bull. Am. Meteorol. Soc. 85, 381–394. https://doi.org/10.1175/BAMS-85-3-381

Sakumura, C., Bettadpur, S., Bruinsma, S., 2014. Ensemble prediction and intercomparison analysis of GRACE time-variable gravity field models. Geophys. Res. Lett. 41, 1389–1397. https://doi.org/https://dx.doi.org/10.1002/2013GL058632

Scanlon, B.R., Zhang, Z., Rateb, A., Sun, A., Wiese, D., Save, H., Beaudoing, H., Lo, M.H., Müller-Schmied, H., Döll, P., Beek, R., Swenson, S., Lawrence, D., Croteau, M., Reedy, R.C., 2019. Tracking seasonal fluctuations in land water storage using global models and GRACE satellites. Geophys. Res. Lett. 46, 5254–5264. https://doi.org/10.1029/2018GL081836

Seo, K.W., Ryu, D., Kim, B.M., Waliser, D.E., Tian, B., Eom, J., 2010. GRACE and AMSR-E-based estimates of winter season solid precipitation accumulation in the Arctic drainage region. J. Geophys. Res. Atmos. 115, 1–18. https://doi.org/10.1029/2009JD013504

Stieglitz, M., Ducharne, A., Koster, R., Suarez, M., 2001. The Impact of Detailed Snow Physics on the Simulation of Snow Cover and Subsurface Thermodynamics at Continental Scales. J. Hydrometeorol. 2, 228–242. https://doi.org/10.1175/1525-7541(2001)002<0228:TIODSP>2.0.CO;2

Sturm, M., Holmgren, J., Liston, G.E., 1995. A seasonal snow cover classification system for local to global applications. J. Clim. 8, 1261–1283. https://doi.org/https://doi.org/10.1175/1520-0442(1995)008<1261:ASSCCS>2.0.CO;2

Su, H., Yang, Z.L., Dickinson, R.E., Wilson, C.R., Niu, G.Y., 2010. Multisensor snow data

assimilation at the continental scale: The value of Gravity Recovery and Climate Experiment terrestrial water storage information. J. Geophys. Res. Atmos. 115, 1–14. https://doi.org/10.1029/2009JD013035

Swenson, S., 2010. Assessing High-Latitude Winter Precipitation from Global Precipitation Analyses Using GRACE. J. Hydrometeorol. 11, 405–420. https://doi.org/10.1175/2009JHM1194.1

Swenson, S., Wahr, J., 2006. Post-processing removal of correlated errors in GRACE data. Geophys. Res. Lett. 33, 1–4. https://doi.org/https://dx.doi.org/10.1029/2005GL025285

Syed, T.H., Famiglietti, J.S., Rodell, M., Chen, J., Wilson, C.R., 2008. Analysis of terrestrial water storage changes from GRACE and GLDAS. Water Resour. Res. 44, 1–15. https://doi.org/https://dx.doi.org/10.1029/2006WR005779

Takala, M., Luojus, K., Pulliainen, J., Derksen, C., Lemmetyinen, J., Kärnä, J.-P., Koskinen, J., Bojkov, B., 2011. Estimating northern hemisphere snow water equivalent for climate research through assimilation of space-borne radiometer data and ground-based measurements. Remote Sens. Environ. 115, 3517–3529. https://doi.org/https://dx.doi.org/10.1016/j.rse.2011.08.014

Tapley, B.D., Bettadpur, S., Watkins, M., Reigber, C., 2004. The gravity recovery and climate experiment: Mission overview and early results. Geophys. Res. Lett. 31, 1–4. https://doi.org/10.1029/2004GL019920

Tapley, B.D., Watkins, M.M., Flechtner, F., Reigber, C., Bettadpur, S., Rodell, M., Sasgen, I., Famiglietti, J.S., Landerer, F.W., Chambers, D.P., Reager, J.T., Gardner, A.S., Save, H., Ivins, E.R., Swenson, S.C., Boening, C., Dahle, C., Wiese, D.N., Dobslaw, H., Tamisiea, M.E., Velicogna, I., 2019. Contributions of GRACE to understanding climate change. Nat. Clim. Chang. 9, 358–369. https://doi.org/10.1038/s41558-019-0456-2

Tedesco, M., Kelly, R., Foster, J.L., Chang, A.T.C., 2004. AMSR-E/Aqua Daily L3 Global Snow Water Equivalent EASE-Grids Version 2. NASA National Snow and Ice Data Center Distributed Active Archive Center, Boulder, Colorado, USA. NASA DAAC at the National Snow and Ice Data Center. https://doi.org/10.5067/amsr-e/ae_dysno.002

Tedesco, M., Narvekar, P.S., 2010. Assessment of the NASA AMSR-E SWE Product. IEEE J.

Sel. Top. Appl. Earth Obs. Remote Sens. 3, 141–159. https://doi.org/10.1109/JSTARS.2010.2040462

Toure, A.M., Rodell, M., Yang, Z.-L., Beaudoing, H., Kim, E., Zhang, Y., Kwon, Y., 2016. Evaluation of the Snow Simulations from the Community Land Model, Version 4 (CLM4). J. Hydrometeorol. 17, 153–170. https://doi.org/https://dx.doi.org/10.1175/JHM-D-14-0165.1

Van Dijk, A.I.J.M., Renzullo, L.J., Wada, Y., Tregoning, P., 2014. A global water cycle reanalysis (2003-2012) merging satellite gravimetry and altimetry observations with a hydrological multi-model ensemble. Hydrol. Earth Syst. Sci. 18, 2955–2973. https://doi.org/10.5194/hess-18-2955-2014

Verseghy, D., Brown, R., Wang, L., 2017. Evaluation of CLASS snow simulation over Eastern Canada. J. Hydrometeorol. 18, 1205–1225. https://doi.org/10.1175/JHM-D-16-0153.1

Wahr, J., Swenson, S., Velicogna, I., 2006. Accuracy of GRACE mass estimates. Geophys. Res. Lett. 33, 1–5. https://doi.org/https://dx.doi.org/10.1029/2005GL025305

Wang, W., Cui, W., Wang, X., Chen, X., 2016. Evaluation of GLDAS-1 and GLDAS-2 Forcing Data and Noah Model Simulations over China at the Monthly Scale. J. Hydrometeorol. 17, 2815–2833. https://doi.org/https://dx.doi.org/10.1175/JHM-D-15-0191.1

Zhou, X., Matthes, H., Rinke, A., Klehmet, K., Heim, B., Dorn, W., Klaus, D., Dethloff, K., Rockel, B., 2014. Evaluation of Arctic Land Snow Cover Characteristics, Surface Albedo, and Temperature during the Transition Seasons from Regional Climate Model Simulations and Satellite Data. Adv. Meteorol. 2014. https://doi.org/10.1155/2014/604157

5. Analyzing the contribution of snow water equivalent to the terrestrial water storage over Canada

5.1. Article presentation

The objective of this article was to study the spatial and temporal relationship between TWSA/SWEA-derived from GRACE and GlobSnow2/AMSR-E/CMC SWEA. The comparison was conducted to understand the impacts of snow mass on the transient terrestrial water storage (TWS) during the snow season (from December to March). A number of fifteen basins were chosen to cover most parts of the Canadian territory. This article follows the first objective of this study and it is intended to provide a general insight into areas where the assimilation of GRACE data into a hydrological model may improve SWE estimations.

In order to consider the contribution of each storage compartment to the transient water storage at the basin scale, the WGHM simulations were used. All WGHM water storage compartments, including canopy, wetland, groundwater, surface water, and soil moisture storage were considered. The temporal means of WGHM storage components were calculated and their basin-averaged values were plotted at the pie charts for each of the fifteen basins. The general methodology for analyzing the association between TWSA and SWEA was summarized in Figure 5.2. The GRACE TWSA (or SWEA) can be compared directly to the multisource SWE products. GRACE-derived SWEA was estimated by subtracting the WGHM water compartments. After applying the masking and spatial averaging steps, monthly water storage and snow mass values were converted to anomalies based on the time-mean baseline (2002-2011). In the next step, a basin-by-basin GRACE TWSA (or SWEA) versus multisource SWEA Spearman's rank correlation coefficients were calculated. Then, correlation results were classified to determine the areas of agreement and insignificant results are filtered out. Finally, the RMSE metric was calculated between GRACE-derived TWSA (or SWEA) and each of the multisource SWEA products.

Analyzing the contribution of snow water equivalent to the terrestrial water storage over Canada

by Ala Bahrami, Kalifa Goïta, Ramata Magagi

Hydrological Processes

ISSN: 0885-6087

Volume 34, No. 2, January 2020, pp. 175-188

Analyzing the contribution of snow water equivalent to the terrestrial water storage over Canada

Ala Bahrami[1], Kalifa Goïta [1], and Ramata Magagi [1]

[1] Centre d'applications et de recherches en télédétection, Département de géomatique appliquée, Université de Sherbrooke, Sherbrooke, Québec, Canada

Abstract: In this study, the spatial and temporal variabilities of terrestrial water storage anomaly (TWSA) and snow water equivalent anomaly (SWEA) information obtained from the Gravity Recovery and Climate Experiment (GRACE) twin satellites data were analyzed in conjunction with multisource snow products over several basins in the Canadian landmass. Snow water equivalent (SWE) data were extracted from three different sources: Global Snow Monitoring for Climate Research version 2 (GlobSnow2), Advanced Microwave Scanning Radiometer-Earth Observing System (AMSR-E), and Canadian Meteorological Centre (CMC). The objective of the study was to understand whether SWE variations have a significant contribution to terrestrial water storage anomalies in the Canadian landmass. The period considered was from December 2002 to March 2011. Significant relationships were observed between TWSA and SWEA for most of the fifteen basins considered (53% to 80% of the basins, depending on the SWE products considered). The best results were obtained with the CMC SWE products, compared to satellite-based SWE data. Stronger relationships were found in snow-dominated basins (R_s >= 0.7), such as the Liard [root mean square error (RMSE) = 21.4 mm] and Peace Basins (RMSE = 26.76 mm). However, despite high snow accumulation in the north of Quebec, GRACE showed weak or insignificant correlations with SWEA, regardless of the data sources. The same behavior was observed in the Western Hudson Bay Basin. In both regions, it was found that the contribution of non-SWE compartments, including wetland, surface water, as well as soil water storages has a significant impact on the variations of total storage. These components were estimated using the WaterGAP Global Hydrology Model (WGHM) simulations and then subtracted from GRACE observations. The GRACE-derived SWEA correlation results showed improved relationships with three SWEA products. The improvement is particularly important in the sub-basins of the Hudson Bay, where very weak and insignificant results were previously found with GRACE TWSA data. GRACE-derived SWEA showed a significant relationship with CMC data in 93% of the basins (13% more

than GRACE TWSA). Overall, the results indicated the important role of SWE on terrestrial water storage variations.

Keywords: Snow water equivalent, Terrestrial water storage, GRACE, WGHM, GlobSnow2, AMSR-E, CMC SWE data.

Résumé:

Dans cette étude, les variabilités spatiales et temporelles des anomalies du stock d'eau terrestre (TWSA) et des anomalies d'équivalent en eau de la neige (SWEA) obtenues à partir des données des satellites Gravity Recovery and Climate Experiment (GRACE) ont été analysées avec diffèrent produits de neige sur plusieurs bassins au Canada. Les données d'équivalent en eau de la neige (SWE) sont issues de trois différentes sources: Global Snow Monitoring for Climate Research version 2 (GlobSnow2), Advanced Microwave Scanning Radiometer - Earth Observing System (AMSR-E) et le Centre météorologique canadien (CMC). L'objectif de l'étude était de comprendre si les variabilités de SWE ont une contribution significative aux anomalies de stock d'eau terrestre dans la masse continentale canadienne. La période considérée est de décembre 2002 à mars 2011. Des relations significatives ont été observées entre TWSA et SWEA pour la plupart des quinze bassins considérés (53% à 80% des bassins, selon les produits SWE considérés). Les meilleurs résultats ont été obtenus avec les produits CMC SWE, par rapport aux données SWE satellitaires. Des relations plus fortes ont été trouvées dans les bassins dominés par la neige (Rs> = 0,7), tels que le bassin versant de la Liard [erreur quadratique moyenne (RMSE) = 21,4 mm] et le bassin versant de la Peace (RMSE = 26,76 mm). Cependant, malgré une forte accumulation de neige dans le nord du Québec, GRACE a montré des corrélations faibles ou insignifiantes avec SWEA, quelque soit la source de données. Le même comportement a été observé dans le bassin versant ouest de la Baie d'Hudson. Dans les deux régions, il a été constaté que la contribution des compartiments non-SWE, y compris les zones humides, les eaux de surface, ainsi que les stocks d'eau du sol a un effet significatif sur les variations du stock total. Ces composantes ont été estimées à l'aide des simulations du modèle hydrologique mondial WaterGAP (WGHM), puis soustraites des observations GRACE. Les résultats de corrélation SWEA dérivés de GRACE ont montré une amélioration des relations avec les trois produits de neige. L'amélioration est particulièrement importante dans les sous-bassins de la Baie d'Hudson,

où des résultats très faibles et insignifiants ont été précédemment trouvés avec les données GRACE TWSA. La SWEA dérivée de GRACE a montré une relation significative avec les données CMC dans 93% des bassins (13% de plus que GRACE TWSA). En somme, les résultats ont indiqué le rôle important du SWE sur les variations du stock d'eau terrestre.

Mots-clés : Équivalent en eau de la neige, Stock total d'eau terrestre, GRACE, Modèle WGHM, GlobSnow2, AMSR-E, Données SWE de CMC.

5.2. Introduction

Snow cover has considerable influence on Earth's climate system (Déry, Sheffield, & Wood, 2005). Global and regional predictions of future climate depend on reliable estimation of snow mass or snow water equivalent (SWE) and snow cover (Swenson & Lawrence, 2012). To better monitor snow processes globally, the spatial and temporal variability of SWE and snow cover onset, persistence, and disappearance are required (Hancock et al., 2013; Ma et al., 2017; Zhang & Ma, 2018). Accurate estimation of snow dates and snow cover changes is crucial for snow albedo feedbacks that accentuates climate change (Barnett, Adam, & Lettenmaier, 2005; Déry et al., 2005; Toure et al., 2016). In many parts of the Northern Hemisphere, the land surface hydrology is strongly affected by the ablation of snow mass, and freshwater supply depends on its melt (Barnett et al., 2005). Snow displays important spatial and temporal variabilities, depending on landscape, topography, forest cover and geographical location. The measurement of snow is challenging. Because of the limitations of ground-based methods to characterize the snowpack, especially in areas with high snow spatial variability, both satellite remote sensing measurements and land surface model simulations are considered as alternative solutions (Zhang et al., 2014). Among satellite measurement techniques, gravimetric retrievals of terrestrial water storage anomaly (TWSA) from the Gravity Recovery and Climate Experiment (GRACE; Tapley et al., 2004) have the ability to monitor the redistribution of integrated freshwater resources on land, including canopy water, surface water, soil moisture, snow, and groundwater (Famiglietti & Rodell, 2013). Over snow-covered areas, gravimetric changes during snow accumulation and ablation phase can be captured by the GRACE measurements (Forman, Reichle, & Rodell, 2012). This unique potential of gravimetric measurements enables us to sense integrated TWS changes, which is not feasible by other remote sensing means (Forman & Reichle, 2013).

A number of studies have focused on SWE estimation using GRACE TWS retrievals. A common and simple strategy to extract snow storage is to subtract directly land surface model estimates of soil moisture, surface water, and groundwater storages from the total GRACE signal. This approach was used by (Niu et al., 2007), who estimated SWE from GRACE data by subtracting groundwater storage simulated by a land surface model (LSM). Their results evaluated with ground-based and satellite-based SWE estimates showed that GRACE-derived SWE were more accurate than microwave retrievals in deep snow regions. Ramillien et al. (2005) developed an iterative inverse method based on a generalized least-squares inversion to isolate the contribution of snow mass from monthly GRACE observations. Based on this numerical strategy, the contribution of snow mass was determined by solving a function defined by a linear combination of the spherical harmonic coefficients measured by GRACE and some a prior information from climate models. Frappart et al. (2006, 2011) compared the annual cycles of GRACE-derived SWE retrievals, as presented by (Ramillien et al., 2005), with satellite microwave observations, global land surface models, climatologies of snow depth, snowfall, and SWE. Their results over North America illustrated a relatively good agreement between GRACE snow retrievals and existing snow mass products. Seo et al., (2010) and Swenson (2010) developed two satellite-based methods including GRACE and passive microwave emission to assess solid precipitation accumulation during cold-season and compared the results with global precipitation and reanalysis products. Behrangi et al. (2018, 2017) used GRACE observations to estimate precipitation accumulation over high mountainous and latitude areas. They highlighted the importance of GRACE observations in quantifying and assessing snowfall products. In these aforementioned studies, the water balance approach was used to estimate solid precipitation accumulation, and the importance of GRACE-based measurements was highlighted as a benchmark to understand the hydrologic cycle. It is also possible to decompose GRACE observations into individual water storage components by implementing a more sophisticated data assimilation approach (Zaitchik, Rodell, & Reichle, 2008).

A number of studies have examined the impact of GRACE data assimilation into land surface model at basin and gridded scales in order to improve SWE and water storage estimations (Eicker et al., 2014; Forman et al., 2012; Kumar et al., 2016; Schumacher, Kusche, & Döll, 2016; Su et al., 2010; Zaitchik et al., 2008). The analyses of the results showed that, in general, the performance of GRACE data assimilation varied depending on the domain of study and the data

assimilation structure. Based on previous research, a better understanding of the relationship between snow water equivalent anomaly (SWEA) and GRACE-derived TWSA could be very beneficial to better guide the assimilation process. Indeed, this relationship could display different spatial and temporal behaviors on a given territory, which could possibly reveal if the assimilation of GRACE is worth doing to improve modeled SWE estimates.

The objective of this research is to study the spatial and temporal relationship between TWSA/SWEA-derived from GRACE and multisource SWEA. SWE data were extracted from three different sources: the European Space Agency (ESA) Global Snow Monitoring for Climate Research (version 2.0 – GlobSnow2), the Advanced Microwave Scanning Radiometer-Earth Observing System (AMSR-E), and the Canadian Meteorological Center (CMC). The comparison was conducted to understand the impacts of snow mass on the transient terrestrial water storage (TWS) during the winter season. More specifically, we address the following scientific questions:

1. How do temporal patterns of SWEA vary over Canadian basins?

2. Can we consider snow mass changes as the dominant component of TWS variabilities during snow season?

3. Does the relationship between GRACE TWSA and multisource SWEA products (GlobSnow2, AMSR-E, and CMC) at the basin scale provide instructive information for monitoring snow mass changes in Canada?

This study will help to better understand whether SWEA has a significant contribution to TWSA in the Canadian landmass. It is also intended to provide a general insight on areas where the assimilation of GRACE data into a land surface model may eventually improve modeled SWE estimations.

5.3. Materials

5.3.1. GRACE Total Water Storage Data

Remote sensing observations from the GRACE mission consisted of twin satellites that measure range-rate variations between both satellites and collect monthly estimates of Earth's gravity field changes (Tapley et al., 2004). The hydrological signal detected by GRACE can provide highly

accurate TWS column of water variations with an accuracy of 1.5 cm equivalent water height at a spatial resolution of ~ 200,000 km^2 (Famiglietti & Rodell, 2013). Because of filtering and truncation of GRACE TWS observations (Swenson & Wahr, 2006), surface mass variation signal is attenuated. Therefore, a scaling factor is applied to data (Landerer & Swenson, 2012). The gridded (1°×1°) scaling factors, as well as post-processed GRACE TWS observations, are publicly available since April 2002 via the National Aeronautics and Space Administration (NASA) Jet Propulsion Laboratory's TELLUS website (available at http://grace.jpl.nasa.gov). The mass changes sensed by GRACE include both hydrological mass variations related to integrated terrestrial water storage anomalies and non-hydrological mass changes related to mantle convection and post-glacial rebound (Abelen & Seitz, 2013; Wahr, Swenson, & Velicogna, 2006; Wang et al., 2013). This research focused on the hydrological component, corresponding to GRACE TWSA measurements. We used Release 5 (RL05) level-3 monthly 1°×1° land gridded data products provided by three data centers, including the University of Texas Center for Space Research (CSR), the Deutsches GeoForschungsZentrum (GFZ), as well as NASA's Jet Propulsion Laboratory (JPL). In order to effectively reduce the noise in the gravity solution and produce an ensemble product, we used the arithmetic mean of all three data products (Sakumura, Bettadpur, & Bruinsma, 2014). The linear trends related to the glacial isostatic adjustment (GIA) has been removed from GRACE TELLUS mass grids, based on the model from (Geruo, Wahr, & Zhong, 2013).

5.3.2. Snow Water Equivalent Products

5.3.2.1. CMC

Daily gridded CMC snow depth analysis is based on 6-hourly optimal interpolation of in-situ daily snow observations from the World Meteorological Organization (WMO) information system and the background (or first guess). The initial guess field is provided by a simple snow accumulation and melt model using analyzed temperatures and forecast precipitation from the CMC Global Environmental Multiscale (GEM) forecast model (Brasnett, 1999; Brown, Brasnett, & Robinson, 2003; Brown, Derksen, & Wang, 2010). Monthly SWE estimates were obtained from monthly averaged snow depth analyses using the corresponding mean monthly snow density values derived from snow climate classes identified by (Sturm, Holmgren, & Liston, 1995). This monthly data

set is provided at the spatial scale of 0.25°×0.25° (~24 km × ~24 km) over the Northern Hemisphere from December 2002 to March 2011 and is available via the National Snow and Ice Data Center (NSIDC). CMC SWE product is often considered as one of the most useful global data sources for evaluating SWE simulation (e.g., Forman et al., 2012; Seo et al., 2010; Su et al., 2010; Toure et al., 2016; Zhang et al., 2014). However, it has some limitations, including imperfect accumulation and melt model, and coarse atmospheric forcing, as well as the scarcity of snow stations at higher latitude (Swenson & Lawrence, 2012; Toure et al., 2016).

5.3.2.2. GlobSnow2 Snow Water Equivalent

The monthly GlobSnow2 SWE product was used as a source of SWE data set. The GlobSnow2 SWE (in mm) product is obtained from a combination of ground-based weather station data and passive microwave remote sensing (Takala et al., 2011). The SWE data which is projected into Equal-Area Scalable Earth Grid (EASE-Grid) covers the terrestrial non-mountainous regions of Northern hemisphere, with the exception of glaciers and Greenland. This SWE product is limited between latitudes 35° to 85° with a spatial resolution of 25 km × 25 km. The data are available from December 2002 to March 2011 and can be accessed via the Finnish Meteorological Institute website (http://www.globsnow.info/swe). GlobSnow2 can provide useful information for peak accumulation and the seasonal pattern of SWE development, and it is considered to be the superior snow product among satellite Earth observation of snow estimates (Hancock, Baxter, Evans, & Huntley, 2013; Larue et al., 2017).

5.3.2.3. AMSR-E-derived SWE Product

The monthly level-3 AMSR-E/Aqua SWE product was used in this study. Like GlobSnow2, it was also derived from passive microwave measurements, but with an empirical equation based on the brightness temperature difference at 19 and 37 GHz (Chang, Foster, & Hall, 1987; Kelly, 2009). The data are available freely via the National Snow and Ice Data Center (NSIDC) web site, in 25^2 km^2 EASE-Grid format (Tedesco et al., 2004). In this study, we used AMSR-E SWE data set for Northern Hemisphere, for the snow season (December to March), from 2002 to 2011.

5.3.3. WGHM Terrestrial Water Storage

The Water-Global Assessment and Prognosis Global Hydrology Model (WGHM) is part of the

Water-Global Assessment and Prognosis (WaterGAP) model (Döll et al., 2014; Müller Schmied et al., 2016a, 2014; Müller Schmied, 2017; Müller Schmied et al., 2016b). It calculates water fluxes and storages on global land area. The WGHM model version 2.2c used here was calibrated to match long-term observed average river discharge at 1319 calibration basins which cover ~ 50% of global drainage (Müller Schmied et al., 2014). The model was driven by WATCH Forcing Data methodology applied to ERA-Interim (WFDEI; Weedon et al., 2014) which is scaled to monthly precipitation sums provided by the Global Precipitation Climatology Center (GPCC; Schneider et al., 2014). In the standard version of the WGHM model, the gridded Moderate Resolution Imaging Spectroradiometer (MODIS) land cover product (MOD12Q1) for the year 2004 was used. The extents of lakes and wetlands, required for the calculation of WGHM water storage, were extracted from the global lakes and wetlands database (Müller Schmied et al., 2014). The total integrated terrestrial water storage of the WGHM was calculated by summing the different water storage components, including canopy, snow, soil, groundwater, lakes, man-made reservoirs, wetlands, and rivers. The model outputs are provided at 0.5°×0.5° spatial resolution for the global land area, excluding Antarctica, on a monthly temporal resolution from December 2002 to March 2011. In this study, we used WGHM water storage compartments related to snow season (December to March) from 2002 to 2011. We aggregated model spatial resolution to 1°×1° by averaging all grid points falling in a 1° grid cell corresponding to GRACE grid. The research software of the WGHM model is not publicly available, while the model output is accessible on request to the modeling team (www.watergap.de) or via the Inter-Sectoral Impact Model Intercomparison Project (ISIMIP) website (https://esg.pik-potsdam.de/projects/isimip/).

5.3.4. Study Area

The basins considered in the study cover most parts of the Canadian landmass (Figure 5.1). Except for the Fraser basin, they are all included within three large scale basins, namely Mackenzie (including Athabasca, Bear and Peel, Liard, Peace, and Slave), Hudson Bay (including Churchill, South Western of Hudson Bay, La Grande, Nelson, Northeastern Hudson Bay, Nottaway, Ungava Bay, Western Hudson Bay), and Saint Lawrence (including Saint Lawrence River). Table 1 gives the basin characteristics (areas, forest fractional cover, and elevation). In summary, the basin study domain contains fifteen basins (Table 5.1), where we analyzed the regional TWSA and SWEA relationships. The majority of these basins are categorized as medium size basins, with the

exception of those with areas larger than 1,000, 000 km^2. Based on the 2010 North American land cover data, 67% of the basins have a forest coverage of more than 50%.

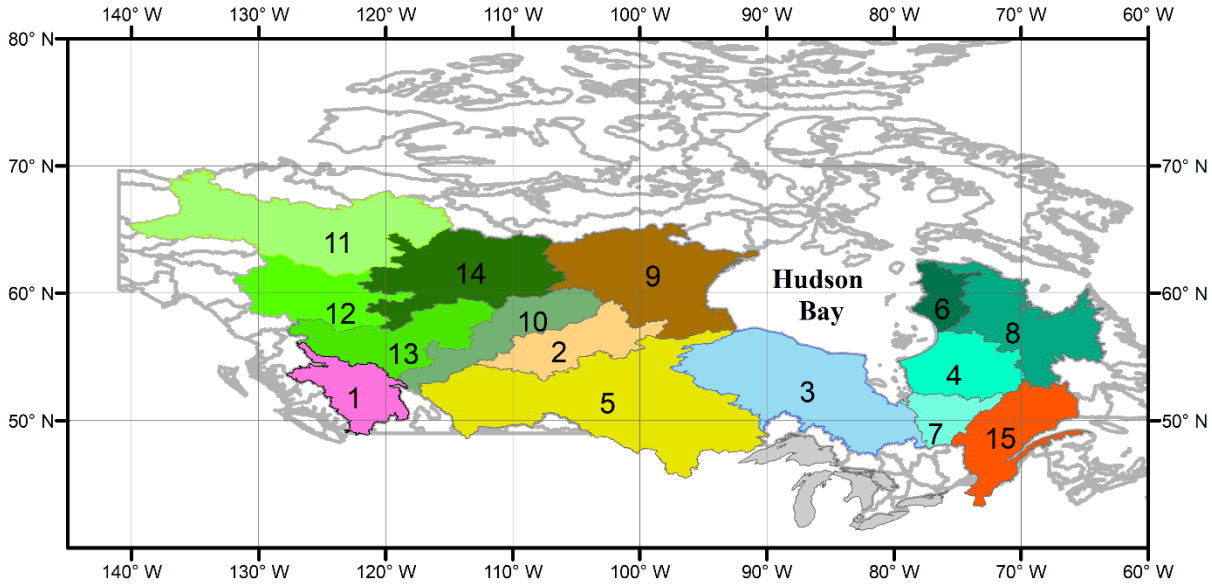

Figure 5.1. Overview location of the fifteen Canadian river basins considered. Information about the basin is presented in Table 5.1.

Table 5.1. Basin areas, forest fractional cover, and elevation. Location of the basins can be seen in Figure 5.1.

Basin ID	Basin Name	Area (km^2)	Percentage of the forest cover	Average elevation (m)
1	Fraser	231924.0	70.2	1192.8
2	Churchill	258817.1	60.7	446.7
3	Southwestern of Hudson Bay	735761.7	63.3	205.9
4	La Grande	268720.9	58.7	329.4
5	Nelson	1112976.0	32.7	525.7
6	Northeastern Hudson Bay	100467.4	2.7	160.1
7	Nottaway	144967.9	63.2	326.4
8	Ungava Bay	380791.9	25.7	352.9
9	Western Hudson Bay	492467.5	21.2	232.9
10	Athabasca	272726.4	64.3	610.4
11	Bear and Peel	498350.3	34.2	538.7
12	Liard	274955.2	71.3	992.2
13	Peace	323134.6	74.3	845.4
14	Slave	430091.1	53.5	342.3
15	Saint Lawrence River	365385.0	79.8	431.4

5.4. Methods

In order to consider the contribution of each storage compartment to the transient water storage at the basin scale, the simulations of WGHM model were used. All WGHM water storage compartments, including canopy water storage (CWS), wetland storage (WS), groundwater storage (GWS), surface water storage (SWS), and soil moisture storage (SMS) were considered. In this study, the summation of lake, river, and reservoir storage variations was used to determine the surface water storage compartment. Monthly storage at basin scale was estimated by averaging all grid cell values within the basin for the corresponding month. In the next step, the temporal mean of each WGHM storage component was calculated by averaging all monthly data from December to March (hereafter referred to as DJFM) for the nine snow seasons (2002-2011). Finally, the time-mean storage percentages were plotted as the pie chart for each of the fifteen studied basins.

In the second part of the methodology, the procedure of the correlation analysis between multiple sources of data is explained. The methodology proposed to analyze the relationship between TWSA and SWEA is summarized in Figure 5.2. GRACE-derived TWSA (or SWEA) was compared to the three data sources of SWEA including, GlobSnow 2, AMSR-E, and CMC.

The GRACE TWSA (or SWEA) can be compared directly to the multisource SWE products. GRACE SWEA is estimated by subtracting the WGHM contributions of canopy water storage anomalies (CWSA), wetland storage anomalies (WSA), groundwater storage anomalies (GWSA), surface water storage anomalies (SWSA), and soil moisture storage anomalies (SMSA) from GRACE derived TWSA. The SWEA was estimated according to the following equation:

$$SWEA = TWSA - CWSA - WSA - GWSA - SWSA - SMSA \tag{5.1}$$

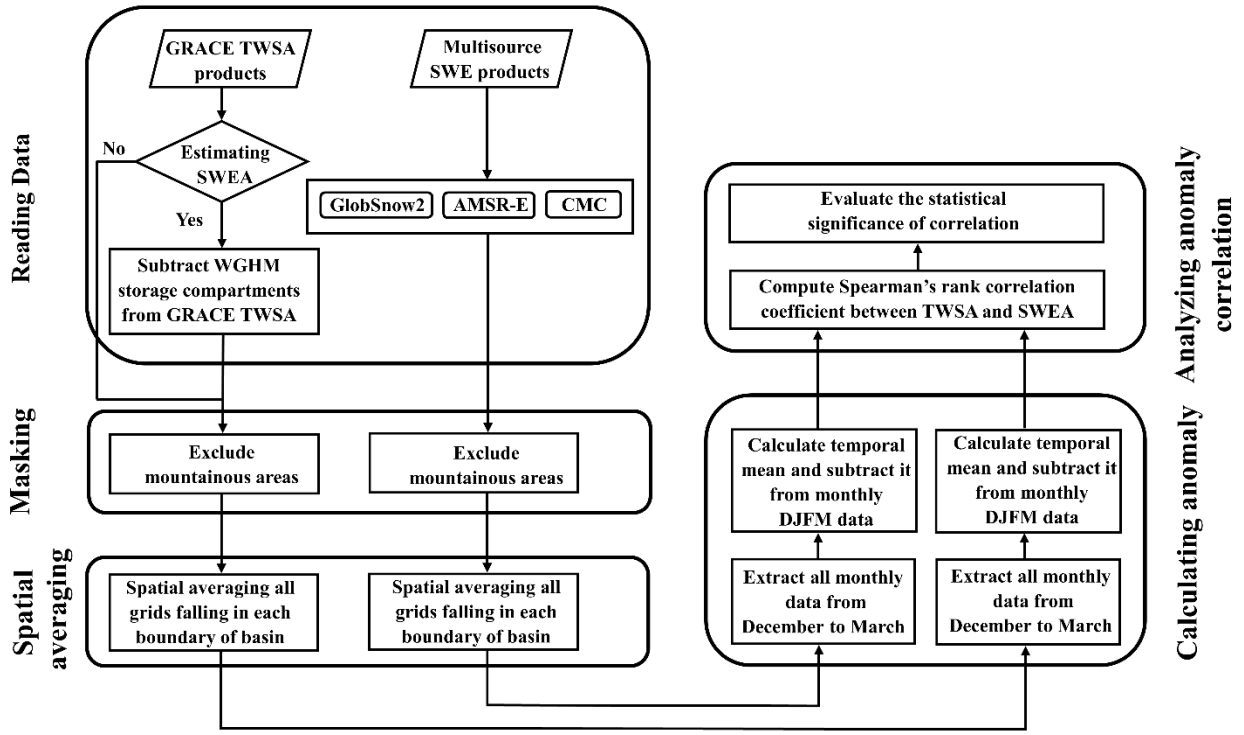

Figure 5.2. Flowchart for preprocessing and comparing GRACE-derived TWSA/SWEA to the multisource SWEA products.

As the mountainous areas were excluded in the GlobSnow products, a topographical mask was applied to each data, including GRACE, AMSR-E, and CMC to exclude areas of high elevation. In order to mask out these areas, we simply extracted grid cells of GlobSnow located in the topographical complex region. Then, based on the geographical information (pixel centers) of these areas and the usage of the Nearest-neighbors method, the pixel centers related to each source of data, (GRACE, AMSR-E, and CMC) were excluded. Note that in the GlobsSnow2 SWE products, observations that fall inside the grid cells with a height standard deviations above 200 m were excluded from data, as the GlobSnow SWE products were deemed unreliable in those areas (Takala et al., 2011).

The analysis of TWSA versus SWE changes at the basin scale was performed to investigate the spatial variability of TWSA versus SWEA in the Canadian river basins, which have different land covers, topographies, climates, and snow accumulation regimes. The basin scale analysis could be less affected by uncertainties, due to the very coarse resolution of GRACE data. In order to obtain

the basin value of a specific month (e.g., March 2003), we spatially averaged all grid cells that fell within each boundary of the basin (in total fifteen watersheds) for that period.

In the basin scale anomaly computation, firstly all available DJFM data for the nine snow seasons (2002-2011) were extracted. The period from December to March was considered as the snow season. For example, the 2003 snow season covers monthly data from December 2002 to March 2003. Missing data were excluded from the analysis (e.g., January 2011). The snow period was limited to March, since the quality of SWE products (especially remote sensing-based SWE) may be affected by frequent snowmelts which occur after March in several areas included in the study. Then, the temporal means of each data were calculated by averaging all available monthly basin-averaged DJFM data. Finally, the temporal means from the available DJFM data were subtracted in order to calculate corresponding data anomaly.

A basin-by-basin GRACE TWSA (or SWEA) versus multisource SWEA Spearman's rank correlation coefficients (Iman & Conover, 1979) were calculated between the datasets over the time period considered. Spearman's correlation is appropriate for nonlinear relationships by applying a rank transformation of the datasets (Schumacher et al., 2015). The rank-order correlation coefficient between the ranks R_i of GRACE TWSA (or SWEA) and the ranks S_i of the existing SWEA products is defined as follows

$$R_s = \frac{\sum_{i=1}^{N}\left(R_i - \overline{R}\right)\left(S_i - \overline{S}\right)}{\sqrt{\sum_{i=1}^{N}\left(R_i - \overline{R}\right)^2 \sum_{i=1}^{N}\left(S_i - \overline{S}\right)^2}} \tag{5.2}$$

Where $\overline{R}$ and $\overline{S}$ are mean of the data set ranks and N is the number of months, respectively. The statistical significances of the calculated R_s were also assessed using a t-statistic, with a significance level of 0.05, and categorized in two groups of significant R_s (p-value < 0.05) and no-significant R_s (p-value ≥ 0.05). Furthermore, the correlation results were classified to determine the areas of agreement between TWSA and SWEA and the insignificant results were filtered out. Possible reasons for disagreement, including weak correlations were discussed. It was hypothesized that higher monthly correlations between TWSA and SWEA occur if either SWE variability contributes mainly to the transient total water storage variation, or if snow mass changes

proportionally with water mass variation.

In the final step, the root mean square errors (RMSEs) between GRACE-derived TWSA (or SWEA) and each of the multisource SWEA products were analyzed in order to evaluate the overall performance of the relationships.

5.5. Results

5.5.1. WGHM storage compartment

The pie chart results of each storage compartment to the total water storage for fifteen basins in the snow season are summarized in Figure 5.3.

In all of the studied basins, the contribution of the canopy water storage during snow accumulation season is less than 1% of the total storage. Therefore, the impact of canopy storage on the variation of the total storage could be considered negligible in all basins.

Results show that the Western Hudson Bay Basin has the highest percentage of wetland storage (53%), while the Fraser Basin has the lowest value of contribution (0%). In general, the contribution of the wetland storage is significant in the majority of the basins. In nine out of the fifteen watersheds, the wetland storage represents more than 20% of the total water storage. This is particularly true in the sub-basins of the Hudson Bay, such as Nottaway and Western Hudson Bay Basins.

Based on the results of WGHM time mean storage during snow season, the contribution of groundwater storage varies between 2% to 6% in all studied basins. As the significance of modeled groundwater storage for different basins is not so strong, its changes during the cold season could not be a substantial component of the total storage variations.

The contribution of the surface water storage compartment (river, reservoir, and lake storage) is shown in Figure 5.3. The highest surface water storage percentage value (62%) is achieved in the La Grande Basin covering most of distributed lakes and reservoirs. The lowest percentage (2%) of surface water storage belongs to the mountainous areas of the Fraser Basin. The importance of surface water storage is more significant in areas surrounding the Hudson Bay.

Results presented in Figure 5.3 show that the Northeastern Hudson Bay Basin located in the north of Quebec Province has the highest snow storage component (61%). The minimum SWE percentage value (15%) is found in the Slave Basin. For thirteen out of the fifteen basins, SWE represents at least 20% of TWS according to WGHM simulation and reaches an average of up to 30% when all basins are combined.

The contribution of the soil moisture storage is moderate in most of the basins, according to Figure 5.3. It varies between 4% and 44%. The highest SMS contribution is found in the Liard Basin, while the lowest one is obtained in the La Grande Basin. It is important to indicate that after SWE and wetland storage, the soil moisture contains the most important water storage component during winter.

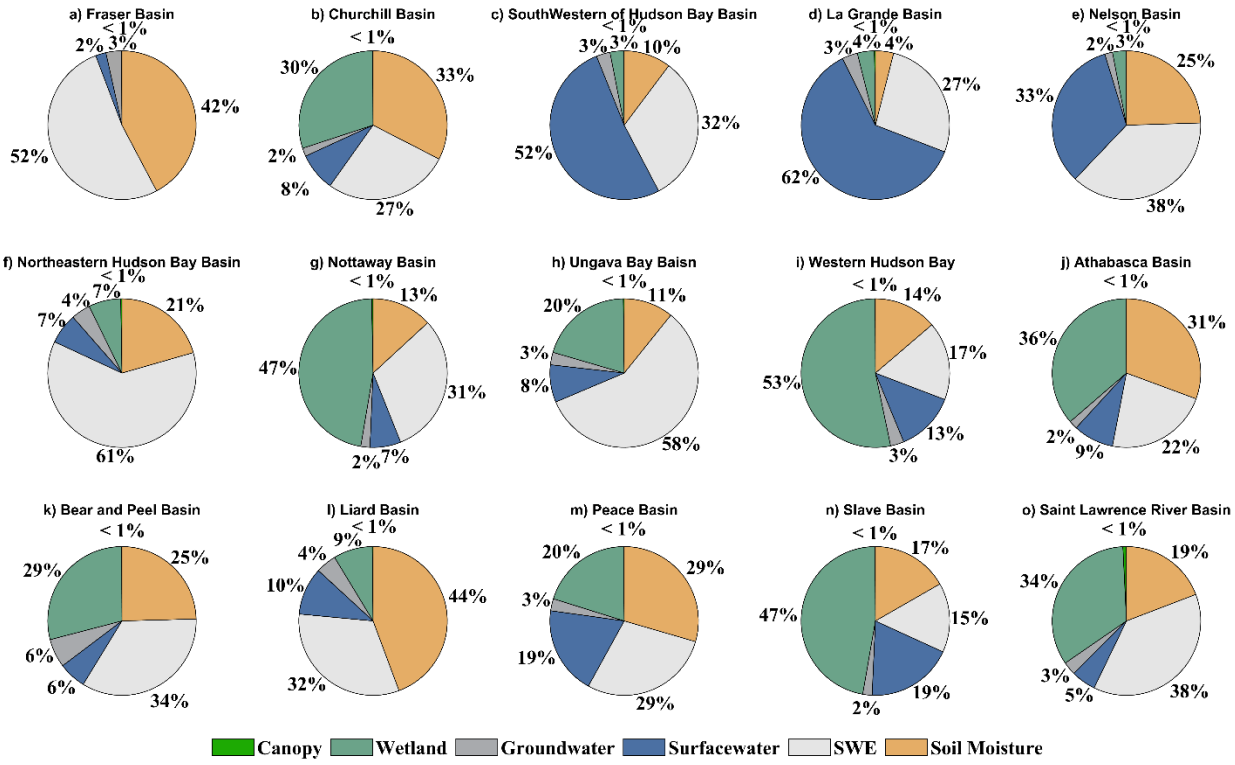

Figure 5.3. WGHM time mean storage compartment, including canopy, wetland, groundwater, surface water, SWE, and soil moisture in the fifteen studied basins during the snow seasons from 2002 to 2011.

5.5.2. Correlation assessment

We investigated TWSA-SWEA and SWEA-SWEA relationships on a basin-scale over the study period from 2002 to 2011. Thus, average basin scale TWSA and SWEA time series from GRACE were respectively compared to each of the three SWEA data sources, that is, GlobSnow2, AMSR-E, and CMC. Table 5.2 summarizes the Spearman correlations, and Table 5.3 provides the related RMSE values. The terrestrial water storage and snow water equivalent anomalies related to each source of data for fifteen basins are shown in Figure 5.4 and Figure 5.5.

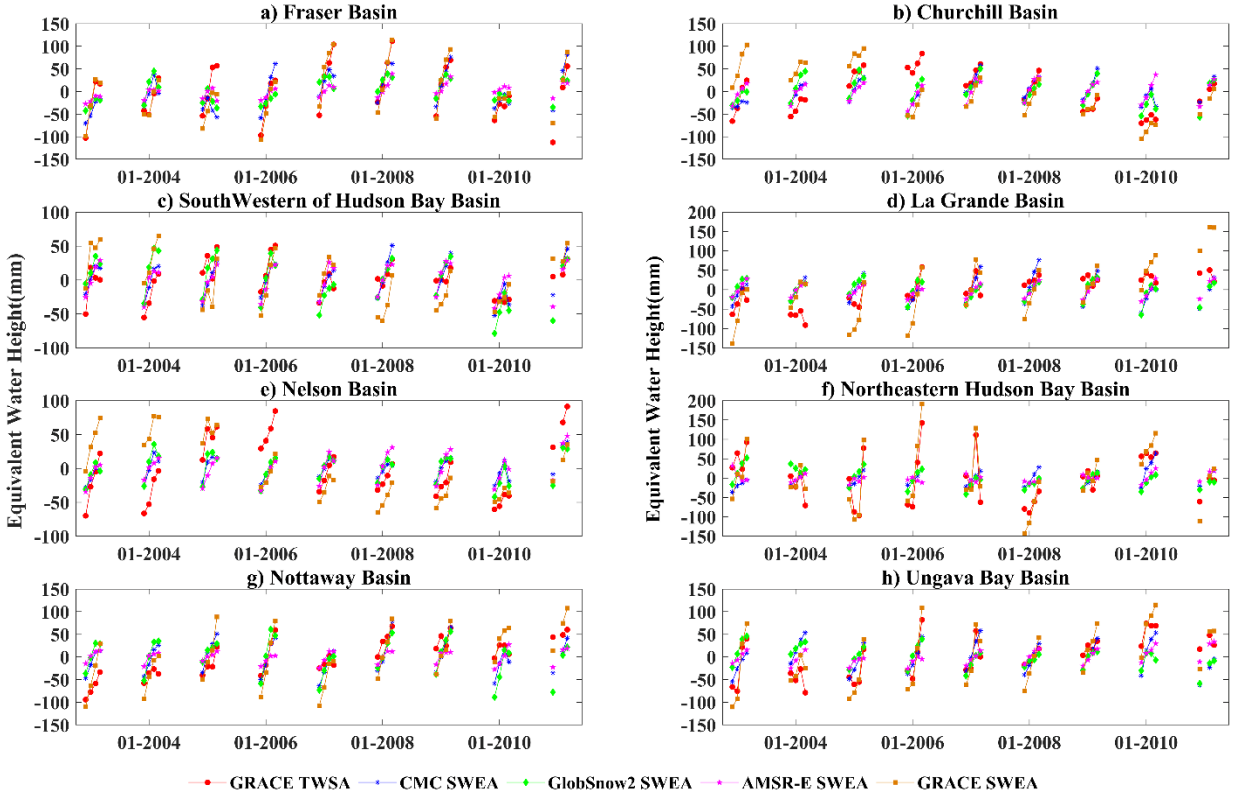

Figure 5.4. Basin-average DJFM time series of GRACE TWSA, CMC SWEA, GlobSnow2 SWEA, AMSR-E SWEA, and GRACE SWEA for the Fraser, Churchill, Southwestern of Hudson Bay, La Grande, Nelson, Northeastern Hudson Bay, Nottaway, Ungava Bay Basins from December 2002 until March 2011.

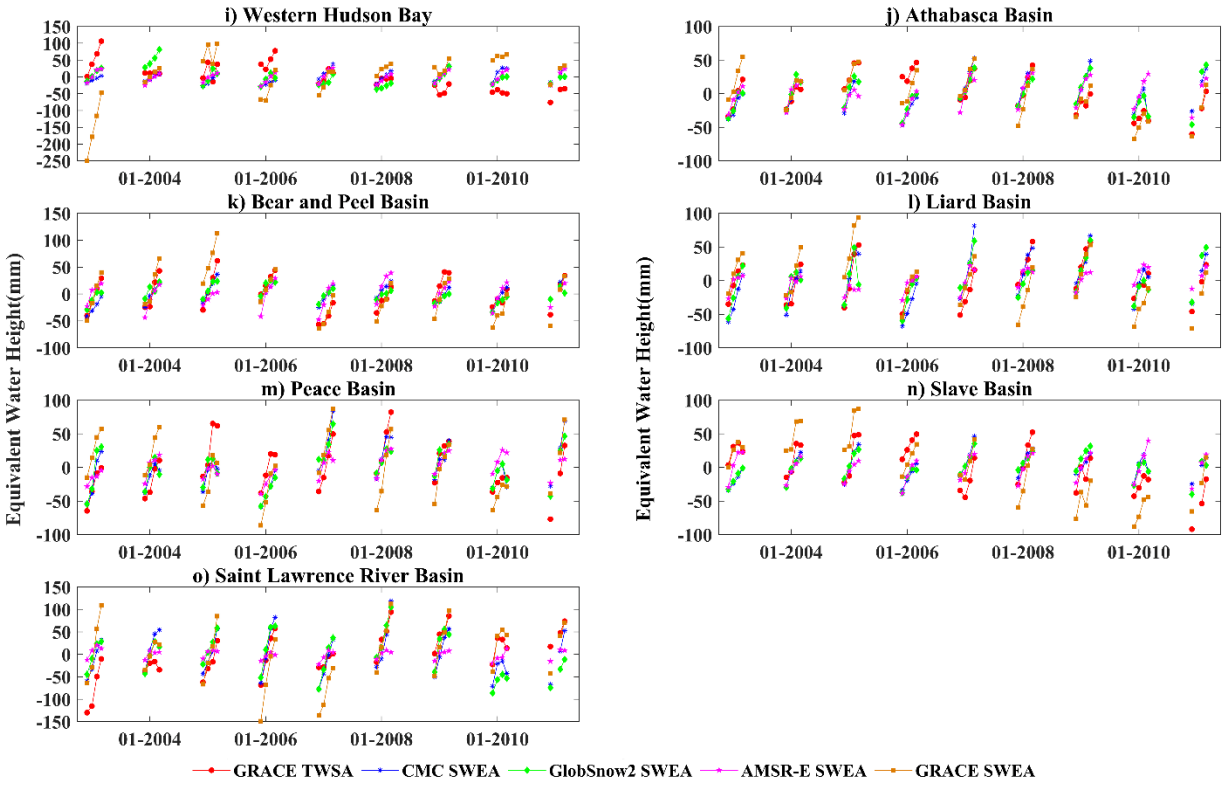

Figure 5.5. Basin-average DJFM time series of GRACE TWSA, CMC SWEA, GlobSnow2 SWEA, AMSR-E SWEA, and GRACE SWEA for the Western Hudson Bay, Athabasca, Bear and Peel, Liard, Peace, Slave, Saint Lawrence River Basins from December 2002 until March 2011.

Table 5.2. Basin averaged statistical results between GRACE derived TWSA and SWEA and GlobSnow2/AMSR-E/CMC SWEA for fifteen basins from December 2002 to March 2011. Entries marked with an asterisk indicate insignificant R_s results.

Basin ID	Basin Name	R_s					
		TWSAversus SWEA			SWEA versus SWEA		
		GRACE-GlobSnow2	GRACE-AMSR-E	GRACE-CMC	GRACE-GlobSnow2	GRACE-AMSR-E	GRACE-CMC
1	Fraser	0.6	0.7	0.7	0.7	0.7	0.8
2	Churchill	0.6	0.3*	0.4	0.6	0.3	0.3*
3	Southwestern of Hudson Bay	0.6	0.5	0.6	0.5	0.5	0.5
4	La Grande	0.0*	0.1*	0.1*	0.3	0.6	0.5
5	Nelson	0.6	0.5	0.6	0.5	0.3*	0.4
6	Northeastern Hudson Bay	0.3*	0.1*	0.2*	0.5	0.2*	0.6
7	Nottaway	0.4	0.3*	0.5	0.7	0.6	0.8
8	Ungava Bay	0.2*	0.5	0.4	0.5	0.8	0.7
9	Western Hudson Bay	0.3*	0.1*	-0.3*	0.0*	0.3*	0.4
10	Athabasca	0.5	0.2*	0.4	0.6	0.4	0.6
11	Bear and Peel	0.6	0.6	0.7	0.8	0.6	0.7
12	Liard	0.7	0.5	0.8	0.7	0.2*	0.6
13	Peace	0.7	0.6	0.8	0.7	0.5	0.8
14	Slave	0.3*	0.4	0.4	0.3*	0.4	0.3
15	Saint Lawrence River	0.5	0.2*	0.6	0.5	0.6	0.7

Table 5.3. Basin averaged RMSE results between GRACE derived TWSA and SWEA and GlobSnow2/AMSR-E/CMC SWEA for fifteen basins from December 2002 to March 2011.

Basin ID	Basin Name	RMSE (mm)					
		TWSAversus SWEA			SWEAversus SWEA		
		GRACE-GlobSnow2	GRACE-AMSR-E	GRACE-CMC	GRACE-GlobSnow2	GRACE-AMSR-E	GRACE-CMC
1	Fraser	46.0	46.2	39.3	44.4	47.0	32.7
2	Churchill	38.1	42.9	40.4	44.3	51.8	53.9
3	South Western of Hudson Bay	27.2	23.2	21.2	35.0	31.4	31.0
4	La Grande	45.9	41.0	47.5	69.7	63.9	64.4
5	Nelson	37.0	38.8	35.7	39.3	44.1	41.1
6	Northeastern Hudson Bay	57.4	60.8	59.3	67.6	74.7	65.0
7	Nottaway	47.1	39.9	37.1	45.4	49.4	35.7
8	Ungava Bay	46.7	38.7	43.1	54.9	51.2	44.2
9	Western Hudson Bay	41.9	40.2	47.7	73.4	67.7	65.4
10	Athabasca	26.3	30.3	28.6	25.2	29.7	27.9
11	Bear and Peel	23.8	24.5	22.4	32.3	35.8	32.0
12	Liard	23.5	25.2	21.4	31.6	39.5	33.1
13	Peace	28.5	29.5	26.8	29.4	36.5	27.9
14	Slave	32.3	30.7	32.4	44.3	43.3	42.9
15	Saint Lawrence River	51.0	48.6	43.2	53.5	58.0	43.3

The Spearman's correlation and RMSE values used to assess the basin-based spatial and temporal correlation between GRACE TWSA observations and GlobSnow2 SWEA are presented in Table 5.2 and Table 5.3. There is a significant relationship between TWSA and SWEA for 10 out of the 15 basins (67%) considered in the study. The highest correlations (R_s = 0.7) are found in the western part of the country, that is, Liard (RMSE = 23.5 mm) and Peace (RMSE = 28.5 mm) while weak and insignificant results are obtained in the La Grande, Northeastern Hudson Bay, Ungava Bay, Western Hudson Bay, and Slave Basins.

Summary of the basin-based analysis of GRACE TWSA against AMSR-E SWEA presented in Table 5.2 and Table 5.3 shows the highest R_s value (0.7) in the Fraser Basin and the lowest (R_s = 0.1) in the La Grande, the Northeastern Hudson Bay, and Western Hudson Bay Basins. The RMSE values fall between the range of 23.2 mm to 60.8 mm. Overall, in 53% (8 out of 15) of the basins, GRACE TWSA has significant relationship with AMSR-E data. It can be interpreted that the total water storage changes as sensed by GRACE were quite linked to the variation of AMSR-E SWEA. On the other hand, if we observe that changes in total water storage were quite linked to changes in snow water equivalent over a time window (2002-2011), we can obtain a significant and strong relationship between GRACE and AMSR-E at any studied basin. Insignificant or weak relationship occurs mostly in the sub-basins of Hudson Bay, Athabasca, and Saint Lawrence River Basins.

In Table 5.2, significant correlations are obtained between GRACE TWSA and CMC SWEA for 12 out of the 15 basins considered (80% of the basins). It can be seen in Figure 5.4 and Figure 5.5, that changes in TWS are linked to variations in SWE. Stronger relationships can be seen in snow-dominated basins (R_s >= 0.7), such as Liard (RMSE = 21.4 mm) and Peace Basins (RMSE = 26.8 mm). From this analysis based on CMC data, it appears more clearly that GRACE TWS variability is highly influenced by SWEA during winter in several basins. However, similar to GlobSnow2 and AMSR-E, CMC does not provide significant results in the La Grande, Northeastern Hudson Bay, and Western Hudson Bay Basins (Figure 5.4d,f and Figure 5.5(i)). The influence of other water components, such as surface water or wetlands may be more important in these areas. To better understand, different water storage components simulated by WGHM were subtracted from GRACE observations in order to estimate the GRACE-derived SWEA. Then, this latter was compared to multisource SWEA. The summary of statistical correlation results is presented below.

The basin-based relationship between GRACE and GlobSnow2 SWEA provides the highest R_s value (0.8) for the Bear and Peel Basin with RMSE value of the 32.3 mm (Table 5.2 and 5.3). About 87% of the basins show significant correlation results. In contrary to what is observed from GRACE TWSA versus GlobSnow2 relationship, GRACE-derived SWEA has significant relationship with GlobSnow2 in the Quebec area, where SWEAs exhibit strong variability in both space and time. As it can be seen in Figure 5.4, the temporal variations of GRACE derived SWEA in the La Grande and Ungava Basins are more consistent with GlobSnow2 SWE changes. Insignificant correlations are found for Slave and Western Hudson Basins with RMSE values of 44.26 and 73.42, respectively.

The highest R_s value (0.8) between GRACE and AMSR-E SWEA is achieved in the Ungava Basin. Overall, 11 out of 15 basins (73%) show significant relationships between GRACE and AMSR-E during snow accumulation season. The minimum value of RMSE (29.7 mm) is obtained in the Athabasca, while the maximum value of RMSE (74.7 mm) appears in the Northeastern of the Hudson Bay. It is worth mentioning that similar to GlobSnow2, the correlation results between GRACE derived SWEAs and AMSR-E in the Quebec area are significantly improved. In Figure 5.4 we can observe that in the north of Quebec the temporal variations of GRACE SWEA are more related to AMSR-E than GRACE TWSA. The insignificant results are obtained in the Nelson, Northeastern Hudson Bay, Western Hudson Bay, and Liard Basins.

The comparison of the GRACE-derived SWEA and CMC-derived SWEA shows that the maximum correlation is achieved in the Fraser, Nottaway, and Peace Basins (R_s = 0.8). In the Peace Basin, we obtained the highest value of correlation with the minimum value of RMSE among all basin. The RMSE values fall within the range of 27.9 mm to 65.4 mm with a median value of 41.1 mm. Overall, GRACE derived SWEA shows significant relationship with CMC data in 93% of the basins (13% more than GRACE TWSA). The minimum (R_s = 0.3) and insignificant value is found in the Churchill Basin. In contrast to GRACE TWSA, the correlation results in the sub-basins of Hudson Bay show strong correspondence with CMC data. For example, in the Western Hudson Bay Basin, the insignificant Spearman's correlation value is increased from -0.3 to the significant value of 0.4.

5.6. Discussion

Regarding the basin-based correlation results of GRACE-derived TWSA versus GlobSnow2/AMSR-E/CMC SWEA data, it appears that GRACE TWSAs are generally quite linked to SWE variations during snow accumulation season. Higher correlation values can be found in the Peace, Fraser and Liard Basins where the seasonal signals of SWE are stronger than the other basins. For example, as it can be seen in Figure 5.4, the CMC-derived SWEA in the Fraser Basin falls between the range of -70 mm to 82 mm, while in the Nelson Basin (covers the Canadian Prairie) SWEA varies between -30 mm to 40 mm. Therefore, the seasonal variability of SWEA in the Fraser Basin is much stronger than the Nelson Basin. The RMSE values in these areas are smaller than 40 mm (Table 5.3), which are about 20% of the GRACE-derived TWSA ranges (Figure 5.4). In areas where significant positive correlations are found between GRACE TWSA and multisource SWEA, the snow mass changes appear as a main or dominant component of TWS variabilities. However, in the north of Quebec area and Western Hudson Basins, insignificant or even negative correlation values are obtained.

Based on temporal correlation analyses at the basin scale GRACE-derived SWEA correlates better with multisource SWEA data than GRACE-derived TWSA. This indicates that GRACE SWEA is quite linked to SWEA data. The strongest relationships are found mainly in both eastern and western part of Canada, such as Fraser, Nottaway, Ungava, Bear, and Peel, as well as Peace Basins (R_s = 0.8). We achieved considerable improvement in terms of increasing numbers of significant relationships, especially in the sub-basins of the Hudson Bay. The smallest and largest correlation value improvements fall between the range of 0.1 to 0.7 (Table 5.2). It is worth mentioning that isolating the contributions of wetland, soil moisture, and surface water storage changes from GRACE TWSAs affected the relationship between GRACE and snow products.

Different possible reasons may influence the relationship. First, we should point out the challenge of coarse spatial and temporal resolution in the different products. Variables such as SWE have significant subgrid heterogeneity in horizontal and vertical properties (Mudryk et al., 2015). Spatial aggregation of TWSA and SWEA data at the basin scale whether the size of the basin is small or large smoothes the spatial representation of information. The larger the basin size, the more spatial heterogeneity is lost. In addition, the temporal resolution is reduced to monthly scale,

and this temporal averaging can create a mismatch of TWS and SWE time series, especially in the case of high frequency anomalies (Humphrey, Gudmundsson, & Seneviratne, 2016). Second, in the basins where inconsistencies are observed between TWSA and SWEA data, the GRACE signal may be dominated by the GIA, or/and the inter-annual variations of the GRACE signal (Humphrey et al., 2016). An important issue in the use of GRACE TWS retrievals in Canada is associated to the correction of GRACE observations from secular GIA signals, especially over Hudson Bay, and the Quebec areas (Lambert et al., 2013; Rangelova et al., 2007; Wang et al., 2013). Although the GIA model might not effectively remove the contribution of this background signal from GRACE observations, the inconsistent behavior of GRACE TWS variabilities, compared to multisource SWEA data, might not only be associated to linear trends. It is worth mentioning that the inter-annual variations of GRACE TWS in the areas surrounding Hudson Bay are more uncertain and exhibit considerable noises that influence the information content of the observations (Humphrey et al., 2016; Trautmann et al., 2018). There might be other factors that influence the correlation results, such as a de-aliasing model (tides are poorly modeled over Hudson Bay) in Arctic coastal regions in Canada, and the west coast of Hudson Bay (Humphrey et al., 2016; Rangelova et al., 2007).

It is expected to find high correlations from TWSA-SWEA relationship in areas with high snow accumulation, such as the La Grande, Northeastern Hudson Bay, Nottaway, and Ungava Basins. However, we observe that GRACE TWS does not change proportionally compared to GlobSnow2/AMSR-E/CMC SWE variations. Based on the WGHM water storage compartment results (Figure 5.3), SWE contributes around 30% of the change in water storage over all area of the study covered by the fifteen studied basins. Therefore, we expected to observe high correlation values between GRACE-TWSA and multisource SWEA in basins where the contribution of non-SWE compartments are not so strong. On the other hand, if the contribution of non-SWE storage compartments is important, it implies that the subtraction of their contributions from the total storage should be taken into account. Trautmann et al. (2018) showed that TWS variations in northern latitudes not only are changed by snow variability but also are driven by liquid water (soil moisture, retained water) storage changes. Non-SWE storage anomalies are dominant drivers of inter-annual (high frequency) TWS changes in mid- to high northern latitudes. The best examples of this phenomenon can be found in the sub-basins located in the Quebec area. We observed that after the subtraction of the wetland, surface water storage, and soil moisture contributions from

GRACE derived TWS changes, the correlation results were improved substantially. In the majority of basins, we achieved improved Spearman's correlation values from GRACE SWEA versus multisource SWEA analyses. However, the uncertainties of relationship were increased. The possible reason might be related to the uncertainty of WGHM storage simulations that influenced the correlation relationships.

Our findings agree with the results of Trautmann et al. (2018), who compared modeled TWS to GRACE TWS observation in mid-to-high latitudes. They found that snow mass variations are the main contributor to seasonal TWS variation. Furthermore, Trautmann et al. (2018) achieved weak correlation values with large uncertainties in the Hudson Bay. We can find an agreement between some of our results and previous research in Western Canada. Frappart et al. (2006, 2011) observed strong GRACE-derived SWE signal on North-West Canada and indicated that GRACE could provide an estimate of the spatial and temporal changes of the snow mass. Seo et al. (2010) compared GRACE-derived solid precipitation accumulation against global precipitation and reanalyses products during the winter season (December to February). They obtained a high correlation in the Mackenzie Basin. Our study confirms the significant relationship between GRACE TWSA and SWEA from three different independent data sources.

In addition to the limitations inherent to GRACE derived TWSA data, the uncertainty of WGHM simulation may influence the correlation results. Like other models, water storages simulated by WGHM are affected by several sources of uncertainty, including input data (eg., climate forcing, land cover, water use), modeling approach, and model parameters. To evaluate some of these uncertainties, Khandu et al. (2016) and Müller Schmied et al. (2014) examined the sensitivity of the freshwater fluxes and water storages to climate forcing and human water use. Müller Schmied et al. (2014) showed that by taking into account uncertainties of climate and land cover data, global discharge was changed by 5% whereas actual evapotranspiration was unaffected. In a number of studies, the performance of the WGHM in the simulation of discharge, reservoir, radiation and evapotranspiration was evaluated and it was found that the model estimate in the gridded and basin scales generally outperforms other global models (Masaki et al., 2017; Müller Schmied et al., 2016b; Veldkamp et al., 2018; Wartenburger et al., 2018; Zaherpour et al., 2018, 2019; Zhao et al., 2017). The comparison of seasonal amplitudes of the model to GRACE data showed that WGHM underestimates TWSA in the southern hemisphere and the tropics, but compares favorably

with GRACE in the northern hemisphere (Scanlon et al., 2019). For example, in northern midlatitudes (20-50ºN), WGHM underestimates GRACE TWSA seasonal amplitudes by 3% with the RMSE value of 52.7 mm. From most of the studies, it generally appears that WGHM performs reasonably well to simulate water storage and fluxes. This could explain the improved results found in this study using GRACE derived-SWEA. However, more calibration/data assimilation efforts are still ongoing to improve WGHM model estimates (www.globalcda.de).

The uncertainty of the SWE product is another issue that should be considered. It is well-known that CMC SWE estimations are not reliable in some areas, particularly in high latitudes, where precipitation gauges are sparsely located (Brown et al., 2010), or in areas covered by small sparse lakes. In northern latitudes (i.e., northern Québec, ~ 55º N), the snow analysis depends on GEM forcing precipitation rather than snow observations (Brown & Brasnett, 2010). In these areas, GEM tends to be biased low (~ 0.1-0.4 mm day^{-1}) in comparison to the Climate Research Unit (CRU) observational database (Verseghy, Brown, & Wang, 2017). Both CMC and GlobSnow datasets tend to be biased low in locations where snow observations come from airports and or coastal areas. Therefore, SWE values in these locations should be analyzed with caution (Verseghy et al., 2017). The evaluation of the GlobSnow2 and AMSR-E in a number of studies showed that the satellite remote sensing snow products underestimate SWE compared to ground-based SWE measurements (Hancock et al., 2013; Larue et al., 2017; Tedesco et al., 2004; Tedesco & Narvekar, 2010). Different factors influence the uncertainty of remote sensing SWE products. The main sources of uncertainty may be related to the algorithms considered, the sensitivity of the microwave frequencies to snow mass, land cover types and forest cover fraction, geographical location, the saturation of the signal penetration in high snow conditions, or the presence of wet snow (Hancock et al., 2013; Larue et al., 2017). We observe that the time series of multisource SWEA variations in the Western Hudson Bay Basin (Figure 5.5i) are equal or closer to zero. The possible reasons for weak or insignificant correlations found in this basin may be linked to the limitations of SWEA.

5.7. Conclusions

This paper analyzed the linkage between terrestrial water storage and snow water equivalent anomalies derived from GRACE and snow water equivalent anomalies from three different

sources (GlobSnow2, AMSR-E, and CMC) over fifteen basins covering most of the Canadian landmass from 2002 to 2011.

Regarding the WGHM model simulations in the entire study domain, we found the main contributors to TWS, including snow water equivalent, wetland storage, soil moisture, and surface water. Results highlighted the importance of both SWE and non-SWE compartments on the variabilities of total storage.

The results indicated the significant relationships between GRACE and SWEAs for 53% to 80% of the basins covering the study area, depending on the SWE product used. The strongest TWS-SWE correlation results were obtained with CMC dataset. The RMSE values fell between a range of 21.2 (mm) to 60.8 (mm). The overall performance of the analysis results illustrated that GRACE had significant correlations with multisource snow products in the majority of studied basins with the exception of the north of Quebec area as well as Western Hudson Bay.

Compared to GRACE TWS, in general, we obtained improved agreement between GRACE-derived SWEA and multisource SWE products. The percentage of basins showing a significant dependency between GRACE and GlobSnow2, AMSR-E, and CMC varied between a range of 73% to 93%. The strong concordances were achieved mainly between GRACE and CMC. Furthermore, we found that isolating and subtracting the contribution of non-SWE components from GRACE observations during snow accumulation season improved the relationship between GRACE and SWE products in the Quebec region. However, in areas surrounding the Hudson Bay GRACE observations are contaminated by the considerable noise, generating higher RMSE values compared to other basins.

Overall, the results found at the basin scale, highlight the important role of SWE on terrestrial water storage variations during the winter. The analyses yielded important insights on the patterns of TWSA and SWEA relationships at the coarse resolution. In general, we found that snow mass variations are the main contributor to seasonal TWS variations. However, in the basins where the contributions of wetland, surface water, and soil water storages are significant, their impacts on total water storage should not be ignored.

In a nutshell, GRACE data may have the potential for validating and improving global and regional

land surface models in the areas, where the seasonal TWS variations are influenced by snow mass changes during winter. Thus, it is expected that the integration of the basin-averaged GRACE TWS retrievals with land surface models through data assimilation methods, may improve SWE simulations in such areas. Further research on the long-term, seasonal and sub-seasonal variabilities, error covariance of GRACE data on the gridded scale, may be helpful to extract its main hydrological features, and better understand its linkage with snow water equivalent at the local scale.

5.8. Data availability statement

The data that support the findings of this study are available from the first author upon reasonable request.

Acknowledgment

The authors would like to thank the Natural Sciences and Engineering Research Council of Canada (NSERC) for the financial support of this project. We thank NASA MEaSUREs Program for supporting Gravity Recovery and Climate Experiment Tellus data. The authors thank the National Snow and Ice Data Center for distributing snow water equivalent data, the Meteorological Service of Canada for supporting Canadian Meteorological Centre data products, as well as Hannes Müller Schmied for supplying Water-Global Assessment and Prognosis Global Hydrology Model data sets and technical details of the model. The authors acknowledge the comments and helpful suggestions of two anonymous referees and the editor that helped to improve the manuscript significantly.

References

Abelen, S., & Seitz, F. (2013). Relating satellite gravimetry data to global soil moisture products via data harmonization and correlation analysis. *Remote Sensing of Environment*, *136*, 89–98. https://dx.doi.org/10.1016/j.rse.2013.04.012

Barnett, T. P., Adam, J. C., & Lettenmaier, D. P. (2005). Potential impacts of a warming climate on water availability in snow-dominated regions. *Nature*, *438*(7066), 303–309. https://doi.org/10.1038/nature04141

Behrangi, A., Gardner, A. S., Reager, J. T., & Fisher, J. B. (2017). Using GRACE to constrain precipitation amount over cold mountainous basins. *Geophysical Research Letters*, *44*(1), 219–227. https://doi.org/10.1002/2016GL071832

Behrangi, A., Gardner, A., Reager, J. T., Fisher, J. B., Yang, D., Huffman, G. J., & Adler, R. F. (2018). Using GRACE to estimate snowfall accumulation and assess gauge undercatch corrections in high latitudes. *Journal of Climate*, *31*(21), 8689–8704. https://doi.org/10.1175/JCLI-D-18-0163.1

Brasnett, B. (1999). A global analysis of snow depth for numerical weather prediction. *Journal of Applied Meteorology*, *38*(6), 726–740. https://doi.org/https://doi.org/10.1175/1520-0450(1999)038<0726:AGAOSD>2.0.CO;2

Brown, R., & Brasnett, B. (2010). Canadian Meteorological Centre (CMC) Daily Snow Depth Analysis Data, Version 1. https://doi.org/10.5067/W9FOYWH0EQZ3

Brown, R. D., Brasnett, B., & Robinson, D. (2003). Gridded North American monthly snow depth and snow water equivalent for GCM evaluation. *Atmosphere - Ocean*, *41*(1), 1–14. https://doi.org/10.3137/ao.410101

Brown, R., Derksen, C., & Wang, L. (2010). A multi-data set analysis of variability and change in Arctic spring snow cover extent, 1967-2008. *Journal of Geophysical Research Atmospheres*, *115*(16), 1–16. https://dx.doi.org/10.1029/2010JD013975

Chang, A.T.C, Foster, J.L, Hall, D. K. (1987). Nimbus-7 SMMR Derived Monthly Global Snow Cover and Snow Depth. *Annals of Glaciology*, *9*, 39–44. https://doi.org/10.3189/S0260305500200736

Déry, S. J., Sheffield, J., & Wood, E. F. (2005). Connectivity between Eurasian snow cover extent and Canadian snow water equivalent and river discharge. *Journal of Geophysical Research*, *110*(D23), 1–14. https://dx.doi.org/10.1029/2005JD006173

Döll, P., Müller Schmied, H., Schuh, C., Portmann, F. T., & Eicker, A. (2014). Global-scale assessment of groundwater depletion and related groundwater abstractions: Combining hydrological modeling with information from well observations and GRACE satellites. *Water Resources Research*, *50*(7), 5698–5720. https://doi.org/10.1002/2014WR015595

Eicker, A., Schumacher, M., Kusche, J., Döll, P., & Schmied, H. M. (2014). Calibration/Data Assimilation Approach for Integrating GRACE Data into the WaterGAP Global Hydrology Model (WGHM) Using an Ensemble Kalman Filter: First Results. *Surveys in Geophysics*, *35*(6), 1285–1309. https://dx.doi.org/10.1007/s10712-014-9309-8

Famiglietti, J. S., & Rodell, M. (2013). Environmental science. Water in the balance. *Science (New York, N.Y.)*, *340*(6138), 1300–1301. https://dx.doi.org/10.1126/science.1236460

Forman, B. A., & Reichle, R. H. (2013). The spatial scale of model errors and assimilated retrievals in a terrestrial water storage assimilation system. *Water Resources Research*, *49*(11), 7457–7468. https://doi.org/10.1002/2012WR012885

Forman, B. A., Reichle, R. H., & Rodell, M. (2012). Assimilation of terrestrial water storage from GRACE in a snow-dominated basin. *Water Resources Research*, *48*(1), 1–14. https://doi.org/10.1029/2011WR011239

Frappart, Frédéric, Ramillien, G., Biancamaria, S., Mognard, N. M., & Cazenave, A. (2006). Evolution of high-latitude snow mass derived from the GRACE gravimetry mission (2002–2004). *Geophysical Research Letters*, *33*(2), 1–5. https://dx.doi.org/10.1029/2005GL024778

Frappart, Frederic, Ramillien, G., & Famiglietti, J. S. (2011). Water balance of the Arctic drainage system using GRACE gravimetry products. *International Journal of Remote Sensing*, *32*(2), 431–453. https://dx.doi.org/10.1080/01431160903474954

Geruo, A., Wahr, J., & Zhong, S. (2013). Computations of the viscoelastic response of a 3-D compressible Earth to surface loading: an application to Glacial Isostatic Adjustment in Antarctica and Canada. *Geophysical Journal International*, *192*(2), 557–572. https://dx.doi.org/10.1093/gji/ggs030

Hancock, S., Baxter, R., Evans, J., & Huntley, B. (2013). Evaluating global snow water equivalent products for testing land surface models. *Remote Sensing of Environment*, *128*, 107–117. https://doi.org/10.1016/j.rse.2012.10.004

Humphrey, V., Gudmundsson, L., & Seneviratne, S. I. (2016). Assessing Global Water Storage Variability from GRACE: Trends, Seasonal Cycle, Subseasonal Anomalies and Extremes. *Surveys in Geophysics*, *37*(2), 357–395. https://dx.doi.org/10.1007/s10712-016-9367-1

Iman, R. L., & Conover, W. J. (1979). The use of the rank transform in regression. *Technometrics*, *21*(4), 499–509. https://doi.org/10.1080/00401706.1979.10489820

Kelly, R. (2009). The AMSR-E Snow Depth Algorithm: Description and Initial Results. *Journal of The Remote Sensing Society of Japan*, *29*(1), 307–317. https://dx.doi.org/10.11440/rssj.29.307

Khandu, Forootan, E., Schumacher, M., Awange, J. L., & Müller Schmied, H. (2016). Exploring the influence of precipitation extremes and human water use on total water storage (TWS) changes in the Ganges-Brahmaputra-Meghna River Basin. *Water Resources Research*, *52*(3), 2240–2258. https://doi.org/10.1002/2015WR018113

Kumar, S. V., Zaitchik, B. F., Peters-Lidard, C. D., Rodell, M., Reichle, R., Li, B., … Ek, M. (2016). Assimilation of Gridded GRACE terrestrial water storage estimates in the North American land data assimilation system. *Journal of Hydrometeorology*, *17*(7), 1951–1972. https://dx.doi.org/10.1175/JHM-D-15-0157.1

Lambert, A., Huang, J., van der Kamp, G., Henton, J., Mazzotti, S., James, T. S., … Barr, A. G. (2013). Measuring water accumulation rates using GRACE data in areas experiencing glacial isostatic adjustment: The Nelson River basin. *Geophysical Research Letters*, *40*(23), 6118–6122. https://dx.doi.org/10.1002/2013GL057973

Landerer, F. W., & Swenson, S. C. (2012). Accuracy of scaled GRACE terrestrial water storage estimates. *Water Resources Research*, *48*(4), 1–11. https://dx.doi.org/10.1029/2011WR011453

Larue, F., Royer, A., De Sève, D., Langlois, A., Roy, A., & Brucker, L. (2017). Validation of GlobSnow-2 snow water equivalent over Eastern Canada. *Remote Sensing of Environment*, *194*, 264–277. https://dx.doi.org/10.1016/j.rse.2017.03.027

Ma, N., Niu, G. Y., Xia, Y., Cai, X., Zhang, Y., Ma, Y., & Fang, Y. (2017). A Systematic Evaluation of Noah-MP in Simulating Land-Atmosphere Energy, Water, and Carbon Exchanges Over the Continental United States. *Journal of Geophysical Research: Atmospheres*, *122*(22), 12,245-12,268. https://doi.org/10.1002/2017JD027597

Masaki, Y., Hanasaki, N., Biemans, H., Schmied, H. M., Tang, Q., Wada, Y., … Hijioka, Y. (2017). Intercomparison of global river discharge simulations focusing on dam operation -

Multiple models analysis in two case-study river basins, Missouri-Mississippi and Green-Colorado. *Environmental Research Letters*, *12*(5), 055002. https://doi.org/10.1088/1748-9326/aa57a8

Mudryk, L. R., Derksen, C., Kushner, P. J., & Brown, R. (2015). Characterization of Northern Hemisphere snow water equivalent datasets, 1981-2010. *Journal of Climate*, *28*(20), 8037–8051. https://dx.doi.org/10.1175/JCLI-D-15-0229.1

Müller Schmied, H., Adam, L., Eisner, S., Fink, G., Flörke, M., Kim, H., … Döll, P. (2016a). Variations of global and continental water balance components as impacted by climate forcing uncertainty and human water use. *Hydrol. Earth Syst. Sci.*, *20*(7), 2877. https://doi.org/10.5194/hess-20-2877-2016

Müller Schmied, H., Eisner, S., Franz, D., Wattenbach, M., Portmann, F. T., Flörke, M., & Döll, P. (2014). Sensitivity of simulated global-scale freshwater fluxes and storages to input data, hydrological model structure, human water use and calibration. *Hydrology and Earth System Sciences*, *18*(9), 3511–3538. https://doi.org/10.5194/hess-18-3511-2014

Müller Schmied, Hannes. (2017). *Evaluation, modification and application of a global hydrological model.* Ph.D. Frankfurt Hydrology Paper 16, Institute of Physical Geography, Goethe University Frankfurt, Frankfurt am Main, Germany.

Müller Schmied, Hannes, Müller, R., Sanchez-Lorenzo, A., Ahrens, B., & Wild, M. (2016b). Evaluation of radiation components in a global freshwater model with station-based observations. *Water (Switzerland)*, *8*(10), 450. https://doi.org/10.3390/w8100450

Niu, G.-Y., Seo, K.-W., Yang, Z.-L., Wilson, C., Su, H., Chen, J., & Rodell, M. (2007). Retrieving snow mass from GRACE terrestrial water storage change with a land surface model. *Geophysical Research Letters*, *34*(15), 1–5. https://dx.doi.org/10.1029/2007GL030413

Ramillien, G., Frappart, F., Cazenave, A., & Guntner, A. (2005). Time variations of land water storage from an inversion of 2 years of GRACE geoids. *Earth and Planetary Science Letters*, *235*(1–2), 283–301. https://dx.doi.org/10.1016/j.epsl.2005.04.005

Rangelova, E., van der Wal, W., Braun, A., Sideris, M. G., & Wu, P. (2007). Analysis of Gravity Recovery and Climate Experiment time-variable mass redistribution signals over North

America by means of principal component analysis. *Journal of Geophysical Research*, *112*(F3), 1–12. https://dx.doi.org/10.1029/2006JF000615

Sakumura, C., Bettadpur, S., & Bruinsma, S. (2014). Ensemble prediction and intercomparison analysis of GRACE time-variable gravity field models. *Geophysical Research Letters*, *41*(5), 1389–1397. https://dx.doi.org/10.1002/2013GL058632

Scanlon, B. R., Zhang, Z., Rateb, A., Sun, A., Wiese, D., Save, H., … Reedy, R. C. (2019). Tracking seasonal fluctuations in land water storage using global models and GRACE satellites. *Geophysical Research Letters*, *46(10)*, 5254-5264. https://doi.org/10.1029/2018GL081836

Schneider, U., Becker, A., Finger, P., Meyer-Christoffer, A., Ziese, M., & Rudolf, B. (2014). GPCC's new land surface precipitation climatology based on quality-controlled in situ data and its role in quantifying the global water cycle. *Theoretical and Applied Climatology*, *115*(1–2), 15–40. https://doi.org/10.1007/s00704-013-0860-x

Schumacher, M., Eicker, A., Kusche, J., Schmied, H. M., & Döll, P. (2015). *Covariance Analysis and Sensitivity Studies for GRACE Assimilation into WGHM*. In: Rizos C., Willis P. (eds) IAG 150 Years. International Association of Geodesy Symposia, vol 143. Springer, Cham. https://doi.org/10.1007/1345_2015_119

Schumacher, M., Kusche, J., & Döll, P. (2016). A systematic impact assessment of GRACE error correlation on data assimilation in hydrological models. *Journal of Geodesy*, *90*(6), 537–559. https://dx.doi.org/10.1007/s00190-016-0892-y

Seo, K. W., Ryu, D., Kim, B. M., Waliser, D. E., Tian, B., & Eom, J. (2010). GRACE and AMSR-E-based estimates of winter season solid precipitation accumulation in the Arctic drainage region. *Journal of Geophysical Research Atmospheres*, *115*(20), 1–18. https://doi.org/10.1029/2009JD013504

Sturm, M., Holmgren, J., & Liston, G. E. (1995). A seasonal snow cover classification system for local to global applications. *Journal of Climate*, *8*(5), 1261–1283. https://doi.org/10.1175/1520-0442(1995)008<1261:ASSCCS>2.0.CO;2

Su, H., Yang, Z. L., Dickinson, R. E., Wilson, C. R., & Niu, G. Y. (2010). Multisensor snow data assimilation at the continental scale: The value of Gravity Recovery and Climate Experiment

terrestrial water storage information. *Journal of Geophysical Research Atmospheres*, *115*(10), 1–14. https://doi.org/10.1029/2009JD013035

Swenson, S. (2010). Assessing High-Latitude Winter Precipitation from Global Precipitation Analyses Using GRACE. *Journal of Hydrometeorology*, *11*(2), 405–420. https://dx.doi.org/10.1175/2009JHM1194.1

Swenson, S. C., & Lawrence, D. M. (2012). A new fractional snow-covered area parameterization for the Community Land Model and its effect on the surface energy balance. *Journal of Geophysical Research Atmospheres*, *117*(21), 1–20. https://doi.org/10.1029/2012JD018178

Swenson, S., & Wahr, J. (2006). Post-processing removal of correlated errors in GRACE data. *Geophysical Research Letters*, *33*(8), 1–4. https://dx.doi.org/10.1029/2005GL025285

Takala, M., Luojus, K., Pulliainen, J., Derksen, C., Lemmetyinen, J., Kärnä, J.-P., … Bojkov, B. (2011). Estimating northern hemisphere snow water equivalent for climate research through assimilation of space-borne radiometer data and ground-based measurements. *Remote Sensing of Environment*, *115*(12), 3517–3529. https://dx.doi.org/10.1016/j.rse.2011.08.014

Tapley, B. D., Bettadpur, S., Ries, J. C., Thompson, P. F., & Watkins, M. M. (2004). GRACE measurements of mass variability in the Earth system. *Science*, *305*(5683), 503–505. https://doi.org/10.1126/science.1099192

Tedesco, M., Kelly, R., Foster, J. L., & Chang, A. T. C. (2004). *AMSR-E/Aqua Daily L3 Global Snow Water Equivalent EASE-Grids Version 2. NASA National Snow and Ice Data Center Distributed Active Archive Center, Boulder, Colorado, USA*. https://doi.org/10.5067/AMSR-E/AE_DYSNO.002.

Tedesco, M., & Narvekar, P. S. (2010). Assessment of the NASA AMSR-E SWE Product. *IEEE Journal of Selected Topics in Applied Earth Observations and Remote Sensing*, *3*(1), 141–159. https://dx.doi.org/10.1109/JSTARS.2010.2040462

Toure, A. M., Rodell, M., Yang, Z.-L., Beaudoing, H., Kim, E., Zhang, Y., & Kwon, Y. (2016). Evaluation of the Snow Simulations from the Community Land Model, Version 4 (CLM4). *Journal of Hydrometeorology*, *17*(1), 153–170. https://dx.doi.org/10.1175/JHM-D-14-0165.1

Trautmann, T., Koirala, S., Carvalhais, N., Eicker, A., Fink, M., Niemann, C., & Jung, M. (2018).

Understanding terrestrial water storage variations in northern latitudes across scales. *Hydrology and Earth System Sciences*, *22*(7), 4061–4082. https://doi.org/10.5194/hess-22-4061-2018

Veldkamp, T. I. E., Zhao, F., Ward, P. J., De Moel, H., Aerts, J. C. J. H., Schmied, H. M., … Wada, Y. (2018). Human impact parameterizations in global hydrological models improve estimates of monthly discharges and hydrological extremes: A multi-model validation study. *Environmental Research Letters*, *13*(5). https://doi.org/10.1088/1748-9326/aab96f

Verseghy, D., Brown, R., & Wang, L. (2017). Evaluation of CLASS snow simulation over Eastern Canada. *Journal of Hydrometeorology*, *18*(5), 1205–1225. https://doi.org/10.1175/JHM-D-16-0153.1

Wahr, J., Swenson, S., & Velicogna, I. (2006). Accuracy of GRACE mass estimates. *Geophysical Research Letters*, *33*(6), 1–5. https://dx.doi.org/10.1029/2005GL025305

Wang, H., Jia, L., Steffen, H., Wu, P., Jiang, L., Hsu, H., … Hu, B. (2013). Increased water storage in North America and Scandinavia from GRACE gravity data. *Nature Geoscience*, *6*(1), 38–42. https://dx.doi.org/10.1038/ngeo1652

Wartenburger, R., Seneviratne, S. I., Hirschi, M., Chang, J., Ciais, P., Deryng, D., … Zhou, T. (2018). Evapotranspiration simulations in ISIMIP2a-Evaluation of spatio-temporal characteristics with a comprehensive ensemble of independent datasets. *Environmental Research Letters*, *13*(7). https://doi.org/10.1088/1748-9326/aac4bb

Weedon, G. P., Balsamo, G., Bellouin, N., Gomes, S., Best, M. J., & Viterbo, P. (2014). The WFDEI meteorological forcing data set: WATCH Forcing data methodology applied to ERA-Interim reanalysis data. *Water Resources Research*, *50*(9), 7505–7514. https://doi.org/10.1002/2014WR015638

Zaherpour, J., Gosling, S. N., Mount, N., Schmied, H. M., Veldkamp, T. I. E., Dankers, R., … Wada, Y. (2018). Worldwide evaluation of mean and extreme runoff from six global-scale hydrological models that account for human impacts. *Environmental Research Letters*, *13*(6), 065015. https://doi.org/10.1088/1748-9326/aac547

Zaherpour, J., Mount, N., Gosling, S. N., Dankers, R., Eisner, S., Gerten, D., … Wada, Y. (2019). Exploring the value of machine learning for weighted multi-model combination of an

ensemble of global hydrological models. *Environmental Modelling and Software*, *114*, 112–128. https://doi.org/10.1016/j.envsoft.2019.01.003

Zaitchik, B. F., Rodell, M., & Reichle, R. H. (2008). Assimilation of GRACE terrestrial water storage data into a land surface model: Results for the Mississippi River basin. *Journal of Hydrometeorology*, *9*(3), 535–548. https://doi.org/10.1175/2007JHM951.1

Zhang, Y. F., Hoar, T. J., Yang, Z. L., Anderson, J. L., Toure, A. M., & Rodell, M. (2014). Assimilation of MODIS snow cover through the data assimilation research testbed and the community Land Model version 4. *Journal of Geophysical Research*, *119*(12), 7091–7103. https://doi.org/10.1002/2013JD021329

Zhang, Y., & Ma, N. (2018). Spatiotemporal variability of snow cover and snow water equivalent in the last three decades over Eurasia. *Journal of Hydrology*, *559*, 238–251. https://doi.org/10.1016/j.jhydrol.2018.02.031

Zhao, F., Veldkamp, T. I. E., Frieler, K., Schewe, J., Ostberg, S., Willner, S., … Yamazaki, D. (2017). The critical role of the routing scheme in simulating peak river discharge in global hydrological models. *Environmental Research Letters*, *12*(7), 075003. https://doi.org/10.1088/1748-9326/aa7250

6. Data Assimilation of satellite-based terrestrial water storage changes into a hydrology land-surface model

6.1. Article presentation

This article intends to incorporate the remote sensing observations into the Environment and Climate Change Canada modeling framework. A semi-distributed model called MESH has been selected for large-scale watershed modeling with consideration of cold region processes in Canada. The main objective of this article investigates how the integration of GRACE TWS observations could improve MESH model predictions of SWE and streamflow. To implement the objective, the EnKS method was used in the snow-dominated Liard Basin of northwestern Canada. Validation of results was conducted for six years (from October 2008 to October 2014) using independent data that were collected at different scales (gridded, basin-scale, and station observations). The general performance of the ensemble-based MESH-GRACE data assimilation system is discussed in details regarding the reduction of model uncertainty and the disaggregation of GRACE observations during the cold season.

In this article, the methodology of implementing the data assimilation framework was summarized in Figure 6.2. The EnkS framework consisted of a two-step procedure, including the forecast and analysis steps. To yield an ensemble of OL and DA, perturbation fields were applied to precipitation, radiation fields (shortwave and longwave), and SWE. The ensemble members were generated from October 2008 to October 2014. The overview of perturbation parameters was presented in Table 6.1. In the forecast step, the time-dependent error covariance and the Kalman gain matrix were computed at the beginning of each month. The model then continues running and stores TWS states. When the computing process reaches the end of the month, the monthly forecast prediction of GRACE TWS was computed. In the analysis step of data assimilation, the monthly-averaged updates for the desired month were divided by the total number of days in the month to obtain the daily fraction of updates. The ensemble was reinitialized, and the MESH model was reset to the beginning of the month. During this step, the daily fraction of updates was added to MESH forecast states over each day. Analysis increments were applied to all TWS compartments of the MESH model, including SWE, the subsurface, and other water storage states. When the

analysis increments were applied for the last day of the month, the forecast step of the next month was launched; this two-step procedure was repeated for the next month, and so on. The complete manuscript is presented below.

Data Assimilation of satellite-based terrestrial water storage changes into a hydrology land-surface model

by Ala Bahrami, Kalifa Goïta, Ramata Magagi , Bruce Davison, Saman Razavi, Mohamed Elshamy, Daniel Princz

Journal of Hydrology

ISSN: 0022-1694

In review for Journal of Hydrology

Data Assimilation of satellite-based terrestrial water storage changes into a hydrology land-surface model

Ala Bahrami[1], Kalifa Goïta [1], Ramata Magagi [1], Bruce Davison[2], Saman Razavi[3], Mohamed Elshamy[3], Daniel Princz[2]

[1] Centre d'applications et de recherches en télédétection (CARTEL), Département de géomatique appliquée, Université de Sherbrooke, Sherbrooke, Québec, Canada

[2] Environment and Climate Change Canada, Saskatoon, Saskatchewan, Canada

[3] Global Institute for Water Security, School of Environment and Sustainability, Saskatoon, Saskatchewan, Canada

Abstract: Accurate estimation of snow mass or snow water equivalent (SWE) over space and time is required for global and regional predictions of the effects of climate change. This work investigates whether integration of remotely sensed terrestrial water storage (TWS) information, which is derived from the Gravity Recovery and Climate Experiment (GRACE), can improve SWE and streamflow simulations within a semi-distributed hydrology land surface model. A data assimilation (DA) framework was developed to combine TWS observations with the MESH (Modélisation Environnementale Communautaire – Surface Hydrology) model using an ensemble Kalman smoother (EnKS). The snow-dominated Liard Basin was selected as a case study. The proposed assimilation methodology reduced bias of monthly SWE simulations at the basin scale by 17.5 % and improved unbiased root-mean-square difference (ubRMSD) by 23 %. At the grid scale, the DA method improved ubRMSD values and correlation coefficients for 85 % and 97 % of the grid cells, respectively. Effects of GRACE DA on streamflow simulations were evaluated against observations from three river gauges, where it effectively improved the simulation of high flows during snowmelt season from April to June. The influence of GRACE DA on the total flow volume and low flows was found to be variable. In general, the use of GRACE observations in the assimilation framework not only improved the simulation of SWE, but also effectively influenced streamflow simulations.

Keywords: GRACE, MESH, Data assimilation, EnKS, Snow water equivalent, Terrestrial water storage

Résumé: Une estimation précise de l'équivalent en eau de la neige (SWE) à travers l'espace et le temps est nécessaire pour les prévisions globales et régionales des effets du changement climatique. Ce travail examine si l'intégration des informations du stock d'eau terrestre (TWS) dérivées des satellites jumeaux Gravity Recovery and Climate Experiment (GRACE), peut améliorer les simulations de SWE et du débit d'eau dans un modèle hydrologique semi-distribué de schéma de surface. Un cadre d'assimilation de données (DA) a été développé pour combiner les observations TWS avec le modèle MESH (Modélisation Environnementale Communautaire - Hydrologie de Surface) en utilisant un ensemble Kalman Smoother (EnKS). Le bassin versant de la Liard dominé par la neige a été choisi comme site d'étude. À l'échelle du bassin versant, la méthodologie d'assimilation proposée a réduit le biais des simulations mensuelles de SWE de 17,5% et amélioré le ubRMSD (unbiased root-mean-square difference) de 23%. À l'échelle de la grille, la méthode DA a amélioré les valeurs ubRMSD et les coefficients de corrélation pour 85% et 97% des cellules de la grille, respectivement. Les effets de GRACE DA sur les simulations de débit ont été évalués par rapport aux observations des débits de trois stations. Ils montrent une amélioration des simulations des débits élevés pendant la saison de fonte de la neige d'avril à juin. Les résultats montrent que l'influence de GRACE DA sur le volume total et les débits d'eau à l'exutoire est variable. En général, l'assimilation des observations GRACE améliore non seulement la simulation de SWE, mais influence également la simulation des estimations de débit d'eau de manière positive.

Mots-clés: GRACE, MESH, Assimilation de données, EnKS, Équivalent en eau de la neige, Stock total d'eau terrestre.

6.2. Introduction

Snow is an important component of terrestrial water storage (TWS), with considerable influence on the short- and long-term behaviors of climate systems (Cohen and Entekhabi, 1999; Su et al., 2010; Walsh, 1984). In northern latitudes and mountainous regions, spring meltwater controls the availability of freshwater resources for more than one-sixth of the world's population (Barnett et al., 2005; Déry et al., 2005; Stieglitz et al., 2001). With respect to terrestrial hydrologic processes, snow water equivalent (SWE) is an important parameter for climatology and hydrology (Foster et

al., 2011). Accurate representation of SWE is thus critical to hydrologists and water resource managers for operational run-off and river discharge forecasts (McCreight et al., 2014; Pulliainen, 2006). Therefore, it is vital that snowpack characteristics are carefully estimated. Ground-based measurements have limitations in terms of characterizing the snowpack, especially in areas with high spatial variability (Liston, 2004). Both satellite remote sensing measurements and land surface model simulations are considered as alternative solutions to estimate snowpack variables (Zhang et al., 2014).

Among satellite measurement techniques with great potential, the Gravity Recovery and Climate Experiment (GRACE, Tapley et al., 2004) has added a unique tool to the existing suite of Earth observations. GRACE measures the redistribution of terrestrial water storage anomalies (TWSA) at regional to global scales (Güntner, 2008). The GRACE mission was launched in March 2002 and has since provided semi-continuous and time-variable gravity measurements for over 15 years, using a constellation of two near-identical satellites that follow each other (Tapley et al., 2019). The mission was extended by launching the GRACE Follow-On (GRACE-FO) in May 2018, with the purpose of continuing the observation of Earth's mass changes (Tapley et al., 2019). The objective of the project is to monitor time-variable components in the variation of the Earth's gravity field to track mass distribution at a large scale in the hydrosphere, cryosphere, and oceans (Tapley et al., 2004). Satellite observations of TWS provide large-scale changes of the total amount of water as the sum of variation in groundwater, soil moisture, SWE, surface water, ice, and water in biomass (Famiglietti and Rodell, 2013). TWSA retrievals have a monthly temporal resolution with an effective spatial (horizontal) resolution that is no better than a few hundred kilometers (~300 km) at midlatitudes (Landerer et Swenson, 2012). Unlike other satellite-based instruments, such as passive microwave sensors, GRACE does not rely upon soil surface and vegetation conditions (Behrangi et al., 2017, 2018). Over snow-dominated areas, the total water storage changes that are captured by GRACE are strongly influenced by snow mass changes during snow accumulation and ablation phases (Forman et al., 2012). However, the disaggregation of GRACE TWS data into individual components, e.g., SWE is difficult making use of land surface models (LSMs, Forman et al., 2012; Zaitchik et al., 2008).

Environment and Climate Change Canada (ECCC) designed a framework called MESH (Modélisation Environnementale Communautaire (MEC) – Surface Hydrology) to couple LSMs

and hydrological models (Pietroniro et al., 2007). As a semi-distributed coupled model, MESH has been developed for large-scale watershed modeling with consideration of cold region processes that are common in Canada. MESH is configured with the Canadian Land Surface Scheme (CLASS, Verseghy, 1991; Verseghy et al., 1993), with hydrological routing implemented from WATFLOOD (Kouwen, 1988; Kouwen et al., 1993), together with lateral flow processes (Mekonnen et al., 2014; Soulis et al., 2011, 2000; Yassin et al., 2019). In this study, CLASS version 3.6 (Verseghy, 2012) simulates vertical energy and water fluxes for the vegetation canopy, snow, and different soil layers. The MESH model is under continuous development by a collaborative team of researchers from ECCC, the Global Institute for Water Security (GIWS, University of Saskatchewan, Saskatoon, SK; Haghnegahdar et al., 2017), and other academic institutions (e.g., McMaster, Waterloo, Wilfrid Laurier Universities).

Different modeling and calibration efforts have been undertaken to improve the performance of MESH in hydrological simulations (Davison et al., 2019, 2006; Dornes et al., 2008; Haghnegahdar and Razavi, 2017; Haghnegahdar et al., 2017, 2015; MacDonald et al., 2009; Mekonnen et al., 2014; Soulis et al., 2011; Yassin et al., 2017). More capabilities have been developed, such as the representation of water management (Yassin et al., 2019) and permafrost (Elshamy et al., 2020). Yassin et al. (2017) used GRACE observations in a multiobjective calibration approach to constrain the model parameters.

In the context of snow, the performance of MESH using CLASS has been evaluated over the Great Lakes Basin (Pietroniro et al., 2007). The validation of results against snow survey observations has indicated that MESH underestimates the SWE estimates (Pietroniro et al., 2007). The major sources of errors in the MESH model simulations are related to the quality of input forcing data, model physical parameterization, and land surface characteristics data. Bearing in mind these limitations of the model, improvements to the performance of MESH are required for the simulation of water storage components.

The data assimilation (DA) technique can incorporate remote sensing observations into hydrological models. In DA methods, hydrological predictions are improved by combining model estimates with observations (Davison et al., 2019), based upon the level of uncertainties that are accounted for in both model predictions and observations (Dunne and Entekhabi, 2005). Many

efforts have focused on integrating GRACE observations into LSMs to improve the accuracy of TWS simulations. The performance of GRACE DA frameworks at grid- and river basin-scales has been tested for different applications, including the estimation of groundwater, soil moisture, global water budgets, drought monitoring, flood and streamflows, and evapotranspiration (Eicker et al., 2014; Girotto et al., 2016, 2017, 2019; Houborg et al., 2012; Khaki et al., 2017a, 2017b; Khaki and Awange, 2019; Kumar et al., 2016; Li et al., 2012; Reager et al., 2015; Schumacher et al., 2018, 2016; Tangdamrongsub et al., 2018, 2015; Van Dijk et al., 2014; Zaitchik et al., 2008). Forman et al. (2012) and Su et al. (2010) investigated the potential for GRACE-derived TWS observations in the data assimilation framework to represent snow budgets accurately. They found that GRACE data assimilation improved modeled SWE in some portions of North American basins (e.g., the Mackenzie Basin). For SWE estimates, Forman et al. (2012) achieved a modest reduction in root-mean-square difference (RMSD) in the Liard Basin (RMSD = 24 mm for OL and RMSD = 19.6 mm for DA).

Xu et al. (2015) applied a one-dimensional version of the Ensemble Kalman filter (1D-EnKF) over the Great Lakes by incorporating SMOS soil moisture retrievals into the MESH model. Results highlighted that the developed DA methodology can improve moisture estimation for both the soil surface and root zone over the crop-dominated grids.

As development of the MESH model continues, some researchers and collaborators have focused upon incorporating remotely sensed products into the modeling system, especially for forecasting applications (Xu et al., 2015; Yassin et al., 2017). Given the importance of GRACE observations in improving changes in estimated terrestrial water storage and its compartments in different LSMs, a question arises whether integrating GRACE observations into the MESH is truly effective. Given the coarse spatial and temporal resolutions of GRACE observations, a robust data assimilation method should be implemented to improve MESH model predictions.

The first specific objective evaluated how the assimilation of basin-averaged GRACE observations could improve MESH model predictions of SWE at both basin and gridded spatial resolution scales. Our second specific objective examined the influence of the developed assimilation framework on streamflow simulation. To achieve these objectives, the ensemble Kalman smoother (EnKS, Evensen and Van Leeuwen, 2000) framework was implemented in the snow-dominated

Liard Basin of northwestern Canada. Validation of results was conducted for six years (from October 2008 to October 2014) using independent data that were collected at different scales (gridded, basin-scale, and station observations). The general performance of the ensemble-based MESH-GRACE data assimilation system is discussed in details regarding the reduction of model uncertainty and the disaggregation of GRACE observations during the cold season. In section 3, the study area and the different data are described, together with the MESH model. In section 4, the details of the developed methodology are explained. Sections 5 and 6 present the results and discussion. Finally, the conclusions of this study are provided in section 7.

6.3. Data and model

6.3.1. Study Area

The study domain that was selected is the Liard River basin, which is a sub-basin of the much larger Mackenzie River basin (Figure 6.1). The watershed of the Liard River drains portions of British Columbia and Alberta, and the Yukon and Northwest Territories of boreal northwestern Canada, spanning longitudes 132°W to 118°W and latitudes 57°N to 63°N. Land cover of the Liard Basin is dominated by sub-polar needleleaf and mixed forest (71%) and grasslands (16%), followed by barren land (7%) and wetlands (4%); a small fraction of its area is covered by water bodies (1.5%) and glaciers (0.5%). The basin is about 275 000 km^2 in area which is greater than the effective area of (~ 150 000 km^2) that can be resolved by GRACE at mid- and high latitudes (Forman et al., 2012; Swenson and Wahr, 2006).

Two main reasons motivated selection of the Liard Basin as the case study. First, preliminary analyses (not presented in this study) revealed that GRACE TWSA seasonal amplitudes in the Liard Basin are dominated by snow mass changes during the snow season (Bahrami et al., 2020). Second, contributions of surface water mass changes from lakes, reservoirs, and river storage to total water storage is not significant, given the very low surface coverage contributions of water bodies and wetlands in the basin.

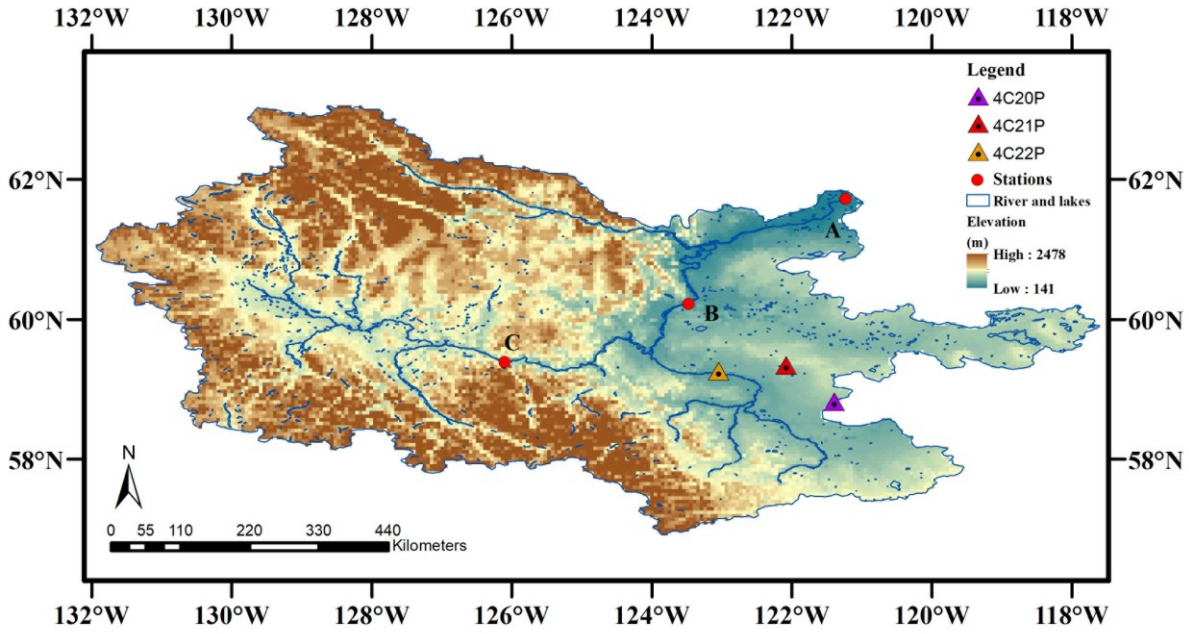

Figure 6.1. Map of the Liard Basin, including the digital elevation model (DEM), basin boundary, locations of streamflow observations, and automated snow survey locations (triangles). Red circles indicate three river stations: (A) Liard River Near the Mouth ; (B) Liard River at Fort Liard; and (C) Liard River at Lower Crossing.

6.3.2. GRACE TWS datasets

The gridded (1°×1°), GRACE-derived TWSA data are publicly available from October 2008 to October 2014, through the NASA Jet Propulsion Laboratory (JPL) TELLUS website (Swenson, 2012). We used Release 5 (RL05) level-3 monthly data products that were provided by three data centers, including the Center for Space Research (CSR) of the University of Texas at Austin, the Deutsches GeoForschungsZentrum (GFZ, the German Research Centre for Geosciences, Potsdam, Germany), and JPL (Pasadena, CA, USA). To effectively reduce the noise in the GRACE data, we used the arithmetic mean of all three data products (Sakumura et al., 2014). Because of filtering and truncation of GRACE TWSA observations, the surface mass variation signal is attenuated (Swenson and Wahr, 2006). Gridded (1°×1°) multiplicative gain factors that are provided by TELLUS were applied to the original GRACE TWS retrievals to restore the signal loss (Landerer and Swenson, 2012). The linear trends that were related to glacial isostatic adjustment (GIA) have

been removed from GRACE TELLUS mass grids, based on the model by Geruo et al. (2013).

6.3.3. Snow Water Equivalent Products

To evaluate the performance of the SWE estimates from MESH, we made use of data that were provided by the Canadian Meteorological Centre (CMC, Dorval, QC). Daily gridded CMC snow depth analysis has been provided by CMC at a spatial resolution of 0.25°×0.25° (~24 km × ~24 km) over the Northern Hemisphere from October 2008 to October 2014 (Brown and Brasnett, 2010). The CMC daily snow depth analysis (Brasnett, 1999) is based upon optimal interpolation of in-situ daily snow observations and the initial guess. The initial guess field is provided by a simple snow accumulation and melt model using analyzed temperature and forecasted precipitation from the Canadian Global Environmental Multiscale (GEM) forecast model. Monthly SWE estimates for the October to June period of each year (Brown and Mote, 2009) were derived from monthly averaged snow depth analyses using the corresponding mean monthly snow density lookup table that was identified by Sturm et al. (1995). The CMC SWE gridded product is often considered as one of the most useful global data sources for evaluating SWE simulations in different studies (Forman et al., 2012; Seo et al., 2010; Su et al., 2010; Toure et al., 2016; Verseghy et al., 2017; Verseghy and MacKay, 2017; Zhang et al., 2014). It should be noted that the CMC SWE product has some limitations, including an imperfect model accumulation and melt model and coarse atmospheric forcing, together with a paucity of snow stations at higher latitudes (Swenson and Lawrence, 2012; Toure et al., 2016). In northern latitudes (~ 55º N), where precipitation gauges are sparsely located (Brown et al., 2010), snow analysis depends upon GEM forcing precipitation rather than snow observations (Brown and Brasnett, 2010). In these areas, GEM tends to be biased low (~ 0.1-0.4 mm day^{-1}) in comparison to the Climate Research Unit (CRU, University of East Anglia, Norwich, England) observational database (Verseghy et al., 2017).

6.3.4. Snow survey observations

Automated snow survey observations are collected and transmitted hourly through the Data Collection System on Geostationary Satellites operated by the National Oceanic and Atmospheric Administration (NOAA). The station-based observations are acquired by the British Columbia Ministry of Environment. Daily SWE observations are publicly available since November 2012

through the provincial snow survey network website. In this study, monthly averaged SWE observations during the snow seasons (November to April) overlapping the study period (i.e. 2013 and 2014) are used to further evaluate the data assimilation performance. The available three automatic snow monitoring stations for this study are the 4C22P (Kiwigana Climate), the 4C21P (Two Island Climate), and 4C20P (Sierra Climate); they are shown in Figure 6.1.

6.3.5. Streamflow observations

Streamflow observations are available from the Water Survey of Canada (WSC) website (http://www.ec.gc.ca/rhc-wsc). Three streamflow records are selected, going from the upper basin to its mouth: the Liard River at Lower Crossing; the Liard River at Fort Liard; and the Liard River Near the Mouth (see Figure 6.1). Gauge-based streamflow observations are used for both the calibration of MESH parameters and the evaluation of the GRACE DA procedure.

6.3.6. MESH model

The prognostic semi-distributed hydrological-land surface model (H-LSM) that was used in this study was developed by Pietroniro et al. (2007). The current version of the MESH model contains an integrated LSM and a river routing system. The geophysical heterogeneity within each grid cell can be defined, based upon a digital elevation model (DEM), land-cover classification, and soil characteristics (Davison et al., 2019). The topographic data are based upon the Canadian Digital Elevation Data (CDED, 2016) at a scale of 1:50 000. Land cover information is extracted from the Land Cover of Canada (LCC, 2010), which is produced based on Landsat satellite images by the Canada Centre for Mapping and Earth Observation (CCMEO), formerly Canada Centre for Remote Sensing (CCRS). Soil texture information comes from Soil Landscapes of Canada (SLC, 2010) data of Agriculture and Agri-Food Canada.

In the MESH model, the desired basin is divided into grids. Each grid is further composed of a number of Grouped Response Units (GRUs; Kouwen et al., 1993). The tile (a specific GRU within a given grid) is the basic computational unit that aggregates different attributes, such as soil and vegetation properties within the grid (Pietroniro and Soulis, 2003). The water storage, energy, and soil prognostic variables for each grid cell are weighted according to the GRUs' percentage area that is occupied inside the grid (Kouwen et al., 1993). The simulated terrestrial water storage in

the MESH model is the sum of several prognostic variables, including intercepted precipitation by the canopy (rain or snow), SWE, snowmelt held in the snow mass, water ponded on the surface, and liquid and frozen water content of soil layers (LQWS and FRWS). Note that in this study, the vertical summation of LQWS and FRWS prognostic states is called the subsurface storage state. The number of soil layers is configurable in MESH, as is their thicknesses. A single-layer snow model is used in MESH to simulate snow mass on bare soil (Verseghy, 1991; Verseghy et al., 1993). Evaluation of simulated SWE of CLASS in the Snow Model Intercomparison Project (SnowMIP) demonstrated that the single-layer model performed as well as multilayer models (Brown et al., 2006).

6.4. Methods

6.4.1. Model configuration

The MESH model for the Liard has been set up at a 0.125º × 0.125º (longitude/latitude) spatial resolution and half-hourly temporal resolution. This yielded a total of 2881 active grids for the basin with seven GRU types, including forest, grass, wetland, barren land, urban, water, and glaciers for the Liard Basin, based on the CCMEO's dataset. A set of seven meteorological inputs are required for the model: incoming shortwave and longwave radiation; precipitation; temperature; barometric pressure; specific humidity; and wind speed. All input-forcing excepted precipitation was obtained from ECCC's GEM Numerical Weather Prediction (NWP) model (Côté et al., 1998a, 1998b; McTaggart-Cowan et al., 2019a, 2019b). Precipitation data were derived from the Canadian Precipitation Analysis (CaPA), which is the analyzed interpolation product of precipitation observations with the model forecast field obtained from the GEM model (Fortin et al., 2018; Lespinas et al., 2015; Mahfouf et al., 2007). Four soil layers with thicknesses of 0.1, 0.25, 0.75, and 3.0 m are used for this model, yielding a total thickness of 4.1 m for the soil column.

Model calibration was implemented using a pseudo multi-objective approach that aggregated three streamflow error metrics, including Percentage Bias (PBIAS), Nash-Sutcliffe Efficiency (NSE, Nash and Sutcliffe, 1970), and Nash-Sutcliffe Efficiency with logarithmic transformation of streamflow (NSE_{log}) at the three selected streamflow stations. NSE emphasizes high flows, while NSE_{log} captures low flows and PBIAS ensures that the total volume is preserved (Krause et al., 2005; Moriasi et al., 2007). Only influential parameters were calibrated as per Haghnegahdar et

al. (2017) for the dominant GRUs (forest, grassland, barren land, and wetland). A total of 49 soil, vegetation, and routing parameters were selected for calibration which was conducted using the Dynamically Dimensioned Search (DDS) method (Tolson and Shoemaker, 2007). Calibration was performed over the October 2003 to October 2008 period, while validation spanned the period October 2008 to October 2014, using a hydrological year that commences October 1st at 00:00 local time. The model was spun up from October 2002 to October 2003 to eliminate the effect of initial conditions. Model performance was satisfactory for all stations, with respective NSE values of 0.73 and 0.78 at the basin outlet for calibration and validation periods, while PBIAS changed from +8% (calibration period) to -5% (validation). October 2008 to October 2014 period was later used for open-loop (OL) and DA simulations.

6.4.2. Data assimilation

The EnKS (Evensen and Van Leeuwen, 2000) approach consists of two major components: forecast (or prediction) and analysis (or update) steps (Evensen, 2003). In the forecast step, the model states are evolved forward in time as an ensemble to estimate errors. In the analysis step, observations are used to update model states for the time period of interest (Dunne and Entekhabi, 2005). In this application, the beginning and end of the assimilation window correspond to the first and last day of the month; a prognostic model refers to the MESH model.

In the EnKS, the nonlinear model *G* propagates the analysis model states, $\mathbf{x}_{k-1,i}^{a}$, sequentially from measurement time *k-1* to the next measurement time step *k* using an ensemble of *N* random realizations of model errors $\mathbf{q}_{k,i}$ to derive the model forecast states $\mathbf{x}_{k,i}^{f}$, as the following

$$x_{k,i}^{f} = \boldsymbol{G}(x_{k-1,i}^{a}, q_{k,i}) \qquad for\ \boldsymbol{i}\ \in\ \boldsymbol{N} \qquad (\mathbf{6}.1)$$

In practice, the model errors are prescribed by applying perturbations to model states and input climate forcing (Forman et al., 2012). Here, for the sake of simplicity, we dropped the ensemble index *i*. In the EnKS method, the analyzed states $\mathbf{x}_{k}^{a}$ are reinitialized, as observations become available, by a weighted linear combination of the model forecast $\mathbf{x}_{k}^{f}$ and the vector of measurement $\mathbf{y_k}$ (Evensen, 2003). This linear combination is written as,

$$x_k^a = x_k^f + \boldsymbol{K_k}\left((\boldsymbol{y_k} + \boldsymbol{\varepsilon_k}) - \boldsymbol{H}\boldsymbol{x_k^f}\right) \quad (\mathbf{6}.2)$$

where $\mathbf{K_k}$ is the Kalman gain and **H** is the measurement vector (or operator) to map the model states linearly into measurement space. Following the work of Forman and Reichle (2013) and Forman et al. (2012), **H** was defined to convert model forecast states to the basin average estimates of TWS. The observations are perturbed by adding random realizations $\boldsymbol{\varepsilon_k}$ of the measurement error (Burgers et al., 1998). In this study, the basin average of GRACE-derived TWSA observations is converted to absolute TWS values by adding the corresponding time-mean (i.e., October 2008 to October 2014) TWS estimates from the MESH simulation.

The second matrix in equation (6.2), i.e., $\boldsymbol{K_k}((\boldsymbol{y_k} + \boldsymbol{\varepsilon_k}) - \boldsymbol{H}\boldsymbol{x_k^f})$, is called the analysis increments (AI). The analysis increments (or updates) transfer the vector of differences between the prediction and measurement to the model prognostic state at the model spatial resolution, based upon the partitioning that is determined by Kalman gain (Girotto *et al.*, 2019). The Kalman gain ($\mathbf{K_k}$) represents the relative weights given to the model forecast states $\mathbf{x}_k^f$ and the observations $\mathbf{y_k}$ during the update state. $\mathbf{K_k}$ is expressed as:

$$\boldsymbol{K_k} = \boldsymbol{P_k^f H^T}\left(\boldsymbol{H P_k^f H^T} + \boldsymbol{R}\right)^{-1} \quad (\mathbf{6}.3)$$

The model forecast (background) error covariance $\mathbf{P_k^f}$ is diagnosed from the sample covariance of the ensemble. Here, **R** is the time-invariant measurement covariance and *T* denotes the transpose operator. In this study, the observation errors are considered to be spatially uncorrelated. Thus, only one scalar value for GRACE observations as a basin average is available for each month (Zaitchik et al., 2008). Following the work of Forman et al. (2012), a constant observation error variance of 289 mm^2 was assigned for GRACE observations in the Liard Basin. A sensitivity analysis for the choice of that error is provided in section 6.6.2.2.

6.4.2.1. Perturbation Setup

In this study, a perturbation module is included to the MESH modeling software. We implemented a customized random field generator developed by the NASA Global Modeling and Assimilation

Office (GMAO, Greenbelt, MD; Reichle et al., 2009). The generation of ensemble spread is maintained by adding perturbations to meteorological forcing and model states (Reichle and Koster, 2003). Based on the variable type, log-normally distributed multiplicative perturbations or normally distributed additive perturbations were generated (Reichle et al., 2007). The precipitation, shortwave radiation, and SWE are subjected to multiplicative perturbations. Longwave radiation received additive normal perturbations. The overview of perturbation parameters is presented in Table 6.1. Following the work of Reichle and Koster (2003) and Forman et al. (2012), two-dimensional pseudo random fields were generated with a horizontal decorrelation length of 2° (latitude/longitude). The temporal correlation of the perturbations was applied through a first-order autoregressive model (AR(1)) with a temporal decorrelation length of one day. Constraints on the perturbed field were applied for every step of the perturbation to avoid physically unfeasible conditions. Both types of multiplicative and additive perturbations were applied every 30 min at the 0.125°× 0.125° spatial resolution. To yield an ensemble of OL, perturbation fields were applied to precipitation, radiation, and SWE, while observations were not integrated with model estimates. The OL ensembles were generated from October 2008 to October 2014 for comparison with data assimilation results.

Following Forman et al. (2012), the major forcing inputs including precipitation and radiation were chosen to limit perturbation to these forcing fields. The perturbation of the other model states rather than SWE, such as soil moisture in different layers, can be added to the current perturbation structure. Because of the effect of creating biases between the ensemble mean and deterministic control (no perturbation, no assimilation) as a result of the specifics of the MESH model or random fields, perturbation of the model state SWE was only considered.

Table 6.1. Perturbation parameters for model state and meteorological forcing

Variable	Perturbation Type	Standard deviation	Temporal Correlation [hours]	Spatial Correlation [°]	Cross correlation with perturbations in		
					P	SW↓	LW↓
Precipitation (P)	Multiplicative	0.5	24	2	1	-0.8	0.5
Shortwave radiation (SW↓)	Multiplicative	0.3	24	2	-0.8	1	-0.5
Longwave radiation (LW↓)	Additive	20 [W m^{-2}]	24	2	0.5	-0.5	1
SWE	Multiplicative	0.0004	24	2			

6.4.2.2. Forecast and analysis approach

Based upon the work of Zaitchik et al. (2008) and Forman et al. (2012), the EnKS assimilation method was developed for the assimilation of GRACE data into the MESH model, version 1.4.1037. The details of a two-step proposed methodology are summarized in Figure 6.2. The following paragraphs explain the method in greater details.

In the first step of the ensemble-based MESH-GRACE data assimilation approach, the MESH model is propagated for month *k* and the model prognostic states of day *j* at 00:00 local time, $\mathbf{x}_{j,k}^{f}$, are stored in memory as a variable $\mathbf{x_{acc}}$. In this application, the model state matrix, $\mathbf{x}_{j,k}^{f}$, has dimensions of $M \times N$, where *M* is the total number of active water storage elements for *N* ensemble realizations. In the Liard Basin, *M* equals to the total numbers of MESH storage compartments, multiplied by the total active tile members for each water storage compartment. Based upon the current set-up of MESH in the Liard Basin, *M* equals to 132 249. An ensemble size, *N*, of twenty members was used in the DA framework.

As seen in the left-hand panel of Figure 6.2 (forecast step), the time-dependent error covariance ($\mathbf{P}_{k}^{f}$) and the Kalman gain matrix ($\mathbf{K_k}$) are computed at the beginning of the month (*k*), based upon the model forecast states of the first day (*j*=1). The model then continues running and stores TWS states. When the computing process reaches the end of the month, the monthly forecast prediction of GRACE TWS observations at the basin scale (i.e., Hx_{k}^{f} in equation 6.2) is computed.

In the second step (analysis step) of data assimilation, the monthly-averaged updates for month *k* are divided by the total number of days in the month to obtain the daily fraction of analysis increments (AI_{daily} in figure 6.2). The ensemble is reinitialized, and the MESH model is reset to the beginning of the month. During this step, AI_{daily} values are added to MESH forecast states ($\mathbf{x}_{j,k}^{f}$) over each day, such that update model states $\mathbf{x}_{j,k}^{a}$ are acquired. Analysis increments are applied to all TWS compartments of the MESH model, including SWE, the subsurface, and other water storage states. It is also possible to use prior information from the model to decide where to apply increments as part of a physically-based update approach. When the analysis increments are applied for the last day of the month, the forecast step of the next month is launched; this two-step procedure is repeated for the next month, and so on. For months when GRACE observations are

not available, only the forecast step is activated.

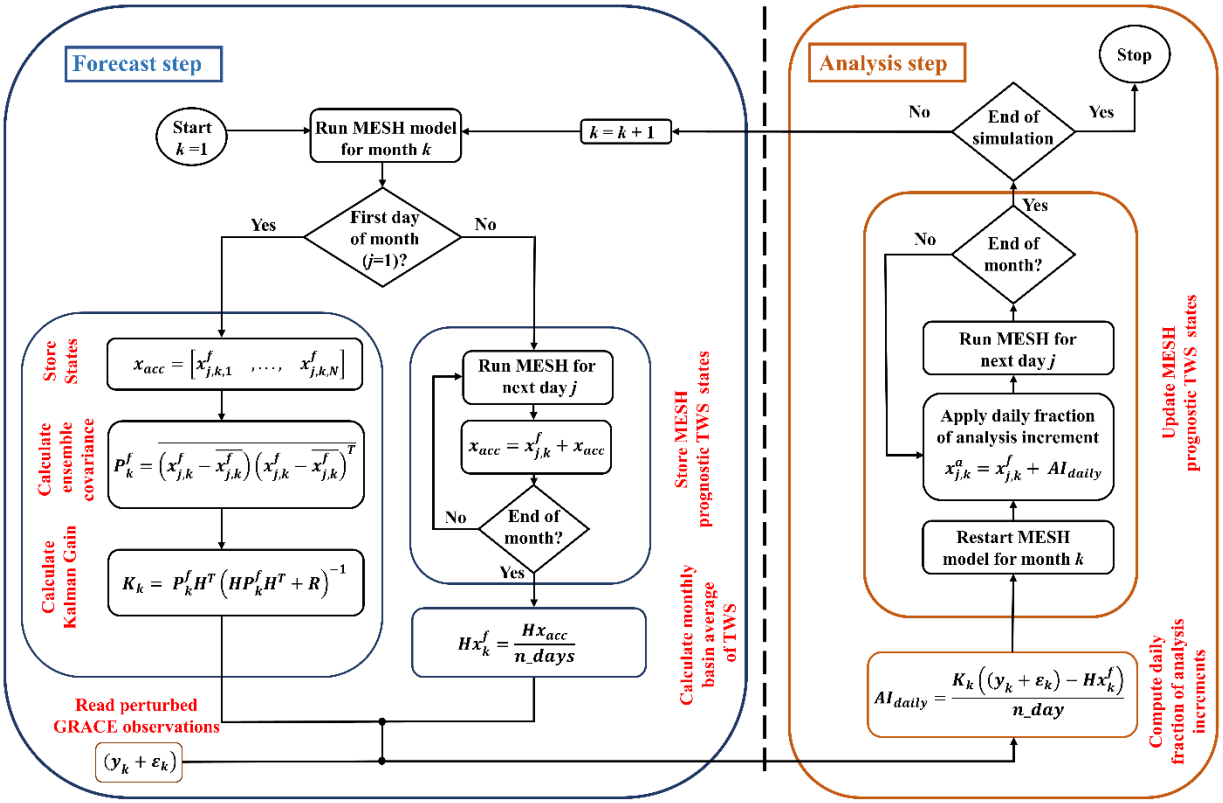

Figure 6.2. Flowchart of MESH-GRACE data assimilation system (modified after Forman et al. 2012).

6.4.3. Evaluation Approach

Different types of evaluation skills were employed to evaluate simulated SWE and streamflow estimates that were obtained from the MESH-GRACE data assimilation framework. Spearman's rank correlations (R_s, Iman and Conover, 1979), PBIAS, and the unbiased root-mean-square difference (ubRMSD, Entekhabi et al., 2010) were computed to compare MESH-derived SWE with independent CMC SWE products and in-situ SWE observation data. The rank-order correlation between the ranks r_i of modeled ensemble mean (OL or DA) and the ranks s_i of the evaluation product is defined as follows (Hamby, 1994):

$$R_s = \frac{\sum_{i=1}^{T}(r_i - \bar{r})\,(s_i - \bar{s})}{\sqrt{\sum_{i=1}^{T}(r_i - \bar{r})^2 \sum_{i=1}^{T}(s_i - \bar{s})^2}} \tag{6.4}$$

where $\bar{r}$ and $\bar{s}$ are time-mean of the data set ranks and T is the total number of months. R_s ranges between -1 and 1 with the optimal value of 1. The statistical significance of the correlation differences was evaluated by using the Fisher's Z-transformation. The null hypothesis (H_0) with the 95% confidence interval was used to evaluate whether the computed R_s differed from zero.

PBIAS indicates the tendency of the simulated data to be larger or smaller than validation values (Gupta et al., 1999). PBIAS was computed as:

$$PBIAS = \frac{\sum_{i=1}^{T}(M_i - O_i) * 100}{\sum_{i=1}^{T}(O_i)} \tag{6.5}$$

where M_i is the modeled ensemble mean (OL or DA) and O_i are the validation data. The optimal value of PBIAS is 0.0, with positive values indicating model overestimation, and negative values indicating model underestimation bias. Similarly, ubRMSD can be expressed as:

$$ubRMSD = \sqrt{\frac{1}{T}\sum_{i=1}^{T}[(M_i - \bar{M}) - (O_i - \bar{O})]^2} \tag{6.6}$$

where $\bar{M}$ and $\bar{O}$ are time-means of modeled ensemble mean (OL or DA). The ubRMSD values near zero indicate that model simulations approach the validation data. The statistical significance of the ubRMSD differences between the OL and DA simulations is determined using the Student's *t* test with the 95% confidence interval.

The simulated streamflow of MESH was validated against streamflow observations that were taken at the three stations (mentioned in Section 6.3) by calculating PBIAS, NSE, and NSE_{log}. NSE ranges between -∞ to 1, where the optimal value equals to 1.0 (Moriasi et al., 2007).

6.5. Results

6.5.1. Terrestrial Water Storage

Daily simulation results of MESH-derived TWS from the OL and DA ensembles and the monthly GRACE TWS retrievals for the Liard Basin are shown in Figure 6.3. Both OL and DA simulations capture the seasonal cycle of TWS. Month-to-month variation in TWS is influenced by the

integration of GRACE observations into the model. Consistent with expectation, in most months, a much better match is found between the DA ensemble and GRACE observations than the OL one. The assimilated TWS ensemble mean lies between both the OL ensemble and GRACE observations, which implies that conditioning of the model can effectively move estimates of the model toward the GRACE observations. It is observed that in some cases, namely year 2012, the number of updates (after assimilation) is small during winter and summer months. In general, the overall performance of the DA procedure is quite promising. It shows how GRACE observations, despite their coarse resolution, can improve estimates of total water storage and effectively influence the uncertainty of the model simulation.

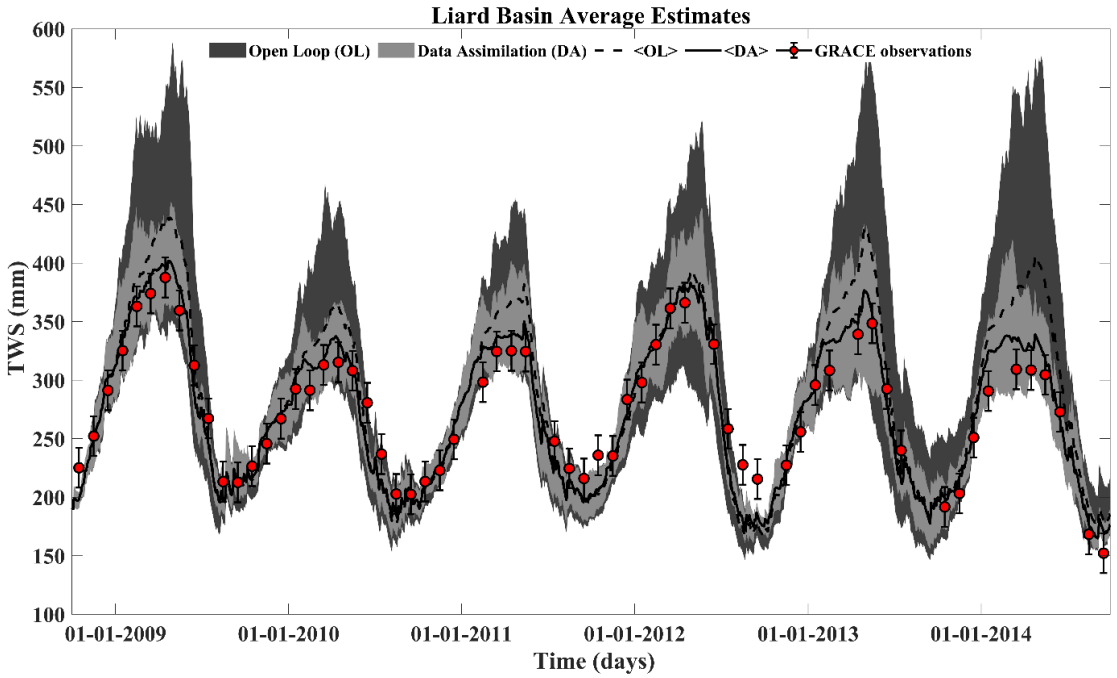

Figure 6.3. Time Series of MESH-derived TWS estimates from the OL (dark gray), DA (light gray) simulation, and the GRACE observations with the error bar of 17 mm in the Liard Basin. The dark and light gray areas show the ranges of OL and DA ensembles, while the thick dashed and solid lines correspond to the respective ensemble means.

6.5.2. Snow Water Equivalent

6.5.2.1. Basin-scale

The influence of GRACE data assimilation on the simulation of SWE was evaluated using monthly

basin-averaged CMC data. Figure 6.4 shows daily MESH-derived SWE estimates from the OL and GRACE DA ensembles with their corresponding ensemble spreads. Monthly averaged CMC values of SWE in the Liard Basin from October to June of each year have been added. Both OL and DA ensembles match the observed seasonal cycle and interannual variability (Figure 6.4). In general, the OL simulations overestimate SWE compared to CMC monthly data. The assimilation results show that integration of GRACE observations into MESH can effectively reduce the snow mass during winter seasons and, consequently, the ensemble averages move toward monthly CMC data. Another apparent feature is that the GRACE DA reduces the uncertainty of the SWE estimates compared to the OL. As a result of data assimilation, an average reduction of 10 mm in ensemble spread was attained.

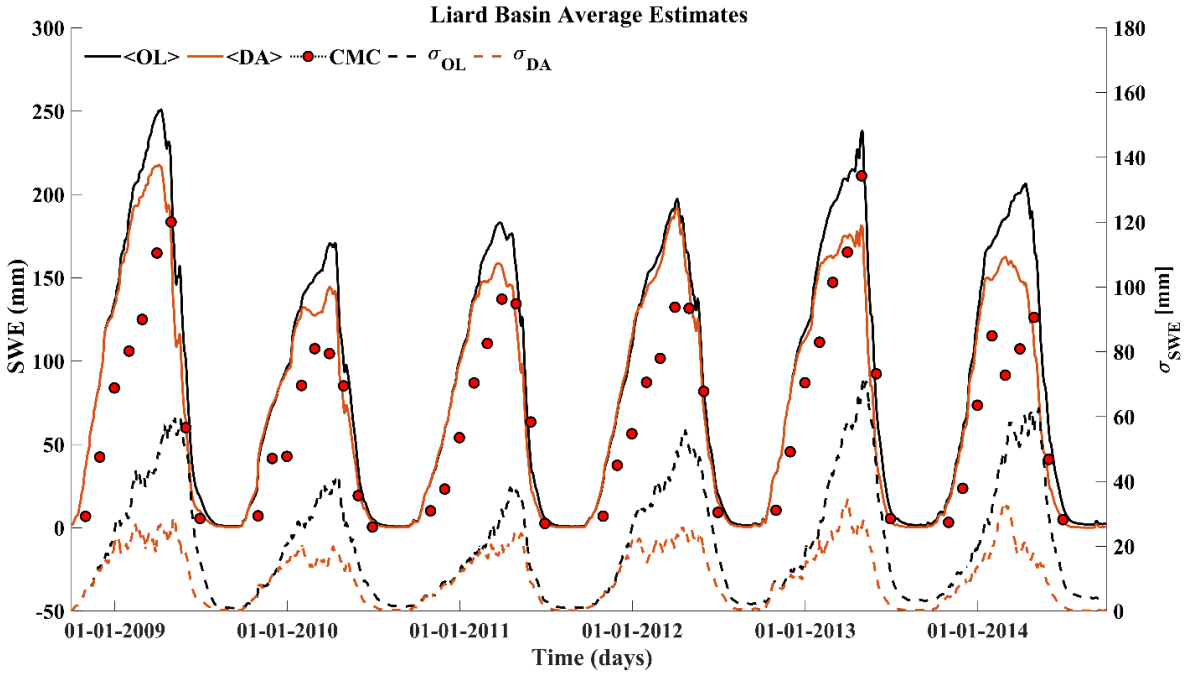

Figure 6.4. Time Series of MESH-derived SWE estimates in the Liard Basin on the left Y-axis and their corresponding ensemble spreads on the right Y-axis. OL and DA ensemble means are shown with solid black and brown lines, respectively. Monthly CMC SWE estimates are represented with solid red circles. OL and DA ensemble spreads are respectively indicated by black and brown dashed lines.

Daily estimates of MESH-derived SWE were converted to a monthly scale for comparison against the CMC data. Summary of the evaluation skills of PBIAS, ubRMSD, and R_s are shown in Figure

6.5. In terms of PBIAS, GRACE DA reduces bias of the simulation by 17%, from +46.7% (for OL) to +29.6% (for DA). The ubRMSD thus decreases from 22.6 mm for OL to 17.7 mm for DA. According to the t-test realized (| *t-value* | = 2.32), this improvement in ubRMSD is statistically significant. Yet, evaluation results for R_s show a very small improvement, i.e., from 0.95 to 0.96. The statistical test that is based upon Fisher's Z-transform with 95% confidence intervals indicates that the difference between OL and DA correlations is not significant. Based upon PBIAS and ubRMSD, assimilation of the GRACE data at the basin scale generally does not only improve the estimation of SWE, but also effectively reduces uncertainty of model estimates.

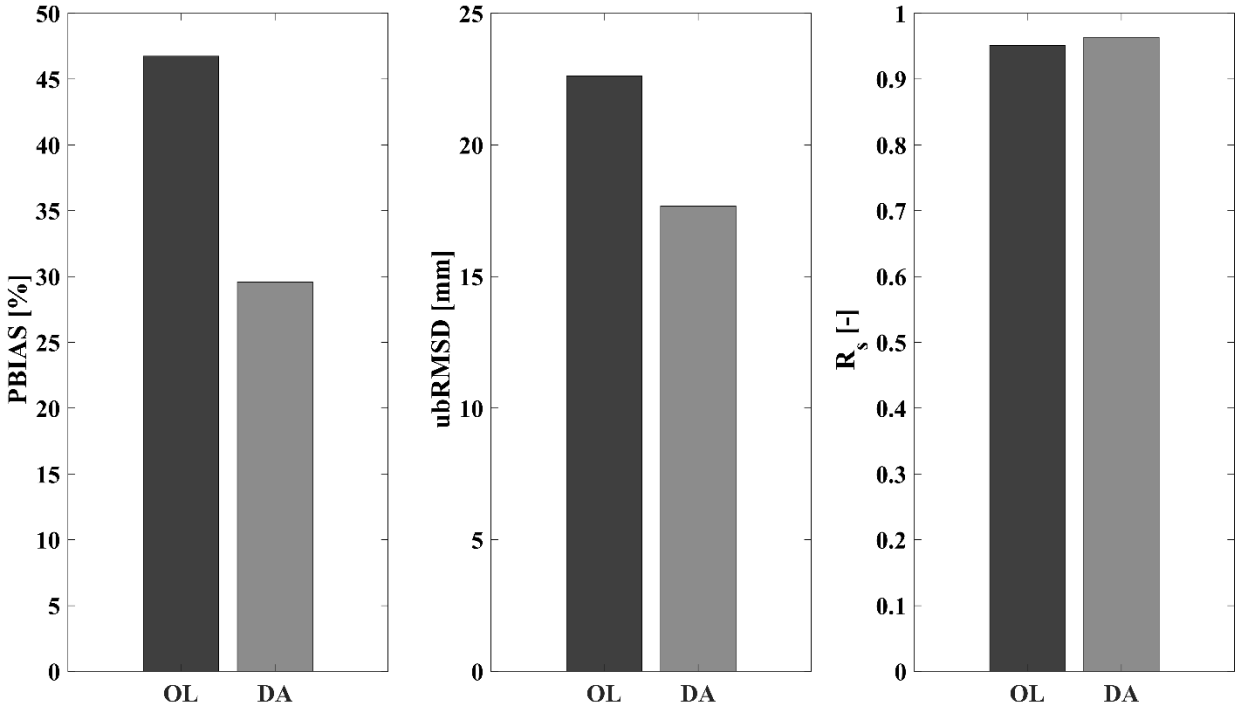

Figure 6.5. Evaluation of the open-loop (OL) and the data assimilation (DA) approaches using Percent bias (PBIAS), unbiased root-mean-square difference (ubRMSD), and Spearman's rank correlations (R_s).

6.5.2.2. Grid scale

In this section, evaluation skills of the DA in terms of correlations (Rs) and ubRMSD are provided at a spatial resolution of 0.125º × 0.125º (longitude/latitude). Monthly CMC SWE data were interpolated on the model grid using the nearest-neighbor approach. Figure 6.6(A) shows ubRMSD

skill for the OL, while Figure 6.6(B) presents the skill difference between DA and OL simulations using blue and red colors to indicate locations of improvement and deterioration, respectively. Significant improvements in ubRMSD are mainly achieved in the Northern Canadian Rockies, Cassiar Mountains and Mackenzie Mountains, which are characterized by larger SWE values compared to the rest of the basin. GRACE DA leads to degraded ubRMSD values at the northwestern and western boundaries of the Liard Basin. The reason for degradation may be related to artifacts that are caused by the perturbation fields over these edge regions. Overall, the ubRMSD values are improved for 85% of the grid cells covering the Liard Basin. The largest improvement that was attained is 165.14 mm. There are statistically significant improvements in terms of the ubRMSD metric in 56% of grid cells. Note that 4% of grid cells experience statistically significant degradations in SWE estimates from the GRACE data assimilation.

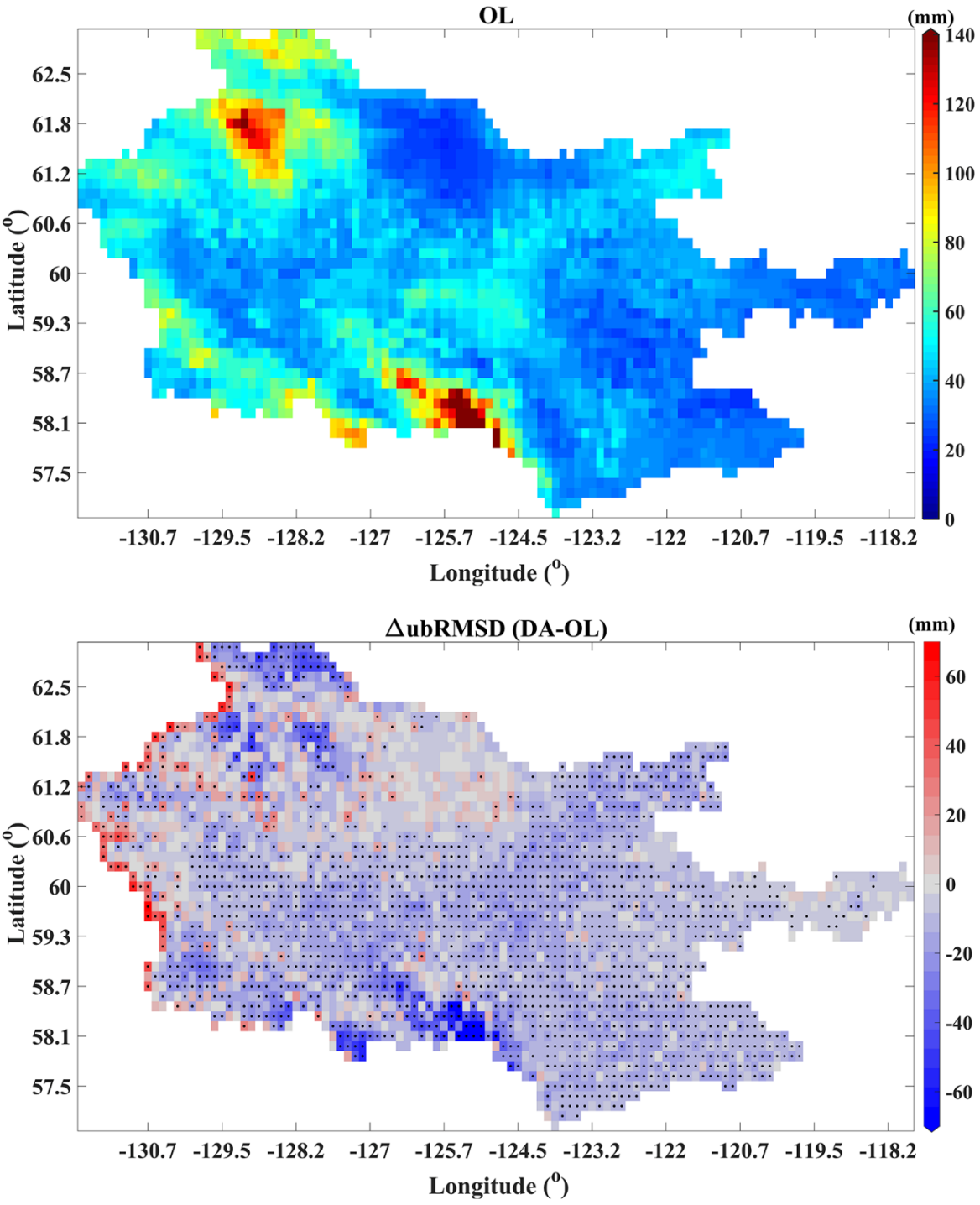

Figure 6.6. Evaluation results of the ubRMSD [mm] of SWE from the OL (A) and the skill difference [mm] between GRACE DA and OL methods (B). Black dots indicate grid cells where the ubRMSD differences are statistically significant at the 95% confidence intervals.

Maps of the correlations (R_s) for the OL and their differences from the GRACE DA are presented in Figure 6.7. Correlation differences fall with the range of -0.25 to 0.26. Grid cells that are shown by black dots (Figure 6.7(B)) indicate that correlation differences between OL vs CMC and DA vs CMC are statistically significant, according to their associated 95% confidence intervals. Compared to the OL method, GRACE DA increased the correlation with CMC SWE data for most grid cells covering the basin, especially in the areas with large annual snow accumulations. Like the pattern of ubRMSD differences in Figure 6.6(B), a decrease in correlations is observed in a few grid cells that are located at the northwestern and western edges of the Liard Basin. Overall, GRACE DA improves the correlation skill values in 97% of the grid cells. Improvements are statistically significant (different from zero) in 61% of these cells. Degradation in the correlations is observed in less than 1% of the grid cells.

In the EnKS method, the ensemble spread is regarded as the standard deviation around the ensemble mean (Evensen, 2003). Here, the time-mean of the monthly ensemble spreads from October 2008 to October 2014 was calculated for both OL and DA methods. Figure 6.8(A) presents the time-mean ensemble spread of MESH-derived SWE for the OL experiment, while Figure 6.8(B) maps the time-mean ensemble spread of the GRACE-DA minus the OL method. For SWE, the mean ensemble spread for the OL over all grid cells in the Liard Basin equals 25.2 mm. Larger ensemble spreads are found in the mountainous areas of the basin, especially in the Northern Canadian Rockies and Mackenzie Mountains, which are dominated by significant seasonal snowpack accumulations. Smaller ensemble spreads are obtained in the grid cells covering non-mountainous areas, including the southeastern and eastern parts of the Liard Basin. After assimilating GRACE observations into the MESH model, the spatially averaged reduction in ensemble spread equals 14.4 mm. With the exception of one grid cell, the ensemble spreads of GRACE DA are smaller than those obtained by the OL method. The larger reductions in the uncertainty of SWE estimates (dark blue in Figure 6.8(B)) mainly occur in areas where the OL produced large ensemble spreads (dark brown in Figure 6.8(A)). In summary, constraining model forecasts by implementing GRACE DA effectively reduced the uncertainty in the MESH-derived SWE. Larger reductions in the ensemble spreads are mainly achieved in areas where significant reductions in the ubRMSD (actual error) values are observed.

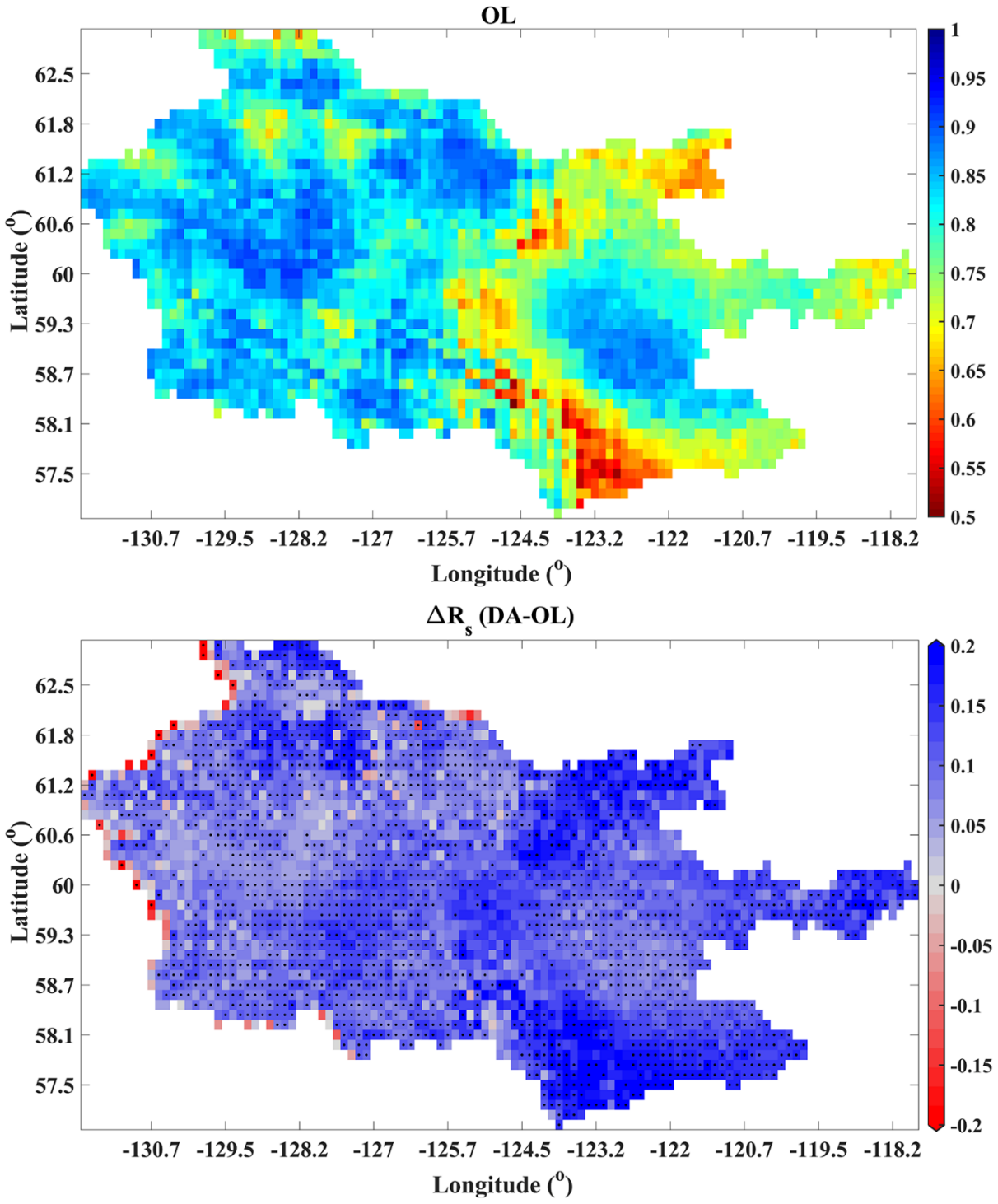

Figure 6.7. Evaluation results of Spearman's rank correlations (R_s) of SWE from the OL (A) and the skill difference ΔR_s between GRACE DA and OL methods (B). Black dots indicate grid cells where the correlation differences between DA and OL results are statistically significant according to their respective 95% confidence intervals.

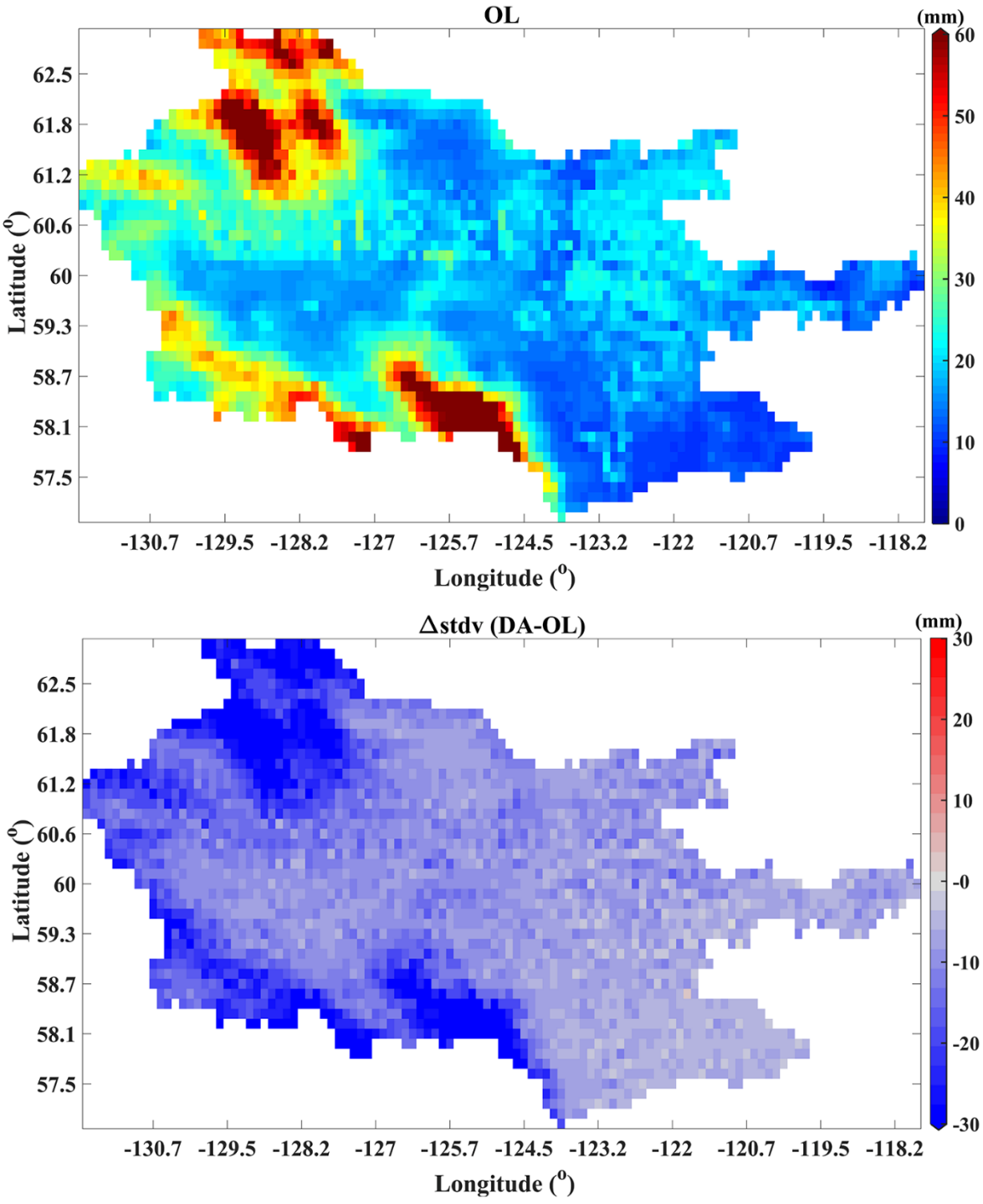

Figure 6.8. Time mean ensemble spread at gridded scale from October 2008 to October 2014 for OL (A) and the difference between ensemble spread of the GRACE DA and OL (B).

6.5.2.3. Comparison with snow measurements

This study uses mainly CMC SWE as a reference product for the comparisons. However, to further assess the assimilation results, the OL and DA SWE simulations were compared against independent ground-based monthly snow survey observations from the three stations available (Section 3.2.2.4). Because of the data limitations of the automatic stations over the study period, the evaluation could be conducted during only two snow seasons (2013 and 2014). To perform each comparison, MESH SWE simulations had to be matched in space and time with snow survey observations. Then, evaluation metrics were computed across time. The results are presented in Table 6.2. During the onset of snow the OL, DA, in-situ observations, and CMC SWE estimates agree quite well, especially from November to January as small updates were applied to MESH model estimates. From February to April when much snow masses were reduced from model simulations, differences between SWE estimates were observed. Figure 6.9 shows a time series of the OL and GRACE DA ensemble means along with snow survey observations and CMC SWE.

In terms of PBIAS skill, the GRACE DA reduces the bias in the SWE at 4C22P (+29.6% for OL, 15.8% for DA) and 4C20P (+18.2% for OL, -1.7% for DA). However, the absolute value of PBIAS was increased at the station 4C21P from -2% for OL to -14.1% for DA. The evaluation results for the ubRMSD skill shows that GRACE DA leads to slight degradations at two snow survey sites compared to OL. The correlation skill values were slightly reduced as a result of the assimilation for all three sites. However, the degradation of DA skills for both ubRMSD and Rs were not statistically significant at the 95% confidence level relative to the OL simulations. In general, the effect of GRACE DA on SWE estimates at the three snow survey stations was found to be mixed, with some patterns of improvements and degradations observed in the intercomparisons to the open-loop simulations. Overall, with GRACE DA, the metrics obtained with CMC in the grid cell corresponding to each ground-based station are not different from those computed for the stations (Table 6.2). The PBIAS improvement follows roughly the same trends. The ubRMSD values vary in a tight range between 16 and 25 mm in all cases, and the correlations found are quite similar. However, the comparison here is just indicative and should be considered with caution due to representativeness error, as stations only provide punctual measurements, while CMC SWE is gridded.

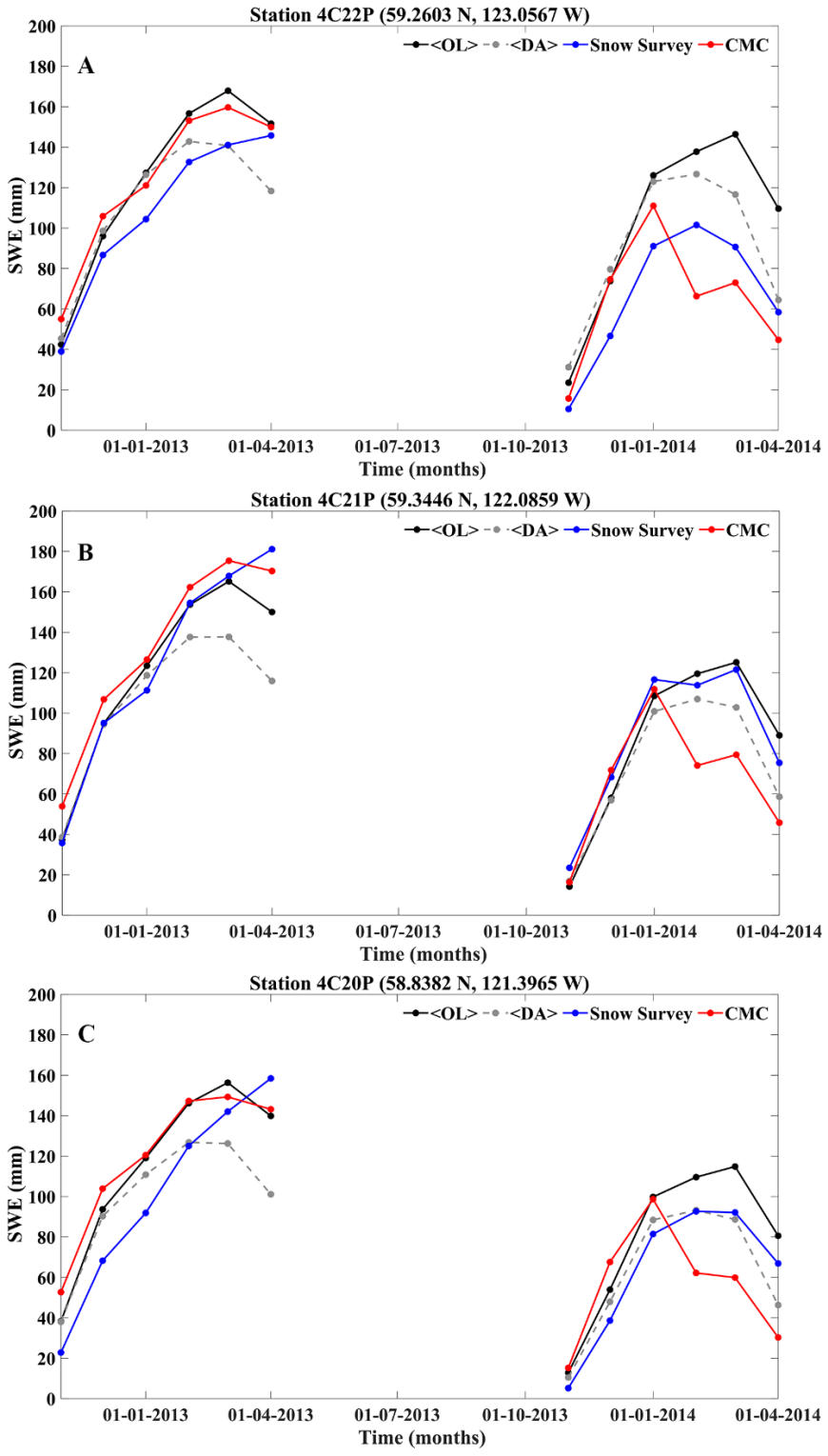

Figure 6.9. Monthly time series comparison of SWE estimates from the OL (black), DA (gray), snow survey observations (blue), and CMC (red) at three snow survey stations: (A) 4C22P, (B)4C21P, and (C) 4C20P.

Table 6.2. Summary of PBIAS, ubRMSD, and R_s skills for OL and GRACE DA at three snow survey stations. Results obtained with CMC for the grid cell corresponding to each station location are also shown.

Station	MESH versus snow survey					
	PBIAS [%]		ubRMSD [mm]		R_s [-]	
	OL	DA	OL	DA	OL	DA
4C22P	+29.6	+15.8	16	16.1	0.92	0.87
4C21P	-2	-14.1	11.4	18.1	0.95	0.87
4C20P	+18.2	-1.7	11.4	20.8	0.95	0.88
	MESH versus CMC					
4C22P	+20.3	+7.4	30.3	24.8	0.76	0.8
4C21P	+3.7	-9.1	24.3	23.4	0.9	0.9
4C20P	+10.9	-7.9	24.6	20.8	0.85	0.9

6.5.3. Streamflow

The performance of OL and GRACE DA in terms of streamflow was evaluated using PBIAS, NSE, and NSE_{log}. Figure 6.10 presents daily MESH-derived streamflow estimates from the OL and GRACE DA ensembles with the corresponding ensemble spreads. Daily averages of the streamflow observations over six years from the three selected river stations were compared against the OL and DA approaches. Evaluations are presented in Table 6.3.

In terms of PBIAS skill, the GRACE DA reduces the bias in the streamflow at Fort Liard from +8.5% for OL to -4.7% for DA. However, the bias skills became slightly worse at the stations Near the Mouth (+3.1% for OL, -9.1% for DA) and Lower Crossing (+4.8% for OL, -9.7% for DA). Changes in the sign of the bias values from negative to positive are related to the reduction of total flow volumes as a result of decreasing snow accumulation. Evaluation results for the NSE skill show that GRACE DA improves high flow peaks during snowmelt seasons from April to June at both Fort Liard (NSE = 0.79 for OL, NSE = 0.83 for DA) and Lower Crossing (NSE = 0.74 for OL, NSE = 0.86 for DA). For example, DA adjusted the streamflow discharge peaks at Fort Liard station by ~2000 m^3 s^{-1} in June 2014. The NSE skill remains unchanged for the Mouth station. Both OL and DA have negative biases in low flow simulations relative to streamflow observations (Figure 6.10). The Assimilation of TWS retrievals has little effect on the low flow estimates during winter seasons. The evaluation results for the NSE_{log} skill reveal that very small degradations in low flows occurred at Lower Crossing during simulation of the DA compared to OL.

The time-mean of daily ensemble spreads from October 2008 to October 2014 of river stations was calculated for both OL and DA methods. Results show that reductions of ensemble spreads that were caused by GRACE DA equal 300.2 m^3 s^{-1} for Near the Mouth, 241.6 m^3 s^{-1} for Fort Liard, and 168.0 m^3 s^{-1} for Lower Crossing.

Table 6.3. Summary of PBIAS, NSE, and NSE_{log} skills for OL and GRACE DA at three river stations.

	PBIAS [%]		NSE [-]		NSE_{log} [-]	
	OL	DA	OL	DA	OL	DA
Liard River Near the Mouth	+3.1	-9.1	0.76	0.76	-0.04	-0.13
Liard River at Fort Liard	+8.5	-4.7	0.79	0.83	-0.07	-0.13
Liard River at Lower Crossing	+4.8	-9.7	0.74	0.86	-1.95	-1.97

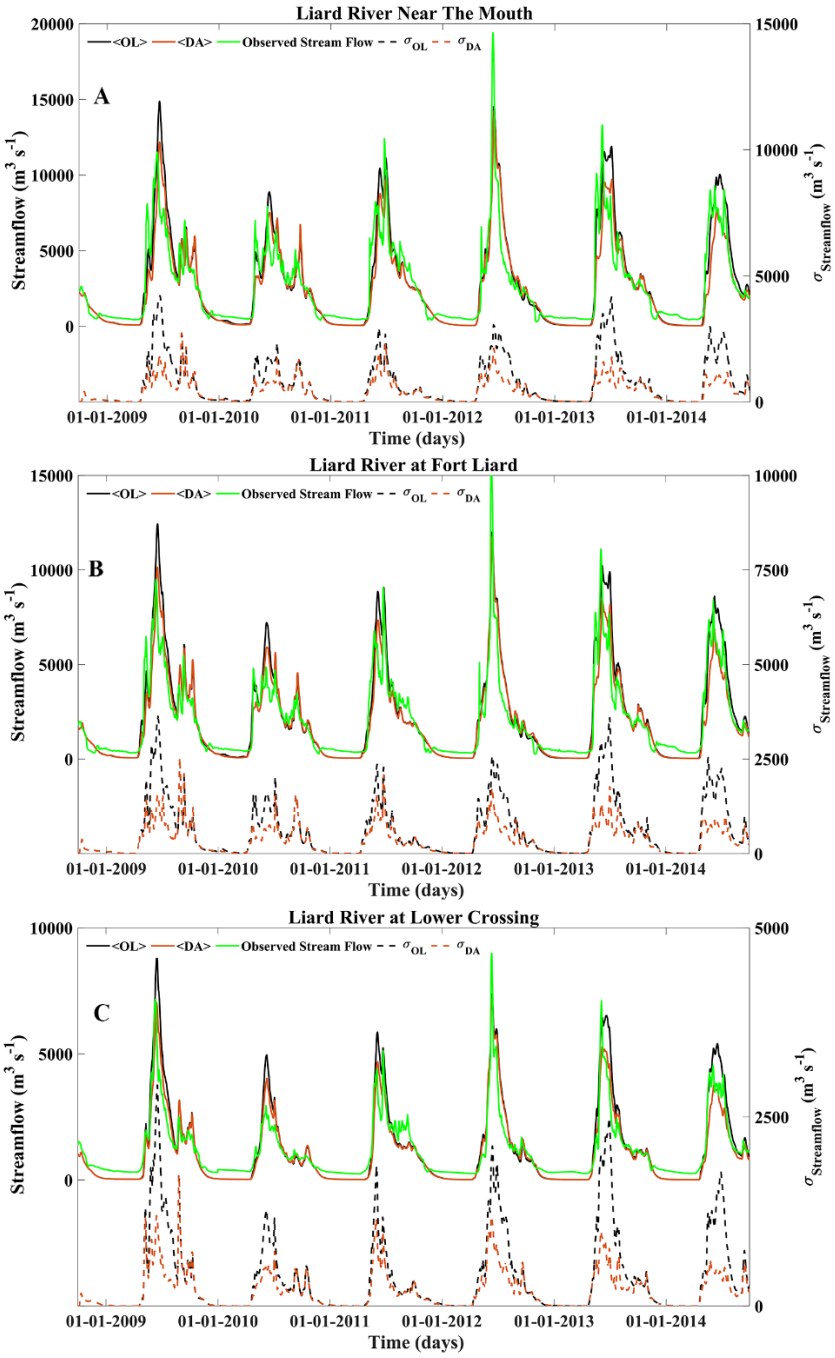

Figure 6.10. Time series of the river streamflow estimates on the left Y-axes and their corresponding ensemble spreads on the right Y-axes at three river stations: (A) Liard River Near the Mouth, (B) Liard river at Fort Liard; and (C) Liard River at Lower Crossing. Solid black and brown lines represent the OL and DA ensemble averages, respectively. Observed streamflows are shown with green solid lines. The OL and DA ensemble spreads are shown as black and brown dashed lines, respectively.

In general, OL does an acceptable job of estimating streamflow, such that a high degree of concordance is achieved between OL simulations and observations. The effect of the GRACE DA on the simulations of streamflow is encouraging. GRACE DA can correct high peaks so that the general evolution of estimated streamflow corresponds to the gauge observations fairly well. The assimilation results show that when the assimilation framework activated, the DA ensemble mean moves closer to the daily observed streamflow observations relative to the OL simulations. The simulation of high flow results using the NSE metric at the Fort Liard and Lower Crossing stations indicates the effects of GRACE assimilation on streamflow simulation. Like the results of modeled SWE, the assimilation effectively reduces ensemble spread for all stations, especially at peak flow times.

6.6. Discussion

6.6.1. Evaluation of the results

The comparison of the OL and DA TWS results versus GRACE-derived TWS retrievals demonstrates that the EnKS method can constrain the amplitude of modeled TWS dynamics, so that close agreement with GRACE observations is obtained. In some cases, the lack of updates is observed. Two possible reasons may cause this small difference. First, the difference is not large between the model predicted TWS and the GRACE-TWS observations. Second, the uncertainty of predicted water storage is small relative to the uncertainty of the observations. As the uncertainties of different soil layers are not included during this experiment, we would expect to observe a small number of updates during summer months. When the uncertainty of model estimates are relatively small in comparison to GRACE observations, a near-zero covariance structure is produced (Forman et al., 2012).

Snow simulation results that were obtained in this study are consistent with Forman et al. (2012) and Su et al. (2010), who demonstrated that SWE estimates could be improved in comparison to the CMC SWE data across portions of North America. The assimilation of GRACE observations into the MESH model shows that SWE estimates in terms of ubRMSD, and Spearman's rank correlations that were estimated at the basin and grid scales have been improved. The MESH-GRACE DA framework generally improved the estimation of SWE in the Liard Basin. The gridded results showed areas in which the greatest improvements in terms of temporal correlation

and ubRMSD were achieved. The gridded scale results reveal that the data assimilation procedure can effectively transfer information from the coarse-scale (~150 000 km^2) GRACE TWS retrievals to the finer scale (~100 km^2) model resolution.

Degradation in the estimation of SWE was observed in some grid cells as a result of GRACE assimilation relative to the OL results (Figures 6.6, 6.7). Loss of skills can be explained by some possible factors. First, the gridded GRACE observations were processed by averaging up to the Liard Basin scale (assuming spatially uncorrelated errors), to make them compatible for integration with the MESH model. However, it is worth pointing out when the gridded GRACE observations are used instead of the basin-averaged TWS values, it is recommended to consider the errors of observations to be spatially correlated (Schumacher et al., 2018, 2016). Forman and Reichle (2013) and Eicker et al. (2014) found that data assimilation of GRACE TWS retrievals performs optimally when observations are assimilated at the smallest spatial scale, i.e., 5º×5º, such that the observation errors become uncorrelated (Girotto et al., 2016). By considering the optimal spatial scale of GRACE data for the DA, the smallest spatial scale in the Liard Basin at which GRACE observation can be reasonably resolved is about 150 000 km^2. Therefore, the use of 1º×1º gridded GRACE observations might not change the results, since the basin size (~275 000 km^2) is not substantially larger than the true resolution of observations. Kumar et al. (2016) assimilated both 1º×1º gridded and basin-averaged GRACE TWSA products into NASA's catchment land surface model (CLSM) over the continental United States (CONUS). They obtained small differences between the DA of basin-averaged and gridded results. Second, in some grid cells where degradations of ubRMSD were observed, OL does a reasonable job in estimating SWE. It is apparent that during the update step, the quantity of reduced mass was larger than what was required to be subtracted from the MESH simulations. Therefore, the ubRMSD values were degraded as a result of GRACE assimilation relative to the OL results. Third, in some grid cells, the correlations between OL simulation results and CMC SWE were not strong compared to the DA results (Figure 6.7). Correlation values obtained with OL in those areas range between 0.5 to 0.7. This may be explained by the pronounced slope effects on snow accumulation in the grid concerned, which are mainly concentrated in the transition zones between the high elevation areas and the lowlands (see Figure 6.1). Also, the lower magnitude of SWE in some grid cells in the eastern part may affect the results. Forth, even though the CMC SWE product is often considered as a very reliable source for the evaluation of modeled SWE, it suffers from some limitations,

including imperfect accumulation and melt model, and coarse atmospheric forcing, together with the scarcity of in situ snow depth measurements in northern latitudes (> 55º N) (Brown and Brasnett, 2010; Brown et al., 2010; Swenson and Lawrence, 2012; Toure et al., 2016). Over northern latitudes and data-sparse areas, CMC SWE analysis depends mostly on the GEM precipitation rather than snow observations. In addition, snow depth observations tend to be biased to coastal locations or large open areas at airports (Brown and Brasnett, 2010). Therefore, in areas experiencing lack of in-situ station data, the evaluation of MESH SWE estimates based on the CMC SWE analysis data becomes likely a model intercomparison rather than a validation with a reference of known uncertainty. The comparison of the assimilation results to independent ground-based snow survey data appears as the best way to validate the results. However, this is limited by the availability of snow measurement stations in the study area. Fortunately, we found three automatic stations (Section 6.5.2.3) and compared the data assimilation results with them, even if the period was limited (2013 and 2014).

A number of distinct remarks could be made from the snow survey evaluation (Figure 6.9). First, DA simulations at the three stations experienced negative biases in March and April 2013 relative to snow observations. This could be explained partly by the fact that GRACE observation was not available in March 2013. Thus, the analysis (or update) in the assimilation procedure in March was not performed. Second, in 2013, MESH simulations (OL and DA) showed maximum SWE in March, while snow observations indicated the maximum values in April. A temporal lag of around 15 days was observed between model simulations and snow observations. Forth, the variations of CMC SWE compared to in-situ observations show a varying level of agreement based on the year and snowmelt occurrence periods (Figure 6.9). This affects the statistics presented in Table 6.2. When the onset period of the snow accumulation is considered (November to January), the agreement improved significantly. For example, the ubRMSD found when comparing OL and DA to the snow survey stations vary from 6.6 mm to 10.9 mm for OL and from 6.2 mm to 9.7 mm for DA. A similar improvement was found when OL and DA are compared to CMC SWE in the grid cells corresponding to station locations (6.2 mm to 9.8 mm for OL and from 4.7 mm to 9.2 mm for DA). Better correlations were also obtained during the onset period (>= 0.94) compared to the whole season (Table 6.2). The lack of data during the snowmelt period did not allow any particular analysis for that specific period. Overall, since the number of data is limited, the findings here should be considered with caution, even if very encouraging results could be seen during the onset

period. It is not possible to draw a clear conclusion on whether GRACE DA improves SWE estimates compared to the OL simulations at this stage of the study. It is also worth to notice, that comparing point-level measurements from automatic stations to gridded values from MESH or CMC may introduce uncertainties due to SWE spatial variations. The limited number of stations used and the short period (2 years) do not allow robust conclusions to be drawn. However, the results shown in Figure 6.9 and Table 6.2 comfort us in using CMC as a reference SWE product in this study, since there is no ideal reliable source of SWE data available.

The assimilation results in the streamflow simulations show that the effect of integrating GRACE observations is small compared to the effects on modeled TWS and SWE estimates. Yet, the developed framework can improve high flows, especially near the peak (summer) of rainfall seasons. Note that fluxes are indirectly updated in the GRACE DA framework; they are subsequently modified as a result of the state vector update (Forman and Reichle, 2013; Schumacher et al., 2018). Therefore, one cannot ignore the influence of GRACE TWS retrievals on streamflow simulations. Estimates of streamflow for flow volume and low flow were slightly degraded at some stations as a result of GRACE assimilation. The degradation of the streamflow estimates in the Liard Basin using NASA's CLSM model has been reported by Forman & Reichle (2013) and by Forman et al. (2012). The loss of skill that is noted in Table 6.3 can be related to different possible reasons. First, SWE is reduced by DA in the Liard Basin, which means less SWE is available to produce snowmelt streamflow. Second, adding subsurface water in the form of surface and root-zone soil moisture during warm seasons leads to more runoff. Yet, water storage increments that were added during the analysis step of assimilation during summer are not sufficient to compensate for deficiencies of the model to simulate adequate streamflow. Third both OL and DA experience negative biases during the winter seasons (December to April) for the simulation of low flows (Figure 6.10). This is particularly obvious during winter when the overland and inter flow components are near zero, and the base flow component is the major contributor to winter runoff (Forman et al., 2012). This negative bias may be related to limitations of the MESH model in generating sufficient base flow at three observed stations.

6.6.2. Assimilation diagnostics

6.6.2.1. Ensemble spread

The ensemble spread is a measure of the uncertainty of the model estimates (Girotto et al., 2019). Assimilation results at the basin and gridded scales revealed that observations can substantially reduce uncertainty of the model between the OL and DA simulations. The results presented here are consistent with the work of Forman et al. (2012), who demonstrated that GRACE DA is valuable for reducing ensemble spread for the estimation of SWE. In this study, large values of SWE ensemble spreads for the OL simulations were encountered in mountainous areas (Northern Canadian Rockies, Cassiar Mountains, and Mackenzie Mountains). In these areas, the actual errors (i.e., the ubRMSD) are also large compared to the other regions. The large uncertainty that is associated with complex terrain may be related to CaPA precipitation forcing and the relatively coarse horizontal resolution of the MESH model (~ 10 km). Lespinas et al. (2015) asserted that current limitations of CaPA can result from different factors, including 1) the scarcity of reliable observations in Canada, 2) problems with observation errors associated with solid precipitation, 3) the presence of biases in GEM precipitation fields, 4) biases that result from data transformation, and 5) verification methodology. Carrera et al. (2010) demonstrated that reliable estimation of SWE over the Canadian Rockies can be acquired by increasing the horizontal resolution of climate forcing, especially the CaPA analysis product. In complex terrain, precipitation and snow accumulation experience high spatial variability due to cloud microphysics and particle transport processes (Schirmer and Jamieson, 2015). Furthermore, in the current Liard model set-up, blowing snow was not considered. However, this option is available in the MESH configuration. Blowing snow (re)distribution can be also an important process that influences accurate snow accumulation (MacDonald et al., 2009). Note that the reduction of uncertainty in the model estimates does not necessarily mean that better estimates are achieved when compared to the validation data (Girotto et al., 2019). For example, in the region near the northwestern and western boundaries of the basin, ensemble spreads were reduced. However, the ubRMSD values are degraded as a result of the GRACE assimilation.

6.6.2.2. Normalized Innovation Sequence

A filter innovation for a given month k, is defined as the difference between the ensemble mean

observation and model forecast, i.e., $\boldsymbol{y_k - Hx_k^f}$. The statistics of the filter innovations is a useful tool to indicate whether or not the choice of the model (Table 6.1) and measurement error parameters is appropriate (Reichle and Koster, 2002). In a linear system with mutually and serially uncorrelated Gaussian model perturbations and observation errors, the normalized innovations (*NI*) should follow a standard normal distribution (zero mean, unit variance, and temporally uncorrelated) (Kumar et al., 2008). Even though the filter used here is a smoother rather than a filter and the MESH model is nonlinear, deviations of the *NI* statistics from the theoretical ideals can be used to diagnose useful information as the performance of the DA procedure (Forman et al., 2012). The normalized innovation is written as:

$$NI_k = \frac{\boldsymbol{y_k - Hx_k^f}}{\sqrt{\boldsymbol{HP_k^f H^T + R}}} \qquad (\mathbf{6.7})$$

where the covariance of innovation, i.e., $\boldsymbol{HP_k^f H^T + R}$, is based on the combination of the background and measurement error and can be used to normalize the innovations (Reichle and Koster, 2002). Then, the statistics (mean and standard deviation) of *NI* are collected as a function of time.

To assess the performance based on the innovation, we did a sensitivity analysis by conducting the data assimilation experiments based on a range of GRACE measurement variance ($\boldsymbol{R}$ in equation 6.7). Thus, four measurement variance values (72.25, 289, 650.25, 1156 mm^2) were chosen following the work of Forman et al. (2012), and other studies who adopted some of the same values (Kumar et al., 2016; Su et al., 2010; Zaitchik et al., 2008). The results of the mean and standard deviation of normalized innovations are shown in Figure 6.11. It is observed that the mean values ($\overline{NI}$) of the normalized innovations using $\boldsymbol{R}$ values of 289 mm^2 and 650.25 mm^2 equal to zero. This implies that the data assimilation simulations are unbiased for these two experiments. The noticeable feature is that the mean innovations using the observation errors of 72.25 mm^2 and 1156 mm^2 have positive and negative biases. It is important to note that with increasing observation error variances, the variance of innovations (σ_{NI}) decreases. This reduction is expected, as an increase in measurement error causes an increase in the dominator of equation 6.7, which leads to a reduction in the standard deviation of the normalized innovation. Based on the information

provided by the normalized innovations, the selection of the observation error between 289 mm^2 (considered in this study) and 650.25 mm^2 indicates a reasonable data assimilation performance for the MESH model (i.e., a σ_{NI} close to unity, and a $\overline{NI}$ close to zero). These findings are consistent with previous data assimilation studies that considered observation variance between 289 mm^2 and 400 mm^2 (Forman et al., 2012; Forman and Reichle, 2013; Kumar et al., 2016; Su et al., 2010; Zaitchik et al., 2008).

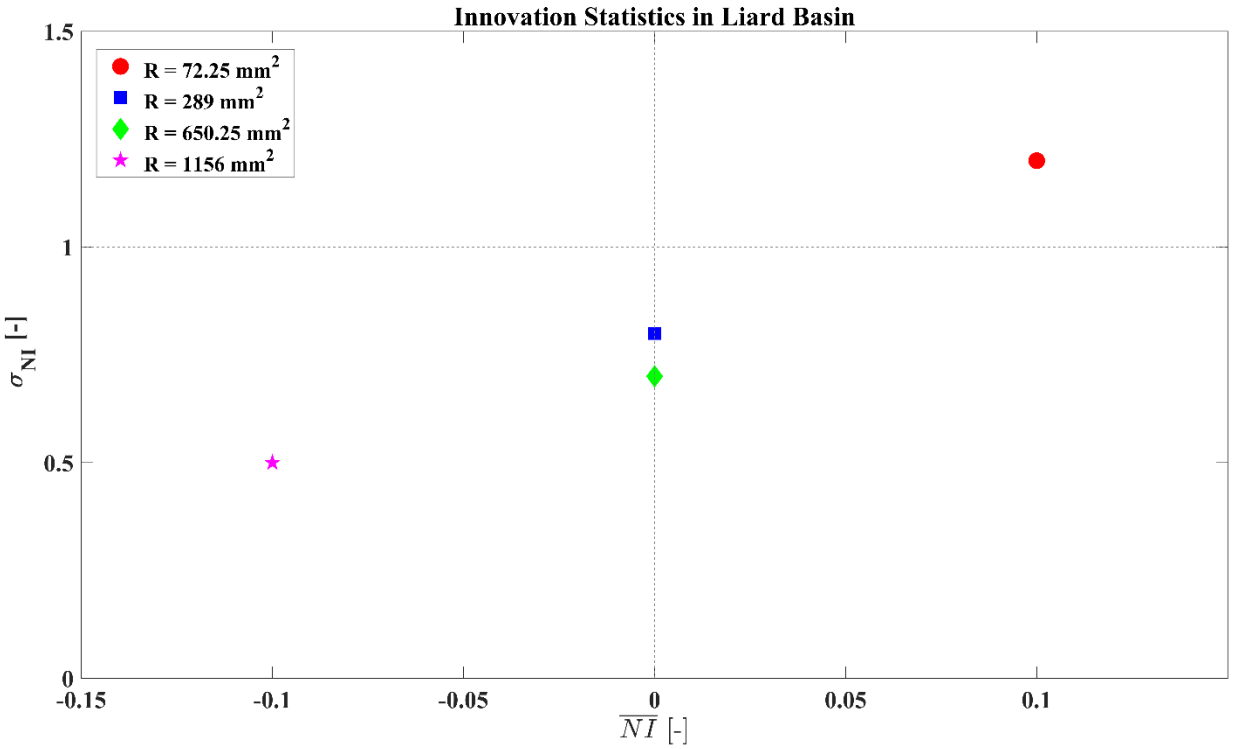

Figure 6.11. Normalized Innovation (NI) statistics for the Liard Basin. The different marker colors correspond to four data assimilation experiments based on observation error variance of 72.25 mm^2 (red circle), 289 mm^2 (blue square), 650.25 mm^2 (green diamond), and 1156 mm^2 (purple star).

6.6.2.3. Analysis increments

Examination of analysis increment (i.e., the difference between update and forecast) can provide another way of realizing the behavior of the data assimilation system (Forman et al., 2012). It shows how much and at what time information from GRACE observations in the data assimilation framework affect the estimation of water storage at different vertical layers (Forman et al., 2012;

Girotto et al., 2019).

Figure 6.12 shows the monthly basin averaged time series (for six years) of ensemble average increments of SWE and subsurface water storage. The negative and positive signs of the increment indicate how the assimilation subtracts and adds water storage. In certain months, such as March 2013, when the GRACE observations were not available, the increments were all zeros. The increments that were applied to SWE and subsurface storage are shown with solid blue and black lines, respectively. Analysis increments were applied to all water storage compartments of the MESH model. The updates of the other components were not significant when compared to SWE and subsurface storage. The summation of SWE increments for six years equals -127.1 mm. Assimilation reduces snow mass from the MESH estimates during the snow accumulation seasons from November to May of each year (Figure 6.12). A small amount of SWE is added back during the spring ablation and snowmelt phases. The summation of the subsurface increments over space and time equals 17.90 mm. Small or near-zero numbers of subsurface updates are possibly related to the perturbation structure, such that the uncertainties of soil water compartments were not included in the system.

The pattern rather than the magnitude of increments (especially SWE) was consistent, to some extent, with those reported by Forman et al. (2012), who assimilated GRACE observations into the CLSM model in the Mackenzie Basin. Together, these results verify that GRACE DA has an effect on reducing snow mass during snow accumulation seasons, but then increases the mass slightly during warm periods. This behavior indicates that GRACE data contain valuable information that helps to constrain the individual model compartments of the MESH model.

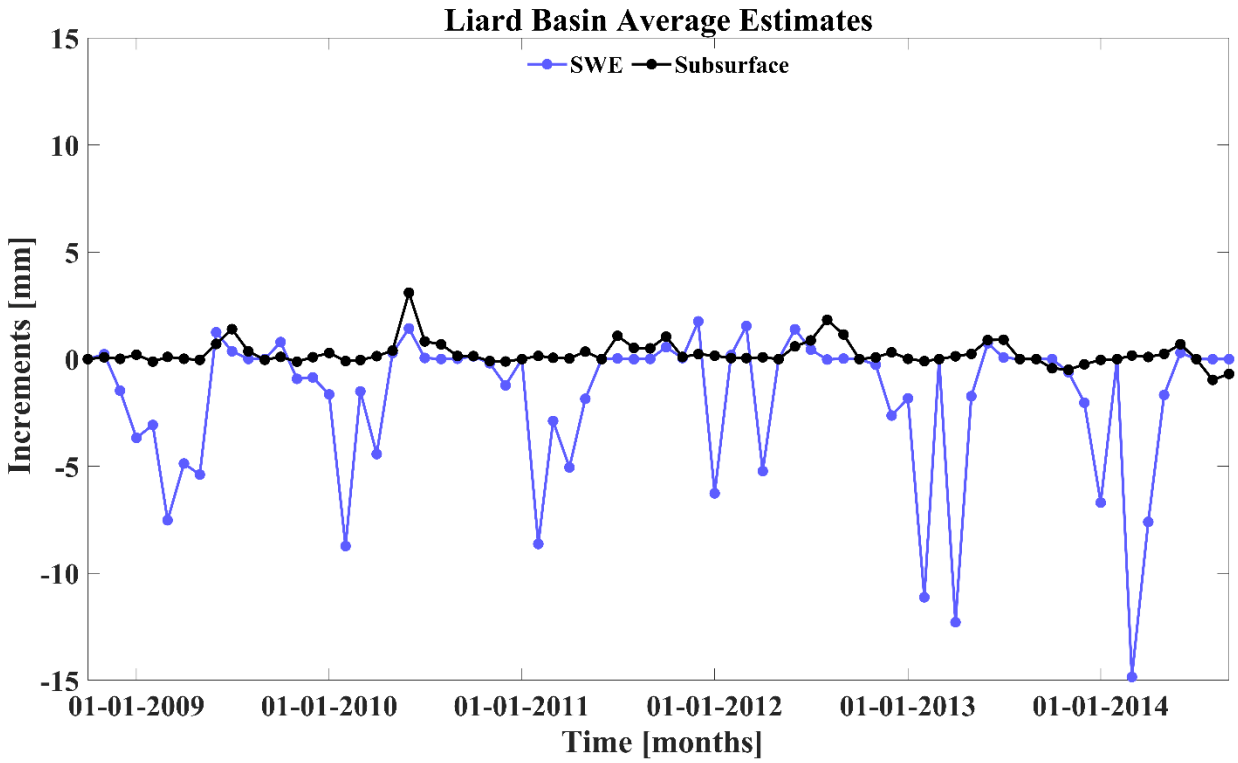

Figure 6.12. Time series of analysis increments for the Liard Basin from October 2008 to October 2014. The solid blue and black lines show monthly mean analysis increments that were calculated for SWE and the subsurface, respectively.

6.7. Conclusion

This study examined the incorporation and development of the ensemble-based MESH-GRACE data assimilation framework into the ECCC community environmental modeling for the first time. The EnKS assimilation method in the Liard Basin was used to integrate GRACE-derived TWS data into the MESH model.

For SWE estimates when compared against the CMC SWE data, data assimilation at the basin scale reduced the bias of the open-loop simulation significantly from +46.7% to +29.6% and improved the unbiased RMSD by ~23%. This confirms that GRACE TWS assimilation has an effect on reducing snow mass during snow accumulation. Data assimilation also reduced significantly the ensemble spreads. In terms of correlations, a negligible improvement was observed (0.95 for OL, 0.96 for DA). At the gridded scale, the DA process showed larger improvements in the ubRMSD compared to the OL, mainly in areas with substantial annual snow

accumulation, particularly in the Northern Canadian Rockies. Overall, the ubRMSD values were improved in 85% of the grid cells. In 56% of grid cells, the ubRMSD improvements were statistically significant. The DA method improved the correlations with CMC SWE in 97% of the grid cells. In 61% of these grid cells, the correlation differences between the OL and DA differed statistically from zero. The GRACE DA approach reduced the ensemble spreads in almost all of the gridded cells. The evaluation of the results based on in-situ observations from November to April presented a varying level of concordance. Due to insufficient snow observations during the snowmelt periods, the evaluation of the results could not be properly conducted.

The impact of GRACE data assimilation on streamflow simulations was evaluated against observations from three river gauges. GRACE DA could effectively improve the simulation of high flows at Lower Crossing (NS = 0.74 for OL, NS = 0.86 for DA) and Fort Liard (NS = 0.76 for OL, NS = 0.83 for DA), while it remained unchanged (NS = 0.76) for the Mouth station. The influence of GRACE DA on total flow volume and low flows was found to be variable. The assimilation procedure can effectively reduce the ensemble spreads in the streamflow simulations, especially during peak flow times.

The assimilation of GRACE TWS retrievals in the Liard Basin provides some valuable insights for ongoing scientific applications. Further works will extend the research to different basins with variable climate regimes and SWE conditions. The use of gridded observations at a finer spatial resolution (1º×1º) will be investigated by considering the full error covariance of the observations. The findings of this research have important implications for evaluating the performance of the MESH-GRACE data assimilation framework for the purpose of improving regional estimates of SWE and streamflow. These results motivate future efforts to understand the influence of GRACE data assimilation on the seasonality and sub-seasonal variability of SWE (at basin-averaged and gridded scales), and investigate whether GRACE-DA leads to changes in the timing of snow accumulation/ablation phases. Moreover, the possibility of extending the developed methodology to multisource data assimilation could be explored to further improve the accuracy of model estimates.

Acknowledgements

Funding for this work was provided by the Natural Sciences and Engineering Research Council of

Canada (NSERC). We thank ECCC for supporting the open-source code of MESH software as well as meteorological forcing. Authors would like to thank the Global Institute for Water Security (GIWS) for providing model setup data. GRACE TELLUS data were supported by the NASA MEaSUREs Program. We are grateful to the Meteorological Service of Canada, and the National Snow and Ice Data Center (Boulder, CO, USA) for distributing SWE data. We thank the NASA Global Modeling and Assimilation Office (GMAO) for providing the open source code for the perturbation module.

References

Bahrami, A., Goïta, K., Magagi, R., 2020. Analyzing the contribution of snow water equivalent to the terrestrial water storage over Canada. Hydrol. Process. 34, 175–188. https://doi.org/10.1002/hyp.13625

Barnett, T.P., Adam, J.C., Lettenmaier, D.P., 2005. Potential impacts of a warming climate on water availability in snow-dominated regions. Nature 438, 303–9. https://doi.org/10.1038/nature04141

Behrangi, A., Gardner, A.S., Reager, J.T., Fisher, J.B., 2017. Using GRACE to constrain precipitation amount over cold mountainous basins. Geophys. Res. Lett. 44, 219–227. https://doi.org/10.1002/2016GL071832

Behrangi, A., Gardner, A., Reager, J.T., Fisher, J.B., Yang, D., Huffman, G.J., Adler, R.F., 2018. Using GRACE to estimate snowfall accumulation and assess gauge undercatch corrections in high latitudes. J. Clim. 31, 8689–8704. https://doi.org/10.1175/JCLI-D-18-0163.1

Brasnett, B., 1999. A global analysis of snow depth for numerical weather prediction. J. Appl. Meteorol. 38, 726–740. https://doi.org/https://doi.org/10.1175/1520-0450(1999)038<0726:AGAOSD>2.0.CO;2

Brown, R., Bartlett, P., MacKay, M., Verseghy, D., 2006. Evaluation of snow cover in CLASS for SnowMIP. Atmosphere-Ocean 44, 223–238. https://doi.org/10.3137/ao.440302

[dataset] Brown, R., Brasnett, B., 2010. Canadian Meteorological Centre (CMC) Daily Snow Depth Analysis Data, Version 1. National Snow and Ice Data Center. https://doi.org/https://doi.org/10.5067/W9FOYWH0EQZ3

Brown, R., Derksen, C., Wang, L., 2010. A multi-data set analysis of variability and change in Arctic spring snow cover extent, 1967-2008. J. Geophys. Res. Atmos. 115, 1–16. https://doi.org/https://dx.doi.org/10.1029/2010JD013975

Brown, R.D., Mote, P.W., 2009. The response of Northern Hemisphere snow cover to a changing climate. J. Clim. 22, 2124–2145. https://doi.org/10.1175/2008JCLI2665.1

Burgers, G., Jan van Leeuwen, P., Evensen, G., 1998. Analysis Scheme in the Ensemble Kalman Filter. Mon. Weather Rev. 126, 1719–1724. https://doi.org/10.1175/1520-0493(1998)126<1719:ASITEK>2.0.CO;2

[dataset] Canadian Digital Elevation Data, 2016. Natural Resources Canada, Canada Centre for Mapping and Earth Observation. http://ftp.geogratis.gc.ca/pub/nrcan_rncan/archive/elevation/geobase_cded_dnec/ (accessed 11.12.19).

Carrera, M.L., Bélair, S., Fortin, V., Bilodeau, B., Charpentier, D., Doré, I., 2010. Evaluation of Snowpack Simulations over the Canadian Rockies with an Experimental Hydrometeorological Modeling System. J. Hydrometeorol. 11, 1123–1140. https://doi.org/10.1175/2010jhm1274.1

Cohen, J., Entekhabi, D., 1999. Eurasian snow cover variability and northern hemisphere climate predictability. Geophys. Res. Lett. https://doi.org/10.1029/1999GL900200

Cooley, S.S., Landerer, F.W., 2019. GRACE/GRACE-FO Level-3 Data Product User Handbook. California.

Côté, J., Desmarais, J.-G., Gravel, S., Méthot, A., Patoine, A., Roch, M., Staniforth, A., 1998b. The Operational CMC–MRB Global Environmental Multiscale (GEM) Model. Part II: Results. Mon. Weather Rev. 126, 1397–1418. https://doi.org/10.1175/1520-0493(1998)126<1397:tocmge>2.0.co;2

Côté, J., Gravel, S., Méthot, A., Patoine, A., Roch, M., Staniforth, A., 1998a. The Operational CMC–MRB Global Environmental Multiscale (GEM) Model. Part I: Design Considerations and Formulation. Mon. Weather Rev. 126, 1373–1395. https://doi.org/10.1175/1520-0493(1998)126<1373:tocmge>2.0.co;2

Davison, B., Fortin, V., Pietroniro, A., Yau, M., Leconte, R., 2019. Parameter-state ensemble

thinning for short-term hydrological prediction. Hydrol. Earth Syst. Sci. 23, 741–762. https://doi.org/10.5194/hess-23-741-2019

Davison, B., Pohl, S., Domes, P., Marsh, P., Pietroniro, A., MacKay, M., 2006. Characterizing snowmelt variability in a land-surface-hydrologic model. Atmosphere-Ocean 44, 271–287. https://doi.org/10.3137/ao.440305

Déry, S.J., Sheffield, J., Wood, E.F., 2005. Connectivity between Eurasian snow cover extent and Canadian snow water equivalent and river discharge. J. Geophys. Res. 110, 1–14. https://doi.org/https://dx.doi.org/10.1029/2005JD006173

Dornes, P.F., Tolson, B.A., Davison, B., Pietroniro, A., Pomeroy, J.W., Marsh, P., 2008. Regionalisation of land surface hydrological model parameters in subarctic and arctic environments. Phys. Chem. Earth, Parts A/B/C 33, 1081–1089. https://doi.org/10.1016/j.pce.2008.07.007

Dunne, S., Entekhabi, D., 2005. An ensemble-based reanalysis approach to land data assimilation. Water Resour. Res. 41, 1–18. https://doi.org/10.1029/2004WR003449

Eicker, A., Schumacher, M., Kusche, J., Döll, P., Schmied, H.M., 2014. Calibration/Data Assimilation Approach for Integrating GRACE Data into the WaterGAP Global Hydrology Model (WGHM) Using an Ensemble Kalman Filter: First Results. Surv. Geophys. 35, 1285–1309. https://doi.org/https://dx.doi.org/10.1007/s10712-014-9309-8

Elshamy, M.E., Princz, D., Sapriza-Azuri, G., Pietroniro, A., Wheater, H.S., Razavi, S., 2020. On the Configuration and Initialization of a Large Scale Hydrological Land Surface Model to Represent Permafrost. Hydrol. Earth Syst. Sci. 24(1), 349–379. https://doi.org/10.5194/hess-2019-206

Entekhabi, D., Reichle, R.H., Koster, R.D., Crow, W.T., 2010. Performance Metrics for Soil Moisture Retrievals and Application Requirements. J. Hydrometeorol. 11, 832–840. https://doi.org/10.1175/2010JHM1223.1

Evensen, G., 2003. The Ensemble Kalman Filter: theoretical formulation and practical implementation. Ocean Dyn. 53, 343–367. https://doi.org/10.1007/s10236-003-0036-9

Evensen, G., Van Leeuwen, P.J., 2000. An ensemble Kalman smoother for nonlinear dynamics. Mon. Weather Rev. 128, 1852–1867. https://doi.org/10.1175/1520-

0493(2000)128<1852:AEKSFN>2.0.CO;2

Famiglietti, J.S., Rodell, M., 2013. Environmental science. Water in the balance. Science 340, 1300–1. https://doi.org/https://dx.doi.org/10.1126/science.1236460

Forman, B.A., Reichle, R.H., 2013. The spatial scale of model errors and assimilated retrievals in a terrestrial water storage assimilation system. Water Resour. Res. 49, 7457–7468. https://doi.org/10.1002/2012WR012885

Forman, B.A., Reichle, R.H., Rodell, M., 2012. Assimilation of terrestrial water storage from GRACE in a snow-dominated basin. Water Resour. Res. 48, 1–14. https://doi.org/10.1029/2011WR011239

Fortin, V., Roy, G., Stadnyk, T., Koenig, K., Gasset, N., Mahidjiba, A., 2018. Ten years of science based on the Canadian Precipitation Analysis: A CaPA system overview and literature Review. Atmos. - Ocean. https://doi.org/10.1080/07055900.2018.1474728

Foster, J.L., Hall, D.K., Eylander, J.B., Riggs, G.A., Nghiem, S. V., Tedesco, M., Kim, E., Montesano, P.M., Kelly, R.E.J., Casey, K.A., Choudhury, B., 2011. A blended global snow product using visible, passive microwave and scatterometer satellite data. Int. J. Remote Sens. 32, 1371–1395. https://doi.org/10.1080/01431160903548013

Geruo, A., Wahr, J., Zhong, S., 2013. Computations of the viscoelastic response of a 3-D compressible Earth to surface loading: an application to Glacial Isostatic Adjustment in Antarctica and Canada. Geophys. J. Int. 192, 557–572. https://doi.org/https://dx.doi.org/10.1093/gji/ggs030

Girotto, M., De Lannoy, G.J.M., Reichle, R.H., Rodell, M., 2016. Assimilation of gridded terrestrial water storage observations from GRACE into a land surface model. Water Resour. Res. 52, 4164–4183. https://doi.org/10.1002/2015WR018417

Girotto, M., De Lannoy, G.J.M., Reichle, R.H., Rodell, M., Draper, C., Bhanja, S.N., Mukherjee, A., 2017. Benefits and pitfalls of GRACE data assimilation: A case study of terrestrial water storage depletion in India. Geophys. Res. Lett. 44, 4107–4115. https://doi.org/10.1002/2017GL072994

Girotto, M., Reichle, R.H., Rodell, M., Liu, Q., Mahanama, S., De Lannoy, G.J.M., 2019. Multi-sensor assimilation of SMOS brightness temperature and GRACE terrestrial water storage

observations for soil moisture and shallow groundwater estimation. Remote Sens. Environ. 227, 12–27. https://doi.org/10.1016/j.rse.2019.04.001

Güntner, A., 2008. Improvement of Global Hydrological Models Using GRACE Data. Surv. Geophys. 29, 375–397. https://doi.org/10.1007/s10712-008-9038-y

Gupta, H.V., Sorooshian, S., Yapo, P.O., 1999. Status of automatic calibration for hydrologic models: Comparison with multilevel expert calibration. J. Hydrol. Eng. 4, 135–143. https://doi.org/10.1061/(ASCE)1084-0699(1999)4:2(135)

Haghnegahdar, A., Razavi, S., 2017. Insights into sensitivity analysis of Earth and environmental systems models: On the impact of parameter perturbation scale. Environ. Model. Softw. 95, 115–131. https://doi.org/10.1016/j.envsoft.2017.03.031

Haghnegahdar, A., Razavi, S., Yassin, F., Wheater, H., 2017. Multi-criteria sensitivity analysis as a diagnostic tool for understanding model behavior and characterizing model uncertainty. Hydrol. Process. 31, 4462–4476. https://doi.org/10.1002/hyp.11358

Haghnegahdar, A., Tolson, B.A., Craig, J.R., Paya, K.T., 2015. Assessing the performance of a semi-distributed hydrological model under various watershed discretization schemes. Hydrol. Process. 29, 4018–4031. https://doi.org/10.1002/hyp.10550

Hamby, D.M., 1994. A review of techniques for parameter sensitivity analysis of environmental models. Environ. Monit. Assess. 32, 135–154. https://doi.org/10.1007/BF00547132

Houborg, R., Rodell, M., Li, B., Reichle, R., Zaitchik, B.F., 2012. Drought indicators based on model-assimilated Gravity Recovery and Climate Experiment (GRACE) terrestrial water storage observations. Water Resour. Res. 48. https://doi.org/10.1029/2011WR011291

Iman, R.L., Conover, W.J., 1979. The use of the rank transform in regression. Technometrics 21, 499–509. https://doi.org/10.1080/00401706.1979.10489820

Khaki, M., Ait-El-Fquih, B., Hoteit, I., Forootan, E., Awange, J., Kuhn, M., 2017a. A two-update ensemble Kalman filter for land hydrological data assimilation with an uncertain constraint. J. Hydrol. 555, 447–462. https://doi.org/10.1016/j.jhydrol.2017.10.032

Khaki, M., Awange, J., 2019. The application of multi-mission satellite data assimilation for studying water storage changes over South America. Sci. Total Environ. 647, 1557–1572.

https://doi.org/10.1016/j.scitotenv.2018.08.079

Khaki, M., Hoteit, I., Kuhn, M., Awange, J., Forootan, E., van Dijk, A.I.J.M., Schumacher, M., Pattiaratchi, C., 2017b. Assessing sequential data assimilation techniques for integrating GRACE data into a hydrological model. Adv. Water Resour. 107, 301–316. https://doi.org/10.1016/j.advwatres.2017.07.001

Kouwen, N., 1988. Watflood: A micro-computer based flood forecasting system based on real-time weather radar. Can. Water Resour. J. 13, 62–77. https://doi.org/10.4296/cwrj1301062

Kouwen, N., Soulis, E.D., Pietroniro, A., Donald, J., Harrington, R.A., 1993. Grouped response units for distributed hydrologic modeling. J. Water Resour. Plan. Manag. 119, 289–305. https://doi.org/10.1061/(ASCE)0733-9496(1993)119:3(289)

Krause, P., Boyle, D.P., Bäse, F., 2005. Comparison of different efficiency criteria for hydrological model assessment. Adv. Geosci. 5, 89–97. https://doi.org/10.5194/adgeo-5-89-2005

Kumar, S. V., Reichle, R.H., Peters-Lidard, C.D., Koster, R.D., Zhan, X., Crow, W.T., Eylander, J.B., Houser, P.R., 2008. A land surface data assimilation framework using the land information system: Description and applications. Adv. Water Resour. 31, 1419–1432. https://doi.org/10.1016/j.advwatres.2008.01.013

Kumar, S.V., Zaitchik, B.F., Peters-Lidard, C.D., Rodell, M., Reichle, R., Li, B., Jasinski, M., Mocko, D., Getirana, A., De Lannoy, G., Cosh, M.H., Hain, C.R., Anderson, M., Arsenault, K.R., Xia, Y., Ek, M., 2016. Assimilation of Gridded GRACE terrestrial water storage estimates in the North American land data assimilation system. J. Hydrometeorol. 17, 1951–1972. https://doi.org/https://dx.doi.org/10.1175/JHM-D-15-0157.1

[dataset] Land Cover of Canada, 2010. Natural Resources Canada; Canada Centre for Remote Sensing. https://open.canada.ca/data/en/dataset/c688b87f-e85f-4842-b0e1-a8f79ebf1133 (accessed 11.12.19).

Landerer, F.W., Swenson, S.C., 2012. Accuracy of scaled GRACE terrestrial water storage estimates. Water Resour. Res. 48, 1–11. https://doi.org/https://dx.doi.org/10.1029/2011WR011453

Lespinas, F., Fortin, V., Roy, G., Rasmussen, P., Stadnyk, T., 2015. Performance evaluation of

the Canadian Precipitation Analysis (CaPA). J. Hydrometeorol. 16, 2045–2064. https://doi.org/10.1175/jhm-d-14-0191.1

Li, B., Rodell, M., Zaitchik, B.F., Reichle, R.H., Koster, R.D., van Dam, T.M., 2012. Assimilation of GRACE terrestrial water storage into a land surface model: Evaluation and potential value for drought monitoring in western and central Europe. J. Hydrol. 446–447, 103–115. https://doi.org/10.1016/j.jhydrol.2012.04.035

Liston, G.E., 2004. Representing subgrid snow cover heterogeneities in regional and global models. J. Clim. 17, 1381–1397. https://doi.org/10.1175/1520-0442(2004)017<1381:RSSCHI>2.0.CO;2

MacDonald, M.K., Pomeroy, J.W., Pietroniro, A., 2009. Parameterizing redistribution and sublimation of blowing snow for hydrological models: Tests in a mountainous subarctic catchment, in: Hydrological Processes. Wiley-Blackwell, pp. 2570–2583. https://doi.org/10.1002/hyp.7356

Mahfouf, J.-F., Brasnett, B., Gagnon, S., 2007. A Canadian Precipitation Analysis (CaPA) Project: Description and preliminary results. Atmosphere-Ocean 45, 1–17. https://doi.org/10.3137/ao.v450101

McCreight, J.L., Small, E.E., Larson, K.M., 2014. Snow depth, density, and SWE estimates derived from GPS reflection data: Validation in the western U.S. Water Resour. Res. 50, n/a-n/a. https://doi.org/10.1002/2014WR015561

McTaggart-Cowan, R., Vaillancourt, P.A., Zadra, A., Chamberland, S., Charron, M., Corvec, S., Milbrandt, J.A., Paquin-Ricard, D., Patoine, A., Roch, M., Separovic, L., Yang, J., 2019a. Modernization of Atmospheric Physics Parameterization in Canadian NWP. J. Adv. Model. Earth Syst. https://doi.org/10.1029/2019ms001781

McTaggart-Cowan, R., Vaillancourt, P.A., Zadra, A., Separovic, L., Corvec, S., Kirshbaum, D., 2019b. A lagrangian perspective on parameterizing deep convection. Mon. Weather Rev. https://doi.org/10.1175/mwr-d-19-0164.1

Mekonnen, M.A., Wheater, H.S., Ireson, A.M., Spence, C., Davison, B., Pietroniro, A., 2014. Towards an improved land surface scheme for prairie landscapes. J. Hydrol. 511, 105–116. https://doi.org/10.1016/j.jhydrol.2014.01.020

Moriasi, D.N., Arnold, J.G., Van Liew, M.W., Bingner, R.L., Harmel, R.D., Veith, T.L., 2007. Model evaluation guidelines for systematic quantification of accuracy in watershed simulations. Trans. ASABE 50, 885–900.

Nash, J.E., Sutcliffe, J. V., 1970. River flow forecasting through conceptual models part I - A discussion of principles. J. Hydrol. 10, 282–290.

Pietroniro, A., Fortin, V., Kouwen, N., Neal, C., Turcotte, R., Davison, B., Verseghy, D., Soulis, E.D., Caldwell, R., Evora, N., Pellerin, P., 2007. Development of the MESH modelling system for hydrological ensemble forecasting of the Laurentian Great Lakes at the regional scale. Hydrol. Earth Syst. Sci. 11, 1279–1294.

Pietroniro, A., Soulis, E.D., 2003. A hydrology modelling framework for the Mackenzie GEWEX programme. Hydrol. Process. 17, 673–676. https://doi.org/10.1002/hyp.5104

Pulliainen, J., 2006. Mapping of snow water equivalent and snow depth in boreal and sub-arctic zones by assimilating space-borne microwave radiometer data and ground-based observations. Remote Sens. Environ. 101, 257–269. https://doi.org/10.1016/j.rse.2006.01.002

Reager, J.T., Thomas, A.C., Sproles, E.A., Rodell, M., Beaudoing, H.K., Li, B., Famiglietti, J.S., 2015. Assimilation of GRACE terrestrial water storage observations into a land surface model for the assessment of regional flood potential. Remote Sens. 7, 14663–14679. https://doi.org/10.3390/rs71114663

Reichle, R.H., Bosilovich, M.G., Crow, W.T., Koster, R.D., Kumar, S. V., Mahanama, S.P.P., Zaitchik, B.F., 2009. Recent Advances in Land Data Assimilation at the NASA Global Modeling and Assimilation Office, in: Park, S.K., Xu, L. (Eds.), Data Assimilation for Atmospheric, Oceanic and Hydrologic Applications. Springer Berlin Heidelberg, pp. 407–428. https://doi.org/10.1007/978-3-540-71056-1_21

Reichle, R.H., Koster, R.D., 2002. Land data assimilation with the ensemble Kalman filter: assessing model error parameters using innovations, in: S. Hassanizadeh, R. Schotting, W. Gray, G.P. (Ed.), XIV International Conference on Computational Methods in Water Resources. Elsevier, New York, Delf, Netherlands, pp. 1387–1394.

Reichle, R., Koster, R., 2003. Assessing the impact of horizontal error correlations in background

fields on soil moisture estimation. J. Hydrometeorol. 4, 1229–1243. https://doi.org/10.1175/1525-7541(2003)004<1229:ATIOHE>2.0.CO;2

Reichle, R.H., Koster, R.D., Liu, P., Mahanama, S.P.P., Njoku, E.G., Owe, M., 2007. Comparison and assimilation of global soil moisture retrievals from the Advanced Microwave Scanning Radiometer for the Earth Observing System (AMSR-E) and the Scanning Multichannel Microwave Radiometer (SMMR). J. Geophys. Res. 112, D09108. https://doi.org/10.1029/2006JD008033

Sakumura, C., Bettadpur, S., Bruinsma, S., 2014. Ensemble prediction and intercomparison analysis of GRACE time-variable gravity field models. Geophys. Res. Lett. 41, 1389–1397. https://doi.org/https://dx.doi.org/10.1002/2013GL058632

Schirmer, M., Jamieson, B., 2015. Verification of analysed and forecasted winter precipitation in complex terrain. Cryosphere 9, 587–601. https://doi.org/10.5194/tc-9-587-2015

Schumacher, M., Forootan, E., van Dijk, A.I.J.M., Müller Schmied, H., Crosbie, R.S., Kusche, J., Döll, P., 2018. Improving drought simulations within the Murray-Darling Basin by combined calibration/assimilation of GRACE data into the WaterGAP Global Hydrology Model. Remote Sens. Environ. 204, 212–228. https://doi.org/10.1016/j.rse.2017.10.029

Schumacher, M., Kusche, J., Döll, P., 2016. A systematic impact assessment of GRACE error correlation on data assimilation in hydrological models. J. Geod. 90, 537–559. https://doi.org/10.1007/s00190-016-0892-y

Seo, K.W., Ryu, D., Kim, B.M., Waliser, D.E., Tian, B., Eom, J., 2010. GRACE and AMSR-E-based estimates of winter season solid precipitation accumulation in the Arctic drainage region. J. Geophys. Res. Atmos. 115, 1–18. https://doi.org/10.1029/2009JD013504

[dataset] Soil Landscapes of Canada, 2010. Agriculture and Agri-Food Canada. http://sis.agr.gc.ca/cansis/nsdb/slc/v3.2/index.html (accessed 11.12.19).

Soulis, E.D., Craig, J.R., Fortin, V., Liu, G., 2011. A simple expression for the bulk field capacity of a sloping soil horizon. Hydrol. Process. 25, 112–116. https://doi.org/10.1002/hyp.7827

Soulis, E.D., Snelgrove, K.R., Kouwen, N., Seglenieks, F., Verseghy, D.L., 2000. Towards closing the vertical water balance in Canadian atmospheric models: Coupling of the land surface scheme class with the distributed hydrological model watflood. Atmos. - Ocean 38,

251–269. https://doi.org/10.1080/07055900.2000.9649648

Stieglitz, M., Ducharne, A., Koster, R., Suarez, M., 2001. The impact of detailed snow physics on the simulation of snow cover and subsurface thermodynamics at continental scales. J. Hydrometeorol. 2, 228–242. https://doi.org/10.1175/1525-7541(2001)002<0228:TIODSP>2.0.CO;2

Sturm, M., Holmgren, J., Liston, G.E., 1995. A seasonal snow cover classification system for local to global applications. J. Clim. 8, 1261–1283. https://doi.org/10.1175/1520-0442(1995)008<1261:ASSCCS>2.0.CO;2

Su, H., Yang, Z.L., Dickinson, R.E., Wilson, C.R., Niu, G.Y., 2010. Multisensor snow data assimilation at the continental scale: The value of Gravity Recovery and Climate Experiment terrestrial water storage information. J. Geophys. Res. Atmos. 115, 1–14. https://doi.org/10.1029/2009JD013035

[dataset] Swenson, S.C., 2012. GRACE monthly land water mass grids NETCDF RELEASE 5.0. Ver. 5.0. Physical Oceanography Distributed Active Archive. Centerhttps://doi.org/http://dx.doi.org/10.5067/TELND-NC005

Swenson, S.C., Lawrence, D.M., 2012. A new fractional snow-covered area parameterization for the Community Land Model and its effect on the surface energy balance. J. Geophys. Res. Atmos. 117, 1–20. https://doi.org/10.1029/2012JD018178

Swenson, S., Wahr, J., 2006. Post-processing removal of correlated errors in GRACE data. Geophys. Res. Lett. 33, 1–4. https://doi.org/https://dx.doi.org/10.1029/2005GL025285

Tangdamrongsub, N., Han, S.C., Tian, S., Schmied, H.M., Sutanudjaja, E.H., Ran, J., Feng, W., 2018. Evaluation of groundwater storage variations estimated from GRACE data assimilation and state-of-the-art land surface models in Australia and the North China Plain. Remote Sens. 10, 483. https://doi.org/10.3390/rs10030483

Tangdamrongsub, N., Steele-Dunne, S.C., Gunter, B.C., Ditmar, P.G., Weerts, A.H., 2015. Data assimilation of GRACE terrestrial water storage estimates into a regional hydrological model of the Rhine River basin. Hydrol. Earth Syst. Sci. 19, 2079–2100. https://doi.org/10.5194/hess-19-2079-2015

Tapley, B.D., Bettadpur, S., Watkins, M., Reigber, C., 2004. The gravity recovery and climate

experiment: Mission overview and early results. Geophys. Res. Lett. 31, 1–4. https://doi.org/10.1029/2004GL019920

Tapley, B.D., Watkins, M.M., Flechtner, F., Reigber, C., Bettadpur, S., Rodell, M., Sasgen, I., Famiglietti, J.S., Landerer, F.W., Chambers, D.P., Reager, J.T., Gardner, A.S., Save, H., Ivins, E.R., Swenson, S.C., Boening, C., Dahle, C., Wiese, D.N., Dobslaw, H., Tamisiea, M.E., Velicogna, I., 2019. Contributions of GRACE to understanding climate change. Nat. Clim. Chang. 9, 358–369. https://doi.org/10.1038/s41558-019-0456-2

Tolson, B.A., Shoemaker, C.A., 2007. Dynamically dimensioned search algorithm for computationally efficient watershed model calibration. Water Resour. Res. 43, 1–16. https://doi.org/10.1029/2005WR004723

Toure, A.M., Rodell, M., Yang, Z.-L., Beaudoing, H., Kim, E., Zhang, Y., Kwon, Y., 2016. Evaluation of the snow simulations from the Community Land Model, Version 4 (CLM4). J. Hydrometeorol. 17, 153–170. https://doi.org/https://dx.doi.org/10.1175/JHM-D-14-0165.1

Van Dijk, A.I.J.M., Renzullo, L.J., Wada, Y., Tregoning, P., 2014. A global water cycle reanalysis (2003-2012) merging satellite gravimetry and altimetry observations with a hydrological multi-model ensemble. Hydrol. Earth Syst. Sci. 18, 2955–2973. https://doi.org/10.5194/hess-18-2955-2014

Verseghy, D.L., 1991. Class-A Canadian land surface scheme for GCMS. I. Soil model. Int. J. Climatol. 11, 111–133. https://doi.org/10.1002/joc.3370110202

Verseghy, D.L., 2012. The Canadian land surface scheme (version 3.6)-technical documentation, Environment Canada.

Verseghy, D., Brown, R., Wang, L., 2017. Evaluation of CLASS snow simulation over Eastern Canada. J. Hydrometeorol. 18, 1205–1225. https://doi.org/10.1175/JHM-D-16-0153.1

Verseghy, D.L., MacKay, M.D., 2017. Offline implementation and evaluation of the Canadian Small Lake Model with the Canadian Land Surface Scheme over Western Canada. J. Hydrometeorol. 18, 1563–1582. https://doi.org/10.1175/JHM-D-16-0272.1

Verseghy, D.L., McFarlane, N.A., Lazare, M., 1993. CLASS - a Canadian land surface scheme for GCMs, II. Vegetation model and coupled runs. Int. J. Climatol. 13, 347–370.

Walsh, J.E., 1984. Snow Cover and Atmospheric Variability: Changes in the snow covering the earth's surface affect both daily weather and long-term climate. Am. Sci. 72, 50–57.

Xu, X., Tolson, B.A., Li, J., Staebler, R.M., Seglenieks, F., Haghnegahdar, A., Davison, B., 2015. Assimilation of SMOS soil moisture over the Great Lakes basin. Remote Sens. Environ. 169, 163–175. https://doi.org/10.1016/j.rse.2015.08.017

Yassin, F., Razavi, S., Elshamy, M., Davison, B., Sapriza-Azuri, G., Wheater, H., 2019. Representation and improved parameterization of reservoir operation in hydrological and land-surface models. Hydrol. Earth Syst. Sci. 23, 3735–3764. https://doi.org/10.5194/hess-23-3735-2019

Yassin, F., Razavi, S., Wheater, H., Sapriza-Azuri, G., Davison, B., Pietroniro, A., 2017. Enhanced identification of a hydrologic model using streamflow and satellite water storage data: A multicriteria sensitivity analysis and optimization approach. Hydrol. Process. 31, 3320–3333. https://doi.org/10.1002/hyp.11267

Zaitchik, B.F., Rodell, M., Reichle, R.H., 2008. Assimilation of GRACE terrestrial water storage data into a land surface model: Results for the Mississippi River basin. J. Hydrometeorol. 9, 535–548. https://doi.org/10.1175/2007JHM951.1

Zhang, Y.F., Hoar, T.J., Yang, Z.L., Anderson, J.L., Toure, A.M., Rodell, M., 2014. Assimilation of MODIS snow cover through the data assimilation research testbed and the community Land Model version 4. J. Geophys. Res. 119, 7091–7103. https://doi.org/10.1002/2013JD021329

7. General Discussion

This section gives an overarching discussion of the thesis. Each of the article manuscripts that constitute the heart of the research (Chapters 4, 5, 6) includes its discussion.

7.1. Spatiotemporal analysis

Based on gridded correlation results of GRACE-derived TWSA versus GlobSnow2/AMSR-E/CMC SWEA data, stronger correlation values could be found in the areas with important snowfall. These findings, to some extent, are consistent with the results of Frappart *et al.* (2006) and Frappart *et al.* (2011). Positive and significant correlation results were found mainly in southern Québec, Ontario, and the Canadian Prairies. In contrary to GRACE, the model simulations of GLDAS derived TWSA had strong linkages with snow products in the Québec-Labrador area. Correlation results obtained with GLDAS showed the dependency on the latitudinal variations. Weak or insignificant correlation results between GLDAS and snow mass datasets were mainly attained in higher latitudes. Based on basin-averaged results, GRACE-derived TWSA retrievals were generally associated with SWEA data sets. Higher correlation values with smaller RMSE were found in western Canada (e.g., Peace, Fraser, and Liard basins). Yet, in the northern Québec area and western Hudson Basins, insignificant or even negative correlation values were obtained. The statistical results between GRACE-derived SWEA and multisource SWEA data sets indicated that improved correlations were obtained in the majorities of basins when the contributions of water storage compartments (e.g., wetland, surface water) were subtracted from GRACE data. Different possible reasons that influence the correlation results at gridded and basin-averaged spatial resolutions are discussed below.

The uncertainty of GRACE observations is a function of measurement error (systematic and random), GIA, signal leakage errors, and background gravity model errors. Note that each of these sources of uncertainties may influence correlations results. This study did not investigate any of the uncertainties mentioned, that can affect GRACE data. The uncertainty analysis is out of the scope of this work. However, possible explanations of the weak correlations found in some of the regions in Canada may be related to GRACE uncertainties or because of the influence of the other storage components in the water column measured by GRACE. Over the Canadian territory, in particular near the Hudson Bay region, GRACE measures secular trends from ice-load histories

(Lambert *et al.*, 2013; Rangelova *et al.*, 2007; Wang *et al.*, 2013). Even though a GIA model correction removed secular trends from Level-3 GRACE-Tellus mass grids, this adjustment adds some uncertainty in the estimation of water storage anomalies. Lambert *et al.* (2013) recommended that GIA adjustments were more efficient when the GIA model correction was combined with GPS observations. Furthermore, GRACE TWSA signal can be decomposed into long-term (linear and inter-annual), seasonal, and sub-seasonal residual components. In areas surrounding Hudson Bay, GRACE observations are more uncertain and exhibit considerable noises that influence the information content of the observations (Humphrey *et al.*, 2016; Trautmann *et al.*, 2018). This could be a possible explanation of weak correlations results found all around the Hudson Bay area up to northern Québec in this study. However, further analyses using temporal decomposition of GRACE signal are required for more insights. It is also possible that in the northern latitudes (e.g. northern Québec) the dominance of the sub-seasonal compartment of the signal might influence the correlation results.

Another issue is the limitation and uncertainty of GLDAS model simulations. First, incomplete or simplified representation of water and energy budgets (e.g. snow layer scheme) can influence model simulations. In these conditions, the model might not capture snow mass variations, especially in high latitudes and mountainous regions over western Canada (Mudryk *et al.*, 2015; Syed *et al.*, 2008). GLDAS also has limitations in capturing seasonal variations in monthly TWS changes compared to GRACE (Wang *et al.*, 2016).

In addition, the uncertainty of WGHM simulation may influence the correlation results. Like other models, several sources of uncertainty, including input data (eg., climate forcing, land cover, water use), modeling approach, and model parameters have effects on the WGHM simulations. In this research, the uncertainty of model simulation was not evaluated. Yet in a number of studies, it was found that the model estimates outperform other global models (Müller Schmied *et al.*, 2014; Veldkamp *et al.*, 2018; Wartenburger *et al.*, 2018; Zaherpour *et al.*, 2018). The performance of WGHM in northern midlatitudes (20-50ºN), showed that WGHM underestimates GRACE TWSA seasonal amplitudes by 3% with a RMSE value of 52.7 mm. Note that, more calibration/data assimilation efforts are still ongoing to improve WGHM model estimates.

SWE retrievals from Remote passive microwave have still large uncertainties because of dense vegetation, wet snow, and deep snow conditions. Larue *et al.* (2017) validated the GlobSnow2 and AMSR-E SWE values against in-situ SWE measurements in eastern Canada. They found that GlobSnow2 underestimated SWE, and still has large errors (RMSE = 94.1 ± 20.3 mm). AMSR-E also underestimates SWE, and has very large errors (RMSE = 165.6 mm). It is well-known that CMC SWE estimations are not reliable in some areas, particularly in high latitudes, where surface snow depth observations are sparsely located, and they are unlikely to be representative of snow cover over the prevailing land cover (Brown and Brasnett, 2010). Brown *et al.* (2018) evaluated the annual maximum SWE (SWEM) based on manual gravimetric snow surveys over the Saint-Maurice River basin in southern Québec. The results showed that CMC underestimated SWEM over the study domain (RMSE = 81.3 mm, BIAS = -58.1 mm, R = 0.53). But CMC could capture the interannual variability in regionally averaged SWEM. Therefore, SWE values in these locations should be analyzed with caution (Verseghy *et al.*, 2017).

Finally, we should point out the challenges of spatiotemporal correlation analysis at the spatial and temporal resolution scales. Variables such as SWE have significant subgrid variability in horizontal and vertical properties (Mudryk *et al.*, 2015). The computation of SWEA and TWSA at the basin scale smoothes the spatial heterogeneity of snow and terrestrial water storage characteristics, respectively. In addition, the temporal resolution of GRACE data is reduced to a monthly scale. This temporal averaging can create a mismatch with TWS and SWE time series, especially in the case of high frequency anomalies (Humphrey *et al.*, 2016).

7.2. MESH-GRACE data assimilation

7.2.1. Evaluation of results

The assimilation of GRACE observation into the MESH model demonstrated that the EnKS method could constrain the amplitude of modeled TWS dynamics so that close agreement with GRACE observations is obtained. This indicated that the assimilation procedure can effectively transfer information from the coarse-scale (~150 000 km^2) GRACE TWS retrievals to the finer scale (~100 km^2) model resolution. Based on ubRMSD and Spearman's rank correlations, the assimilation of GRACE observations improved SWE simulations at both basin and grid scales. In general, the MESH-GRACE DA framework influenced effectively the estimation of SWE in the

Liard Basin. Snow simulation results were consistent with Forman *et al.* (2012) and Su *et al.* (2010), who demonstrated the effects of the GRACE data assimilation in the improvement of model SWE estimates across portions of North America, using models other than MESH. The streamflow simulations showed that the influence of integrating GRACE observations was small compared to modeled TWS and SWE estimates. Different possible reasons that influence the assimilation results at gridded and basin-averaged spatial resolutions are discussed below.

In some cases, namely the year 2012, the lack of updates in TWS simulation was observed. Two possible reasons may cause this small difference. First, the difference between the model forecast and observation was not large. Second, the uncertainty of predicted water storage was small relative to the uncertainty of the observations. This led to a near-zero covariance structure in the Kalman gain (Forman *et al.*, 2012).

Loss of ubRMSD skill in the estimation of SWE observed in 44% of grid cells (4% of them statistically significant) as a result of GRACE assimilation can be explained by different possible factors. First, the gridded GRACE observations were processed by averaging up to the Liard Basin scale to make them compatible with the MESH model. Note that, as Liard basin size (~275 000 km^2) is not substantially larger than the true resolution of observations, the usage of gridded (1º×1º) observations might not influence the results. Even though the implementation of assimilation based on gridded GRACE data is an advantage, observations should be assimilated at the smallest spatial scale, i.e., 5º×5º, such that their errors become uncorrelated (Girotto *et al.*, 2019). Second, in grid cells where degradations of ubRMSD were observed, OL did a reasonable job in estimating SWE. Third, the limitations of CMC SWE analysis data in northern latitudes (> 55º N) should also be considered. Over northern areas, CMC SWE analysis depends mostly on the GEM precipitation forecast rather than snow depth observations (Brown and Brasnett, 2010). Moreover, snow depth observations tend to be biased to coastal locations or large open areas at airports. Therefore, due to the scarcity of in-situ observations in northern latitudes, the evaluation of MESH SWE estimates based on the CMC SWE analysis data stands like a comparison of model to model.

Different distinct features are observed from the snow survey evaluation (Figure 6.9). First, GRACE data assimilation for SWE simulations at three stations had negative biases in March and April 2013 relative to snow observations. This might be explained partly because GRACE

observation was not available in March 2013. Thus, the analysis (or update) procedure in March was not performed. Second, in 2013, MESH simulations (OL and DA) had maximum SWE in March, while snow observations showed maximum values in April. A temporal lag around 15 days could be observed between model simulations and snow observations. It is worth mentioning that, comparing point-level measurements to the 0.125º×0.125º grid resolution of the MESH model is not easy and may introduce representativeness error due to SWE spatial variations of MESH SWE estimates and ground-based measurements. It is important to highlight that, the number of in-situ measurements that fall inside the Liard Basin is not large enough to cover the entire study area. The reason is that the acquisition of SWE observations in northern latitude basins is a difficult task (installation of stations, maintenance). Therefore, due to the insufficiency of snow survey observations in the Liard Basin, the conclusions about the comparison of model estimates to in-situ observations cannot be drawn clearly. Third, the GRACE DA method performed effectively in the snow season of 2014, such that a close agreement between MESH SWE estimates and snow observations was obtained. Forth, CMC SWE estimates are not in direct contrast to snow survey observations. It can be observed in Figure 6.9 that, CMC SWE estimates agree well with automated SWE measurements especially in 2013. Less than 20 mm difference between CMC SWE and snow stations is observed. Note that the comparison between CMC SWE values and snow survey observations was not applied to evaluate the CMC SWE product (this evaluation is out of the scope of this study). The purpose was to see whether in the three different geographical locations CMC showed comparable results to GRACE DA and in-situ measurements. As it is mentioned before, CMC faces challenges in the estimation of SWE, especially in northern latitude areas (> 55°). Even though the evaluation of CMC SWE product is an interesting research topic, it is beyond the scope of this study.

The streamflow simulations show that the effect of the assimilation of GRACE observations was small compared to the effects on modeled TWS and SWE estimates. Yet, the developed framework can improve high flows, particularly near the rainfall seasons. Estimates of streamflow for flow volume and low flow were slightly degraded at some stations as a result of GRACE assimilation. The loss of skill could be related to different possible reasons. First, SWE is reduced by DA in the Liard Basin, which means less SWE is available to produce snowmelt streamflow. Second, water storage increments that were added during the update step of assimilation during summer were not sufficient to compensate for deficiencies of the model to simulate adequate streamflow. Third both

OL and DA had negative biases during the winter season (December to April) for the simulation of low flows. These biases could be related to the limitation of the MESH model in generating sufficient base flow at the three observed stations.

7.2.2. Assimilation diagnostics

Results at the basin and gridded scales revealed that the uncertainty of OL simulations was reduced substantially after constraining model predictions. Forman *et al.* (2012) attained similar findings in the Liard Basin by making use of the CLSM model. In this study, large values of SWE ensemble spreads for the OL simulations were located mainly in mountainous areas (e.g., Mackenzie Mountains). In these regions, the ubRMSD values were also large compared to the other regions. The large uncertainty that was associated with complex terrain may be related to the uncertainties of CaPA forcing (Lespinas *et al.*, 2015) and the horizontal resolution of the MESH model (Carrera *et al.*, 2010). Furthermore, blowing snow processes was not incorporated into the MESH model. This process can be simulated using the physically-based PBSM model that takes into account wind direction and speed, and other aspects (MacDonald *et al.*, 2009). Note that the reduction of uncertainty in the model estimates does not necessarily mean that better estimates are achieved when compared to the evaluation data (Girotto *et al.*, 2019). For example, in the region near the northwestern and western boundaries of the basin, ensemble spreads were reduced, but the ubRMSD values were degraded as a result of the GRACE assimilation.

The statistics of the filter innovations are useful tools to indicate whether or not the choice of the model (Table 6.1) and measurement error parameters is appropriate. The results of the mean and standard deviation of normalized innovation are presented in Figure 6.11 based on four different GRACE measurement variance values of 72.25 mm^2, 289 mm^2, 650.25 mm^2, and 1156 mm^2. It was observed that the mean values ($\overline{NI}$) of the normalized innovations for $\boldsymbol{R}$ values of 289 mm^2 and 650.25 mm^2 were equal to zero. This reveals that the data assimilation simulations are unbiased for these two experiments. The noticeable feature is that the mean innovations using two observation errors of 72.25 mm^2 and 1156 mm^2 had positive and negative biases. Moreover, the innovation variance (σ_{NI}) values were decreased as a result of increasing measurement errors. Based on the information provided from the normalized innovations, the selection of the observation error between 289 mm^2 and 650.25 mm^2 indicates a reasonable data assimilation

performance for the MESH model (i.e., a σ_{NI} close to unity, and $\overline{NI}$ close to zero). These findings are consistent with previous data assimilation studies that considered observation variance between 289 mm^2 and 400 mm^2 (Forman et al., 2012; Forman and Reichle, 2013; Kumar et al., 2016; Su et al., 2010; Zaitchik et al., 2008).

Examination of analysis increment (i.e., the difference between update and forecast) showed how much and at what time information from GRACE observations affected the estimation of water storage at different vertical layers (Forman *et al.*, 2012; Girotto *et al.*, 2019). The pattern rather than the magnitude of increments (especially SWE) was consistent, to some extent, with those reported by Forman *et al.* (2012). Analysis increments applied to MESH water storage compartments indicated that assimilation reduced snow mass during the snow accumulation seasons from November to May of each year. A small amount of SWE is added back during the spring ablation and snowmelt phases. Small or near-zero numbers of subsurface updates were possibly related to the perturbation structure, such that the uncertainties of soil water compartments were not included in the system.

8. Conclusion and perspective work

8.1. Conclusion

The research aimed to develop a data assimilation framework to integrate GRACE observations into the MESH model. To implement the principal objective of this study, GRACE observations, as along with a suite of remote-sensing products, model simulations, and snow analysis products were utilized to find out locations where gravimetric retrievals are highly influenced by snow mass variations. The main contributions and originalities of this thesis can be summarized as follow:

1. For the first time, a comprehensive experimental study of assessing GRACE observations with regard to three different SWE products has been conducted, to determine areas in Canada where SWE is the major contributor to the total terrestrial water storage.

2. GRACE data assimilation framework was developed into the MESH modeling framework in Liard Basin for the first time to improve snow water equivalent and streamflow estimates.

Following the first objective of the research, the spatiotemporal association between GRACE TWSA retrievals and three sources of snow products was investigated at the gridded (1°×1° grid cells) and basin-averaged spatial resolutions. Results showed significant relationships between GRACE and SWE anomalies for 52% to 62% of the grid cells covering the study area, depending on the SWE product. Based on the basin-averaged results, significant relationships were found between GRACE and SWEAs for 53% to 80% of the basins covering the study area. Overall, results support hypothesis I and indicate the important role of SWEA on the TWSA variations during the snow season in areas with dominant snow mass.

GRACE-derived TWSA retrievals in the snow-dominated basin were assimilated into the MESH model using the EnKS method. During six years of data assimilation, the integration of GRACE TWSA observations was found to have positive effects on the snow budgets and streamflow estimates compared to the open-loop (with assimilation) simulation. At the basin scale, GRACE DA reduced the bias by 17.1% and improved the unbiased RMSD by ~23%. At the grid cell spatial resolution, ubRMSD values were improved in 85% of the grid cells, and in 56% of the grids the

ameliorations were statistically significant. Furthermore, data assimilation led to improved correlation values in 97% of the grid cells (61% of these grid cells were statistically significant). It was shown that the implementation of the ensemble smoother method improves MESH SWE estimates, thus hypothesis II is supported. In addition, the performance of the methodology was evaluated for streamflow simulations at the three selected streamflow stations. GRACE DA could improve the simulation of high flows at Lower Crossing and Fort Liard stations. The influence of GRACE DA on total flow volume and low flows was found to be variable. It is worth mentioning that, the integration of satellite observations could effectively reduce the ensemble spreads (uncertainty) at the basin, gridded, and station-based simulations. The findings of this study are encouraging and suggest the potential for further improvements of model simulation through using GRACE observations with a finer spatial resolution.

8.2. Outlook

The investigation of the relationship between GRACE and multisource of SWE revealed that further works are required to consider the temporal decomposition of GRACE signal into the long-term, inter-annual, seasonal, and sub-seasonal residuals. Undoubtedly, proper treatment of signal contamination from nearby land hydrology and adjusted GIA effects should be considered carefully. Further research on the consideration of error covariance of GRACE data on the gridded scale, may be helpful to understand autocorrelation effects and extracting the main hydrological features.

Further work will extend the research to different basins with variable climate regimes and snow budgets conditions. The use of gridded observations at a finer spatial resolution (e.g., 3º×3º) will be investigated by considering the full error covariance of the observations. The findings at such finer resolution will have important implications for evaluating the performance of the MESH-GRACE data assimilation framework for the purpose of improving regional estimates of SWE, soil moisture, and water and energy fluxes.

It is interesting to further develop the assimilation methodology to integrate parameters (e.g., minimum depth to consider 100% cover of snow on the ground surface) during the assimilation procedure. The calibration of model parameters, such as snow-related variables will present a relatively new research area. The simultaneous estimation of water storage states and model

parameter values can be beneficial for accurate model simulations.

The possibility of extending the developed methodology to multivariate and multisensor data assimilation could be explored to further improve the accuracy of model estimates. Future works can investigate the individual and joint assimilation of GRACE and GRACE-FO observations with other satellite-based measurements. This embedded framework will be implemented into the MESH software. The data assimilation results will be evaluated by comparing against a large suite of reference data products. In the next step, findings of this implementation can be compared with results from an operational data assimilation system such as CaLDAS that has been developed at ECCC.

It is encouraging to benefit from extending the MESH-GRACE data assimilation framework based on fully Bayesian methods (e.g., Particle Filter). The effects of multiple filtering methods could be evaluated on the hydrological model simulations. Various aspects of the filters, e.g., the stability of ensemble members, ensemble distributions, the system error covariances should be analyzed.

References (except for articles)

Alavi, N., Bélair, S., Fortin, V., Zhang, S., Husain, S. Z., Carrera, M. L. and Abrahamowicz, M. (2016) Warm Season Evaluation of Soil Moisture Prediction in the Soil, Vegetation and Snow (SVS) Scheme. Journal of Hydrometeorology, p. JHM-D-15-0189.1.

Bahrami, A., Goïta, K. and Magagi, R. (2020) Analyzing the contribution of snow water equivalent to the terrestrial water storage over Canada. Hydrological Processes, vol. 34, n°2, p. 175-188.

Barnett, T. P., Adam, J. C. and Lettenmaier, D. P. (2005) Potential impacts of a warming climate on water availability in snow-dominated regions. Nature, vol. 438, n°7066, p. 303-9.

Barnett, T. P., Dumenil, L., Schlese, U., Roeckner, E. and Latif, M. (1989) The effect of Eurasian snow cover on regional and global climate variations. Journal of the Atmospheric Sciences, vol. 46, n°5, p. 661-685.

Behrangi, A., Gardner, A. S., Reager, J. T. and Fisher, J. B. (2017) Using GRACE to constrain precipitation amount over cold mountainous basins. Geophysical Research Letters, vol. 44, n°1, p. 219-227.

Behrangi, A., Gardner, A., Reager, J. T., Fisher, J. B., Yang, D., Huffman, G. J. and Adler, R. F. (2018) Using GRACE to estimate snowfall accumulation and assess gauge undercatch corrections in high latitudes. Journal of Climate, vol. 31, n°21, p. 8689-8704.

Benoit, R., Pellerin, P., Kouwen, N., Ritchie, H., Donaldson, N., Joe, P. and Soulis, E. D. (2000) Toward the use of coupled atmospheric and hydrologic models at regional scale. Monthly Weather Review, vol. 128, n°6, p. 1681-1706.

Bettadpur, S. (2012) GRACE Product Specification Document. Center for Space Research, The University of Texas at Austin, p. 1-77 .

Bettadpur, S. (2018) GRACE Level-2 Gravity Field Product User Handbook. Center for Space Research, The University of Texas at Austin, p. 1-21.

Bras, R. L. (1990) Hydrology : an introduction to hydrologic science. Addison-Wesley.

Brown, R., Bartlett, P., MacKay, M. and Verseghy, D. (2006) Evaluation of snow cover in

CLASS for SnowMIP. Atmosphere-Ocean, vol. 44, n°3, p. 223-238.

Brown, R. and Brasnett, B. (2010) Canadian Meteorological Centre (CMC) Daily Snow Depth Analysis Data, Version 1. National Snow and Ice Data Center.

Brown, R., Tapsoba, D. and Derksen, C. (2018) Evaluation of snow water equivalent datasets over the Saint-Maurice river basin region of southern Québec. Hydrological Processes, vol. 32, n°17, p. 2748-2764.

Burgers, G., Jan van Leeuwen, P. and Evensen, G. (1998) Analysis Scheme in the Ensemble Kalman Filter. Monthly Weather Review, vol. 126, n°6, p. 1719-1724.

Canadian Digital Elevation Data (2016). Natural Resources Canada, Canada Centre for Mapping and Earth Observation.

Carrassi, A., Bocquet, M., Bertino, L. and Evensen, G. (2018) Data assimilation in the geosciences: An overview of methods, issues, and perspectives. Wiley Interdisciplinary Reviews: Climate Change, vol. 9, n°5, p. 50.

Carrera, M. L., Bélair, S. and Bilodeau, B. (2015) The Canadian Land Data Assimilation System (CaLDAS): Description and Synthetic Evaluation Study. Journal of Hydrometeorology, vol. 16, n°3, p. 1293-1314.

Carrera, M. L., Bélair, S., Fortin, V., Bilodeau, B., Charpentier, D. and Doré, I. (2010) Evaluation of Snowpack Simulations over the Canadian Rockies with an Experimental Hydrometeorological Modeling System. Journal of Hydrometeorology, vol. 11, n°5, p. 1123-1140.

Chambers, D. P., Cazenave, A., Champollion, N., Dieng, H., Llovel, W., Forsberg, R., von Schuckmann, K. and Wada, Y. (2016) Evaluation of the Global Mean Sea Level Budget between 1993 and 2014. Surveys in Geophysics. Springer Netherlands.

Chambers, D. P., Wahr, J. and Nerem, R. S. (2004) Preliminary observations of global ocean mass variations with GRACE. Geophysical Research Letters, vol. 31, n°13, p. 1-4.

Chang, A. T. C., Foster, J. L. et Hall, D. K. (1996) Effects of forest on the snow parameters derived from microwave measurements during the BOREAS Winter Field Campaign. Hydrological Processes, vol. 10, n°12, p. 1565-1574.

Chen, F., Mitchell, K., Schaake, J., Xue, Y., Pan, H.-L., Koren, V., Duan, Q. Y., Ek, M. and Betts, A. (1996) Modeling of land surface evaporation by four schemes and comparison with FIFE observations. Journal of Geophysical Research: Atmospheres, vol. 101, n°D3, p. 7251-7268.

Clarke, R. T. (1973) A review of some mathematical models used in hydrology, with observations on their calibration and use. Journal of Hydrology, vol. 19, n°1, p. 1-20.

Cohen, J. (1989) The effect of snow cover on the climate. Proc. 45th Eastern snow conference, Lake Placid, NY, 1988, vol. 4, n°7, p. 27-41.

Cohen, J. and Entekhabi, D. (1999) Eurasian snow cover variability and northern hemisphere climate predictability. Geophysical Research Letters. John Wiley & Sons, Ltd.

Cooley, S. S. and Landerer, F. W. (2019) GRACE/GRACE-FO Level-3 Data Product User Handbook. Jet Propulsion Laboratory California Institute of Technology, p. 1-58.

Côté, J., Desmarais, J.-G., Gravel, S., Méthot, A., Patoine, A., Roch, M. and Staniforth, A. (1998b) The Operational CMC–MRB Global Environmental Multiscale (GEM) Model. Part II: Results. Monthly Weather Review, vol. 126, n°6, p. 1397-1418.

Côté, J., Gravel, S., Méthot, A., Patoine, A., Roch, M. and Staniforth, A. (1998a) The Operational CMC–MRB Global Environmental Multiscale (GEM) Model. Part I: Design Considerations and Formulation. Monthly Weather Review, vol. 126, n°6, p. 1373-1395.

Davison, B. (2016) Improving Hydrologic Prediction in Canada using a Land Surface Scheme with Data Assimilation of Precipitation and Streamflow. PhD dissertation, McGill University, Montreal, Canada.

Davison, B., Fortin, V., Pietroniro, A., Yau, M. and Leconte, R. (2019) Parameter-state ensemble thinning for short-term hydrological prediction. Hydrology and Earth System Sciences, vol. 23, n°2, p. 741-762.

Davison, B., Pohl, S., Domes, P., Marsh, P., Pietroniro, A. and MacKay, M. (2006) Characterizing snowmelt variability in a land-surface-hydrologic model. Atmosphere-Ocean, vol. 44, n°3, p. 271-287.

Derksen, C., Toose, P., Rees, A., Wang, L., English, M., Walker, A. and Sturm, M. (2010) Development of a tundra-specific snow water equivalent retrieval algorithm for satellite

passive microwave data. Remote Sensing of Environment, vol. 114, n°8, p. 1699-1709.

Déry, S. J., Sheffield, J. and Wood, E. F. (2005) Connectivity between Eurasian snow cover extent and Canadian snow water equivalent and river discharge. Journal of Geophysical Research, vol. 110, n°D23, p. 1-14.

Döll, P., Fritsche, M., Eicker, A. and Müller Schmied, H. (2014a) Seasonal Water Storage Variations as Impacted by Water Abstractions: Comparing the Output of a Global Hydrological Model with GRACE and GPS Observations. Surveys in Geophysics, vol. 35, n°6, p. 1311-1331.

Döll, P., Müller Schmied, H., Schuh, C., Portmann, F. T. and Eicker, A. (2014b) Global-scale assessment of groundwater depletion and related groundwater abstractions: Combining hydrological modeling with information from well observations and GRACE satellites. Water Resources Research, vol. 50, n°7, p. 5698-5720.

Dornes, P. F., Tolson, B. A., Davison, B., Pietroniro, A., Pomeroy, J. W. and Marsh, P. (2008) Regionalisation of land surface hydrological model parameters in subarctic and arctic environments. Physics and Chemistry of the Earth, Parts A/B/C, vol. 33, n°17-18, p. 1081-1089.

Dunn, C., Bertiger, W., Bar-Sever, Y., Desai, S., Haines, B., Kuang, D., Franklin, G., Harris, I., Kruizinga, G., Meehan, T., Nandi, S., Nguyen, D., Rogstad, T., Thomas, J. B., Tien, J., Romans, L., Watkins, M., Wu, S. C., Bettadpur, S. and Kim, J. (2003) Instrument of Grace: GPS augments gravity measurements. GPS World, vol. 14, n°2, p. 16-28.

Dunne, S. and Entekhabi, D. (2005) An ensemble-based reanalysis approach to land data assimilation. Water Resources Research, vol. 41, n°2, p. 1-18.

Eicker, A., Schumacher, M., Kusche, J., Döll, P. and Schmied, H. M. (2014) Calibration/Data Assimilation Approach for Integrating GRACE Data into the WaterGAP Global Hydrology Model (WGHM) Using an Ensemble Kalman Filter: First Results. Surveys in Geophysics, vol. 35, n°6, p. 1285-1309.

Elshamy, M. E., Princz, D., Sapriza-Azuri, G., Pietroniro, A., Wheater, H. S. and Razavi, S. (2020) On the Configuration and Initialization of a Large Scale Hydrological Land Surface Model to Represent Permafrost. Hydrology and Earth System Sciences, vol. 24, n°1, p. 349-

379.

Entekhabi, D., Reichle, R. H., Koster, R. D. and Crow, W. T. (2010) Performance Metrics for Soil Moisture Retrievals and Application Requirements. Journal of Hydrometeorology, vol. 11, n°3, p. 832-840.

Essery, R., Rutter, N., Pomeroy, J., Baxter, R., Stahli, M., Gustafsson, D., Barr, A., Bartlett, P. and Elder, K. (2009) SnowMIP2: An evaluation of forest snow process simulation. Bulletin of the American Meteorological Society, vol. 90, n°8, p. 1130-1135.

Etchevers, P., Martin, E., Brown, R., Fierz, C., Lejeune, Y., Bazile, E., Boone, A., Dai, Y. J., Essery, R., Fernandez, A., Gusev, Y., Jordan, R., Koren, V., Kowalczyk, E., Nasonova, N. O., Pyles, R. D., Schlosser, A., Shmakin, A. B., Smirnova, T. G., Strasser, U., Verseghy, D., Yamazaki, T. and Yang, Z. L. (2004) Validation of the energy budget of an alpine snowpack simulated by several snow models (SnowMIP project). Annals of Glaciology, vol. 38, p. 150-158.

Etchevers, P., Martin, E., Brown, R., Fierz, C., Lejeune, Y., Bazile, E., Boone, A., Dai, Y. J., Essery, R., Fernandez, A., Gusev, Y., Jordan, R., Kowalczyk, E., Nasonova, N. O., Pyles, R. D., Schlosser, A. and Shmakin, A. B. (2002) SnowMIP, an intercomparison of snow models : first results International Snow Science Workshop, p. 353-360. Penticton, British Columbia.

Evensen, G. (2003) The Ensemble Kalman Filter: theoretical formulation and practical implementation. Ocean Dynamics, vol. 53, n°4, p. 343-367.

Evensen, G. (2009) Data assimilation: The ensemble Kalman filter. Data Assimilation (Second Edition): The Ensemble Kalman Filter. Springer Science & Business Media.

Evensen, G., Carlo, M. and Carlo, M. (1994) Sequential data assimilation with a nonlinear quasi-geostrophic model using Monte Carlo methods to forecast error statistics. Journal of Geophysical Research, vol. 99, n°C5, p. 10143–10162.

Evensen, G. and Van Leeuwen, P. J. (2000) An ensemble Kalman smoother for nonlinear dynamics. Monthly Weather Review, vol. 128, n°6, p. 1852-1867.

Famiglietti, J. S., Lo, M., Ho, S. L., Bethune, J., Anderson, K. J., Syed, T. H., Swenson, S. C., de Linage, C. R. and Rodell, M. (2011) Satellites measure recent rates of groundwater depletion

in California's Central Valley. Geophysical Research Letters, vol. 38, n°3, p. n/a-n/a.

Famiglietti, J. S. and Rodell, M. (2013) Environmental science. Water in the balance. Science (New York, N.Y.), vol. 340, n°6138, p. 1300-1.

Fletcher, C. G., Kushner, P. J., Hall, A. and Qu, X. (2009) Circulation responses to snow albedo feedback in climate change. Geophysical Research Letters, vol. 36, n°9, p. L09702.

Forman, B. A. and Reichle, R. H. (2013) The spatial scale of model errors and assimilated retrievals in a terrestrial water storage assimilation system. Water Resources Research, vol. 49, n°11, p. 7457-7468.

Forman, B. A., Reichle, R. H. and Rodell, M. (2012) Assimilation of terrestrial water storage from GRACE in a snow-dominated basin. Water Resources Research, vol. 48, n°1, p. 1-14.

Forootan, E., Rietbroek, R., Kusche, J., Sharifi, M. a., Awange, J. L., Schmidt, M., Omondi, P. and Famiglietti, J. (2014) Separation of large scale water storage patterns over Iran using GRACE, altimetry and hydrological data. Remote Sensing of Environment, vol. 140, p. 580-595.

Fortin, V., Roy, G., Stadnyk, T., Koenig, K., Gasset, N. and Mahidjiba, A. (2018) Ten Years of Science Based on the Canadian Precipitation Analysis: A CaPA System Overview and Literature Review†. Atmosphere - Ocean.

Foster, J. L., Hall, D. K., Eylander, J. B., Riggs, G. A., Nghiem, S. V., Tedesco, M., Kim, E., Montesano, P. M., Kelly, R. E. J., Casey, K. A. and Choudhury, B. (2011) A blended global snow product using visible, passive microwave and scatterometer satellite data. International Journal of Remote Sensing, vol. 32, n°5, p. 1371-1395.

Frappart, F., Ramillien, G., Biancamaria, S., Mognard, N. M. and Cazenave, A. (2006) Evolution of high-latitude snow mass derived from the GRACE gravimetry mission (2002–2004). Geophysical Research Letters, vol. 33, n°2, p. 1-5.

Frappart, F., Ramillien, G. and Famiglietti, J. S. (2011) Water balance of the Arctic drainage system using GRACE gravimetry products. International Journal of Remote Sensing, vol. 32, n°2, p. 431-453.

Gaborit, É., Fortin, V., Xu, X., Seglenieks, F., Tolson, B., Fry, L. M., Hunter, T., Anctil, F. and

Gronewold, A. D. (2017) A hydrological prediction system based on the SVS land-surface scheme: Efficient calibration of GEM-Hydro for streamflow simulation over the Lake Ontario basin. Hydrology and Earth System Sciences, vol. 21, n°9, p. 4825-4839.

Ganji, A., Sushama, L., Verseghy, D. and Harvey, R. (2015) On improving cold region hydrological processes in the Canadian Land Surface Scheme. Theoretical and Applied Climatology.

Girotto, M., De Lannoy, G. J. M., Reichle, R. H. et Rodell, M. (2016) Assimilation of gridded terrestrial water storage observations from GRACE into a land surface model. Water Resources Research, vol. 52, n°5, p. 4164-4183.

Girotto, M., De Lannoy, G. J. M., Reichle, R. H., Rodell, M., Draper, C., Bhanja, S. N. and Mukherjee, A. (2017) Benefits and pitfalls of GRACE data assimilation: A case study of terrestrial water storage depletion in India. Geophysical Research Letters, vol. 44, n°9, p. 4107-4115.

Girotto, M., Reichle, R. H., Rodell, M., Liu, Q., Mahanama, S. and De Lannoy, G. J. M. (2019) Multi-sensor assimilation of SMOS brightness temperature and GRACE terrestrial water storage observations for soil moisture and shallow groundwater estimation. Remote Sensing of Environment, vol. 227, p. 12-27.

Gong, G., Entekhabi, D., Cohen, J. and Robinson, D. (2004) Sensitivity of atmospheric response to modeled snow anomaly characteristics. Journal of Geophysical Research : Atmospheres, vol. 109, n°6, p. 1-13.

GRACE Mission Operation Status (2016). Derived from http://www2.csr.utexas.edu/grace/operations/mission_status/

Güntner, A. (2008) Improvement of Global Hydrological Models Using GRACE Data. Surveys in Geophysics, vol. 29, n°4-5, p. 375-397.

Güntner, A., Stuck, J., Werth, S., Döll, P., Verzano, K. and Merz, B. (2007) A global analysis of temporal and spatial variations in continental water storage. Water Resources Research, vol. 43, n°5.

Haghnegahdar, A. and Razavi, S. (2017) Insights into sensitivity analysis of Earth and environmental systems models: On the impact of parameter perturbation scale.

Environmental Modelling and Software, vol. 95, p. 115-131.

Haghnegahdar, A., Razavi, S., Yassin, F. and Wheater, H. (2017) Multi-criteria sensitivity analysis as a diagnostic tool for understanding model behavior and characterizing model uncertainty. Hydrological Processes, vol. 31, n°25, p. 4462-4476.

Haghnegahdar, A., Tolson, B. A., Craig, J. R. and Paya, K. T. (2015) Assessing the performance of a semi-distributed hydrological model under various watershed discretization schemes. Hydrological Processes, vol. 29, n°18, p. 4018-4031.

Heiskanen, W. A. and Moritz, H. (1967) Physical Geodesy. Geological Magazine. San Francisco, London : W. H. Freeman and Company.

Houborg, R., Rodell, M., Li, B., Reichle, R. and Zaitchik, B. F. (2012) Drought indicators based on model-assimilated Gravity Recovery and Climate Experiment (GRACE) terrestrial water storage observations. Water Resources Research, vol. 48, n°7.

Houtekamer, P. L., Mitchell, H. L., Pellerin, G., Buehner, M., Charron, M., Spacek, L. and Hansen, B. (2005) Atmospheric data assimilation with an ensemble Kalman filter: Results with real observations. Monthly Weather Review, vol. 133, n°3, p. 604-620.

Houtekamer, P. L. and Zhang, F. (2016) Review of the ensemble Kalman filter for atmospheric data assimilation. Monthly Weather Review. American Meteorological Society.

Humphrey, V., Gudmundsson, L. and Seneviratne, S. I. (2016) Assessing Global Water Storage Variability from GRACE: Trends, Seasonal Cycle, Subseasonal Anomalies and Extremes. Surveys in Geophysics, vol. 37, n°2, p. 357-395.

Husain, S. Z., Alavi, N., Bélair, S., Carrera, M., Zhang, S., Fortin, V., Abrahamowicz, M. and Gauthier, N. (2016) The multibudget Soil, Vegetation, and Snow (SVS) scheme for land surface parameterization: Offline warm season evaluation. Journal of Hydrometeorology, vol. 17, n°8, p. 2293-2313.

Iman, R. L. and Conover, W. J. (1979) The use of the rank transform in regression. Technometrics, vol. 21, n°4, p. 499-509.

Kelly, R. (2009) The AMSR-E Snow Depth Algorithm: Description and Initial Results. Journal of The Remote Sensing Society of Japan, vol. 29, n°1, p. 307-317.

Khaki, M. and Awange, J. (2019) The application of multi-mission satellite data assimilation for studying water storage changes over South America. Science of the Total Environment, vol. 647, p. 1557-1572.

Khaki, M., Forootan, E., Kuhn, M., Awange, J., van Dijk, A. I. J. M., Schumacher, M. and Sharifi, M. A. (2018) Determining water storage depletion within Iran by assimilating GRACE data into the W3RA hydrological model. Advances in Water Resources, vol. 114, p. 1-18.

Khaki, M., Hoteit, I., Kuhn, M., Awange, J., Forootan, E., van Dijk, A. I. J. M., Schumacher, M. and Pattiaratchi, C. (2017a) Assessing sequential data assimilation techniques for integrating GRACE data into a hydrological model. Advances in Water Resources, vol. 107, p. 301-316.

Khaki, M., Schumacher, M., Forootan, E., Kuhn, M., Awange, J. L. and van Dijk, A. I. J. M. (2017b) Accounting for spatial correlation errors in the assimilation of GRACE into hydrological models through localization. Advances in Water Resources, vol. 108, p. 99-112.

Koren, V., Schaake, J., Mitchell, K., Duan, Q.-Y., Chen, F. and Baker, J. M. (1999) A parameterization of snowpack and frozen ground intended for NCEP weather and climate models. Journal of Geophysical Research: Atmospheres, vol. 104, n°D16, p. 19569-19585.

Kouwen, N. (1988) Watflood: A micro-computer based flood forecasting system based on real-time weather radar. Canadian Water Resources Journal, vol. 13, n°1, p. 62-77.

Kouwen, N. (2018) WATFLOOD/CHARM Canadian Hydrological And Routing Model. Waterloo, Ontario : 289 p.

Kouwen, N., Soulis, E. D., Pietroniro, A., Donald, J. and Harrington, R. A. (1993) Grouped response units for distributed hydrologic modeling. Journal of Water Resources Planning and Management, vol. 119, n°3, p. 289-305.

Kumar, S. V., Zaitchik, B. F., Peters-Lidard, C. D., Rodell, M., Reichle, R., Li, B., Jasinski, M., Mocko, D., Getirana, A., De Lannoy, G., Cosh, M. H., Hain, C. R., Anderson, M., Arsenault, K. R., Xia, Y. and Ek, M. (2016) Assimilation of Gridded GRACE terrestrial water storage estimates in the North American land data assimilation system. Journal of Hydrometeorology, vol. 17, n°7, p. 1951-1972.

Lambert, A., Huang, J., van der Kamp, G., Henton, J., Mazzotti, S., James, T. S., Courtier, N. and

Barr, A. G. (2013) Measuring water accumulation rates using GRACE data in areas experiencing glacial isostatic adjustment: The Nelson River basin. Geophysical Research Letters, vol. 40, n°23, p. 6118-6122.

Land Cover of Canada (2010) Natural Resources Canada; Canada Centre for Remote Sensing.

Landerer, F. W. and Swenson, S. C. (2012) Accuracy of scaled GRACE terrestrial water storage estimates. Water Resources Research, vol. 48, n°4, p. 1-11.

Langlois, A., Bergeron, J., Brown, R., Royer, A., Harvey, R., Roy, A., Wang, L. and Thériault, N. (2014) Evaluation of CLASS 2.7 and 3.5 Simulations of Snow Properties from the Canadian Regional Climate Model (CRCM4) over Québec, Canada*. Journal of Hydrometeorology, vol. 15, n°4, p. 1325-1343.

Larue, F., Royer, A., De Sève, D., Langlois, A., Roy, A. and Brucker, L. (2017) Validation of GlobSnow-2 snow water equivalent over Eastern Canada. Remote Sensing of Environment, vol. 194, p. 264-277.

Lespinas, F., Fortin, V., Roy, G., Rasmussen, P. and Stadnyk, T. (2015) Performance Evaluation of the Canadian Precipitation Analysis (CaPA). Journal of Hydrometeorology, vol. 16, n°5, p. 2045-2064.

Li, B., Rodell, M., Kumar, S., Beaudoing, H. K., Getirana, A., Zaitchik, B. F., de Goncalves, L. G., Cossetin, C., Bhanja, S., Mukherjee, A., Tian, S., Tangdamrongsub, N., Long, D., Nanteza, J., Lee, J., Policelli, F., Goni, I. B., Daira, D., Bila, M., de Lannoy, G., Mocko, D., Steele-Dunne, S. C., Save, H. and Bettadpur, S. (2019) Global GRACE Data Assimilation for Groundwater and Drought Monitoring: Advances and Challenges. Water Resources Research, vol. 55, n°9, p. 7564-7586.

Li, B., Rodell, M., Zaitchik, B. F., Reichle, R. H., Koster, R. D. and van Dam, T. M. (2012) Assimilation of GRACE terrestrial water storage into a land surface model: Evaluation and potential value for drought monitoring in western and central Europe. Journal of Hydrology, vol. 446-447, p. 103-115.

Llovel, W., Willis, J. K., Landerer, F. W. and Fukumori, I. (2014) Deep-ocean contribution to sea level and energy budget not detectable over the past decade. Nature Climate Change, vol. 4, n°11, p. 1031-1035.

Lo, M. H., Famiglietti, J. S., Yeh, P. J. F. and Syed, T. H. (2010) Improving parameter estimation and water table depth simulation in a land surface model using GRACE water storage and estimated base flow data. Water Resources Research, vol. 46, n°5.

Luo, Y., Arnold, J., Allen, P. and Chen, X. (2012) Baseflow simulation using SWAT model in an inland river basin in Tianshan Mountains, Northwest China. Hydrology and Earth System Sciences, vol. 16, n°4, p. 1259-1267.

MacDonald, M. K., Pomeroy, J. W. and Pietroniro, A. (2009) Parameterizing redistribution and sublimation of blowing snow for hydrological models: Tests in a mountainous subarctic catchment. Hydrological Processes, vol. 23, n°18, p. 2570-2583. Wiley-Blackwell.

Mahfouf, J.-F., Brasnett, B. and Gagnon, S. (2007) A Canadian Precipitation Analysis (CaPA) Project: Description and Preliminary Results. Atmosphere-Ocean, vol. 45, n°1, p. 1-17.

Margulis, S. A. (2014) Introduction to Hydrology (First Edition).

McCreight, J. L., Small, E. E. and Larson, K. M. (2014) Snow depth, density, and SWE estimates derived from GPS reflection data: Validation in the western U. S. Water Resources Research, vol. 50, p. 6892-6909.

McTaggart-Cowan, R., Vaillancourt, P. A., Zadra, A., Separovic, L., Corvec, S. and Kirshbaum, D. (2019b) A Lagrangian Perspective on Parameterizing Deep Convection. Monthly Weather Review.

McTaggart-Cowan, R., Vaillancourt, P. A., Zadra, A., Chamberland, S., Charron, M., Corvec, S., Milbrandt, J. A., Paquin-Ricard, D., Patoine, A., Roch, M., Separovic, L. and Yang, J. (2019a) Modernization of Atmospheric Physics Parameterization in Canadian NWP. Journal of Advances in Modeling Earth Systems.

Mekonnen, M. A., Wheater, H. S., Ireson, A. M., Spence, C., Davison, B. and Pietroniro, A. (2014) Towards an improved land surface scheme for prairie landscapes. Journal of Hydrology, vol. 511, p. 105-116.

Milbrandt, J. A., Bélair, S., Faucher, M., Vallée, M., Carrera, M. L. and Glazer, A. (2016) The pan-canadian high resolution (2.5 km) deterministic prediction system. Weather and Forecasting, vol. 31, n°6, p. 1791-1816.

Moore, R. J. (2007) The PDM rainfall-runoff model. Hydrology and Earth System Sciences, vol. 11, n°1, p. 483-499.

Mudryk, L. R., Derksen, C., Kushner, P. J. and Brown, R. (2015) Characterization of Northern Hemisphere snow water equivalent datasets, 1981-2010. Journal of Climate, vol. 28, n°20, p. 8037-8051.

Müller Schmied, H., Eisner, S., Franz, D., Wattenbach, M., Portmann, F. T., Flörke, M. and Döll, P. (2014) Sensitivity of simulated global-scale freshwater fluxes and storages to input data, hydrological model structure, human water use and calibration. Hydrology and Earth System Sciences, vol. 18, n°9, p. 3511-3538.

Nash, J. E. and Sutcliffe, J. V. (1970) River flow forecasting through conceptual models part I - A discussion of principles. Journal of Hydrology, vol. 10, n°3, p. 282-290.

Niu, G.-Y., Seo, K.-W., Yang, Z.-L., Wilson, C., Su, H., Chen, J. and Rodell, M. (2007) Retrieving snow mass from GRACE terrestrial water storage change with a land surface model. Geophysical Research Letters, vol. 34, n°15, p. 1-5.

Niu, G. Y. and Yang, Z. L. (2006) Assessing a land surface model's improvements with GRACE estimates. Geophysical Research Letters, vol. 33, n°7, p. 1-4.

Pietroniro, A., Fortin, V., Kouwen, N., Neal, C., Turcotte, R., Davison, B., Verseghy, D., Soulis, E. D., Caldwell, R., Evora, N. and Pellerin, P. (2007) Development of the MESH modelling system for hydrological ensemble forecasting of the Laurentian Great Lakes at the regional scale. Hydrology and Earth System Sciences, vol. 11, n°4, p. 1279-1294.

Pietroniro, A. and Soulis, E. D. (2003) A hydrology modelling framework for the Mackenzie GEWEX programme. Hydrological Processes, vol. 17, n°3, p. 673-676.

Princz, D. (2017) Standalone MESH, Development Updates. Environment and Climate Change Canada (ECCC), Saskatoon, p. 1-19.

Pulliainen, J. (2006) Mapping of snow water equivalent and snow depth in boreal and sub-arctic zones by assimilating space-borne microwave radiometer data and ground-based observations. Remote Sensing of Environment, vol. 101, n°2, p. 257-269.

Ramillien, G., Frappart, F., Cazenave, A. and Guntner, A. (2005) Time variations of land water

storage from an inversion of 2 years of GRACE geoids. Earth and Planetary Science Letters, vol. 235, n°1-2, p. 283-301.

Ramillien, G., Frappart, F., Güntner, A., Ngo-Duc, T., Cazenave, A. and Laval, K. (2006) Time variations of the regional evapotranspiration rate from Gravity Recovery and Climate Experiment (GRACE) satellite gravimetry. Water Resources Research, vol. 42, n°10.

Rangelova, E., van der Wal, W., Braun, A., Sideris, M. G. and Wu, P. (2007) Analysis of Gravity Recovery and Climate Experiment time-variable mass redistribution signals over North America by means of principal component analysis. Journal of Geophysical Research, vol. 112, n°F3, p. 1-12.

Reager, J. (2012) Terrestrial water storage across scales : Applications of the GRACE satellite mission for global hydrology. PhD dissertation, University of California Irvine, Irvine, United States, p. 1-111.

Reager, J. T. and Famiglietti, J. S. (2009) Global terrestrial water storage capacity and flood potential using GRACE. Geophysical Research Letters, vol. 36, n°23, p. 1-6.

Reager, J. T., Thomas, B. F. and Famiglietti, J. S. (2014) River basin flood potential inferred using GRACE gravity observations at several months lead time. Nature Geoscience, vol. 7, n°8, p. 588-592.

Reager, J. T., Thomas, A. C., Sproles, E. A., Rodell, M., Beaudoing, H. K., Li, B. and Famiglietti, J. S. (2015) Assimilation of GRACE terrestrial water storage observations into a land surface model for the assessment of regional flood potential. Remote Sensing, vol. 7, n°11, p. 14663-14679.

Refsgaard, J. C. (1997) Parameterisation, calibration and validation of distributed hydrological models. Journal of Hydrology, vol. 198, n°1-4, p. 69-97.

Reichle, R. H., Bosilovich, M. G., Crow, W. T., Koster, R. D., Kumar, S. V., Mahanama, S. P. P. and Zaitchik, B. F. (2009) Recent Advances in Land Data Assimilation at the NASA Global Modeling and Assimilation Office. *In* S. K. Park and L. Xu (dir.), Data Assimilation for Atmospheric, Oceanic and Hydrologic Applications. Springer Berlin Heidelberg, p. 407-428

Reichle, R. and Koster, R. (2003) Assessing the impact of horizontal error correlations in background fields on soil moisture estimation. Journal of Hydrometeorology, vol. 4, n°6, p.

1229-1243.

Reichle, R. H., Koster, R. D., Liu, P., Mahanama, S. P. P., Njoku, E. G. and Owe, M. (2007) Comparison and assimilation of global soil moisture retrievals from the Advanced Microwave Scanning Radiometer for the Earth Observing System (AMSR-E) and the Scanning Multichannel Microwave Radiometer (SMMR). Journal of Geophysical Research, vol. 112, n°D9, p. 1-14.

Richey, A. S., Thomas, B. F., Lo, M. H., Famiglietti, J. S., Swenson, S. and Rodell, M. (2015) Uncertainty in global groundwater storage estimates in a Total Groundwater Stress framework. Water Resources Research, vol. 51, n°7, p. 5198-5216.

Rignot, E., Velicogna, I., Van Den Broeke, M. R., Monaghan, A. and Lenaerts, J. (2011) Acceleration of the contribution of the Greenland and Antarctic ice sheets to sea level rise. Geophysical Research Letters, vol. 38, n°5.

Robinson, D. A., Dewey, K. F. and Heim, R. R. (1993) Global snow cover monitoring: an update. Bulletin - American Meteorological Society, vol. 74, n°9, p. 1689-1696.

Rodell, M., Chen, J., Kato, H., Famiglietti, J. S., Nigro, J. and Wilson, C. R. (2007) Estimating groundwater storage changes in the Mississippi River basin (USA) using GRACE. Hydrogeology Journal, vol. 15, n°1, p. 159-166.

Rodell, M., Famiglietti, J. S., Wiese, D. N., Reager, J. T., Beaudoing, H. K., Landerer, F. W. and Lo, M. H. (2018) Emerging trends in global freshwater availability. Nature, vol. 557, n°7707, p. 651-659.

Rodell, M., Houser, P. R., Jambor, U., Gottschalck, J., Mitchell, K., Meng, C.-J., Arsenault, K., Cosgrove, B., Radakovich, J., Bosilovich, M., Entin*, J. K., Walker, J. P., Lohmann, D. and Toll, D. (2004) The Global Land Data Assimilation System. Bulletin of the American Meteorological Society, vol. 85, n°3, p. 381-394.

Rodell, M., Mcwilliams, E. B., Famiglietti, J. S., Beaudoing, H. K. and Nigro, J. (2011) Estimating evapotranspiration using an observation based terrestrial water budget. Hydrological Processes, vol. 25, n°26, p. 4082-4092.

Rodell, M., Velicogna, I. and Famiglietti, J. S. (2009) Satellite-based estimates of groundwater depletion in India. Nature, vol. 460, n°7258, p. 999-1002.

Rott, H., Yueh, S. H., Cline, D. W., Duguay, C., Essery, R., Haas, C., Hélière, F., Kern, M., Macelloni, G., Malnes, E., Nagler, T., Pulliainen, J., Rebhan, H. and Thompson, A. (2010) Cold Regions Hydrology High-Resolution Observatory for Snow and Cold Land Processes. Proceedings of the IEEE, vol. 98, n°5, p. 752-765.

Roy, A. (2014) Modélisation de l'émission micro-onde hivernale en forêt boréale canadienne. PhD dissertation, Université de Sherbrooke, Sherbrooke, Canada, p. 1-242.

Roy, A., Royer, A. et Turcotte, R. (2010) Improvement of springtime streamflow simulations in a boreal environment by incorporating snow-covered area derived from remote sensing data. Journal of Hydrology, vol. 390, n°1-2, p. 35-44.

Roy, A., Royer, A., Wigneron, J. P., Langlois, A., Bergeron, J. et Cliche, P. (2012) A simple parameterization for a boreal forest radiative transfer model at microwave frequencies. Remote Sensing of Environment, vol. 124, p. 371-383.

Rutter, N., Essery, R., Pomeroy, J., Altimir, N., Andreadis, K., Baker, I., Barr, A., Bartlett, P., Boone, A., Deng, H., Douville, H., Dutra, E., Elder, K., Ellis, C., Feng, X., Gelfan, A., Goodbody, A., Gusev, Y., Gustafsson, D., Hellström, R., Hirabayashi, Y., Hirota, T., Jonas, T., Koren, V., Kuragina, A., Lettenmaier, D., Li, W. P., Luce, C., Martin, E., Nasonova, O., Pumpanen, J., Pyles, R. D., Samuelsson, P., Sandells, M., Schädler, G., Shmakin, A., Smirnova, T. G., Stähli, M., Stöckli, R., Strasser, U., Su, H., Suzuki, K., Takata, K., Tanaka, K., Thompson, E., Vesala, T., Viterbo, P., Wiltshire, A., Xia, K., Xue, Y. and Yamazaki, T. (2009) Evaluation of forest snow processes models (SnowMIP2). Journal of Geophysical Research Atmospheres, vol. 114, n°6, p. 1-18.

Saberi, N., Kelly, R., Flemming, M. et Li, Q. (2020) Review of snow water equivalent retrieval methods using spaceborne passive microwave radiometry. International Journal of Remote Sensing. Taylor and Francis Ltd.

Sakumura, C., Bettadpur, S. and Bruinsma, S. (2014) Ensemble prediction and intercomparison analysis of GRACE time-variable gravity field models. Geophysical Research Letters, vol. 41, n°5, p. 1389-1397.

Sapriza-Azuri, G., Gamazo, P., Razavi, S. and Wheater, H. S. (2018) On the appropriate definition of soil profile configuration and initial conditions for land surface-hydrology

models in cold regions. Hydrology and Earth System Sciences, vol. 22, n°6, p. 3295-3309.

Sasgen, I., Konrad, H., Ivins, E. R., Van Den Broeke, M. R., Bamber, J. L., Martinec, Z. and Klemann, V. (2013) Antarctic ice-mass balance 2003 to 2012: Regional reanalysis of GRACE satellite gravimetry measurements with improved estimate of glacial-isostatic adjustment based on GPS uplift rates. Cryosphere, vol. 7, n°5, p. 1499-1512.

Sasgen, I., van den Broeke, M., Bamber, J. L., Rignot, E., Sørensen, L. S., Wouters, B., Martinec, Z., Velicogna, I. and Simonsen, S. B. (2012) Timing and origin of recent regional ice-mass loss in Greenland. Earth and Planetary Science Letters, vol. 333-334, p. 293-303.

Scanlon, B. R., Zhang, Z., Rateb, A., Sun, A., Wiese, D., Save, H., Beaudoing, H., Lo, M. H., Müller-Schmied, H., Döll, P., Beek, R., Swenson, S., Lawrence, D., Croteau, M. and Reedy, R. C. (2019) Tracking seasonal fluctuations in land water storage using global models and GRACE satellites. Geophysical Research Letters, vol. 46, n°10, p. 5254-5264.

Scanlon, B. R., Zhang, Z., Save, H., Sun, A. Y., Müller Schmied, H., van Beek, L. P. H., Wiese, D. N., Wada, Y., Long, D., Reedy, R. C., Longuevergne, L., Döll, P. and Bierkens, M. F. P. (2018) Global models underestimate large decadal declining and rising water storage trends relative to GRACE satellite data. Proceedings of the National Academy of Sciences, vol. 115, n°6, p. 1080-1089.

Schumacher, M. (2012) Assimilation of GRACE data into a global hydrological model using an ensemble Kalman filter. Master thesis, University of Bonn, Bonn, Germany, p. 1-81.

Schumacher, M. (2016) Methods for assimilating remotely-sensed water storage changes into hydrological models. PhD dissertation, University of Bonn, Bonn, Germany, p. 1-195.

Schumacher, M., Forootan, E., van Dijk, A. I. J. M., Müller Schmied, H., Crosbie, R. S., Kusche, J. and Döll, P. (2018) Improving drought simulations within the Murray-Darling Basin by combined calibration/assimilation of GRACE data into the WaterGAP Global Hydrology Model. Remote Sensing of Environment, vol. 204, p. 212-228.

Schumacher, M., Kusche, J. and Döll, P. (2016) A systematic impact assessment of GRACE error correlation on data assimilation in hydrological models. Journal of Geodesy, vol. 90, n°6, p. 537-559.

Seo, K. W., Ryu, D., Kim, B. M., Waliser, D. E., Tian, B. and Eom, J. (2010) GRACE and

AMSR-E-based estimates of winter season solid precipitation accumulation in the Arctic drainage region. Journal of Geophysical Research Atmospheres, vol. 115, n°20, p. 1-18.

Sheard, B. S., Heinzel, G., Danzmann, K., Shaddock, D. A., Klipstein, W. M. and Folkner, W. M. (2012) Intersatellite laser ranging instrument for the GRACE follow-on mission. Journal of Geodesy, vol. 86, n°12, p. 1083-1095.

Shepherd, A., Ivins, E., Rignot, E., Smith, B., Van Den Broeke, M., Velicogna, I., Whitehouse, P., Briggs, K., Joughin, I., Krinner, G., Nowicki, S., Payne, T., Scambos, T., Schlegel, N., Geruo, A., Agosta, C., Ahlstrøm, A., Babonis, G., Barletta, V., Blazquez, A., Bonin, J., Csatho, B., Cullather, R., Felikson, D., Fettweis, X., Forsberg, R., Gallee, H., Gardner, A., Gilbert, L., Groh, A., Gunter, B., Hanna, E., Harig, C., Helm, V., Horvath, A., Horwath, M., Khan, S., Kjeldsen, K. K., Konrad, H., Langen, P., Lecavalier, B., Loomis, B., Luthcke, S., McMillan, M., Melini, D., Mernild, S., Mohajerani, Y., Moore, P., Mouginot, J., Moyano, G., Muir, A., Nagler, T., Nield, G., Nilsson, J., Noel, B., Otosaka, I., Pattle, M. E., Peltier, W. R., Pie, N., Rietbroek, R., Rott, H., Sandberg-Sørensen, L., Sasgen, I., Save, H., Scheuchl, B., Schrama, E., Schröder, L., Seo, K. W., Simonsen, S., Slater, T., Spada, G., Sutterley, T., Talpe, M., Tarasov, L., Van De Berg, W. J., Van Der Wal, W., Van Wessem, M., Vishwakarma, B. D., Wiese, D. and Wouters, B. (2018) Mass balance of the Antarctic Ice Sheet from 1992 to 2017. Nature. Nature Publishing Group.

Soil Landscapes of Canada (2010) Agriculture and Agri-Food Canada.

Sood, A. and Smakhtin, V. (2015) Global hydrological models: a review. Hydrological Sciences Journal, vol. 60, n°4, p. 549-565.

Soulis, E. D., Craig, J. R., Fortin, V. and Liu, G. (2011) A simple expression for the bulk field capacity of a sloping soil horizon. Hydrological Processes, vol. 25, n°1, p. 112-116.

Soulis, E. D., Kouwen, N., Pietroniro, A., Seglenieks, F. R., Snelgrove, K. R., Pellerin, P., Shaw, D. W. and Martz, L. W. (2005) A framework for hydrological modelling in MAGS. *In* J. W. P. and A. P. C.Spence (dir.), Prediction in Ungauged Basins: Approaches for Canada's Cold Regions. Canadian Water Resources Association, p. 119-138.

Soulis, E. D. and Seglenieks, F. R. (2008) The MAGS integrated modeling system. Cold Region Atmospheric and Hydrologic Studies. The Mackenzie GEWEX Experience, Berlin,

Heidelberg : Springer Berlin Heidelberg, vol. 2, p. 445-473.

Soulis, E. D., Snelgrove, K. R., Kouwen, N., Seglenieks, F. and Verseghy, D. L. (2000) Towards closing the vertical water balance in Canadian atmospheric models: Coupling of the land surface scheme class with the distributed hydrological model watflood. Atmosphere - Ocean, vol. 38, n°1, p. 251-269.

Stieglitz, M., Ducharne, A., Koster, R. and Suarez, M. (2001) The Impact of Detailed Snow Physics on the Simulation of Snow Cover and Subsurface Thermodynamics at Continental Scales. Journal of Hydrometeorology, vol. 2, n°3, p. 228-242.

Sturm, M., Holmgren, J. and Liston, G. E. (1995) A seasonal snow cover classification system for local to global applications. Journal of Climate, vol. 8, n°5, p. 1261-1283.

Sturm, M., Taras, B., Liston, G. E., Derksen, C., Jonas, T. and Lea, J. (2010) Estimating Snow Water Equivalent Using Snow Depth Data and Climate Classes. Journal of Hydrometeorology, vol. 11, p. 1380-1394.

Su, H., Yang, Z. L., Dickinson, R. E., Wilson, C. R. and Niu, G. Y. (2010) Multisensor snow data assimilation at the continental scale: The value of Gravity Recovery and Climate Experiment terrestrial water storage information. Journal of Geophysical Research Atmospheres, vol. 115, n°10, p. 1-14.

Sun, A. Y., Green, R., Swenson, S. and Rodell, M. (2012) Toward calibration of regional groundwater models using GRACE data. Journal of Hydrology, vol. 422-423, p. 1-9.

Swenson, S. (2010) Assessing High-Latitude Winter Precipitation from Global Precipitation Analyses Using GRACE. Journal of Hydrometeorology, vol. 11, n°2, p. 405-420.

Swenson, S. C. (2012) GRACE monthly land water mass grids NETCDF RELEASE 5.0. Ver. 5.0. Physical Oceanography Distributed Active Archive Center.

Swenson, S. C. and Lawrence, D. M. (2014) Assessing a dry surface layer-based soil resistance parameterization for the Community Land Model using GRACE and FLUXNET-MTE data. Journal of Geophysical Research: Atmospheres, vol. 119, n°17, p. 10,299-10,312.

Swenson, S. C. and Lawrence, D. M. (2015) A GRACE-based assessment of interannual groundwater dynamics in the Community Land Model. Water Resources Research, p. 8817-

8833.

Swenson, S. and Wahr, J. (2006) Post-processing removal of correlated errors in GRACE data. Geophysical Research Letters, vol. 33, n°8, p. 1-4.

Syed, T. H., Famiglietti, J. S., Chen, J., Rodell, M., Seneviratne, S. I., Viterbo, P. and Wilson, C. R. (2005) Total basin discharge for the Amazon and Mississippi River basins from GRACE and a land-atmosphere water balance. Geophysical Research Letters, vol. 32, n°24, p. 1-5.

Syed, T. H., Famiglietti, J. S., Rodell, M., Chen, J. and Wilson, C. R. (2008) Analysis of terrestrial water storage changes from GRACE and GLDAS. Water Resources Research, vol. 44, n°2, p. 1-15.

Takala, M., Luojus, K., Pulliainen, J., Derksen, C., Lemmetyinen, J., Kärnä, J.-P., Koskinen, J. and Bojkov, B. (2011) Estimating northern hemisphere snow water equivalent for climate research through assimilation of space-borne radiometer data and ground-based measurements. Remote Sensing of Environment, vol. 115, n°12, p. 3517-3529.

Tangdamrongsub, N., Han, S. C., Tian, S., Schmied, H. M., Sutanudjaja, E. H., Ran, J. and Feng, W. (2018) Evaluation of groundwater storage variations estimated from GRACE data assimilation and state-of-the-art land surface models in Australia and the North China Plain. Remote Sensing, vol. 10, n°3, p. 483.

Tangdamrongsub, N., Steele-Dunne, S. C., Gunter, B. C., Ditmar, P. G., Sutanudjaja, E. H., Sun, Y., Xia, T. and Wang, Z. (2017) Improving estimates of water resources in a semi-arid region by assimilating GRACE data into the PCR-GLOBWB hydrological model. Hydrology and Earth System Sciences, vol. 21, n°4, p. 2053-2074.

Tangdamrongsub, N., Steele-Dunne, S. C., Gunter, B. C., Ditmar, P. G. and Weerts, A. H. (2015) Data assimilation of GRACE terrestrial water storage estimates into a regional hydrological model of the Rhine River basin. Hydrology and Earth System Sciences, vol. 19, n°4, p. 2079-2100.

Tapley, Byron D., Bettadpur, S., Ries, J. C., Thompson, P. F. and Watkins, M. M. (2004b) GRACE measurements of mass variability in the Earth system. Science, vol. 305, n°5683, p. 503-505.

Tapley, B. D., Bettadpur, S., Watkins, M. and Reigber, C. (2004a) The gravity recovery and

climate experiment: Mission overview and early results. Geophysical Research Letters, vol. 31, n°9, p. 1-4.

Tapley, B. D., Watkins, M. M., Flechtner, F., Reigber, C., Bettadpur, S., Rodell, M., Sasgen, I., Famiglietti, J. S., Landerer, F. W., Chambers, D. P., Reager, J. T., Gardner, A. S., Save, H., Ivins, E. R., Swenson, S. C., Boening, C., Dahle, C., Wiese, D. N., Dobslaw, H., Tamisiea, M. E. and Velicogna, I. (2019) Contributions of GRACE to understanding climate change. Nature Climate Change, vol. 9, n°5, p. 358-369.

Tedesco, M., Derksen, C., Deems, J. S. et Foster, J. L. (2014) Remote sensing of snow depth and snow water equivalent. Remote Sensing of the Cryosphere (p. 73-98). Chichester, UK : John Wiley & Sons, Ltd.

Tedesco, M., Kelly, R., Foster, J. L. and Chang, A. T. C. AMSR-E/Aqua Daily L3 Global Snow Water Equivalent EASE-Grids Version 2. NASA National Snow and Ice Data Center Distributed Active Archive Center, Boulder, Colorado, USA (2004). NASA DAAC at the National Snow and Ice Data Center.

Tian, S., Tregoning, P., Renzullo, L. J., van Dijk, A. I. J. M., Walker, J. P., Pauwels, V. R. N. and Allgeyer, S. (2017) Improved water balance component estimates through joint assimilation of GRACE water storage and SMOS soil moisture retrievals. Water Resources Research, vol. 53, n°3, p. 1820-1840.

Trautmann, T., Koirala, S., Carvalhais, N., Eicker, A., Fink, M., Niemann, C. and Jung, M. (2018) Understanding terrestrial water storage variations in northern latitudes across scales. Hydrology and Earth System Sciences, vol. 22, n°7, p. 4061-4082.

Vachon, F., Goïta, K., De Sève, D. et Royer, A. (2010) Inversion of a snow emission model calibrated with in situ data for snow water equivalent monitoring. IEEE Transactions on Geoscience and Remote Sensing, vol. 48, n°1, p. 59-71.

Van Dijk, A. I. J. M., Renzullo, L. J., Wada, Y. and Tregoning, P. (2014) A global water cycle reanalysis (2003-2012) merging satellite gravimetry and altimetry observations with a hydrological multi-model ensemble. Hydrology and Earth System Sciences, vol. 18, n°8, p. 2955-2973.

Veldkamp, T. I. E., Zhao, F., Ward, P. J., De Moel, H., Aerts, J. C. J. H., Schmied, H. M.,

Portmann, F. T., Masaki, Y., Pokhrel, Y., Liu, X., Satoh, Y., Gerten, D., Gosling, S. N., Zaherpour, J. and Wada, Y. (2018) Human impact parameterizations in global hydrological models improve estimates of monthly discharges and hydrological extremes: A multi-model validation study. Environmental Research Letters, vol. 13, n°5, p. 1-16.

Velicogna, I., Sutterley, T. C. and Van Den Broeke, M. R. (2014) Regional acceleration in ice mass loss from Greenland and Antarctica using GRACE time-variable gravity data. Geophysical Research Letters, vol. 41, n°22, p. 8130-8137.

Velicogna, I. and Wahr, J. (2005) Greenland mass balance from GRACE. Geophysical Research Letters, vol. 32, n°18, p. 1-4.

Verseghy, D. L. (1991) Class-A Canadian land surface scheme for GCMS. I. Soil model. International Journal of Climatology, vol. 11, n°2, p. 111-133.

Verseghy, D. L. (2012) The Canadian land surface scheme (version 3.6)-technical documentation. Environment Canada.

Verseghy, D., Brown, R. and Wang, L. (2017) Evaluation of CLASS snow simulation over Eastern Canada. Journal of Hydrometeorology, vol. 18, n°5, p. 1205-1225.

Verseghy, D. L. and MacKay, M. D. (2017) Offline Implementation and Evaluation of the Canadian Small Lake Model with the Canadian Land Surface Scheme over Western Canada. Journal of Hydrometeorology, vol. 18, n°6, p. 1563-1582.

Verseghy, D. L., McFarlane, N. A. and Lazare, M. (1993) CLASS - a Canadian land surface scheme for GCMs, II. Vegetation model and coupled runs. International Journal of Climatology, vol. 13, n°4, p. 347-370.

Vishwakarma, B. D., Devaraju, B. and Sneeuw, N. (2018) What is the spatial resolution of GRACE satellite products for hydrology? Remote Sensing, vol. 10, n°6.

Voss, K. A., Famiglietti, J. S., Lo, M., De Linage, C., Rodell, M. and Swenson, S. C. (2013) Groundwater depletion in the Middle East from GRACE with implications for transboundary water management in the Tigris-Euphrates-Western Iran region. Water Resources Research, vol. 49, n°2, p. 904-914.

Wahr, J., Molenaar, M. and Bryan, F. (1998) Time variability of the Earth's gravity field:

Hydrological and oceanic effects and their possible detection using GRACE. Journal of Geophysical Research B: Solid Earth, vol. 103, n°B12, p. 30205-30229.

Walsh, J. E. (1984) Snow Cover and Atmospheric Variability: Changes in the snow covering the earth's surface affect both daily weather and long-term climate. American Scientist, vol. 72, n°1, p. 50-57.

Wang, H., Jia, L., Steffen, H., Wu, P., Jiang, L., Hsu, H., Xiang, L., Wang, Z. and Hu, B. (2013) Increased water storage in North America and Scandinavia from GRACE gravity data. Nature Geoscience, vol. 6, n°1, p. 38-42.

Wang, W., Cui, W., Wang, X. and Chen, X. (2016) Evaluation of GLDAS-1 and GLDAS-2 Forcing Data and Noah Model Simulations over China at the Monthly Scale. Journal of Hydrometeorology, vol. 17, n°11, p. 2815-2833.

Wartenburger, R., Seneviratne, S. I., Hirschi, M., Chang, J., Ciais, P., Deryng, D., Elliott, J., Folberth, C., Gosling, S. N., Gudmundsson, L., Henrot, A. J., Hickler, T., Ito, A., Khabarov, N., Kim, H., Leng, G., Liu, J., Liu, X., Masaki, Y., Morfopoulos, C., Müller, C., Schmied, H. M., Nishina, K., Orth, R., Pokhrel, Y., Pugh, T. A. M., Satoh, Y., Schaphoff, S., Schmid, E., Sheffield, J., Stacke, T., Steinkamp, J., Tang, Q., Thiery, W., Wada, Y., Wang, X., Weedon, G. P., Yang, H. and Zhou, T. (2018) Evapotranspiration simulations in ISIMIP2a-Evaluation of spatio-temporal characteristics with a comprehensive ensemble of independent datasets. Environmental Research Letters, vol. 13, n°7.

Watkins, M. M., Wiese, D. N., Yuan, D.-N., Boening, C. et Landerer, F. W. (2015) Improved methods for observing Earth's time variable mass distribution with GRACE using spherical cap mascons. Journal of Geophysical Research: Solid Earth, vol. 120, n°4, p. 2648-2671.

Wolff, M. (1969) Direct measurements of the Earth's gravitational potential using a satellite pair. Journal of Geophysical Research, vol. 74, n°22, p. 5295-5300.

Wouters, B., Bamber, J. L., Van Den Broeke, M. R., Lenaerts, J. T. M. and Sasgen, I. (2013) Limits in detecting acceleration of ice sheet mass loss due to climate variability. Nature Geoscience, vol. 6, n°8, p. 613-616.

Wouters, B., Chambers, D. and Schrama, E. J. O. (2008) GRACE observes small-scale mass loss in Greenland. Geophysical Research Letters, vol. 35, n°20.

Xu, X., Tolson, B. A., Li, J., Staebler, R. M., Seglenieks, F., Haghnegahdar, A. and Davison, B. (2015) Assimilation of SMOS soil moisture over the Great Lakes basin. Remote Sensing of Environment, vol. 169, p. 163-175.

Yang, F., Kumar, A., Wang, W., Juang, H.-M. M. H. and Kanamitsu, M. (2001) Snow-Albedo feedback and seasonal climate variability over North America. Journal of Climate, vol. 14, n°22, p. 4245-4248.

Yassin, F., Razavi, S., Elshamy, M., Davison, B., Sapriza-Azuri, G. and Wheater, H. (2019) Representation and improved parameterization of reservoir operation in hydrological and land-surface models. Hydrology and Earth System Sciences, vol. 23, n°9, p. 3735-3764.

Yassin, F., Razavi, S., Wheater, H., Sapriza-Azuri, G., Davison, B. and Pietroniro, A. (2017) Enhanced identification of a hydrologic model using streamflow and satellite water storage data: A multicriteria sensitivity analysis and optimization approach. Hydrological Processes, vol. 31, n°19, p. 3320-3333.

Yeh, P. J.-F., Swenson, S. C., Famiglietti, J. S. and Rodell, M. (2006) Remote sensing of groundwater storage changes in Illinois using the Gravity Recovery and Climate Experiment (GRACE). Water Resources Research, vol. 42, n°12, p. n/a-n/a.

Yirdaw, S. Z., Snelgrove, K. R., Seglenieks, F. R., Agboma, C. O. and Soulis, E. D. (2009) Assessment of the WATCLASS hydrological model result of the Mackenzie River basin using the GRACE satellite total water storage measurement. Hydrological Processes, vol. 23, n°23, p. 3391-3400.

Zaherpour, J., Gosling, S. N., Mount, N., Schmied, H. M., Veldkamp, T. I. E., Dankers, R., Eisner, S., Gerten, D., Gudmundsson, L., Haddeland, I., Hanasaki, N., Kim, H., Leng, G., Liu, J., Masaki, Y., Oki, T., Pokhrel, Y., Satoh, Y., Schewe, J. and Wada, Y. (2018) Worldwide evaluation of mean and extreme runoff from six global-scale hydrological models that account for human impacts. Environmental Research Letters, vol. 13, n°6, p. 065015.

Zaitchik, B. F., Rodell, M. and Reichle, R. H. (2008) Assimilation of GRACE terrestrial water storage data into a land surface model: Results for the Mississippi River basin. Journal of Hydrometeorology, vol. 9, n°3, p. 535-548.

Zhang, Y. F., Hoar, T. J., Yang, Z. L., Anderson, J. L., Toure, A. M. and Rodell, M. (2014)

Assimilation of MODIS snow cover through the data assimilation research testbed and the community Land Model version 4. Journal of Geophysical Research, vol. 119, n°12, p. 7091-7103.

Zhao, L. and Yang, Z. L. (2018) Multi-sensor land data assimilation: Toward a robust global soil moisture and snow estimation. Remote Sensing of Environment, vol. 216, p. 13-27.

Appendix 1. MESH input files

MESH_parameters_CLASS.ini

MESH_parameters_CLASS.ini

```
Liard@Mouth 10ED002                                                                                 01 TITLE
G.Saprisa code - M.Elshamy                                                                          02 NAME
GIWS                                                                                                03 PLACE
   61.55   -121.40     40.00     40.00     50.00   -1.0    1 2881   7                              04 DEGLAT/DEGLON/ZRFM/ZRFH/ZBLD/GC/ILW/NL/NM
  0.990   0.010   0.000   0.000   0.000   2.000   8.532   0.000   0.000                             05 5xFCAN/4xLAMX
  0.582   1.216   0.000   0.000   0.000   1.983   2.080   0.000   0.000                             06 5xLNZ0/4xLAMN
  0.062   0.036   0.000   0.000   0.000  11.966  13.669   0.000   0.000                             07 5xALVC/4xCMAS
  0.477   0.478   0.000   0.000   0.000   1.302   1.302   0.000   0.000                             08 5xALIC/4xROOT
223.361 125.000   0.000   0.000          49.482  47.087   0.000   0.000                             09 4xRSMN/4xQA50
  0.229   0.875   0.000   0.000           0.763   0.732   0.000   0.000                             10 4xVPDA/4xVPDB
100.000 100.000   0.000   0.000           5.000   5.000   0.000   0.000                             11 4xPSGA/4xPSGB
  0.031   0.414   1.000  50.000                                                                      12 DRN/SDEP/FARE/DD
  0.04    0.1     0.242   0.001  1  Forest                                                          13 XSLP/XDRAINH/MANN/KSAT/MID
    73.2      43.3      65.987                                                                      14 3xSAND
     5.2      29.1      17.486                                                                      15 3xCLAY
     5.2      0.00      0.00                                                                        16 3xORGM
   5.000     7.000     8.000     15.00     0.000     0.000                                          17 3xTBAR/TCAN/TSNO/TPND
   0.300     0.300     0.300     0.000     0.000     0.000     0.000                                18 3xTHLQ/3xTHIC/ZPND
  0.0000    0.0000     0.00      0.000     0.000     1.000                                          19 RCAN/SCAN/SNO/ALBS/RHOS/GRO

  0.000   0.000   0.000   1.000   0.000   0.000   0.000   0.000   4.925                             05 5xFCAN/4xLAMX
  0.000   0.000   0.000   0.022   0.000   0.000   0.000   0.000   1.023                             06 5xLNZ0/4xLAMN
  0.000   0.000   0.000   0.051   0.000   0.000   0.000   0.000   5.223                             07 5xALVC/4xCMAS
  0.000   0.000   0.000   0.488   0.000   0.000   0.000   0.000   1.000                             08 5xALIC/4xROOT
  0.000   0.000   0.000  77.665           0.000   0.000   0.000  46.036                             09 4xRSMN/4xQA50
  0.000   0.000   0.000   0.630           0.000   0.000   0.000   0.638                             10 4xVPDA/4xVPDB
  0.000   0.000   0.000 100.000           0.000   0.000   0.000   5.000                             11 4xPSGA/4xPSGB
  0.378   1.134   1.000  50.000                                                                      12 DRN/SDEP/FARE/DD
  0.03    0.1     0.131   0.001  2  Grass                                                           13 XSLP/XDRAINH/MANN/KSAT/MID
    72.1      49.7      70.020                                                                      14 3xSAND
     5.0      21.4      23.682                                                                      15 3xCLAY
     7.8      0.00      0.00                                                                        16 3xORGM
   5.000     7.000     8.000     15.00     0.000     0.000                                          17 3xTBAR/TCAN/TSNO/TPND
   0.300     0.300     0.300     0.000     0.000     0.000     0.000                                18 3xTHLQ/3xTHIC/ZPND
  0.0000    0.0000     0.00      0.000     0.000     1.000                                          19 RCAN/SCAN/SNO/ALBS/RHOS/GRO

  0.000   0.000   0.000   1.000   0.000   0.000   0.000   0.000   2.795                             05 5xFCAN/4xLAMX20 (not used, but 4x integer values are required)
  0.000   0.000   0.000   0.028   0.000   0.000   0.000   0.000   0.683                             06 5xLNZ0/4xLAMN21 (not used, but 4x integer values are required)
  0.000   0.000   0.000   0.085   0.000   0.000   0.000   0.000   2.823                             07 5xALVC/4xCMAS22 IHOUR/IMINS/IJDAY/IYEAR
  0.000   0.000   0.000   0.251   0.000   0.000   0.000   0.000   1.000                             08 5xALIC/4xROOT
  0.000   0.000   0.000  86.272           0.000   0.000   0.000  33.272                             09 4xRSMN/4xQA50
  0.000   0.000   0.000   0.828           0.000   0.000   0.000   1.256                             10 4xVPDA/4xVPDB
  0.000   0.000   0.000 100.000           0.000   0.000   0.000   5.000                             11 4xPSGA/4xPSGB
  0.956   1.059   1.000   5.00                                                                       12 DRN/SDEP/FARE/DD
  0.001   0.1     0.206   0.001  3  wetland                                                         13 XSLP/XDRAINH/MANN/KSAT/MID
    56.4      59.2      49.164                                                                      14 3xSAND
    16.1       6.1      12.015                                                                      15 3xCLAY
     5.4     20.00     20.00                                                                       16 3xORGM
   5.000     7.000     8.000     15.00     0.000     0.000                                          17 3xTBAR/TCAN/TSNO/TPND
   0.300     0.300     0.300     0.000     0.000     0.000     0.000                                18 3xTHLQ/3xTHIC/ZPND
  0.0000    0.0000     0.00      0.000     0.000     1.000                                          19 RCAN/SCAN/SNO/ALBS/RHOS/GRO

  0.000   0.000   0.000   0.000   1.000   0.000   0.000   0.000   0.000                             05 5xFCAN/4xLAMX
  0.000   0.000   0.000   0.000  -3.000   0.000   0.000   0.000   0.000                             06 5xLNZ0/4xLAMN
  0.000   0.000   0.000   0.000   0.071   0.000   0.000   0.000   0.000                             07 5xALVC/4xCMAS
  0.000   0.000   0.000   0.000   0.327   0.000   0.000   0.000   0.000                             08 5xALIC/4xROOT
  0.000   0.000   0.000   0.000           0.000   0.000   0.000   0.000                             09 4xRSMN/4xQA50
  0.000   0.000   0.000   0.000           0.000   0.000   0.000   0.000                             10 4xVPDA/4xVPDB
  0.000   0.000   0.000   0.000           0.000   0.000   0.000   0.000                             11 4xPSGA/4xPSGB
  0.729   1.232   1.000  50.00                                                                       12 DRN/SDEP/FARE/DD
  0.1     0.1     0.368   0.007  4 BarrenLand                                                       13 XSLP/XDRAINH/MANN/KSAT/MID
    73.0      45.1      66.165                                                                      14 3xSAND
     6.4      29.6      20.441                                                                      15 3xCLAY
     7.4      0.00      0.00                                                                        16 3xORGM
   5.000     7.000     8.000     15.00     0.000     0.000                                          17 3xTBAR/TCAN/TSNO/TPND
   0.300     0.300     0.300     0.000     0.000     0.000     0.000                                18 3xTHLQ/3xTHIC/ZPND
  0.0000    0.0000     0.00      0.000     0.000     0.000                                          19 RCAN/SCAN/SNO/ALBS/RHOS/GRO

  0.000   0.000   0.000   0.000   1.000   0.000   0.000   0.000   0.000                             05 5xFCAN/4xLAMX
  0.000   0.000   0.000   0.000   0.300   0.000   0.000   0.000   0.000                             06 5xLNZ0/4xLAMN
  0.000   0.000   0.000   0.000   0.090   0.000   0.000   0.000   0.000                             07 5xALVC/4xCMAS
  0.000   0.000   0.000   0.000   0.150   0.000   0.000   0.000   0.000                             08 5xALIC/4xROOT
  0.000   0.000   0.000   0.000           0.000   0.000   0.000   0.000                             09 4xRSMN/4xQA50
  0.000   0.000   0.000   0.000           0.000   0.000   0.000   0.000                             10 4xVPDA/4xVPDB
  0.000   0.000   0.000   0.000           0.000   0.000   0.000   0.000                             11 4xPSGA/4xPSGB
  1.000   4.100   1.000  50.00                                                                       12 DRN/SDEP/FARE/DD
  0.04    0.1     0.010   0.01   5 Urban                                                            13 XSLP/XDRAINH/MANN/KSAT/MID
   22.00     22.00     22.00                                                                       14 3xSAND
   35.00     35.00     35.00                                                                       15 3xCLAY
    5.00      0.00      0.00                                                                       16 3xORGM
   5.000     7.000     8.000     15.00     0.000     0.000                                          17 3xTBAR/TCAN/TSNO/TPND
   0.300     0.300     0.300     0.000     0.000     0.000     0.000                                18 3xTHLQ/3xTHIC/ZPND
  0.0000    0.0000     0.00      0.000     0.000     0.000                                          19 RCAN/SCAN/SNO/ALBS/RHOS/GRO

  0.000   0.000   0.000   0.000   1.000   0.000   0.000   0.000   0.000                             05 5xFCAN/4xLAMX
  0.000   0.000   0.000   0.000  -9.200   0.000   0.000   0.000   0.000                             06 5xLNZ0/4xLAMN
  0.000   0.000   0.000   0.000   0.010   0.000   0.000   0.000   0.000                             07 5xALVC/4xCMAS
  0.000   0.000   0.000   0.000   0.200   0.000   0.000   0.000   0.000                             08 5xALIC/4xROOT
  0.000   0.000   0.000   0.000           0.000   0.000   0.000   0.000                             09 4xRSMN/4xQA50
  0.000   0.000   0.000   0.000           0.000   0.000   0.000   0.000                             10 4xVPDA/4xVPDB
  0.000   0.000   0.000   0.000           0.000   0.000   0.000   0.000                             11 4xPSGA/4xPSGB
  0.000   4.100   1.000   5.00                                                                       12 DRN/SDEP/FARE/DD
  0.001   0.1     0.04    0.1    6  Water                                                           13 XSLP/XDRAINH/MANN/KSAT/MID
 100.000  100.000   100.000                                                                              14 3xSAND
   0.000     0.000     0.000                                                                             15 3xCLAY
   0.000     0.000     0.000                                                                             16 3xORGM
   5.000     7.000     8.000     15.00     0.000     0.000                                          17 3xTBAR/TCAN/TSNO/TPND
   0.300     0.300     0.300     0.000     0.000     0.000     0.000                                18 3xTHLQ/3xTHIC/ZPND
  0.0000    0.0000     0.00      0.000     0.000     0.000                                          19 RCAN/SCAN/SNO/ALBS/RHOS/GRO

  0.000   0.000   0.000   0.000   1.000   0.000   0.000   0.000   0.000                             05 5xFCAN/4xLAMX20 (not used, but 4x integer values are required)
  0.000   0.000   0.000   0.000  -6.000   0.000   0.000   0.000   0.000                             06 5xLNZ0/4xLAMN21 (not used, but 4x integer values are required)
  0.000   0.000   0.000   0.000   0.700   0.000   0.000   0.000   0.000                             07 5xALVC/4xCMAS22 IHOUR/IMINS/IJDAY/IYEAR
  0.000   0.000   0.000   0.000   0.700   0.000   0.000   0.000   0.000                             08 5xALIC/4xROOT
  0.000   0.000   0.000   0.000           0.000   0.000   0.000   0.000                             09 4xRSMN/4xQA50
  0.000   0.000   0.000   0.000           0.000   0.000   0.000   0.000                             10 4xVPDA/4xVPDB
  0.000   0.000   0.000   0.000           0.000   0.000   0.000   0.000                             11 4xPSGA/4xPSGB
  0.000   4.100   1.000   5.00                                                                       12 DRN/SDEP/FARE/DD
  0.001   0.1     0.04    0.1    7  SnowICe                                                         13 XSLP/XDRAINH/MANN/KSAT/MID
   33.34     33.34     33.34                                                                       14 3xSAND
   33.33     33.33     33.33                                                                       15 3xCLAY
   33.31     33.31     33.31                                                                       16 3xORGM
   5.000     7.000     8.000     15.00     0.000     0.000                                          17 3xTBAR/TCAN/TSNO/TPND
   0.300     0.300     0.300     0.000     0.000     0.000     0.000                                18 3xTHLQ/3xTHIC/ZPND
  0.0000    0.0000     0.00      0.000     0.000     0.000                                          19 RCAN/SCAN/SNO/ALBS/RHOS/GRO

      1       365         1       365                                                               20 (not used, but 4x integer values are required)
   2002      2003      2002      2003                                                               21 (not used, but 4x integer values are required)
     18         0       274      2008                                                               22 IHOUR/IMINS/IJDAY/IYEAR0
```

MESH_input_run_options.ini

MESH_input_run_options.ini

```
MESH input run options file                    # comment line 1                                  | *
##### Control Flags #####                      # comment line 2                                  | *
----#                                          # comment line 3                                  | *
   32                                          # Number of control flags                         | I5
HOURLYFLAG            60                       #01 hourly flag                                  | A20, I4
IDISP                  0                       #02 Vegetation Displacement Height Calculation   | A20, I4
IZREF                  1                       #03 Atmospheric Model Reference Height           | A20, I4
IPCP                   1                       #04 Rainfall-Snowfall Partition distribution     | A20, I4
ITC                    2                       #05 Canopy and Ground-Surface Temp Iter Scheme   | A20, I4
ITCG                   2                       #06 Canopy and Ground-Surface Temp Iter Scheme   | A20, I4
ITG                    2                       #07 Canopy and Ground-Surface Temp Iter Scheme   | A20, I4
IWF                    1                       #08 Water Flow control                           | A20, I4
IPAI                   0                       #09 CLASS Input Leaf-Area Index Override         | A20, I4
IHGT                   0                       #10 CLASS Input Vegetation Height Override       | A20, I4
IALC                   0                       #11 CLASS Input Canopy Albedo Override           | A20, I4
IALS                   0                       #12 CLASS Input Snow Albedo Override             | A20, I4
IALG                   0                       #13 CLASS Input Soil Albedo Override             | A20, I4
BASINRAINFLAG          3  hf=360               #14 basin rain flag                              | A20, I4
BASINLONGWAVEFLAG      3                       #15 basin longwave flag                          | A20, I4
BASINSHORTWAVEFLAG     3                       #16 basin shortwave flag                         | A20, I4
BASINTEMPERATUREFLAG   3                       #17 basin temperature flag                       | A20, I4
BASINWINDFLAG          3                       #18 basin wind flag                              | A20, I4
BASINPRESFLAG          3                       #19 basin pressure flag                          | A20, I4
BASINHUMIDITYFLAG      3                       #20 basin humidity flag                          | A20, I4
SHDFILEFLAG            1                       #21 basin shed file flag                         | A20, I4
FROZENSOILINFILFLAG    0                       #22 frozen soil infiltration flag                | A20, I4
INTERPOLATIONFLAG      0
SAVERESUMEFLAG         4                       # set it 4 in case of saving  the resume
RESUMEFLAG             4                       # set it 4 in case of reading from resume
OUTFIELDSFLAG          1
PRINTRFFR2CFILEFLAG    0
PRINTRCHR2CFILEFLAG    0
AUTOCALIBRATIONFLAG    1
METRICSSPINUP        457
BASEFLOWFLAG           1
STREAMFLOWOUTFLAG      daily
##### Output Grid selection #####             #15 comment line 15                              | *
----#                                          #16 comment line 16                              | *
    0   #Maximum 5 points                     #17 Number of output grid points                 | I5
---------#---------#---------#---------#---------#  #18 comment line 18                        | *
      1709                                     #19 Grid number                                  | 5I10
         1                                     #20 Land class                                   | 5I10
CLASSOUT                                       #21 Output directory                             | 5A10
##### Output Directory #####                  #22 comment line 22                              | *
---------#                                     #23 comment line 23                              | *
results                                        #24 Output Directory for total-basin files       | A10
##### Simulation Run Times #####              #25 comment line 25                              | *
---#---#---#---#                               #26 comment line 26                              | *
2008 275   0   0                               #27 Start year, day, hour, minute (2012 275   0   0)          | 4I4
2009 274   0   0                               #28 Stop year, day, hour, minute  (2012 306   0   0)          | 4I4
```

MESH_input_soil_levels.txt

MESH_input_soil_levels.txt

```
1    0.10    0.10
2    0.25    0.35
3    0.75    1.10
4    3.00    4.10
```

MESH_parameters_hydrology.ini

MESH_parameters_hydrology.ini

```
1.1.a04:MESH Hydrology Parameters input file                # 01version number and comment line 1                                | A8
##### Option Flags #####                                    # 02comment line 2                                                  | *
----#                                                       # 03comment line 3                                                  | *
    2                                                       # 04Number of option flags                                          | *
    0                                                       # 05[reserved]                                                      | *
    0                                                       # 06[reserved]                                                      | *
##### River roughness factor ( 1.713) (5 classes maximum)    # 07comment line 7                                                  | *
-----#-----#-----#-----#-----#                              # 08comment line 8                                                  | *
  0.210   1.713   0.206   0.498   0.410                         # 09River roughness factor                                                  | 5F6.3
##### GRU class independent hydrologic parameters #####     # 10comment line 10                                                 | *
-------#                                                    # 11comment line 11                                                 | *
       2                                                    # Number of GRU independent hydrologic parameters
       0.167                                                # WrchrgIni (BASEFLOWFLAG = 1, 2)
       0.200                                                # QbIni (BASEFLOWFLAG = 1, 2)
##### GRU class dependent hydrologic parameters #####       # 18comment line 18                                                 | *
-------#                                                    # 19comment line 19                                                 | *
       7                                                    # 20Number of GRUs (must match number in mesh_parameters_class.ini file)      | I8
       11                                                   # 21Number of GRU dependent hydrologic parameters     ??????       | I8
--Forest-W--Grass-W--Wetland--Barrenland-Urban----Water-----SnowIce------## 22comment line 22                                                  | *
   0.030     0.257     0.312     0.11      0.25      0.11      0.11       # ZSNL
   0.09      0.09      0.09      0.09      0.09      0.09      0.09       # ZPLS
   0.26      0.26      0.26      0.26      0.26      0.26      0.26       # ZPLG
   0.00      0.00      0.00      0.00      0.00      0.00      0.00       # FRZC
   2.00      2.00      2.00      2.00      2.00      2.00      2.00       # CMAX
   0.00      0.00      0.00      0.00      0.00      0.00      0.00       # CMIN
   1.00      1.00      1.00      1.00      1.00      1.00      1.00       # B
   0.00      0.00      0.00      0.00      0.00      0.00      0.00       # K1
   0.00      0.00      0.00      0.00      0.00      0.00      0.00       # K2
  33.909    45.128    40.768    55.021    45.397     2.5       2.5       # dgwsh (BASEFLOWFLAG = 1)/WF_LZFPWR (BASEFLOWFLAG = 2)
   0.62929   0.47777   0.76877   0.43000   0.35680   0.00001   0.00001    # agwsh (BASEFLOWFLAG = 1)/WF_LZFA (BASEFLOWFLAG = 2)
```

MESH_input_streamflow.txt

MESH_input_streamflow.txt

```
MRB 13years 2002-2014
3   4748    4748    24  2002    1   0
3702    -7286   10ED002
3617    -7408   10ED001
3565    -7566   10BE001
725 576 419
722 573 420
719 570 423
718 560 425
705 550 420
695 542 418
683 536 423
672 530 424
658 525 415
655 520 410
661 516 408
652 512 412
648 508 408
643 504 405
640 500 395
636 496 388
634 493 388
633 490 390
630 487 393
628 484 386
626 480 382
624 476 380
621 472 381
618 468 375
615 464 368
610 460 364
598 456 359
586 452 354
577 448 359
570 444 354
563 440 350
```

minmax_parameters.txt

minmax_parameters.txt

```
Reserved 1 - THEXTRA                                !ROW 1
0.0000                                              !min
0.0001                                              !max
Reserved 2 - ICE_INDEX                              !ROW 2
0.0000                                              !min
0.0001                                              !max
Reserved 3 - GWSCALE                                !ROW 3
0.0000                                              !min
0.0001                                              !max
River roughness factor (WF_R2) (5 classes maximum) !ROW 4
0.0200                                              !min
2.0000                                              !max
WF_R2 - CLASS 2                                     !ROW 5
0.0200                                              !min
2.0000                                              !max
WF_R2 - CLASS 3                                     !ROW 6
0.0200                                              !min
2.0000                                              !max
WF_R2 - CLASS 4                                     !ROW 7
0.0200                                              !min
2.0000                                              !max
WF_R2 - CLASS 5                                     !ROW 8
0.0200                                              !min
2.0000                                              !max
maximum soil porosity                               !ROW 9
0.0000                                              !min
1.0000                                              !max
depth from surface to bottom of rooting zone for maximum water holding capacity, m !ROW 10
0.0000                                              !min
4.1000                                              !max
Surface saturations [0.75 - 1.0]                    !ROW 11
0.0000                                              !min
1.0000                                              !max
Overnight minimum to cause ice lens after major melt -[50 - 0.0 ωC] !ROW 12
-50.00                                              !min
0.0000                                              !max
DRNROW - DRAINAGE INDEX, CALCULATED DRAINAGE IS MULTIPLIED BY THIS VALUE                    !ROW 13
0.0000 0.0000 0.0000 0.0000 0.0000 0.0000 0.0000 0.0000   !min DRNROW
1.0000 1.0000 1.0000 1.0000 1.0000 1.0000 1.0000 1.0000   !max
SDEPROW - THE PERMEABLE DEPTH OF THE SOIL COLUMN                                            !ROW 14
0.0000 0.0000 0.0000 0.0000 0.0000 0.0000 0.0000 0.0000    !min SDEPROW
100.00 100.00 100.00 100.00 100.00 100.00 100.00 100.00    !max
FARAROW - WHEN RUNNING A MOSAIC, THE FRACTIONAL AREA THAT THIS TILE REPRESENTS IN A GRID CELL !ROW 15
0.0000 0.0000 0.0000 0.0000 0.0000 0.0000 0.0000 0.0000    !min FARAROW
5.0000 5.0000 5.0000 5.0000 5.0000 5.0000 5.0000 5.0000    !max
DDENROW - THE DRAINAGE DENSITY OF THE GRU IN m/m2                                  !ROW 16
0.0000 0.0000 0.0000 0.0000 0.0000 0.0000 0.0000 0.0000    !min DDENROW
100.00 100.00 100.00 100.00 100.00 100.00 100.00 100.00    !max
XSLPROW - AVERAGE OVERLAND SLOPE OF A GIVEN GRU                                             !ROW 17
0.0001 0.0001 0.0001 0.0001 0.0001 0.0001 0.0001 0.0001    !min XSLPROW
1.0000 1.0000 1.0000 1.0000 1.0000 1.0000 1.0000 1.0000    !max
XDNROW - HORIZONTAL CONDUCTIVITY AT A DEPTH OF h0 DIVIDED BY HORIZONTAL CONDUCTIVITY AT SURFACE !ROW 18
0.0010 0.0010 0.0010 0.0010 0.0010 0.0010 0.0010 0.0010    !min XDNROW
1.0000 1.0000 1.0000 1.0000 1.0000 1.0000 1.0000 1.0000    !max
MANNROW - MANNING ROUGHNESS COEFFICIENT                                                     !ROW 19
0.0010 0.0010 0.0010 0.0010 0.0010 0.0010 0.0010 0.0010    !min MANNROW
2.0000 2.0000 2.0000 2.0000 2.0000 2.0000 2.0000 2.0000    !max
KSROW - HORIZONTAL CONDUCTIVITY AT SURFACE                                                  !ROW 20
0.0000 0.0000 0.0000 0.0000 0.0000 0.0000 0.0000 0.0000    !min KSROW
1.0200 1.0200 1.0200 1.0200 1.0200 1.0200 1.0200 1.0200    !max
SANDROW - PERCENTAGES OF SAND CONTENT OF SOIL LAYER 1                                       !ROW 21
-5.000 -5.000 -5.000 -5.000 -5.000 -5.000 -5.000 -5.000    !min % OF SAND not organic in soil layer 1
100.00 100.00 100.00 100.00 100.00 100.00 100.00 100.00    !max
CLAYROW - PERCENTAGES OF CLAY CONTENT OF SOIL LAYER 1                                       !ROW 22
0.0000 0.0000 0.0000 0.0000 0.0000 0.0000 0.0000 0.0000    !min % OF CLAY not organic or sand in soil layer 1
100.00 100.00 100.00 100.00 100.00 100.00 100.00 100.00    !max
ORGMROW - PERCENTAGES OF ORGANIC MATTER OF SOIL LAYER 1                                     !ROW 23
0.0000 0.0000 0.0000 0.0000 0.0000 0.0000 0.0000 0.0000    !min % OF ORGANIC in soil layer 1
100.00 100.00 100.00 100.00 100.00 100.00 100.00 100.00    !max
SANDROW - PERCENTAGES OF SAND CONTENT OF SOIL LAYER 2                                       !ROW 24
-5.000 -5.000 -5.000 -5.000 -5.000 -5.000 -5.000 -5.000    !min % OF SAND not organic in soil layer 2
100.00 100.00 100.00 100.00 100.00 100.00 100.00 100.00    !max
CLAYROW - PERCENTAGES OF CLAY CONTENT OF SOIL LAYER 2                                       !ROW 25
0.0000 0.0000 0.0000 0.0000 0.0000 0.0000 0.0000 0.0000    !min % OF CLAY not organic or sand in soil layer 2
100.00 100.00 100.00 100.00 100.00 100.00 100.00 100.00    !max
ORGMROW - PERCENTAGES OF ORGANIC MATTER OF SOIL LAYER 2                                     !ROW 26
0.0000 0.0000 0.0000 0.0000 0.0000 0.0000 0.0000 0.0000    !min % OF ORGANIC in soil layer 2
100.00 100.00 100.00 100.00 100.00 100.00 100.00 100.00    !max
SANDROW - PERCENTAGES OF SAND CONTENT OF SOIL LAYER 3                                       !ROW 27
-5.000 -5.000 -5.000 -5.000 -5.000 -5.000 -5.000 -5.000    !min % OF SAND not organic in soil layer 3
100.00 100.00 100.00 100.00 100.00 100.00 100.00 100.00    !max
CLAYROW - PERCENTAGES OF CLAY CONTENT OF SOIL LAYER 3                                       !ROW 28
0.0000 0.0000 0.0000 0.0000 0.0000 0.0000 0.0000 0.0000    !min % OF CLAY not organic or sand in soil layer 3
100.00 100.00 100.00 100.00 100.00 100.00 100.00 100.00    !max
ORGMROW - PERCENTAGES OF ORGANIC MATTER OF SOIL LAYER 3                                     !ROW 29
0.0000 0.0000 0.0000 0.0000 0.0000 0.0000 0.0000 0.0000    !min % OF ORGANIC in soil layer 3
100.00 100.00 100.00 100.00 100.00 100.00 100.00 100.00    !max
ZSNLROW - LIMITING SNOW DEPTH BELOW WHICH COVERAGE IS < 100%                                !ROW 30
0.0000 0.0000 0.0000 0.0000 0.0000 0.0000 0.0000 0.0000    !min ZSNLROW    **From MESH_parameters_hydrology.ini
5.0000 5.0000 5.0000 5.0000 5.0000 5.0000 5.0000 5.0000    !max
ZPLSROW - MAXIMUM WATER PONDING DEPTH FOR SNOW-COVERED AREAS                                !ROW 31
0.0000 0.0000 0.0000 0.0000 0.0000 0.0000 0.0000 0.0000    !min ZPLSROW
1.0000 1.0000 1.0000 1.0000 1.0000 1.0000 1.0000 1.0000    !max
ZPLGROW - MAXIMUM WATER PONDING DEPTH FOR SNOW-FREE AREAS                                   !ROW 32
0.0000 0.0000 0.0000 0.0000 0.0000 0.0000 0.0000 0.0000    !min ZPLGROW
1.0000 1.0000 1.0000 1.0000 1.0000 1.0000 1.0000 1.0000    !max
FZRCROW - COEFFICIENT FOR THE FROZEN SOIL INFILTRATION PARAMETERIC EQUATION                  !ROW 33
0.0000 0.0000 0.0000 0.0000 0.0000 0.0000 0.0000 0.0000    !min FZRCROW
3.0000 3.0000 3.0000 3.0000 3.0000 3.0000 3.0000 3.0000    !max
LNZ0ROW - NATURAL LOGARITHM OF THE ROUGHNESS LENGTH FOR LAND COVER CATEGORY 1                !ROW 34
-20.00 -20.00 -20.00 -20.00 -20.00 -20.00 -20.00 -20.00    !min LNZ0ROW1   Column 1 **Atmospheric parameters from MESH_parameters_CLASS.INI
100.00 100.00 100.00 100.00 100.00 100.00 100.00 100.00    !max
ALVCROW - VISIBLE ALBEDO FOR LAND COVER CATEGORY 1                                          !ROW 35
0.0000 0.0000 0.0000 0.0000 0.0000 0.0000 0.0000 0.0000    !min ALVCROW1
100.00 100.00 100.00 100.00 100.00 100.00 100.00 100.00    !max
ALICROW - NEAR INFRARED ALBEDO FOR LAND COVER CATEGORY 1                                    !ROW 36
0.0000 0.0000 0.0000 0.0000 0.0000 0.0000 0.0000 0.0000    !min ALICROW1
100.00 100.00 100.00 100.00 100.00 100.00 100.00 100.00    !max
RSMNROW - MINIMUM STOMATAL RESISTANCE FOR THE VEGETATION TYPE 1                             !ROW 37
0.0000 0.0000 0.0000 0.0000 0.0000 0.0000 0.0000 0.0000    !min RSMNROW1
1000.0 1000.0 1000.0 1000.0 1000.0 1000.0 1000.0 1000.0    !max
VPDAROW - COEFFICIENT GOVERNING THE RESPONSE OF STOMATES TO VAPOR PRESSURE DEFICIT - COMMON VALUE 0.5 !ROW 38
0.0000 0.0000 0.0000 0.0000 0.0000 0.0000 0.0000 0.0000    !min VPDAROW1
100.00 100.00 100.00 100.00 100.00 100.00 100.00 100.00    !max
PSGAROW - COEFFICIENT GOVERNING THE RESPONSE OF STOMATES TO SOIL WATER SUCTION -OMMON VALUE 100 !ROW 39
```

Appendix 2: Publications

Peer-reviewed publications

Bahrami, A., Goïta, K and Magagi, R., *Analyzing the contribution of snow water equivalent to the terrestrial water storage over Canada*, Hydrological Processes, Vol. 34, No. 2 (2020), pp. 175-188. https://doi.org/10.1002/hyp.13625

Bahrami, A., Goïta, K., Magagi, R., Davison, B., Razavi, S., Elshamy, M., and Princz, D., *Data Assimilation of satellite-based terrestrial water storage changes into a hydrology land-surface model*, Journal of Hydrology, Submitted in December 2019 (under review).

Conferences

Bahrami, A., Goïta, K., Magagi, R., Davison, B., Razavi, S., Elshamy, M., and Princz, D., *Data Assimilation approach for integrating satellite-based water storage changes into a hydrology land-surface model in Canadian basin*, 27*th* IUGG General Assembly, July. 8-18 (2019), Montréal, Canada (Poster presentation).

Bahrami, A., Goïta, K., Magagi, R., Davison, B., Razavi, S., Elshamy, M., and Princz, D., *Assimilation of satellite-based data into a hydrology land-surface model in Canada*, Colloque L'Association Québécoise de Télédétection (L'AQT) and La recherche en hydrologie au Québec (L'RHQ), May. 15-17 (2019), Sherbrooke, Canada (Oral presentation).

Bahrami, A., Goïta, K., Magagi, R., Razavi, S., Elshamy, M., Haghnegahdar, A., and Davison, B., *Integration of GRACE data into a hydrology land-surface model in a snow dominated Canadian basin*, Canadian Geophysical Union (CGU) Annual Joint Meeting, June. 10-14 (2018), Niagara Falls, Canada (Oral presentation).

Bahrami, A., Goïta, K., and Magagi, R., *Analysis of GRACE Terrestrial Water Storage Anomaly versus Snow Water Equivalent*, Canadian Geophysical Union (CGU) Annual Joint Meeting, June. 10-14 (2018), Niagara Falls, Canada (Oral presentation).

Bahrami, A., Goïta, K., Razavi, S., Magagi, R., Elshamy, M., Haghnegahdar, A., Davison, B., and Yassin, F.A., *Assimilation of GRACE derived terrestrial water storage data into Canadian land surface and hydrology model*, American Geophysical Union (AGU) Fall Meeting, Dec. 12-

16 (2016), San Francisco, USA (Poster presentation). https://doi.org/10.13140/RG.2.2.32902.73280